NTNU
Norwegian University of
Science and Technology

Within plate gabbroic intrusion at 565 Ma in the Uppermost Allochthon

A regional, geochemical and
geochronological study of the Umbukta
gabbro, north-central Norway

Anne Bruland Høyen

Geology
Submission date: July 2016
Supervisor: Allan George Krill, IGB
Co-supervisor: Trond Slagstad, NGU

Norwegian University of Science and Technology
Department of Geology and Mineral Resources Engineering

Abstract

A part of the Kjerringfjell Group in the Rödingsfjället Nappe Complex in the Uppermost Allochthon of north-central Norway was mapped during this thesis. The rocks in this area mainly compose of garnet-biotite gneiss, garnet-mica schist, two-mica gneiss, garnet-two mica gneiss, quartzite, pegmatite, and garnet amphibolite, and the host rock of garnet-biotite gneiss are intruded by the Umbukta gabbro and mafic dykes. The contact-zone between the gabbro and the garnet-biotite gneiss consists of contact-zone granitoid, mafic- dyke and enclaves, and granitic veins, which show evidence of mingling processes. At Umbukta and Østre Sauvatnet, mafic dykes cut the gabbro, the garnet-biotite gneiss and the quartzite.

Major- and trace element geochemical analyses were made for the Umbukta gabbro and the mafic dykes. The gabbro (represents a cumulate composition) and the mafic dykes show a tholeiitic geochemical signature. The trace element geochemistry of the rocks shows an enriched REE pattern relative to chondrite. The trace elements in the MORB normalized spider diagram mainly show an enriched pattern of the trace elements, except for Y and Yb, and the primitive mantle normalized spider diagram shows a relative enriched geochemical pattern relative to the primitive mantle, with no negative anomalies for Nb, Ta or Ti. The trace element geochemical patterns of the chondrite-, MORB-, and primitive mantle normalized spider diagrams indicate an intracontinental environment. The tectonic discrimination diagrams point to an intracontinental rift or a back-arc setting.

Geochronological analyses were conducted on the Umbukta gabbro and the host rock for age determination, with the use of the LA-ICP-MS method. The Umbukta gabbro yields a U-Pb zircon age of 565±20 Ma, and the U-Pb detrital zircon age population of the host rock mainly shows depositional ages between 1000 and 1900 Ma. The youngest age of the analysed detrital zircons was 1000 Ma, and point to depositional age younger than 1000 Ma.

The U-Pb zircon age and the geochemical signature of the Umbukta gabbro and the mafic dykes show many similarities with the gabbros in the Seiland Igneous Province (SIP), in Finnmark of northern Norway. The SIP is placed in the Kalak Nappe Complex (KNC) within the Middle Allochthon. The Umbukta gabbro could stem from the same source as the gabbros in the Seiland Igneous Province (SIP). This possible correlation should lead to a reconsideration of the interpretation of the tectonostratigraphy of the Scandinavian Caledonides. The KNC and SIP is traditionally interpreted to belong to the Middle Allochthon, and the Umbukta gabbro and mafic

dykes in the Kjerringfjell Group is placed within the Uppermost Allochthon. The results of this study suggest a possible correlation of the rocks in the KNC and SIP with the rocks in the Kjerringfjell Group in the Uppermost Allochthon.

Sammendrag

En del av Kjerringfjell gruppen i Øverste Allochthon i sørlige Nord- Norge har blitt kartlagt i denne oppgaven. Bergartene i dette området består hovedsakelig av granat-biotitt gneis, granat-glimmer skifer, to-glimmer gneis, granat-to glimmer gneis, kvartsitt, pegmatitt og granat amfibolitt og vertsbergarten som består av granat-biotitt gneis er intrudert av Umbukta gabbroen og mafiske ganger. Kontaktsonen mellom gabbroen og granat-biotitt gneisen består av kontakt-sone granittoid, mafiske ganger og -enklaver og granittiske årer og her er kan man se bevis på mingling prosesser. Ved Umbukta og Østre Sauvatnet blir gabbroen, granat-biotitt gneisen og kvartsitten kuttet av de mafiske gangene.

Geokjemisk analyse av hoved- og sporelementer har blitt utført på Umbukta gabbroen og de mafiske gangene. Gabbroen (representerer en kumulat sammensetning) og de mafiske gangene viser en tholeiitisk geokjemisk signatur. De geokjemiske sporelementene i gabbroen og de mafiske gangene viser en beriket REE trend relativ til kondrittisk sammensetning. Det MORB normaliserte spor element diagrammet viser hovedsakelig berikning av spor elementene, bortsett fra Y og Yb, og det primitive mantel normaliserte spor element diagrammet viser en relativ berikelse av spor elementene og viser ingen negativ anomali for Nb, Ta eller Ti. De geokjemiske sporelementene i bergartene indikerer et intrakontinentalt miljø, og de tektoniske diskriminasjons diagrammene peker mot en intrakontinental rifting eller en back-arc setting.

Geokronologisk analyse for aldersbestemmelse ble utført på Umbukta gabbroen og vertsbergarten. Aldersbestemmelsen ble bestemt ved bruk av U-Pb zirkon analyse, hvor det ble benyttet LA-ICP-MS metoden. Umbukta gabbroen er blitt datert til en U-Pb zirkon alder på 565±20 Ma og de detritisk zirkon aldrene av vertsbergarten viser til avsetnings provenansaldre som hovedsakelig strekker seg mellom 1000- 1900 Ma. Den yngste detrital zirkon alderen som ble analysert var 1000 Ma og antyder en avsetningsalder yngre enn 1000 Ma.

U-Pb zirkon alderen og den geokjemiske signaturen av Umbukta gabbroen viser til mange likheter med gabbroene som befinner seg i Seiland Igneous Province (SIP) i Finnmark i Nord-Norge. SIP ligger plassert i Kalak Nappe Kompleks (KNC), som ligger i Midtre Allochthon. Disse dataene har ført til spekulasjoner om Umbukta gabbroen kan stamme fra samme kilde som gabbroene i SIP. Denne mulige korrelasjonen bør lede til en ny vurdering av den tradisjonelle tolkningen av tektonostratigrafien av de Skandinaviske Kaledonidene. KNC og SIP er tradisjonelt tolket til å tilhøre Midtre Allochthon mens Umbukta gabbroen i Kjerringfjell Gruppa tilhører Øverste Allochthon. I denne oppgaven har det blitt foreslått en mulig

korrelasjon mellom bergartene i KNC og SIP med bergartene i Kjerringfjell Gruppen i Øverste Allochthon.

Acknowledgements

This master thesis has been carried out at the Department of Geology and Mineral Resources Engineering (IGB) at the Norwegian University of Science and Technology (NTNU), Trondheim, and in collaboration with the Geological Survey of Norway (NGU). Professor Allan Krill (NTNU) and Dr. Trond Slagstad (NGU) have been the main supervisors for this project.

I would especially like to thank my supervisors, Krill and Slagstad, for their support during both fieldwork and guidance through this project. The door has always been open, and even in busy times they always were able to find time for discussion or practical help. I also would like to thank Dr. Nolwenn Coint at NGU for excellent guidance in thin section examinations. Their encouragement and expertise has truly benefitted my project. NTNU supported for thin sections and NGU for geochemical analysis, which made this project possible. Moreover, I would like to thank my dad (Stein P. Høyen) for stepping in as my field assistant whenever it was needed, and my classmates for many good discussions, and a special thanks to Anette Utgården Granseth for assisting in final stage of editing.

Anne Bruland Høyen

Trondheim 08.07.2016

Table of contents

Figure list

Introduction

The studied area is part of the Uppermost Allochthon of the north-central Caledonides in Nordland, Norway. The examined plutonic rock at Umbukta, now referred to as the Umbukta gabbro, and the gneisses are located within in the Rödingsfjället Nappe Complex, which is located west of the city of Mo i Rana, at the border to Sweden (Figure 1). The Rödingsfjället Nappe Complex is divided into six nappes and covers most of the Rana region (Melezhik et al., 2015). The Ravnålia Nappe is one of the six nappes of the Rödingsfjället Nappe Complex, and is divided into three lithostratigraphic units, the Kjerringfjellet Group, the Dunderland Formation, and the Ørtfjellet Group, and the Kjerringfjellet Group is placed at the bottom of the Ravnålia Nappe (Melezhik et al., 2015). In this thesis mapping has been performed in part of the Kjerringfjell Group, and the geology of the mapped area mainly consists of gabbro, mafic dykes, garnet-biotite gneiss, garnet-mica schist, two-mica gneiss, quartzite, chloritized garnet-biotite gneiss, pegmatite and granitic veins.

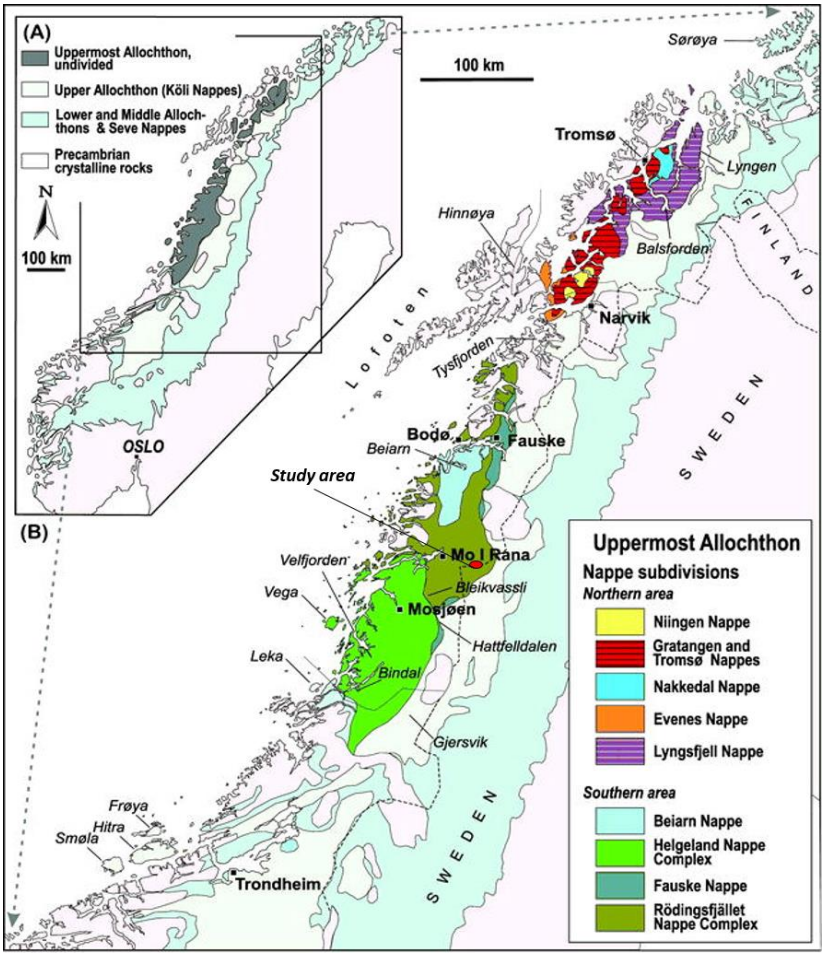

Figure 1: The figure is showing a tectonostratigraphic map of north-central Norway. The study area is marked with a red circle, and is located northeast of Mo i Rana in the Rödingsfjället Nappe Complex, close to the boarder of Sweden. Figure is modified from Roberts et al. (2007).

The Rödingsfjället Nappe Complex has received little attention, and little research has been performed in the area. The present work has focused on unravelling some of the geology in part of the Kjerringfjellet Group. This has included field observations, petrographic descriptions and geochemical analysis. The fieldwork has focussed on mapping the different rock lithologies and the contact relations between the Umbukta gabbro and the garnet-biotite gneiss. The classification of the rocks is based on thin-section examination. Major- and trace-element geochemistry of the Umbukta gabbro is presented, as well as isotopic age dating of the rock. Based on the gathered data, interpretations of geological processes, relations to tectonic environment and some ideas of possible tectonostratigraphic implications are presented. The present data show that the Umbukta gabbro has an older intrusive age and is more enriched in REE elements than most other gabbros in the Scandinavian Caledonides. The Umbukta gabbro shows geochemical similarities with the gabbros in the Seiland Igneous Province in the Kalak Nappe Complex in Finnmark, Northern Norway. The similarities apply to age of intrusion and the geochemical signatures of the rocks from the two regions.

The Scandinavian Caledonides have been studied for decades, and the tectonostratigraphy of the allochthons has generally been accepted. Throughout the years the instruments have improved, and more knowledge of tectonic processes have developed (Corfu et al., 2014a). U-Pb geochronology has been improved (Corfu et al., 2014a) and has led to a more precise time estimate of the orogenic processes (Roberts et al., 2006). This has led to some new perspectives of the Scandinavian Caledonides. Recent years, the subdivision of the Scandinavian Caledonides into Lower, Middle, Upper and Uppermost Allochthon has received increasing criticism (Corfu et al., 2014a). The subdivision of the Scandinavian Caledonides may be a too simplified model of a much more complex history.

Aim of thesis

Selection of the study area was based on some unpublished geochronological- and geochemical data of the Umbukta gabbro and some mafic dykes. The intrusion age of the Umbukta gabbro is an uncommon age for most Caledonian gabbros and mafic rocks, and this needed further investigation.

The aim of this research is to contribute new geological data from the Kjerringfjell Group in the Uppermost Allochthon in northern Norway. The geological data is used to perform regional interpretation of the geology of the area, for geological understanding. To accomplish interpretation of the area, geological mapping of the rocks have been central. Geochemistry and geochronology are used to get insight into the origin of the gabbro. Detrital zircon age analyses were made for the host rock of the gabbro for indication of provenance of the metasedimentary rocks, and their maximum age of deposition.

Geological background

The Caledonides

The Scandinavian Caledonides

The Caledonides have been studied throughout several centuries and the orogen extend through Norway and Sweden over a distance of nearly 2000 km (Gee et al., 2008) and dominate the Norwegian geology. The orogen extend from the edge of the Eurasian basin (Gee et al., 2008) in the north to the British Isles in the south, and the Caledonian orogen is also present in North-America as the Appalachians (Van Staal et al., 1998). The Caledonides are separated into the Svalbard Caledonides, the Greenland Caledonides, the Scandinavian Caledonides, and the British Caledonides (Corfu et al., 2014b).

The orogen formed during closure of the Iapetus ocean in the Ordovician- to Early Devonian times (Gee, 1975). Converging plates resulted in collision between Laurentia, Baltica and Avalonia (Corfu et al., 2014b) (Figure 2). First Baltica collided obliquely with Avalonia at about 443 Ma. which has been interpreted to be relatively softly (Cocks and Torsvik, 2006), and soon after Laurentia collided with Baltica in a more energetic way (Cocks and Torsvik, 2006). The Baltic margin subducted beneath Laurentia (Roberts, 2003) and resulted in eastward thrusting of the Baltic plate margin (Grenne et al., 1999). The Caledonian orogen was possibly similar to the modern Himalayan – Tibetan system (Labrousse et al., 2010) before it became deeply eroded.

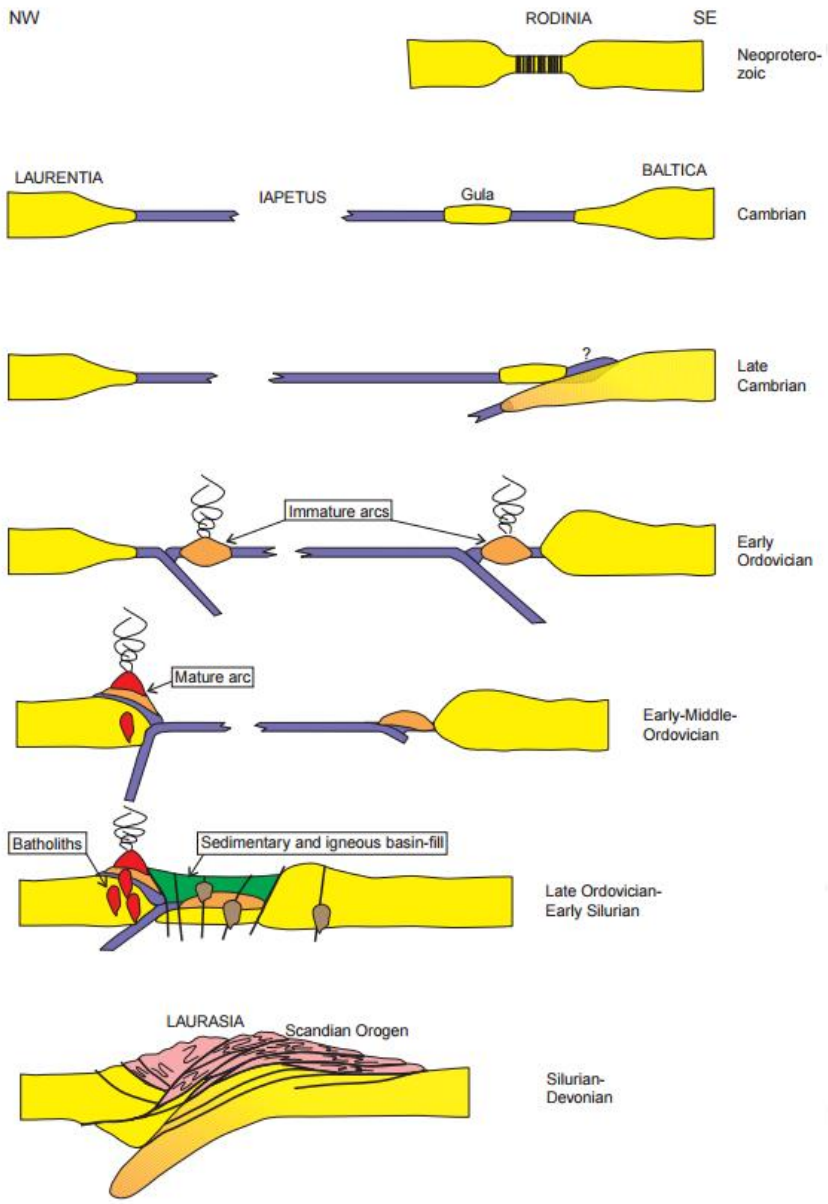

Figure 2: The figure shows an illustration of the different stages of Caledonian plate tectonic evolution. The figure is modified from Grenne et al. (1999)

In this thesis, the focus will be on the Scandinavian Caledonides. The Caledonian orogen is dominated by thrust- and nappe tectonics (Roberts and Gee, 1985). The large-scale structures are major thrust units of approximately east to south-eastward emplacement (Corfu et al., 2014b). The thrust sheets are composed of metasedimentary and igneous rocks from Late Proterozoic to Silurian age and sheets of pre-Caledonian crystalline basement rocks (Roberts and Gee, 1985).The thrust sheets have been separated into Lower, Middle, Upper and Uppermost Allochthons (Roberts and Gee, 1985), resting on an autochthonous-parautochthonous crystalline basement.

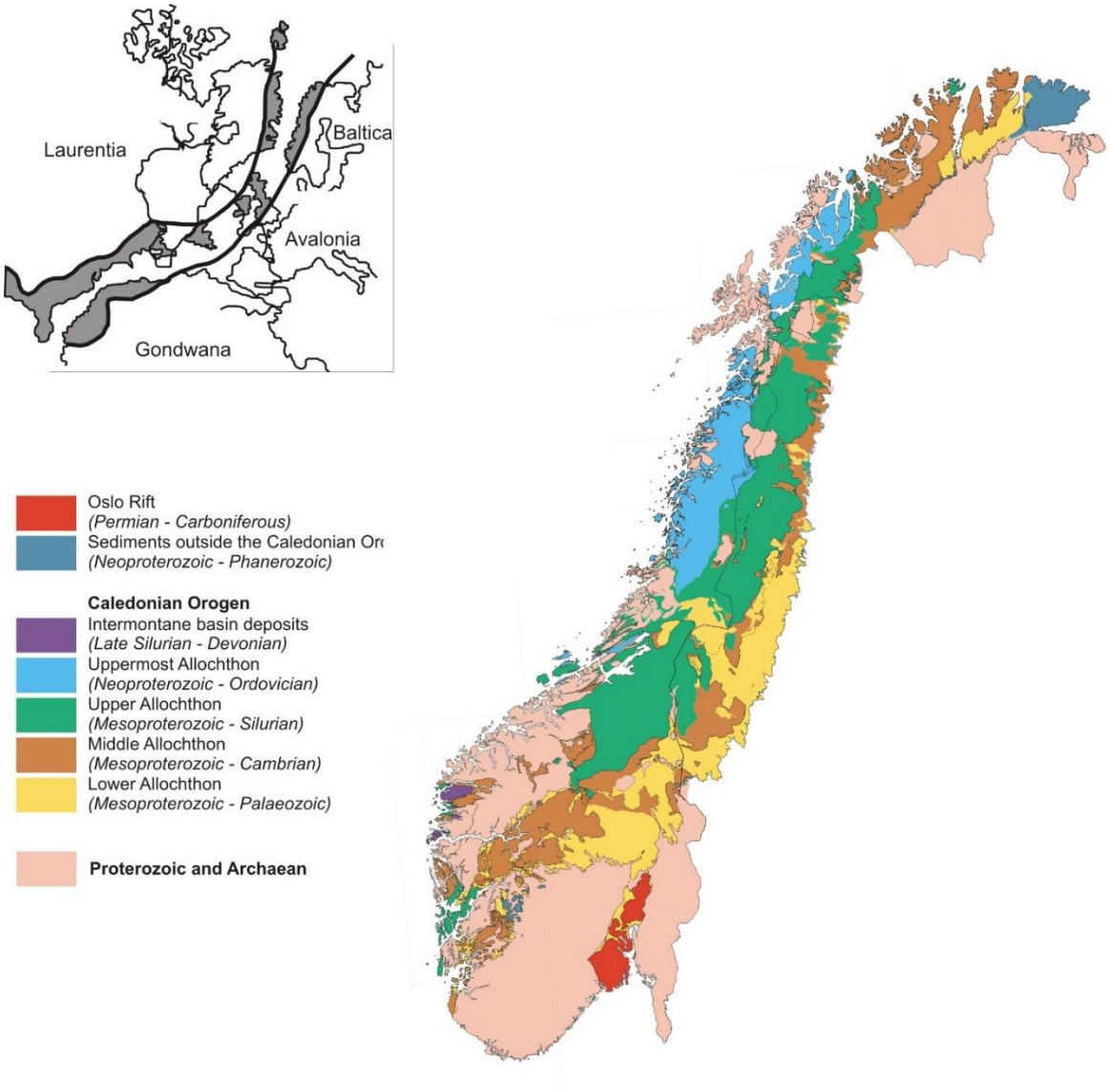

Figure 3: Tectonostratigraphic map of the Scandinavian Caledonides. Map modified from (Slagstad et al., 2014).

Autochthonous–Parautochthonous

The Autochthonous–Parautochthonous basement consist of Archean to Neoproterozoic crystalline rocks of the Fennoscandian shield (Bryhni and Sturt, 1985a, Corfu et al., 2014b), at many localities these rocks are covered with sandstone and shales of Cambrian age (Roberts and Gee, 1985). The basement mainly consist of granites, gneisses, porphyries and migmatites (Roberts and Gee, 1985). The Lower Allochthon was transported on a surface of black shales, which provided as a decollement. Precambrian crystalline rocks west of the decollement occur as antiformal windows, which often are foliated and they may have been laterally transported,

and for these reasons they are referred to as parautochthonous (Gee and Zachrisson, 1979). The basement is generally affected by lower greenshist-facies, but along the coast of western Norway, the crystalline basement rocks are affected by amphibolite-facies metamorphism. In southwestern Norway the basement gneisses are affected by high-grade metamorphism with eclogite bearing rocks (Roberts and Gee, 1985, Corfu et al., 2014a, Andersen and Jamtveit, 1990), and locally there are occurrence of coesite and microdiamonds (Dobrzhinetskaya et al., 1995), which indicate a crustal burial depth up to 125 km (Gee et al., 2008).

Lower Allochthon

The Lower Allochthon is a sediment-dominated Allochthon (Stephens et al., 1985b) and consists of lower and higher nappes. It is interpreted to be a part of Baltica's continental margin (Gee et al., 2008). The lower nappe complex mostly consists of early Palaeozoic to Late Proterozoic sedimentary successions (Bryhni and Sturt, 1985b), including quartzite and shale from Vendian and Lower Cambrian age (Roberts and Gee, 1985, Bryhni and Sturt, 1985b). These sedimentary successions are overlain by grey and black shale from Mid- and Upper Cambrian (Roberts and Gee, 1985), and of some Ordovician limestone. Farther west it is presence of greywacke (Roberts and Gee, 1985). Higher nappes in the Lower Allochthon consist of tillites and underlying fluvial and shallow- marine sandstones from the Late Palaeozoic (Roberts and Gee, 1985). The structures in this allochthon consist of a westward Caledonian thrust front (Stephens et al., 1985b), and the sediments typically contain folds and listric reverse-faulting (Roberts and Gee, 1985). The Lower Allochthon has mostly been exposed to greenshist facies (Roberts and Gee, 1985), but in the westernmost area the rocks have been through amphibolite facies metamorphism (Roberts and Gee, 1985).

Middle Allochthon

The Middle Allochthon mainly consists of metasediments and Precambrian crystalline rocks (Roberts and Gee, 1985), and is interpreted to represent parts of the ocean-ward Baltic basement and their cover rocks (Lundmark and Corfu, 2008). The Jotun Nappe Complex is located in southwestern Norway, and is part of the Middle Allochthon, and consists of a thick unit of Precambrian crystalline rocks, which are highly foliated and mylonitized along their margin (Roberts and Gee, 1985, Lundmark et al., 2007). The metasediments overlying the crystalline rocks have been through highly ductile deformation with penetrative foliation and isoclinal recumbent folding (Roberts and Gee, 1985). In the upper part of the Middle Allochthon the Neoproterozoic sandstones are characterized by mafic dykes (Gee et al., 2008) and metaplutonic complexes (Roffeis et al., 2012). These rocks are located within the Kalak Nappe

Complex in Finnmark of northern Norway (Figure 4). The Kalak Nappe Complex contains the Seiland Igneous Province (SIP), which consists of several intrusive rocks mainly of gabbroic plutons with subordinate intrusives of ultramafic, syenitic and felsic composition (Roberts et al., 2006, Ramsay et al., 1985, Stephens et al., 1985a). This region has a complex geology, and the intrusive rocks in the SIP have an older intrusive age and a different geochemical signature than most other intrusive rocks in the Scandinavian Caledonides. The timing of the intrusive stages has been widely studied and debated (Krogh and Elvevold, 1990).

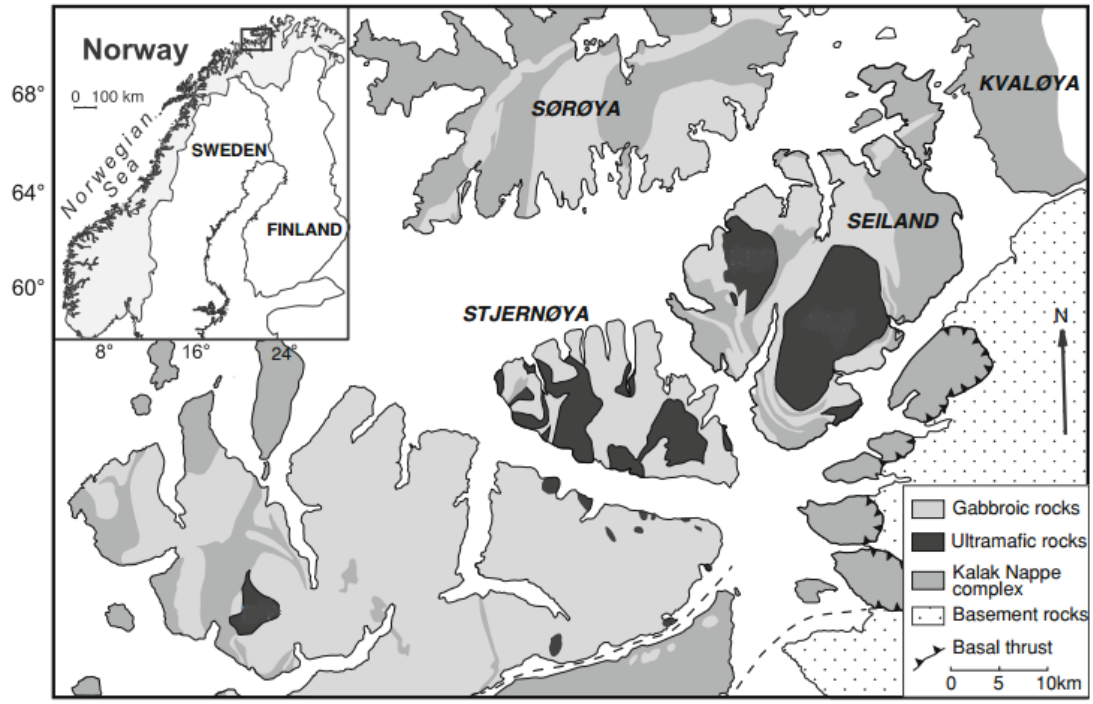

Figure 4: Regional setting of the Kalak Nappe Complex and the Seiland Igneous Province of northern Norway, Finnmark. Figure from Griffin et al. (2013)

Upper Allochthon

The Upper Allochthon is the most complex of the allochthons, because of the extensive Caledonian igneous activity (Roberts and Gee, 1985). The Seve Nappe is the lowest unit of the Upper Allochthon, and is generally of a higher metamorphic grade than the over- and underlying rocks. The Seve Nappe composes of pelitic schist, gneiss, migmatitic gneiss, amphibolite, eclogite and peridotite (Corfu et al., 2014b). The Köli Nappe is located above the Seve Nappe and composes volcanosedimentary rocks (Corfu et al., 2014a). The higher nappes of the Upper Allochthon consist of ophiolites from the Iapetus ocean floor and arc complexes derived from the Baltic margin (Gee et al., 2008). A major unconformitie in the Köli Nappe

separate successions of Late Ordovician and Silurian age from earlier volcanosedimentary complexes that includes ophiolites. This unit has been through greenschist- , granulite- and eclogite facies. The eclogite facies occur in the basaltic units (Roberts and Gee, 1985).

Uppermost Allochthon

The Uppermost Allochthon is the highest tectonic unit of the Allochthons. This Allochthon is dominating in Norland, which is in north-central Norway. The Uppermost Allochthon has affinities to the Laurentian margin or unknown microcontinents (Stephens and Gee, 1985), and composes of the Scandinavian Caledonides most exotic elements (Gee et al., 2008, Stephens et al., 1985a). The nappes in the Uppermost Allochthon are positioned above the Köli nappes (Roberts and Gee, 1985) and composes of the Rödingsfjället-, Helgeland- and Tromsø nappe complexes (Roberts and Gee, 1985, Corfu et al., 2003b). The Helgeland and Rödingsfjället nappe complexes dominate the Uppermost Allochthon (Figure 1), and characteristic for the two nappe complexes is the abundant marble formation, a variety of granitoid batholiths, occurrence of plutons which range in composition from olivine gabbro to leucogranite, and stratabound iron formations. These features separate the Uppermost Allochthon from the rocks recorded in the Baltoscandian- and Iapetus allochthons (Roberts et al., 2007). The abundant marble formations and the magmatic arc related granitoids have led to an interpretation that the Uppermost Allochthon must be derived from the Laurentian margin (Stephens and Gee, 1985, Roberts et al., 2007). Already in the 1980s it was suggested an exotic origin for the rocks in the Uppermost Allochthon, and further work during the last years still supports this interpretation (Roberts et al., 2007)

The Helgeland Nappe Complex is the most studied Nappe Complex in the Uppermost Allochthon, and separates into five nappes (Barnes et al., 2007), which further can divide into two groups (McArthur et al., 2014). One group consist of Upper-, Lower- and Horta nappes and the rocks in these nappes mainly consist of migmatitic gneiss, calc-silicate rocks and marbles (McArthur et al., 2014, Barnes et al., 2007). The other group composes Middle- and Sauren-Torghatten nappes and the rock lithologies in these nappes mainly consist of metaconglomerates, marble, calc-silicate schist and pelitic schist, which are deposited on ultramafic and mafic meta-igneous rocks (McArthur et al., 2014, and references therein). Commonly the rocks in the nappes are highly deformed and of medium-grade metamorphic assemblages (Nordgulen et al., 1993).

The Rödingsfjället Nappe Complex (Figure 5) is divided into six nappes (Melezhik et al., 2015, and references therein), and one of the six nappes is the Ravnålia Nappe, which separates into

three groups; the Kjerringfjell Group, the Dunderland Formation and the Ørtfjellet Group (Melezhik et al., 2015, and references therein). The Kjerringfjell Group is the group that will be considered in the current contribution, and is situated at the bottom of the Ravnålia Nappe. The Kjerringfjell Group mainly consists of metasedimentary rocks of garnet-biotite gneiss and garnet-mica schist intruded by a gabbroic pluton, while the Dunderland Formation and the Ørtfjellet Group have lithologies of abundant marble, mica-schists and iron-ore formation (Melezhik et al., 2015).

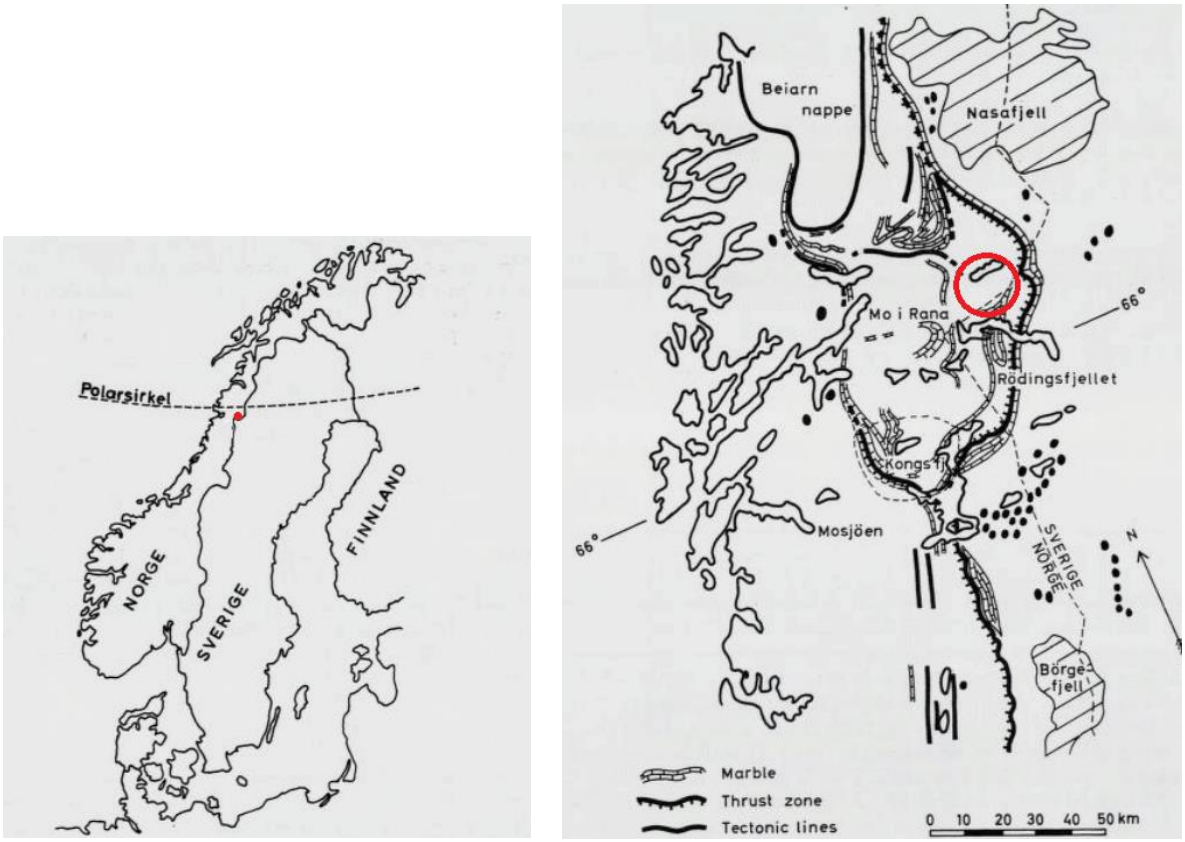

Figure 5: The red dot in the left figure shows the location of the Rödingsfjället Nappe Complex in north-central Norway. To the right the red circle show a more detailed location of the Kjerringfjellet Group. Figure modified from Ramberg (1967).

Extensional tectonics in the Caledonides

After contractional tectonics and formation of the Caledonides, the contractional tectonics changed to extensional in the southern part of the orogen, shortly prior to 400 Ma (Gee et al., 2008). The extensional collapse resulted in sub-vertical shortening and later east-west extension of the Caledonides (Milnes et al., 1997). The main phase of crustal extension and fabric indicate normal top-to-the west or southwest movement (Gee et al., 2008, Milnes et al., 1997). In northern Norway the extensional and contractional relationship appears more complex, and

there is some overlap between contraction and the development of the major extensional detachments (Gee et al., 2008). The deep-crustal imbrication and the collapse of the root, led to the event where deep metamorphic rocks where brought relatively close to the surface (Tucker et al., 2004).

Theory

Diagrams presenting major element data

The major elements are those mainly responsible for the rock forming minerals. They are usually presented as oxides and constitute of more than 0.1 wt. % of the rock (Winter, 2010). Most rocks are made from one or more, of 11 major element oxides. The most common oxides are SiO_2, MgO, FeO (sometime presented as Fe_2O_3), CaO, Al_2O_3, MnO, TiO_2, Na_2O, K_2O, and P_2O_5 (Best, 2003). Major elements are often used to classify igneous rocks, and to study chemical evolution of melts and crystal-melt systems (Winter, 2010).

Fenner diagrams

The Fenner-type variation diagram is a bivariate plot showing major element variation as a function of MgO concentration. First, the Harker diagram was introduced by Harker (1900, 1909) (Wilson, 1993), where silica is used along the x-axis to explore the evolving magma. Silica typically varies little in the early stages of magmatic evolution, because the mafic minerals, which first crystallize from the mafic magma, typically consume MgO and Fe_2O_3. Olivine and pyroxene are usually the first minerals that crystallizes from the magma, and removes elements as the MgO and the Fe_2O_3 (Winter, 2010). To see any trends in the early stages of magma evolution the MgO is assumed to be more appropriate for rock series including abundant mafic members (Wilson, 1993). MgO decreases to the right of the diagram, as the magma evolves and gives indication of the fractional trends of the rock. The Fenner diagram graphically shows variation between samples (Wilson, 1993, Rollinson, 1993). The diagram is compiled for volcanic rocks.

Concern has been expressed about the validity of the binary diagrams, such as the Fenner diagrams. The elements plotted in the diagrams are presented as percent value, and this can lead to artefacts, because the analysed elements all must total to 100%, and this may affect the trends in the variation diagrams. The apparent increase of one or more elements can result from a crystallizing phase, which consume some of the elements, and removes them from the liquid. The remaining elements do not increase their concentration in the liquid, but compose a greater proportion of the remaining liquid. Looking at the percentage it appears as the concentration of the remaining elements increases, when in fact they actually could decrease on an absolute scale (Pearce, 1968, Winter, 2010). So there have been questioned if this graphical treatment of the chemical components generally represent the true variation with respect to each other (Pearce, 1968). Still, there are authors defending the use of the diagrams, because of the vital information

such diagrams give, when used by experienced geologists (Cortés, 2009, Egozcue, 2009). However, there is agreement that the diagrams should be used with some caution.

AFM diagram

The purpose of the AFM diagram is to separate calc-alkaline and tholeiitic magmas. The basis for separation is the iron content. AFM makes up the corners of the triangular diagram (Figure 6), where A = Na_2O + K_2O, F = FeO + 0.8998*Fe_2O_3 (Fe_{tot}) and M = MgO (all in wt%). Tholeiitic basalts typically show a strong iron enrichment in the early stages of differentiation, whereas calc-alkaline basalts trend towards Na_2O + K_2O, because of early crystallization of Fe-Ti oxides suppresses iron enrichment (Riddle, 1993, Sheth et al., 2002). Irvine and Baragar (1971) used rocks from many locations worldwide to create the boundary line (Sheth et al., 2002), which most commonly is used today, to separate the calc-alkaline and tholeiitic magmas.

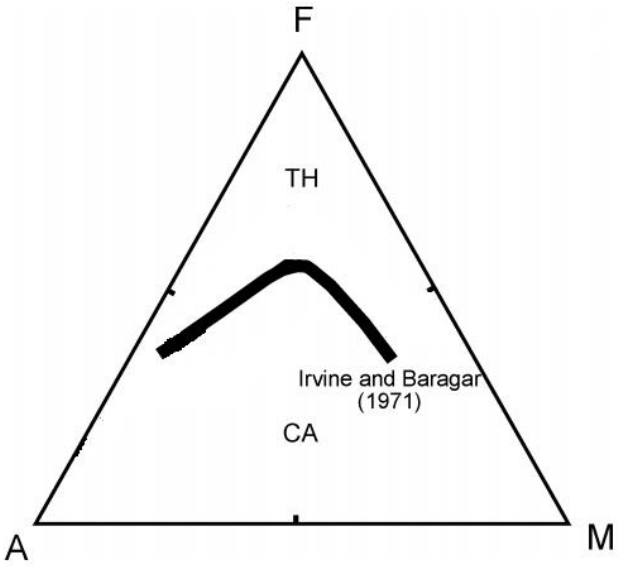

Figure 6: The AFM diagram showing the boundary line, which separates the tholeiitic (TH) and calc-alkaline (CA) fields. The black boundary-line, which separates the two fields is the one made by Irvine and Baragar (1971) (modified from Sheth et al., 2002).

Using discrimination diagrams possible artefacts may occur, and should be taken into consideration. What is generally a problem with discrimination diagrams is their lack of fully representing the total rock chemistry. In the AFM diagram the presented parameters composes of less than 50% of the oxide weight percentages of the total rock composition (Rollinson, 1993). Only four components (Na + K, Fe and Mg) of the whole rock chemistry are used when normalizing to 100%, and this can lead to distortion of the trends (Rollinson, 1993). Some

overlap can occur between the calc-alkaline and tholeiitic fields, especially at the mafic and felsic ends (Sheth et al., 2002). Rocks with mafic composition have been assumed to have a higher proportion of the chemistry presented in the diagram than a felsic rock (Rollinson, 1993). The main usefulness of the AFM diagram is to recognise trends, which may identify rock series (Philpotts, 2003).

Diagrams presenting trace element data

Trace elements usually constitutes less than 0.1 wt. % (1000 ppm) of the rock composition, and are usually given as an element (Winter, 2010, Best, 2003, Rollinson, 1993). The trace elements often substitutes for the major or minor elements, because their concentration are usually too low to form a separate mineral phase, and they are usually more sensitive to different phases than the major elements (Winter, 2010, Best, 2003). The behaviour of the trace elements have made them good indicators for analysing petrological processes (Winter, 2010, Best, 2003, Rollinson, 1993).

Rare earth elements (REE) diagram

The rare earth elements (REE) are a series of metals with atomic numbers from 57 to 71, La – Lu (Hanson, 1980). The REE are stable as 3+ ions and they have almost similar ionic radius (Bau, 1991), so their physical properties are very similar. There is however, a very small difference in the ionic radius, the ionic size decreases with increasing atomic number, and this causes fractionation of the REEs (Bau, 1991, Rollinson, 1993). The REE from La to Sm are usually referred to as the LREE, and these elements have lower atomic number and atomic masses than the elements from Gd to Lu, which is referred to as the HREE (Hanson, 1980, Henderson, 1984). The ionic radius is slightly lager for the LREE than the HREE, and causes the LREE to usually be a bit more incompatible than the HREE, and favours liquid and melts over crystalline phases. The lower ionic radius of the HREE makes them more compatible relative to the LREE, and the HREE usually favours the crystalline phases (Best, 2003).

The REEs are generally immobile during low-grade metamorphism, weathering and hydrothermal alteration (Best, 2003) and are considered as some of the least soluble trace elements. When REE data are presented from a rock sample, they are often normalized to a common reference standard (Rollinson, 1993). The standard most commonly used today, are the values for the chondritic meteorites (Rollinson, 1993). The chondritic meteorites are thought

to be the oldest objects of the solar system and are relatively unfractionated samples of the solar system (McKeegan and Davis, 2003), so they probably approximate the chemical composition of bulk Earth (Winter, 2010). To graphically compare the REEs for different rocks, the Oddo-Harkins effect must be eliminated. This effect is a result of higher concentration of elements with even atomic number than with odd atomic number (Hanson, 1980, Castor and Hedrick, 2006). Normalizing the individual REEs to chondrite, will smooth out the variable concentration from each element (Hanson, 1980). Another important function of the normalization is to identify the fractionated REE groups relative to the chondritic meteorites (Rollinson, 1993). The pattern of the plotted REE data is of petrological interest.

A relatively common anomaly in the chondrite normalized spider diagram is the europium anomaly. Europium (Eu) can occur as both Eu^{2+} and Eu^{3+}, and Eu^{2+} is compatible with plagioclase and can substitute for Ca^{2+}, because of the similarities of the two elements (Best, 2003). When Eu^{2+} substitutes for Ca^{2+} in plagioclase, the REE pattern will either show a positive or a negative anomaly on the diagram. A positive anomaly is an indication of plagioclase accumulation, while a negative anomaly indicates plagioclase fractionation and removal of the plagioclase from the melt (Best, 2003, Winter, 2010).

Primitive mantle- and MORB normalized spider diagrams

Chondrite normalization is not the only reference used for normalization and presentation of the trace elements. An estimated primitive mantle and an average mid-ocean ridge basalts (MORB) are other standards used for normalizing the trace elements (Rollinson, 1993). The primitive mantle- and the MORB normalized spider diagrams have usually a larger range of plotted trace elements then the chondrite normalized REE diagram. Each spider diagram has a slightly different number of presented elements and the order of the elements can varies, but mostly the primitive- and MORB normalized spider diagrams are presented as log-linear diagrams and the elements are ordered with increasing compability from left to right (Best, 2003, Winter, 2010, Rock, 1987).

The primitive mantle is assumed to be the chemical composition of the mantle after core segregation, but before the extraction of the continental crust (Lyubetskaya and Korenaga, 2007, Sun, 1982). The primitive mantle is most frequently used as a compositional reference, when comparing variations between mafic lavas (Rollinson, 1993, Wood et al., 1979). Number of elements presented in the diagram varies from 13 to 19.

The MORB normalized spider diagram normalises the data to an average mid-ocean ridge basalt (MORB), which is the most abundant igneous rock on the planet (Winter, 2010). This diagram is most appropriate to use when analysing evolved basalts, andesites and crustal rocks, because it is more likely that MORB is the parental magma than the primitive mantle (Rollinson, 1993). There is more than one version of the MORB normalized spider diagram, but the one made by Pearce (1983) is the most common. Along the x-axis the elements are ordered with the most mobile elements (Sr, K, Rb and Ba) placed at the left of the diagram and the immobile elements (TH, Ta, Nb, Ce, P, Zr, Hf, Sm, Ti, Y and Yb) are arranged from right to left in order of increasing incompability (Pearce, 1983).

The trace element diagrams are helpful tools in interpretation of different petrological processes. Peaks and troughs in the spider-normalized diagrams provide important information of the source and processes in the origin of the magma (Best, 2003). What may be most troublesome with the usage of the normalized spider diagrams is the lack of one standardized method (Rock, 1987). The main problem with no common standard mainly affects the comparison of different plots. It is difficult to compare different plots if the elements are not normalized to the same normalizing value or have the same element orders (Rock, 1987). The chondrite normalized values are an example of this problem. Individual chondrites sometimes show marked variation between and within both relative and absolute REE abundance, and this has resulted in no standardization value (Masuda et al., 1973, Evensen et al., 1978), just a considerable number of different normalizing values, for the REEs (Masuda et al., 1973). Generally, the trace elements are considered immobile. However, it is important to be aware that changes in fluid composition, increasing temperature or extremely high fluid amount may mobilize otherwise immobile elements (Hastie et al., 2007).

Tectonic discrimination diagrams

Different tectonic environment show variable geochemical signatures and tectonic discrimination diagrams permit rocks of unknown origin to be assigned to its most probable tectonic setting (Pearce, 1996). Discrimination diagrams that have the widest applicability are those based on elements or element ratios that are not sensitive to secondary processes, especially when analysing altered or metamorphosed rocks (Pearce, 1996).

Tectonic discrimination diagrams mostly separate between tectonic environments as mid-ocean ridge basalts (MORB), the MORB can be separated into N-MORB (normal-MORB) and E-MORB (enriched-MORB). Volcanic arc basalts (VAB), which can be distinguished into volcanic arc tholeiitic basalts, volcanic arc calc-alkaline basalts and active continental margin. Collisional settings can separate into continent-continent collision or continental-arc collision. The within plate setting can be subdivided into tholeiites or alkalic affinities, and between intracontinental or ocean-island settings (Rollinson, 1993, Pearce, 1996)

Ti-Zr-Y diagram by Pearce and Cann (1979)

Pearce and Cann (1973) constructed the Ti-Zr-Y diagram for interpretation of tectonic settings of different basalts (Figure 7). They analysed 200 basaltic rocks from different tectonic settings (Pearce and Cann, 1973), and made it possible to discriminate between four different tectonic environments: mid-ocean ridge basalts (MORB), volcanic arc basalts (VAB), ocean island basalts (OIB) and within-plate basalts (WPB). The diagram most effectively discriminate within-plate basalt, known as ocean-island basalt or continental flood basalt (Vermeesch, 2006). The four fields are; Island-arc tholeiites plotting in field A, MORB, island-arc tholeiites and calc-alkaline basalt that all plot in field B, calc-alkaline basalts from volcanic-arc plot in field C, and within-plate basalts plotting in field D (Rollinson, 1993).

A few weaknesses have been notified when using the Ti-Zr-Y diagram. The diagram does identify ocean island basalts (OIB), but cannot separate MORB from island arc basalts (IAB) (Vermeesch, 2006), and anomalous ocean ridge basalt tend to plot as within-plate basalts (Prestvik, 1982). Prestvik (1982) emphasised that great care should be taken when analysing data from altered or metamorphic rocks.

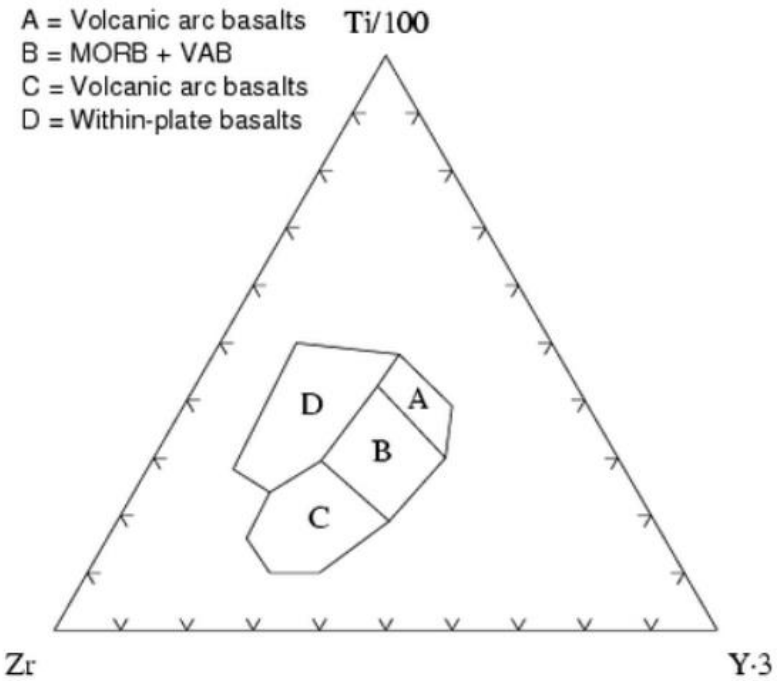

Figure 7 : Ti-Zr-Y diagram constructed by Pearce and Cann (1973) for interpretation of tectonic settings of different basalts.

Zr/Y-Zr diagram (Pearce and Norry, 1979)

The Zr and Y are both high-field strength elements and typically not affected by aqueous fluids or metasomatic alteration. These properties have made the elements suitable in studying metamorphosed and weathered rocks (Pearce and Norry, 1979). The Pearce and Norry (1979) found that the use of Zr/Y ratio plotted against Zr could effectively discriminate between basalts from different tectonic settings (Figure 8). The basalt suites have different Zr/Y ratios, which mainly separate within-plate basalts from other magma types (Pearce and Norry, 1979). The diagram is divided into five fields and the basalts from arcs plot in field A and D, MORB in field B, D and E, and within-plate basalts in field C and E (Rollinson, 1993).

Pearce (1983) also used this diagram to subdivide island-arc basalts into those belonging to oceanic arcs and arcs developed at continental margins. The oceanic-arc basalts plot in the field of island-arc (A, B and D) (Rollinson, 1993) and the continental-arc basalts plot in field C and E, because of the higher values of Zr/Y (Pearce and Norry, 1979). The diagram has been criticized because arc basalt plot in every field (WPB, MORB and calc-alkaline basalt (CAB)) of the diagram (Wang and Glover, 1992).

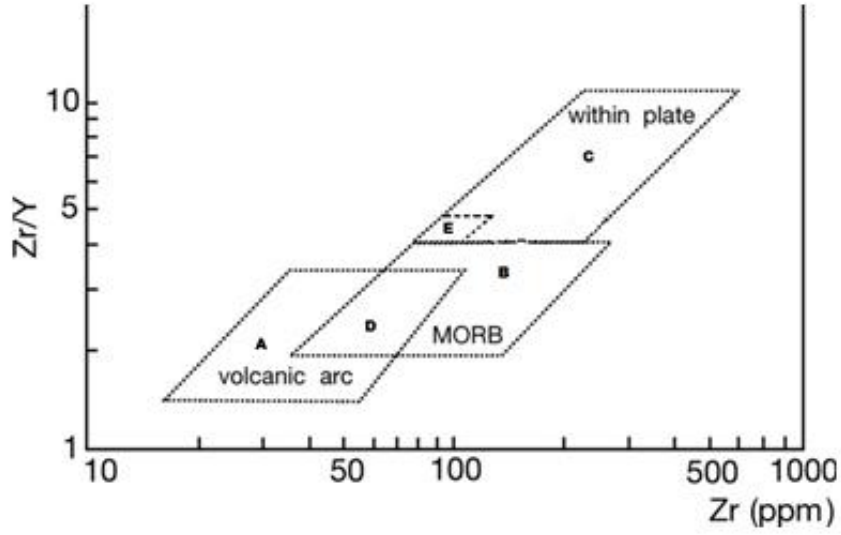

Figure 8: The Zr/Y-Zr diagram by Pearce and Norry (1979). A = volcanic arc basalts B = MORB, C = within-plate basalts, D = MORB and volcanic-arc basalts, E = MORB and within-plate basalt. The scale is logarithmic.

The Zr-Nb-Y diagram (Meschede, 1986)

The triangular discrimination diagram made by Meschede (1986) is based on analysis from 1800 basaltic rocks from different tectonic settings (Meschede, 1986). Meschede used the immobile Nb, Zr, Y elements for discrimination (Figure 9). The diagram separates between two types of MORB, the N-type MORB which is oceanic basalt from mid-ocean ridge environments and E-type MORB which is basalt from plume influenced regions, and generally more enriched in incompatible trace elements. The diagram also separates between within-plate tholeiites and within-plate alkali basalts (Meschede, 1986). Meschede (1986) suggested that Nb could be used to separate different types of ocean-floor basalts, because Nb shows a large spread of concentration between the N-MORB and the E-MORB, which make it a good indicator to the different MORB types. Zr and Y are chosen as elements in this diagram because they show trends of enrichment or depletion which differs from Nb (Meschede, 1986).

The diagram separates into five fields. Within-plate alkali basalts plot in A1, within-plate alkali basalts, and within-plate tholeiites plot in A2, E-type MORB plot in B, within-plate tholeiites plot in C, and N-type MORB plot in field D. Volcanic-arc basalts plot in field C and D, and cannot be further distinguished. It has been pointed out that this diagram has a lot of overlap, and the only certain identified classification is within-plate alkali basalts and E-type MORB (Rollinson, 1993). Wang and Glover (1992) argued that the biggest problem of this diagram was its inability to separate volcanic-arc basalts from N-type MORB or within plate tholeiite.

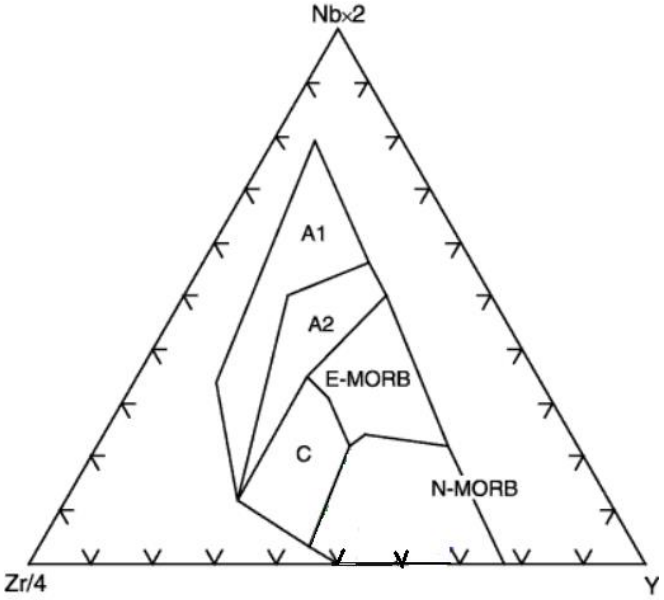

Figure 9: The Zr-Nb-Y discrimination diagram for basalts after Meschede (1986). Following fields are defined as: A1= within-plate alkali basalts, A2 = within-plate alkali basalts and within-plate tholeiites, B= E-type MORB, C= within-plate tholeiites and volcanic arc basalts, D= N-type MORB and volcanic arc basalts.

The La-Y-Nb diagram (Cabanis and Lecolle, 1989)

The triangular diagram made by Cabanis and Lecolle (1989) distinguishes between volcanic basalts, continental basalts and oceanic basalts (Figure 10). This diagram has not been extensively tested, but has the possibility to separate between different MORB types (Rollinson, 1993). The weakness of the element combination is some evidence that La is mobile under hydrothermal conditions (Rollinson, 1993), and may show some distortion relative to La in highly altered or metamorphic rocks (Rollinson, 1993). If the rock is altered or metamorphic, another diagram should be considered. The diagram separates into nine fields. Volcanic-arc basalts plot in field 1, and are subdivided into 1A= calc-alkali basalts, 1C= island-arc tholeiites, and 1B is the overlap between 1A and 1C. Continental basalts plot in 2A and back-arc basin basalts plot in 2B. Oceanic basalts plot in field 3 and are subdivided into 3A= alkali basalts from the Kenya Rift, 3B and 3C= E-type MORB and 3D= N-type MORB.

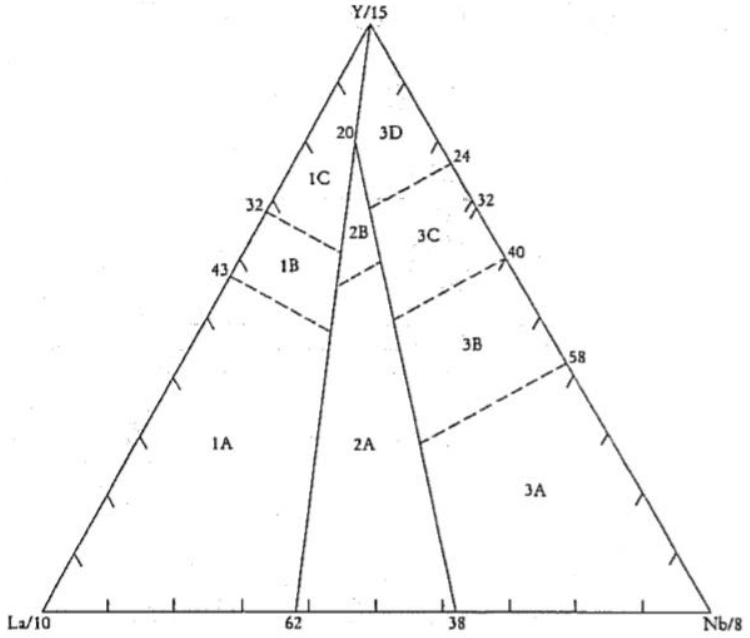

Figure 10: The La-Y-Nb discrimination diagram for basalts after Cabanis and Lecolle (1989). The different fields are defined as: 1= volcanic-arc basalts, and are subdivided into 1A= calc-alkali basalts, 1C= island-arc tholeiites and 1B= overlap between 1A and 1C . Field 2A= continental basalts and 2B= back-arc basin basalts. Field 3= oceanic basalts and is subdivided into 3A= alkali basalts form the Kenya Rift, 3B and 3C= E-type MORB and 3D= N-type MORB. Figure from Rollinson (1993)

The P2O5 – Zr diagram (Floyd and Winchester, 1975)

Floyd and Winchester (1975) made this simple binary plot to allow discrimination between alkalic and tholeiitic magma types (Figure 11). The diagram is based on immobile minor and trace elements to make it usable for analysing altered samples (Floyd and Winchester, 1975). The P_2O_5 content is measured in wt. % and Zr in ppm. The majority of tholeiites have lower values than 0.25 wt.% P_2O_5 and 150 ppm Zr (Floyd and Winchester, 1975). The alkali basalts have higher P_2O_5 than tholeiitic basalts for a given Zr content, and the alkali basalts are more scattered than the tholeiitic basalts (Floyd and Winchester, 1975). A straight line separates the two fields in the binary diagram. The diagram just gives an indication if the sample is alkalic or tholeiitic, because of considerable overlap between the two fields (Rollinson, 1993).

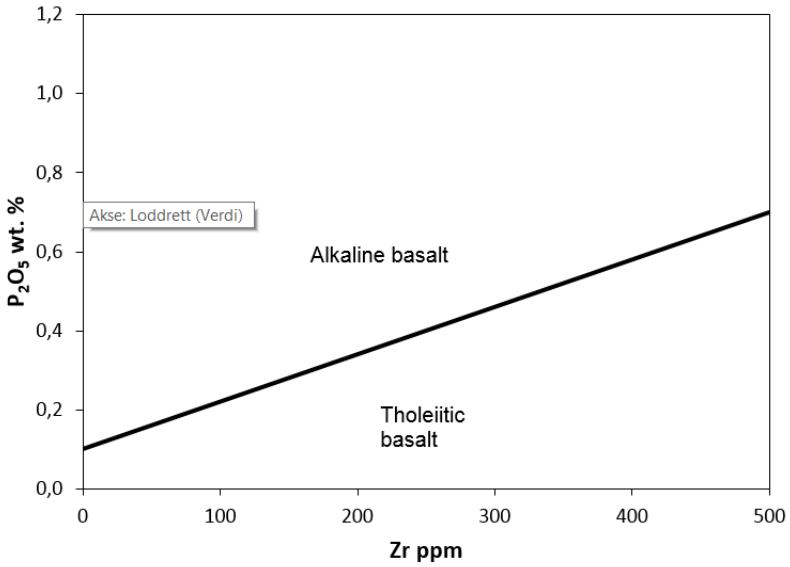

Figure 11: The P_2O_5-Zr discrimination diagram for basalts after Floyd and Winchester (1975) showing the fields of alkali basalts and tholeiitic basalts.

It is important to be aware that the tectonic discrimination diagrams are based on volcanic rocks and the boundarie-lines in these diagrams are mostly drawn by eye (Vermeesch, 2006). A problem with all the diagrams is the overlap between the different fields of tectonic classification (Wang and Glover, 1992), and they seldom provide a clear answer of former tectonic settings and should be used as an indicator and not as a proof. Careful application of these techniques may give useful information not otherwise available (Winter, 2010). "Most of the diagrams require the samples to be extrusive, very slightly altered or unaltered and undifferentiated, primitive basaltic rocks" (Wang and Glover, 1992 p.127).

Hydrothermal alteration and element mobility

Hydrothermal fluids can originate from different sources as seawater, meteoric, connate, juvenile, magmatic or metamorphic water (Pirajno, 2009). Hydrothermal fluids are often defined as hot solutions (~50 to about 500 ^oC), and changes in composition due to chemical reactions as elements dissolves or precipitates in the solution due to changes in temperature, pressure and/or chemical environment (Pirajno, 2009, Putnis and Austrheim, 2010).

Circulation of the hydrothermal fluids or solutions usually affects the rock, which they circulate through, and physio-chemical reaction between the rock and the fluid causes hydrothermal alteration (Pirajno, 2009), where the original minerals are chemically replaced by new minerals, as a result of chemical reactions between the elements in the minerals and the hydrothermal

fluids (Giggenbach, 1984). In contact with aqueous fluids the high field strength (HFS) elements such as Zr, Hf, Nb, Ta, Y, Ti, REE apart from Eu, and possibly La, Th, Ga and Sc, are considered among the most immobile elements (Hastie et al., 2007, Rollinson, 1993). The low field strength (LFS) elements as the Cs, Sr, Rb, Ba, Na and K are considered as mobile (Rollinson, 1993, Pearce, 1983). The transition metals as Co, Ni, V and Cr are also considered to be immobile while Mn, Zn and Cu are mobile (Rollinson, 1993, Pearce, 1983). The main pathways for the hydrothermal fluids commonly occur along fractures, cracks, faults, shear zones and permeable lithologies (Harlov and Austrheim, 2013).

Zircon and U-Pb geochronology

Zircon ($ZrSiO_4$) is a common accessory mineral in sedimentary, igneous and metamorphic rocks and typically ranges in size from about 20 to 200 µm. Larger zircon grains can be up to several centimetre wide (Corfu et al., 2003a). It is a chemically resistant mineral and can survive high temperatures, weathering, transport processes and anatexis (Belousova et al., 2002, Nallusamy, 2014). The resistance and stability of zircon make it retain petrogenetic information, such as protolith characteristics and formation age (Nallusamy, 2014). The U-Th-Pb isotopic dating of zircon has been used for some time to establish rock ages. Zircons can have internal zoning, which is a result of multiple growth events and provide a record of crustal evolution (Hanchar and Rudnick, 1995).

Zircon textures

To observe internal properties in zircon, X-ray or electron scattering techniques must be applied. The best resolution of internal textures is delivered by cathodoluminescence (CL) or backscatter electron (BSE) imaging (Corfu et al., 2003a). Corfu et al. (2003) found that CL images generally are more useful in identifying different growth regions than BSE images. Zircons commonly have elongated prismatic shapes, but the temperature and crystallization rate is believed to reflect the crystal shape (Vavra, 1993, Pupin, 1980). Needle-shaped acicular zircon crystals are believed to result from fast crystallization, and stubby, equant crystals are more common under slow cooling conditions (Corfu et al., 2003a, Belousova et al., 2006). Metamorphically grown or modified zircon crystals are generally subrounded, but euhedral shapes are possible, especially if fluid-rich systems are present (Corfu et al., 2003a).

When zircon crystallization occurs over a substantial time span, individual zircon grains can reflect internal compositional zoning with variation of Zr and Si, but also trace elements as Hf,

P, Y, REE, U and Th (Corfu et al., 2003a, Belousova et al., 2006, Fowler et al., 2002). The chemical variation in the zoned crystals may be a reflection of alternating crystal growth in response to the local environment (Fowler et al., 2002). If the melt, which the zircon crystalizes from, is depleted in Zr, but enriched in Hf, P, Y, REE, U and/or Th, the zircon will change to a composition rich in trace elements and formation of oscillatory growth (Fowler et al., 2002). This is a typical feature of magmatic zircon. The band thicknesses are characterized by μm to mm wide optically and chemically distinct bands parallel to crystal faces (Fowler et al., 2002). The zone composition differs between almost pure zircon and highly enriched in trace elements, and the brighter zones are commonly represented by one or more of the trace elements (Corfu et al., 2003a, Belousova et al., 2006, Fowler et al., 2002). It has also been suggested that oscillatory zoning may be affected by external forces (Hoskin, 2000), which means that the processes occur within the magma system and not at the crystal/melt interface. Hoskin (2000) also presented a model suggesting that oscillatory zoning results from crystal growth velocity, diffusion and cation distribution at the zircon/melt interface.

Detrital zircon

Detrital zircon can be used as a tool for interpretation of source history and provenance of sedimentary systems. Detrital zircon grains do often have a rounded shape, because the zircons have often been through processes of transport and/or weathering.

Analysis of detrital zircons would ideally represent all possible provenances of a sedimentary basin for a complete interpretation of the geological history (Fedo et al., 2003). The various detrital zircon ages present in a sedimentary rock sample generally reflects the ages from the source rock of the sediment (Gehrels et al., 2011). However, many geological factors can affect the detrital zircon age distribution. Sampling of detrital zircon can be quite complex because the detrital zircons may not be representative for the entire set of source rocks for a sedimentary unit (Fedo et al., 2003). Especially ultramafic and mafic rocks may be underrepresented because zircon is not typically found in these rocks (Fedo et al., 2003). Other factors that may affect the age distribution of the detrital zircons are if recycled zircons from older sedimentary units are incorporated during transport, introduction or removal of different sources during sedimentation, and how robust the zircon is from Pb losses (Gehrels et al., 2011), these factors can complicate the interpretation of detrital zircon data.

There is possible to combine a group of samples to characterize a region or terrain, and the robustness of the geological information extracted from the analysed samples depends on the

number of measured zircon grains (Andersen, 2005), their age range, geographic distribution, and the heterogeneity of the detrital zircon distribution (Gehrels et al., 2011). It is estimated that at least 59 randomly selected grains must be analysed to have a 95% confidence detection limit to not miss an age population (Dodson et al., 1988, Fedo et al., 2003). Andersen (2005) recommended at least 35-70 randomly selected grains. To estimate the maximum depositional age of a sedimentary system, the youngest detrital zircon age has often been used, but this has been questioned for both geological and statistical reasons (Andersen, 2005). Usually detrital zircon data are presented in univariate diagrams such as histograms or probability density plots (Andersen, 2005).

Diffusion in zircon

U-Th-Pb isotopic dating of zircon has become an important tool in interpreting crustal events. Trace elements do also tend to incorporate in zircon and are useful as geochemical tracers, such as REE, Y and Hf (Cherniak and Watson, 2001). It is agreement of a slow diffusion rate of Pb, and that it is unlikely that significant amounts of Pb is lost from a crystalline zircon (Cherniak and Watson, 2001, Lee et al., 1997). Water or pressure is not found to have any remarkable effect on diffusion of Pb (Cherniak and Watson, 2001), and most Pb loss in zircon is likely a consequence of recrystallization or Pb transport in zircons with severe radiation damage caused by α-decay (Cherniak and Watson, 2001, Lee et al., 1997). Studies have indicated that lead closure temperatures exceeds 900^{o}C, and that resetting of isotopic age by thermal effects alone is unlikely, or almost unlikely, because extreme conditions as granulite-grade metamorphism and partial melting may affect the isotopic age (Lee et al., 1997).

Diffusion measurements on REEs have also been studied because of several generations of geochemical information stored in a single zircon grain (Cherniak and Watson, 2003). It has been proven a variation in the diffusion rates of the REEs, the heavy REE with smaller ionic radius have a faster diffusion rate than the larger lighter REE (Cherniak et al., 1997, Cherniak and Watson, 2003). A very slow diffusion rate for the REEs was measured by Cherniak et al. (1997), which means that they essentially are immobile under most geological conditions. The closure temperature for the REEs in zircon is estimated to be in excess of 1000^{o}C (Cherniak et al., 1997), which is very high.

Methods

Field work and mapping

Two weeks in the summer of 2013 and three weeks in the summer of 2014 were spent in the field mapping the area of Umbukta, Østre Sauvatnet, Saufjellet and Kallvatnet/Plurdalen. Most of the field area lies above the tree line, and the mapping was performed on outcrops not covered by peat. A white map of the field area with UTM grid was used. The different rock lithologies were given different colours and were drawn in to the map while mapping the field area. Strike and slip were measured on the metasedimentary rocks, using a Silva compass. A handheld lens where used for close up examination of the rock, whenever this was needed.

Sampling

During fieldwork, 76 samples were collected. To document exactly where the rock sample was sampled UTM coordinates were measured with a GPS, and noted. The rock samples were mostly collected in fist sizes, and every sample was given a separate sample bag and marked with a sample number.

To keep track of the collected samples, a sample list was made with sample number, GPS coordinates, rock name and a short sample description. For thin section examination 38 samples were selected. Out of the 38 thin section investigated, 21 detailed descriptions are presented in appendix B, representing 4 gabbros, 2 mafic dyke, 2 garnet-biotite gneisses, 1 garnet-mica schists, 3 garnet two-mica gneisses, 3 contact-zone granitoids, 2 pegmatites, 1 quartzite, 1 two-mica gneiss, 1 granite and 1 chloritised garnet-biotite gneiss. A set of 30 rock samples was analysed for major- and trace element geochemistry. Eleven of the samples were sampled during this fieldwork, 5 samples (4 gabbros and one mafic dyke) were sampled by Ron Boyd (from NGU) during fieldwork in 2008 and 14 samples (5 gabbros, 5 mafic dykes and 4 host rock of garnet-biotite gneiss) were sampled by Trond Slagstad (from NGU) during fieldwork in 2008.

Thin section preparation and microscopy

From different lithologies sampled during fieldwork the thin section laboratory at the Department of Geology and Mineral Resources Engineering at NTNU prepared thin section

with a size of 28x48 mm and thickness of 30 µm, for detailed microscopy examinations. The thin section examinations were performed with polarisation microscopes at NTNU's student laboratory and at NGU's laboratory. At NGU's laboratory the thin section where photographed by a camera mounted on the microscope. Model amount of minerals have been estimated visually, and grain sizes have been measured at NTNU's student laboratory with a measuring tool in the program Espon Perfection V600 Photo Scanner.

Major- and trace element geochemistry

The 30 rock samples were analysed for major- and trace element geochemistry at ALS Global at Piteå in Sweden. The analyses were performed on rock samples from the study area at Umbukta and Østre Sauvatnet. Fifteen of the rock samples were of the Umbukta gabbro, 8 samples of the mafic dykes, 4 sample of the host rock, 2 samples of granite and 1 sample of the contact-zone granitoid. The 13 major oxides where analysed by fused bead, acid digestion and inductively coupled plasma - atomic emission spectroscopy (ICP-AES), and 30 trace elements where analysed by fused bead, acid digestion and inductively coupled plasma–mass spectrometry (ICP-MS). In addition a four acid digestion method was used for the base metals. The descriptions of the methods preformed by ALS Global are based on the descriptions available from ALS Globals website (www.alsglobal.com). The data are presented under Results in the Geochemical analysis section.

Sample preparation, by method PREP-31

Before analysing the rocks samples, they had to be prepared by the method PREP-31, and the forms sent to ALS Global were also marked with method code LOG-22 and PUL-31.

The PREP-31 is the standard sample preparation, which dry, crush, split and pulverize the rock sample. It is important to produce a homogenous analytical sub-sample, which is as representative as possible from the rock sample it was derived from. The sample is logged in a tracking system and a bar code label is attached (method code LOG-22). Then the sample is weighed, dried and crushed to better than 70 % passing a 2 mm (Tyler 9 mesh, US Std. No.10) screen. The sample is finely split up to 250 g and pulverized to better than 85 % passing a 75 micron (Tyler 200 mesh, US Std. No. 200) screen (method code PUL-31).

Whole rock geochemistry, by method ME-ICP06

From a prepared sample 0.200 g was added to lithium metaborate/lithium tetraborate flux (0.90 g), mixed and fused in a furnace at 1000°C. Then the melt was cooled and dissolved in 100 mL solution of 4% nitric acid (HNO_3) and 2% hydrochloric acid (HCl_3). The solution was then analysed by inductively coupled plasma – atomic emission spectroscopy (ICP-AES), and the major elements were reported in weight percentage of the oxide (wt. %).

Trace element geochemistry, by method ME-MS81 and ME-4ACD81

Of the prepared sample 0.200 g was added to lithium metaborate flux (0.90 g), then mixed and fused in a furnace at 1000°C. The melt was then cooled and dissolved in 100 mL solution of 4% nitric acid (HNO_3) and 2% hydrochloric acid (HCl_3). The solution was analysed by inductively coupled plasma – mass spectrometry (ICP-MS), and the results are reported in parts per million (ppm). A four acid digestion were used for base metal analysis (ME-4ACD81).

Methodology for geochronological analysis

Geochronological analysis is a method used for rock age determination. Zircon is a U-Pb bearing mineral and usually suitable for rock dating. The laboratory at NGU has been used for cutting, crushing and splitting samples. In this thesis, four samples were crushed and separated throughout several stages, to single out the zircons from the rest of the rock, for further analysis.

The samples were washed under running water and dried. Then they were crushed using a jawcrusher of the type Fritsch pulverisette 01.703, No. 795, Volt: 380. The crushing was performed two times, to get small enough pieces. After each sample was crushed the jawcrusher was rigorously cleaned. The samples were then split to get representative material for chemical analysis. The rest of the sample was sieved by Endecott sieve shaker for 10 minutes, with 50 rpm. The material was divided into > 250 µm and < 250 µm.

The fine fraction, <250 µm, was further separated on a Wilfley watertable, which uses gravity to separate heavy minerals from lighter ones. A thin film of water moved over the table, with a horizontal asymmetrical movement, back and forth of the table, and the heavy minerals separated from the light minerals. The zircons separate with the heavy minerals due to high specific gravity (4.6 – 4.7 g/cm^3). The lighter minerals moved faster down the board and were first collected in a bowl at the end of the table, the bowl was then switched and the heavier minerals were collected. The samples were dried before further separation.

To remove the most magnetic minerals a vertical Frantz isodynamic magnet-separator (mod. L1) was used. The least magnetic minerals were then separated by heavy liquid (diiodomethane, with a density of 3.3 g/cm^3). The separating process was performed in a separatory funnel. Minerals with lower density than 3.3 g/cm^3 floated to the top and the heavier minerals sank to the bottom.

The heavy minerals separated out by heavy liquids were then sent through a horizontal Frantz magnetic barrier separator (mod. LB-1). For the first round of separation the Frantz was tilted 10^o and the magnet was put on 0.5A. The least magnetic minerals were then separated at 10^o with 1.0A. The next round of separation was at 10^o and 1.5A, and the last round of separation was at 5^o and 1.7A. This process is done to remove impure zircon. As clean zircon as possible is wanted for age dating.

The zircons were picked with tweezers under a binocular microscope, and placed onto a glass plate with a double sided tape. The zircons were mounted in epoxy, polished to approximately half thickness, and cathodoluminescence images (CL) were obtained with a scanning electron microscope (SEM), to reveal internal structures such as growth zoning and core-rim relationships. The SEM used in this thesis was a 1450 Variable Pressure (VP) SEM, manufactured by LEO Electron Microscopy Ltd at the Geological Survey of Norway (NGU), in Trondheim

Zircon age dating was performed at NGU, and conducted with an ELEMENT XR single collector, high resolution ICP-MS, coupled to a UP193-FX 193 nm short-pulse excimer laser ablation system, from New Wave Research. To ablate a small amount of sample, the laser ablation microprobe used a focussed laser beam (Jackson et al., 2004). Using a spot size of 15 µm, a repetition rate of 10 Hz and an energy corresponding to a fluence of 4-5 J/cm^2, the laser was set to ablate single, up to 60 µm long lines. Each analysis included 30 sec of background measurement followed by 30 sec of ablation. For isotopic quantification the ablated material is transported from the sample chamber in a He carrier gas (Jackson et al., 2004) and introduced into the plasma after mixing with Ar gas. The data are acquired in a time-resolved scanning mode for 60 sec, with measurement of the masses ^{202}Hg, ^{204}(Hg + Pb), ^{206}Pb, ^{207}Pb, ^{208}Pb, ^{232}Th and ^{238}U. The interference between ^{204}Pb and ^{204}Hg contained in the Ar gas is corrected by monitoring ^{202}Hg and assuming a ^{204}Hg/^{202}Hg ratio of 0.2293. The ICP-MS was calibrated with measurements of masses 202, 204, 206-208, 232 and 238. For correction of isotopic ratios zircon standard (GJ-1) (Jackson et al., 2004) was used. To check the precision and accuracy 91500 (Wiedenbeck et al., 1995) and an-in house standard (OS-99-14; 1797 ± 3 Ma; (Skår,

2002)) was used. The data were not corrected for common lead, but monitoring of the signal from 204 allowed exclusion of affected data from further calculations. The data were reduced using the GLITTER® software (Van Achterbergh et al., 2001), and the analysed results was plotted and visualized with the Microsoft Excel macro program (Lugwig, 2010).

Results

Geological mapping, field observations and petrography

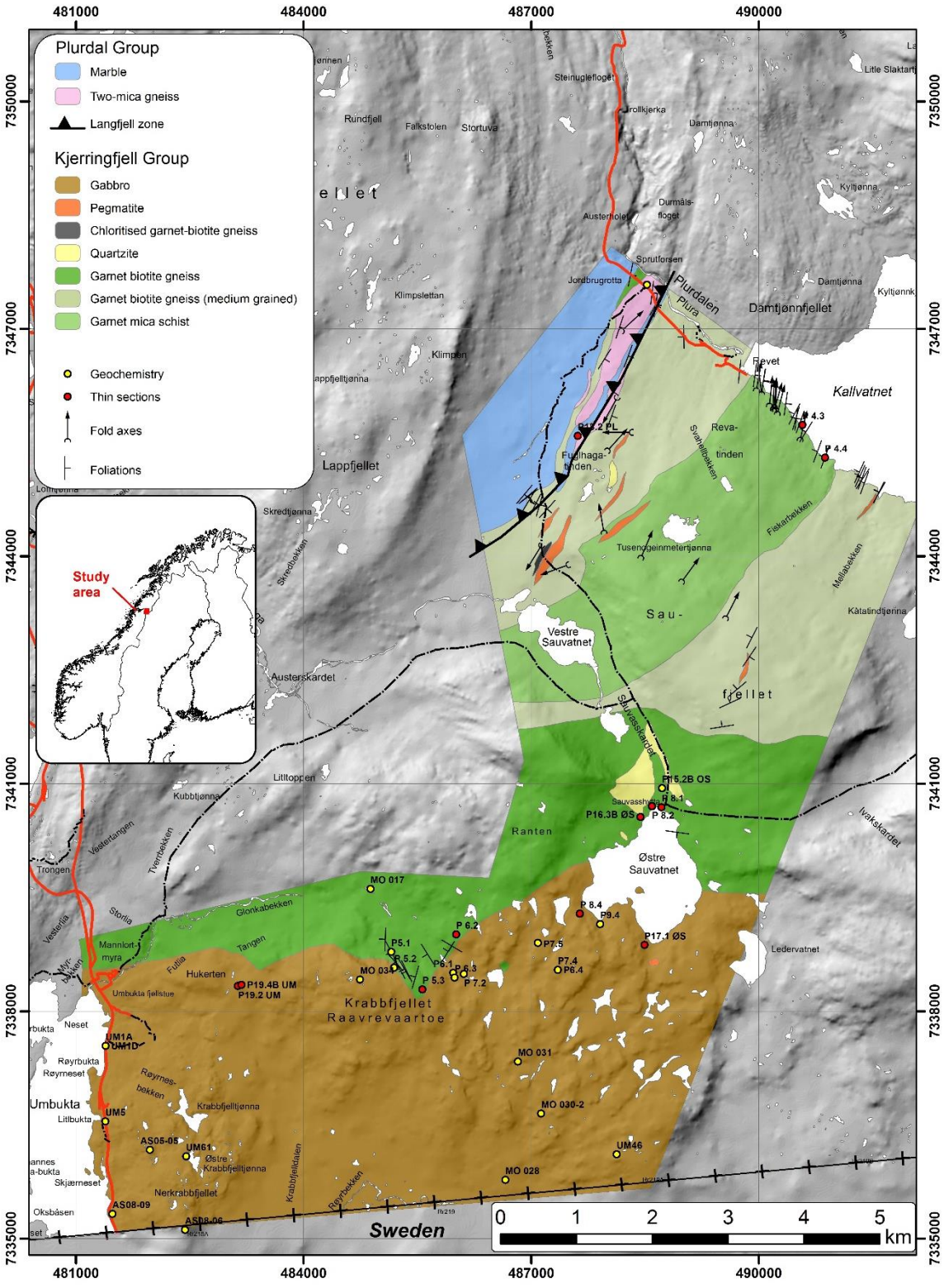

Figure 12: Field map, showing the study area and lithologies mapped during this thesis.

Petrographic descriptions, including mineral assemblages, textures and classification of the rocks are based on field observations and thin section examinations. Modal mineralogy is estimated through thin section examinations.

Kjerringfjell Group, host rock to the Umbukta gabbro

The Kjerringfjell Group consists of garnet-biotite gneiss and can be separated in two different units. The garnet-biotite gneiss at Kallvatnet and Saufjellet, and the garnet-biotite gneiss at Østre Sauvatnet and Umbukta, which is the host rock of the Umbukta gabbro.

The garnet-biotite gneiss at Kallvatnet is medium-grained and lies in contact with garnet-mica schist and they occur in centimetre to meter thick alternating layers. The unit at Kallvatnet also contains layers of garnet amphibolite, pegmatite- and quartz lenses, which is not seen at Østre Sauvatnet and Umbukta. At Østre Sauvatnet and Umbukta the garnet-biotite gneiss is fine-grained and has a more diffuse banding than the garnet-biotite gneiss at Kallvatnet, and it sometimes occurs as garnet-two-mica gneiss. Mafic dykes cutting the garnet-biotite gneiss at Østre Sauvatnet and Umbukta are not seen at Kallvatnet and Saufjellet. Garnet amphibolite and pegmatite lenses are not present in the garnet-biotite gneiss at Østre Sauvatnet and Umbukta. At Kallvatnet and Saufjellet the garnet-mica schist is a bit more dominating rock than the garnet-biotite gneiss, which also distinguishes this unit from the unit at Østre Sauvatnet and Umbukta. The garnet-two-mica gneiss is only present in the garnet-biotite gneiss at Østre Sauvatnet and Umbukta. A clear contact, which separates these two unit has not been mapped during this fieldwork.

Garnet-biotite gneiss and garnet-mica schist at Kallvatnet/Plurdalen and Saufjellet

Kallvatnet/Plurdalen

Kallvatnet is a small lake oriented NW-SE in Plurdalen. The lake is dammed and because of damming and seasonal lowering of the shoreline, the area is perfect for study, with no vegetation covering the rocks. About 2.8 km of exposed rocks were mapped along the lake. The rocks mainly consist of garnet-biotite gneiss and garnet-mica schist. The garnet-biotite gneiss and the garnet-mica schist consist of alternating centimetre to metre thick layers. The garnet-mica schist is often a slightly dominating lithology in this area. The micas in the garnet-mica

schist orients in N-S direction through all of the mapped area at Kallvatnet. The layering of the rocks probably reflect primary bedding, modified by strong deformation, high-grade metamorphism and metamorphic segregation.

Garnet-biotite gneiss*:* The garnet-biotite gneiss is leucocratic, medium-grained and mainly consists of quartz (40-45%), biotite (10-40%), plagioclase (1-25%) and garnet (5-15%). Most samples have accessory minerals of apatite (1-10%), zircon (<1%), epidote (1-2%), muscovite (1%) and chlorite (1%). The rock is heterogeneous and separated in leucocratic and mesocratic millimetre to centimetre thick layers (Figure 13). The mesocratic minerals mainly consist of flaky dark brown biotite, and the leucocratic minerals mainly consist of plagioclase and milky white quartz. Small, red garnet in 0.5 to 2.0 mm size is mostly random distributed throughout the rock, but some samples show a higher concentration of garnet in the biotite rich layers.

In thin section, the garnet-biotite gneiss is fine- to medium grained and characterised by millimetre to centimetre thick layers richer and poorer in garnet and biotite. The rock is relatively quartz rich (Figure 14). The mesocratic layers separates from the leucocratic layers manly by a higher concentration of biotite, but there is also a slightly higher concentration of garnet in the biotite rich layers. The biotite is aligned and defines a foliation in the rock. The layering most likely represents primary bedding, which has been modified by metamorphism. Biotite is brown and lath shaped and shows a slight trend of foliation, and a few grains are altered to chlorite. Garnet is fine- to medium-grained and occurs as euhedral to anhedral crystals, with poikilitic texture and inclusions of quartz, biotite, chlorite and minor titanite. The quartz is fine- to medium grained, have irregular grain-boundaries and undulating extinction. The plagioclase is randomly distributed throughout the rock, fine- to medium grained and has irregular grain-boundaries. A few plagioclase grains show a dusty surface and slight seritization. Accessory phases consist more or less of apatite, zircon, muscovite, epidote (allanite or clinozoisite) and chlorite.

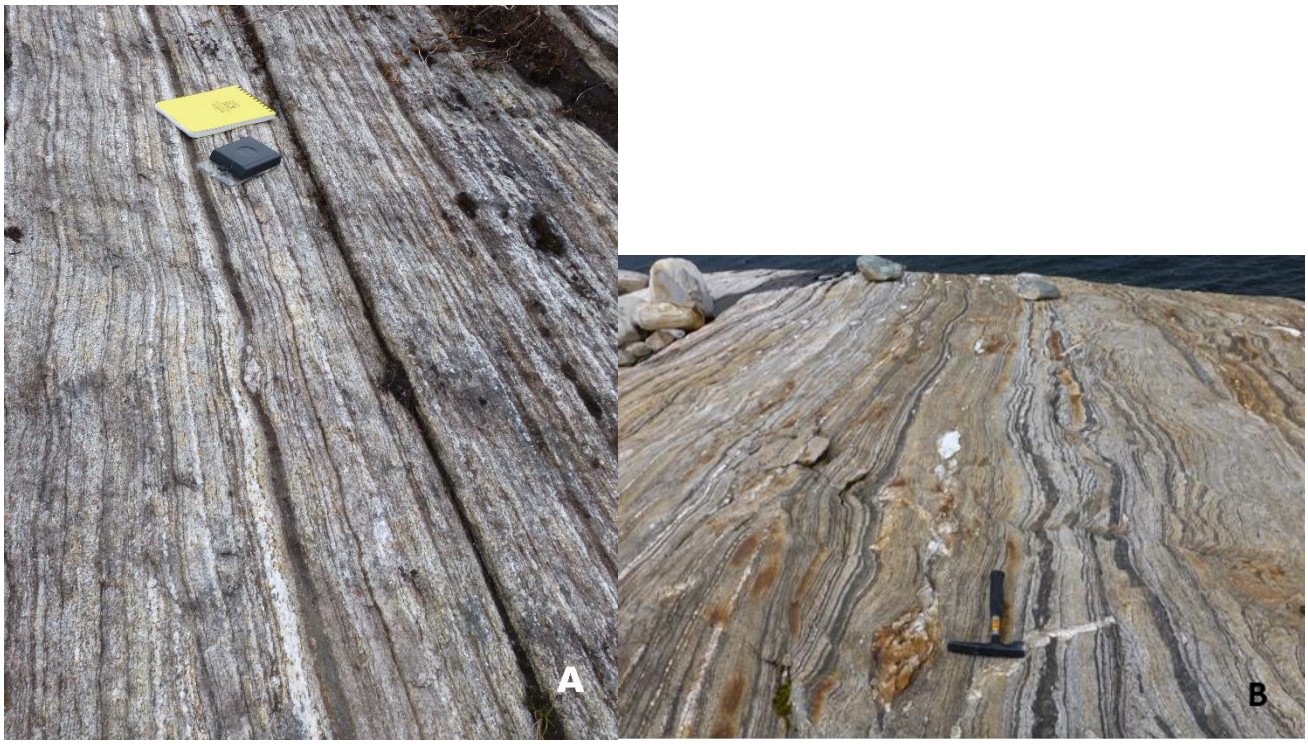

Figure 13: Field photos of the garnet-biotite gneiss at Kallvatnet. Photo A) and B) is from different localities at Kallvatnet. B) GPS: 491326Ø, 7345107N

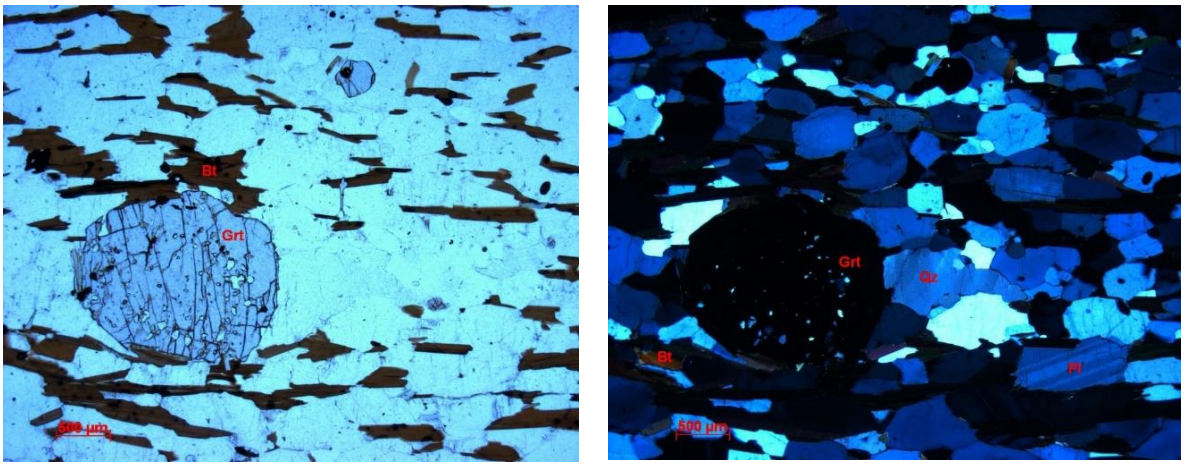

Figure 14: Thin section image of the garnet biotite gneiss. The figure to the left is a plan-polarized photo (ppl), and the figure to the left is cross-polarized photo (xpl) of the garnet-biotite gneiss

Mainly, the garnet-biotite gneiss occurs as alternating layers, but also a more leucocratic garnet-biotite gneiss is present at Kallvatnet, and these layers are folded (Figure 15) and boudinaged. The leucocratic garnet-biotite gneiss contains fine-grained quartz, plagioclase, brown biotite, black amphibole that is acicular, and 1-2 mm sized garnet. The amphibole and garnet are scattered, and the amphibole minerals show a slight N-S orientation (Figure 15).

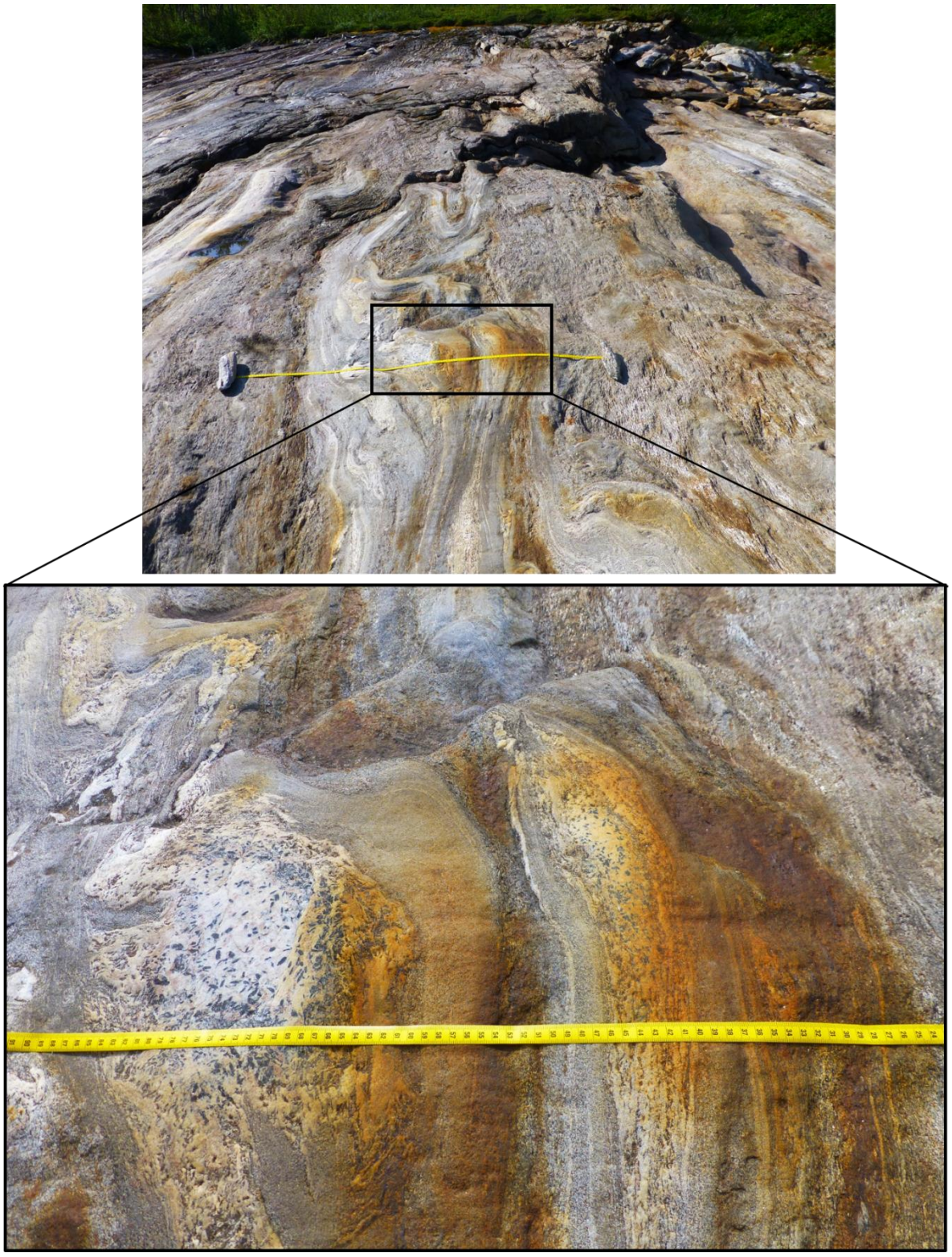

Figure 15: The folded and boudinaged structures of the garnet-biotite gneiss at Kallvatnet. The black grains in the in the white layer of fine-grained quartz and plagioclase, are probably acicular amphibole. (GPS: 490080Ø, 7346240Ø)

Garnet-mica schist: The garnet-mica schist is medium grained, schistose and mica rich (Figure 16). It mainly consists of quartz (40%), muscovite (40%), biotite (10%), garnet (5-10%) and plagioclase (1%), which is an accessory mineral in this rock. The mica grains are aligned and show crenulation folding and the quartz grains are distributed in-between the micas. The garnet is red and occurs in size of 1-2 mm.

Figure 16: Field photos of the garnet-mica schist. Left photo show close-up image of the garnet-mica schist. (GPS: 490866Ø, 7345405N)

In thin section, the muscovite is characterised by kink-banding, and folds around the garnet grains. The garnet is almost euhedral and has a poikilitic texture with inclusions of quartz. The biotite lies in-between the muscovite grains (Figure 17), some biotite grains show pleochroic halos and one grain is chloritized. The quartz grains are fine- to medium grained, have anhedral shape, irregular grain boundaries and undulating extinction.

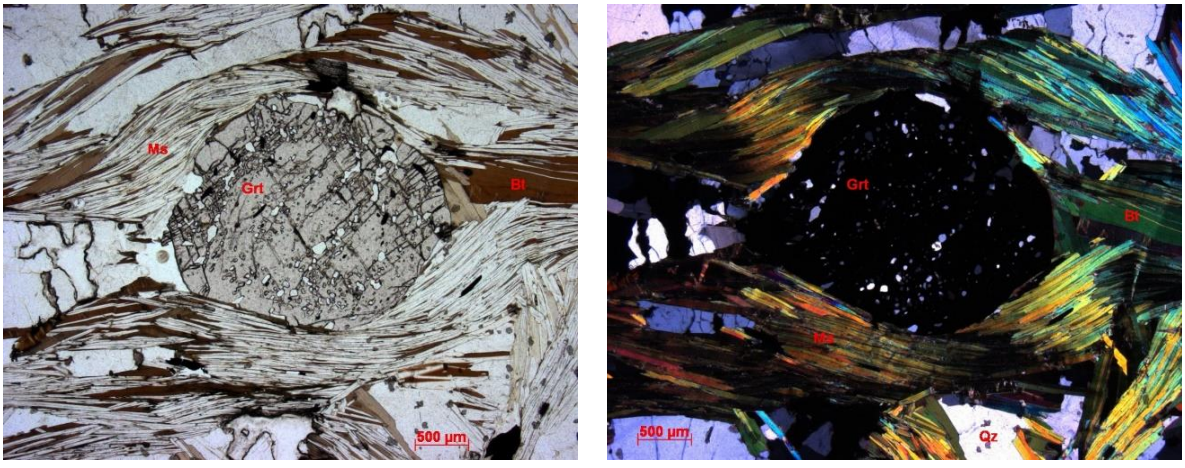

Figure 17: Thin section image of garnet-mica schist, ppl photo to the left and xpl photo to the right

The garnet-mica schist composes more mica, especially muscovite, than the garnet-biotite gneiss, and it has a schistose texture that the garnet-biotite gneiss does not contain. The garnet-biotite gneiss composes more quartz and feldspar and lesser amounts of biotite than the garnet-mica schist. The garnet-biotite gneiss locally sticks out relative to the garnet-mica schist, because of more resistant minerals in the rock.

The unit along Kallvatnet mainly consists of alternating layers of garnet-biotite gneiss and garnet-mica schist, but it also composes layers of garnet amphibolite and veins and lenses of pegmatite and quartz.

Garnet amphibolite: Garnet amphibolite is present in centimetre to metre thick layers. They orient in the same direction as the rest of the rock unit and occur randomly throughout the mapped area. The garnet amphibolites conmposes of fine-grained black amphibole and coarse-grained garnet in sizes from 1 to 8 mm. A few 1 mm thick quartz veins also appear in the garnet amphibolite (Figure 18).

Figure 18: A layer of garnet amphibolite in the garnet-biotite gneiss at Kallvatnet. (GPS: 489979Ø, 7346380N)

Pegmatite: The pegmatite is present in the garnet-biotite gneiss and the garnet-mica schist. The pegmatite is leucocratic, mainly coarse-grained, but a few sample are medium-grained (Figure 19), and mainly consists of plagioclase (50-60%), quartz (25-40%), muscovite (5-15%). Some samples have accessory minerals of chlorite (2-5%), biotite (1%), titanite (<1%) and epidote (clinozoisite) (<1 %). In the coarse-grained pegmatite, twinning in plagioclase crystals is

visible. The pegmatite contains scattered silver- coloured muscovite flakes, and some pegmatites contains biotite where some of the biotite grains show a greenish colour.

Figure 19: Coarse grained pegmatite with silver coloured mica grains in figure A, and medium grained pegmatite in figure B.

In thin section, the plagioclase grains have a dusty appearance, and some grains show seritization and have a poikilitic texture with inclusions of quartz and muscovite. Some samples have inclusions of chlorite and biotite. The plagioclase grains are anhedral and the boundaries are irregular. Quartz grains are anhedral and occur both interstitially and as inclusions. The quartz has undulating extinction, mostly irregular grain boundaries and a few coarser grains show triple junctions. Muscovite mostly occurs as medium- to coarse-grained crystals with lath shapes, and interstitial between the plagioclase grains, and as secondary formed fine-grained crystals inside the plagioclase. A few muscovite grains are also present with an undeveloped crystal shape, probably secondary formed, with a medium-grained skeletal texture. The muscovite, with undeveloped crystal shape, always occurs inside a plagioclase grain and they do show the same crystal orientation (Figure 20). When biotite occurs in a sample, it is medium grained and lath shaped. The biotite appears both interstitial and as inclusions in the plagioclase. Most biotite grains are altered to chlorite (Figure 21).

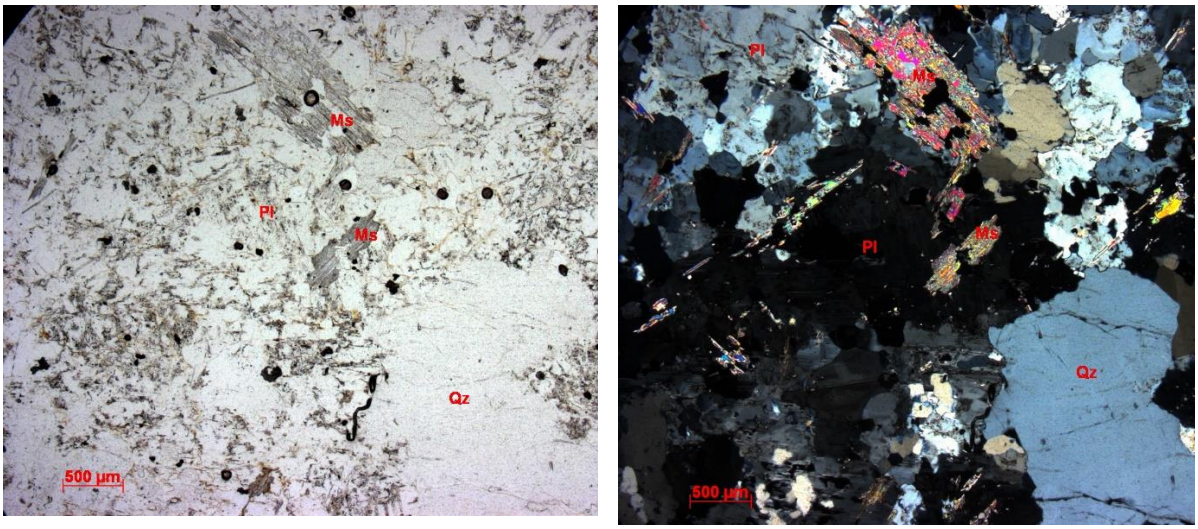

Figure 20: Thin section image of the medium-grained pegmatite. Left photo ppl, and right photo xpl

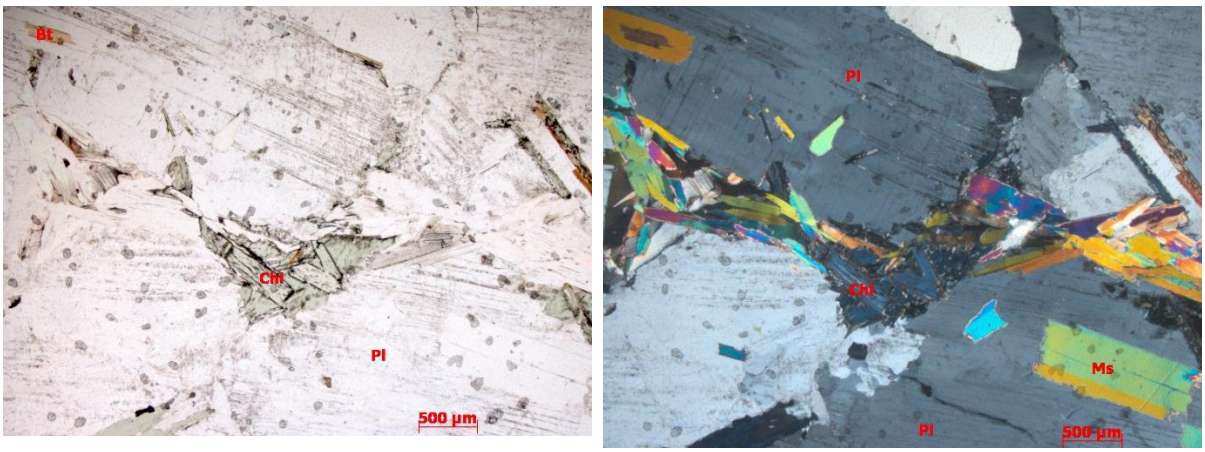

Figure 21: Thin section images of the coarse-grained pegmatite. Left photos ppl, and right photos xpl.

Pegmatite present as centimetre thick veins and centimetre sized boudinaged lenses do not cut the gneissose structure (Figure 22A) in the rock unit at Kallvatnet. The small pegmatitic veins and boudinaged lenses both orient in the same direction as the layering of the unit. Pegmatite is also present in large meter sized lenses. They often occur in clusters of several lenses. These large lenses cut through the foliation of the garnet-biotite gneiss and the garnet-mica schist (Figure 22B).

Figure 22: A) A centimetre thick pegmatite vein in a garnet-mica schist. (GPS: 489979 7346380N) B) Metre sized pegmatite lenses in garnet-biotite gneiss (GPS: 490866Ø, 7345306N). Figure A and B is from the rock unit at Kallvatnet.

Quartz veins and lenses: Only a few, meter-sized quartz lenses are present in the unit at Kallvatnet. The quartz is somewhat impure, and contains a few muscovite grains. The quartz lenses cut the structures of the garnet-biotite gneiss and the garnet-mica schist.

Structures: The rocks at Kallvatnet are folded (Figure 23 A and B). There are crenulation folding in the garnet-mica schist, and z-folds orienting to the east, are registered in thin pegmatite veins. Garnet amphibolite and pegmatite show boudinaged structures (Figure C and D), and the large meter sized pegmatites cut the layering of the garnet-biotite gneiss and garnet-mica schist (Figure E).

Figure 23: A) and B) show field photos of folding rocks, C) and D) show photos of boudinaged structures, E) show a close-up photo of the pegmatite cutting the garnet-biotite gneiss. All photos is from localities at Kallvatnet. (A) GPS: 490287Ø, 7346066N, C) GPS: 490305Ø, 7346063N, D) GPS: 490054Ø, 7346299N, E) GPS: 491581Ø, 7344841N)

Plurdalen and Saufjellet

From Kallvatnet to Saufjellet mapping was carried out from the path in Plurdalen and southeasttward to Saufjellet. Along the path at Plurdalen a small part of the Langfjell zone and some of the marble belonging to the Plura Group was mapped. The Langfjell zone is a thrust front west of the mapped area for this thesis, and the Plura Group is interpreted to be a stratigraphically higher unit than the Kjerringfjell Group. On the path, mostly garnet-biotite gneiss and garnet-mica schist as described at Kallvatnet is occuring, together with two-mica gneiss. In field, the two-mica gneiss looks quite similar to the garnet-biotite gneiss, but there is no presence of garnet and a lesser amount of biotite, which make the two-mica gneiss a bit more leucocratic then the garnet-biotite gneiss. In this area there occur a few lenses with chloritised garnet-biotite gneiss. The chloritised garnet-biotite gneiss appear as meter sized mesocratic lenses and has mostly a width between 5 and 10 meters, and orients in the same direction as the rock unit. In the west the garnet-biotite gneiss and the garnet-mica schist lie in contact with the marbles of the Plurdal Group. The marble is coarse-grained and white.

Two-mica gneiss*:* The two-mica gneiss is leucocratic has a gneissose texture and mostly contains fine- to medium-grained K-feldspar (30%), muscovite (30%), quartz (20%), biotite (10%) and plagioclase (5-10%). The rock is heterogenic and separates into millimetre to centimetre thick layers, which is more or less rich in micas. The mica-rich layers are a bit darker in colour than the mica-poor layers, probably because of a slightly higher concentration of biotite. The micas occur as aligned minerals in the rock. The mica-poor layers have a light, very slight pinkish colour and mainly consist of K-feldspar, quartz and plagioclase, and a few mica grains are present in these layers as well.

In thin section, the two-mica gneiss is characterised by clear orientation of the micas. Muscovite is aligned and defines a foliation in the rock, some places accompanied by greenish-brown biotite. The rock is relatively muscovite rich. K-feldspar, plagioclase and especially the quartz show undulating extinction, and some quartz grains also show ribbon-like extinction, which indicates that the rock has been through deformational processes. The feldspars and the quartz have subhedral grain shape and irregular grain boundaries (Figure 24).

In field, the two-mica gneiss is sometimes difficult to separate from the garnet-biotite gneiss, because they often look quite similar on a distance, and closer examination is needed to separate one lithology form the other. The easiest way to separate between the two rocks is to look for garnet, because garnet only occurs in the garnet-biotite gneiss.

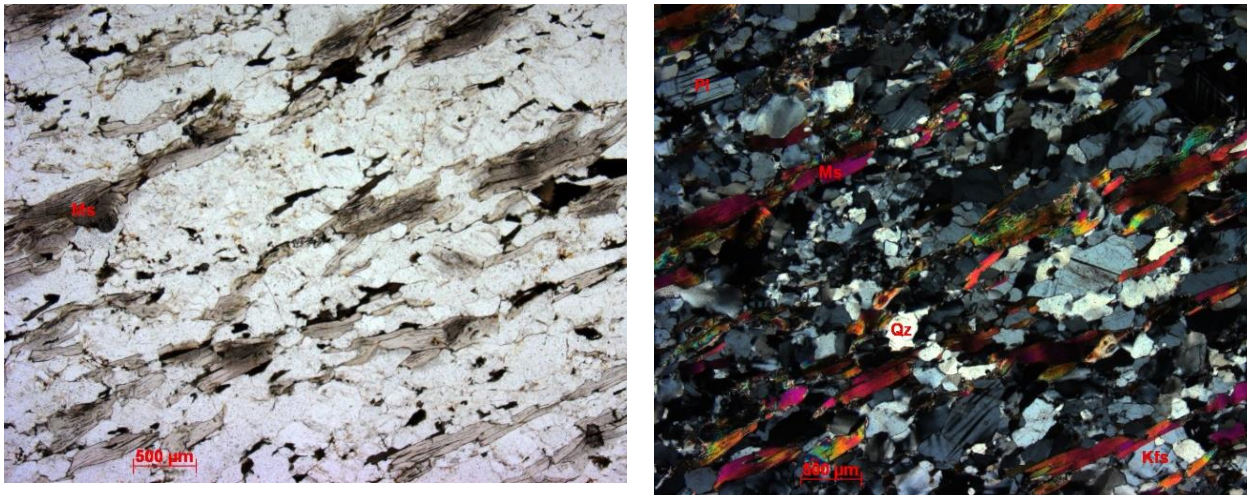

Figure 24: Thin section images of two-mica gneiss. Ppl photo to the left and cpl photo to the left.

The rocks at Saufjellet (Figure 12) are the same as mapped at Kallvatnet. The rocks mainly composes of medium-grained garnet-biotite gneiss and garnet-mica schist, but there also occur quartz- and pegmatite lenses, and layers of garnet amphibolite. Close to the Fuglhagatinden (Figure 12), is an area, kind of a broad belt, with a lot of pegmatite- and some quartz lenses, cutting the structures of garnet-biotite gneiss and garnet-mica schist. The lenses are oriented in a NE-SW direction (Figure 25).

Figure 25: The white pegmatite and quartzite lenses clearly emerge in the landscape. They have a NE-SW orientation.

Chloritised garnet-biotite gneiss:The chloritised garnet-biotite gneiss has a gneissose texture and mostly contains fine-grained quartz (20-25 %), plagioclase (20-25 %), biotite (5-10 %), chlorite (20-25 %), garnet (5 %), epidote + clinozoisite (5 %), calcite (5 %), and accessory

minerals of titanite (1 %) and apatite (1 %). The chloritised garnet-biotite gneiss is mesocratic, and separates into very fine-grained dark layers, and fine-grained lighter layers. The dark and lighter layers vary from millimetre to centimetre thicknesses. The dark layers mainly consist of chlorite and biotite, and the lighter layers mainly composes quartz, plagioclase and biotite. Garnet occurs in both layers in 0.5 to 1.0 cm sizes, and has largest concentration in the lighter layers, showing a brown-red colour.

In thin section, the chloritised garnet-biotite gneiss is mostly fine-grained and characterised by relatively aligned layers of biotite and chlorite. The biotite is fine-grained, mainly lath shaped and has a brown colour, and most of the biotite grains are altered to chlorite (Figure 26). The chlorite has a light green colour. The quartz is mostly fine-grained, have irregular grain-boundaries and show undulating extinction. The plagioclase is fine-grained and most of the plagioclase is partly seritizated. The calcite is fine-grained and mostly randomly distributed in the rock. The garnet and the epidote + clinozoisite occur mostly in the layering where the biotite is least altered to chlorite (Figure 27). The garnet is medium-grained, subhedral and has a poikilitic texture. The epidote + clinozoisite are fine- to medium grained, subhedral and some grains show poikilitic texture. Accessory phases are mostly titanite and apatite.

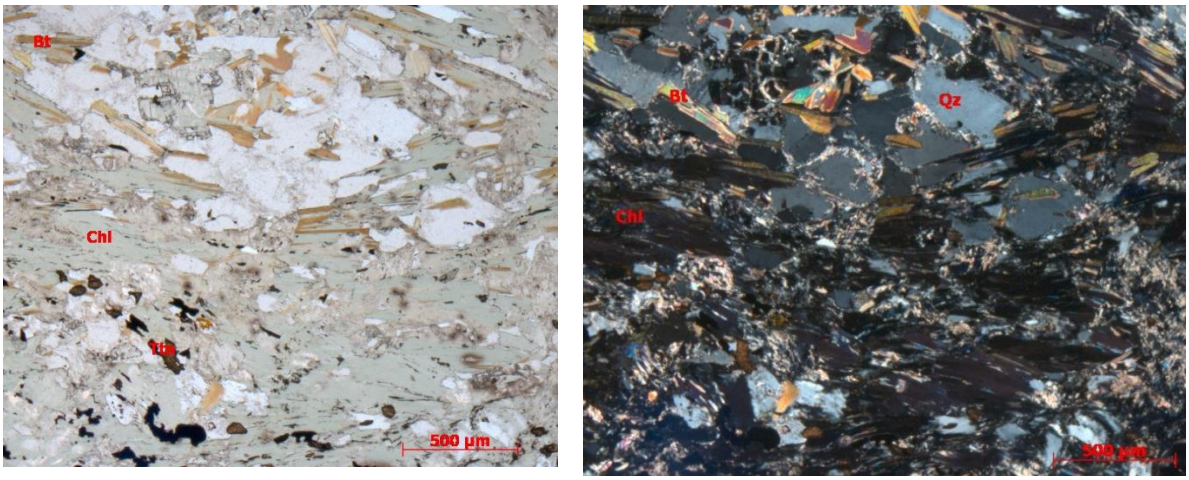

Figure 26: Thin section image of the chloritised garnet-biotite gneiss. Left photo in ppl, showing light green chlorite and brown biotite, right photo in xpl.

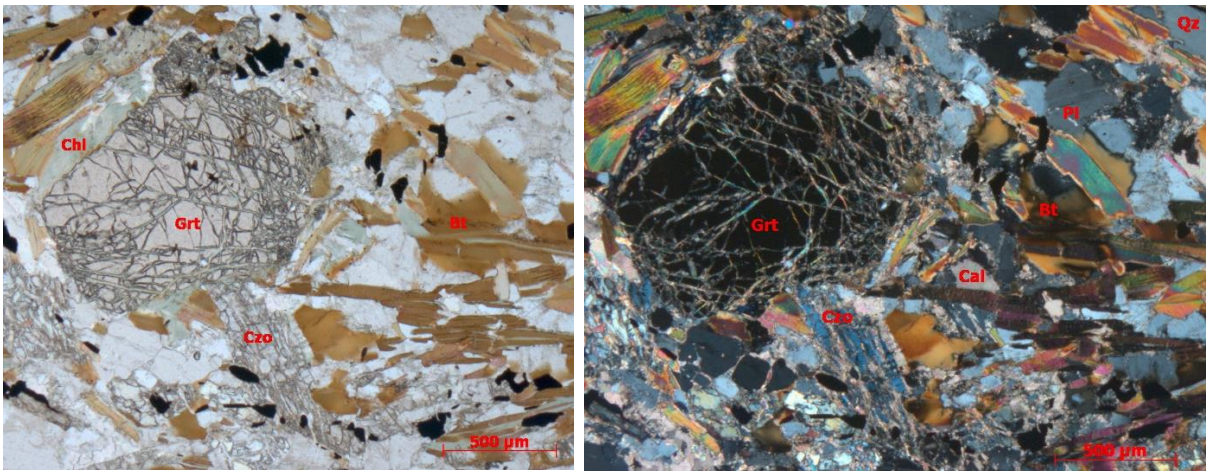

Figure 27: Thin section image of the chloritised garnet-biotite gneiss. Left photo in ppl and right photo in xpl.

Garnet-biotite gneiss and garnet-two-mica gneiss at Østre Sauvatnet and Umbukta

Østre Sauvatnet is a small lake southwest of Saufjellet, and is the location of the contact-zone between the gabbro and garnet-biotite gneiss. This area is characterised by intrusion of mafic-dyke and enclaves, granitic veins, ductile structures and impure quartzites.

After thin section examination, the garnet-biotite gneiss was separated into garnet-biotite gneiss and garnet-two-mica gneiss. These rocks look quite similar in the field, but the garnet-two-mica gneiss composes a larger amount of muscovite, and an overall larger amount of mica than the garnet-biotite gneiss. Since the garnet-biotite gneiss and the garnet-two-mica gneiss were not separated during fieldwork, they were both mapped as garnet-biotite gneiss.

Garnet-biotite gneiss: the garnet-biotite gneiss is fine-grained, heterogeneous and displays light and dark diffuse layers (Figure 28). The layer thickness of the leucocratic and the mesocratic layers varies from millimetre to centimetre sizes. The rock composes fine-grained garnet mainly concentrated in the mesocratic layers. The garnet-biotite gneiss mainly consists of quartz (45%), biotite (40%), garnet (5-10%) and accessory minerals of plagioclase (1%), muscovite (<1%), clinozoisite (1-2%) and chlorite (1%).

Figure 28: Hand specimen of the garnet biotite gneiss at Østre Sauvatnet and Umbukta.

In thin section, the garnet-biotite gneiss is characterised by millimetre to centimetre thick layers richer and poorer in biotite (Figure 29). The biotite is aligned and occur as relatively small subhedral flakes, and defines a nearly continuous foliation in the rock. Biotite also shows pleochroic haloes. Garnet is mostly found in the biotite-rich layers as clusters of small anhedral grains. In the biotite-poorer layers, anhedral quartz is the dominant mineral, and the alignment of the biotite grains is not as clear. The thin-section contains sparse chloritized biotite grains.

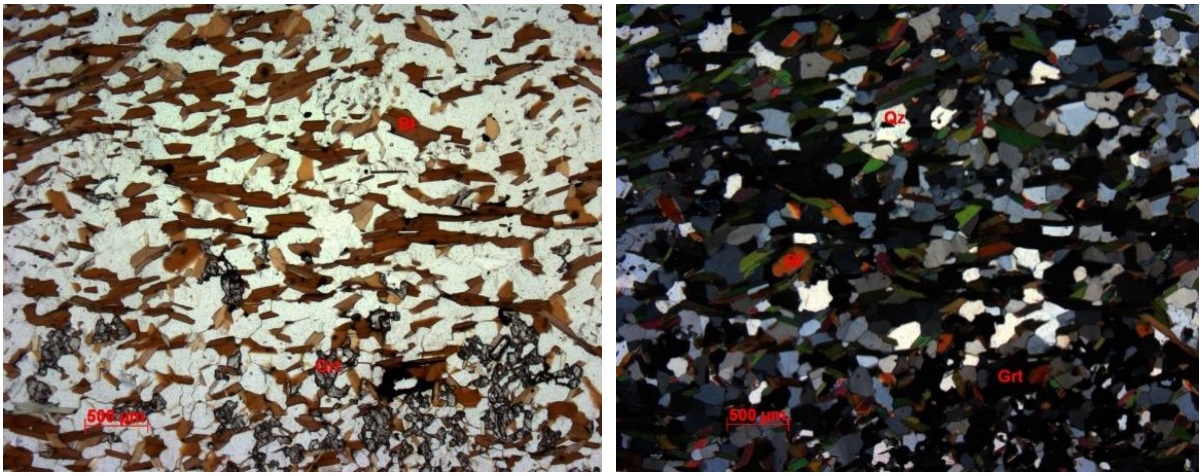

Figure 29: Thin section image of the garnet-biotite gneiss. Left photo in ppl, and right photo in xpl.

Garnet-two-mica gneiss*:* The rock is fine-grained, leucocratic and composes of 0.5-2.0 mm diffuse layers of light or dark minerals (Figure 30). The garnet-two mica gneiss mainly composes quartz (35-40%), muscovite (20-30%), biotite (10-30%), garnet (5-10%), plagioclase (1-5%) and apatite (1%) as an accessory mineral. The light layers are a bit thicker than the darker layers. The darker layers separate from the lighter layers with a higher concentration of biotite. The texture is gneissose and the rock has garnet in sizes from 0.2 to 1.5 cm.

Figure 30: Field photo of the garnet-two mica gneiss at Kallvatnet

In thin section, the garnet-two-mica gneiss shows separation of thin layers richer and poorer in garnet and mica. The mica is aligned and the biotite has a light brown color and is flaky to lath shaped. The muscovite is a bit coarser than the biotite and is lath shaped. The mica concentrates

in millimetre thick foliae and bends around the garnet (Figure 31). The garnet grains are fine- to medium-grained and subhedral. One sample contains some coarser grains of quartz and plagioclase, these few coarser plagioclase grains show seritization, and both the plagioclase and quartz grains have irregular grain-boundaries. One of the examined thin sections does not show as clear alignment of the micas as the other thin sections of the garnet-two-mica gneiss..

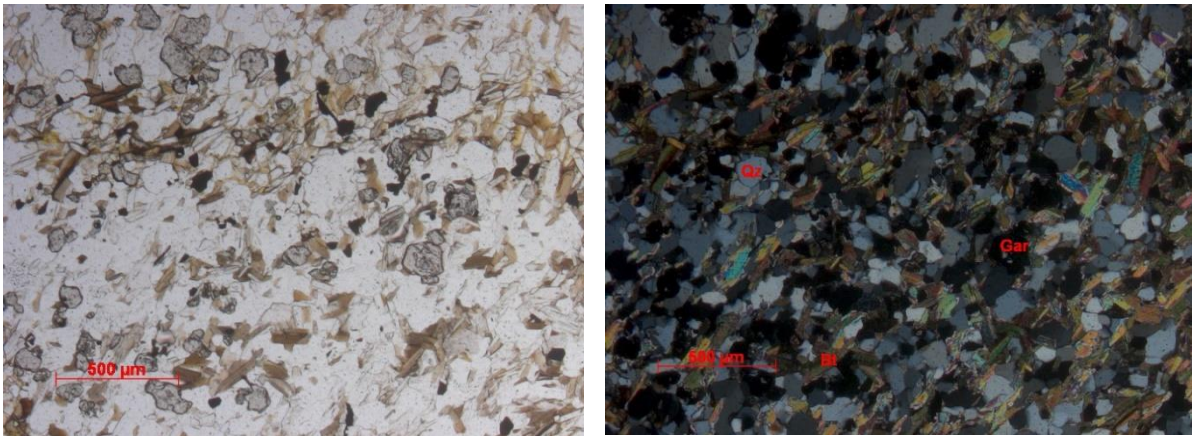

Figure 31: Thin section image of the garnet-two mica gneiss. Left photo in ppl, and right photo in xpl.

Gabbro and mafic dykes at Umbukta and Østre Sauvatnet

Gabbro

Two types of gabbro have been identified at Umbukta, olivine gabbro and hornblende gabbro. They are fine- to coarse-grained, but most examined samples are medium-grained (1-2 mm). The gabbro is locally homogenous, but regionally heterogeneous. Some rock samples show deformation and other samples do not.

Hornblende gabbro*:* the hornblende gabbro mainly composes of plagioclase (20-40%), pyroxene (15-40%), amphibole (5-45%) and biotite (<1-20%). Some hornblende gabbro also contains garnet (5%). Most samples have accessory minerals of apatite (1%) and opaques (1-5%). The hornblende gabbro is mesocratic with scattered minerals of plagioclase and hornblende. Textural variations are mapped inside the gabbro. Typically, the hornblende gabbro is medium-grained, homogeneous and has an almost even distribution of scattered plagioclase and dark minerals of hornblende and some pyroxene, with no sign of deformational structures. Samples showing deformational structures are also seen, as shown in the outcrop in Figure 32, which is a medium-grained hornblende gabbro showing irregularly banded texture. Plagioclase and hornblende are segregated into irregular foliations of 1-5 mm thicknesses, looking almost like black and white tiger stripes.

Figure 32: Field photo of hornblende gabbro showing deformational texture looking like black and white tiger stripes. (GPS: 483025Ø, 7338181N)

The hornblende gabbro typically have preserved primary igneous textures. The hornblende gabbro has plagioclase and pyroxene occurring in ophitic to sub-ophitic texture. Pyroxene is subhedral- to anhedral and many of the pyroxene grains have an altered margin of green amphibole interpreted to be hornblende (Figure 33 A and B). Some thin sections show complete alteration of pyroxene to zoned amphibole with an outer margin of green-brown hornblende and a pale green interior, which is interpreted to be actinolite (Figure 33 C and D). In coarse-grained hornblende gabbro, the amphibole grains have a poikilitic texture with many small inclusions of what probably is quartz, which may result from excess silica in the alteration from pyroxene to amphibole. Plagioclase is euhedral to subhedral and lath shaped with irregular grain boundaries, which indicates a magmatic origin. Biotite does not show any orientation and occurs as anhedral flakes and subhedral elongated grains, with either dark brown or green colour. Some grains show pleochroic halos that probably result from inclusion of small zircons. A few grains in a few thin-sections show chloritization of the biotite. Samples containing garnet show coarse-grained garnet with a scattered distribution.

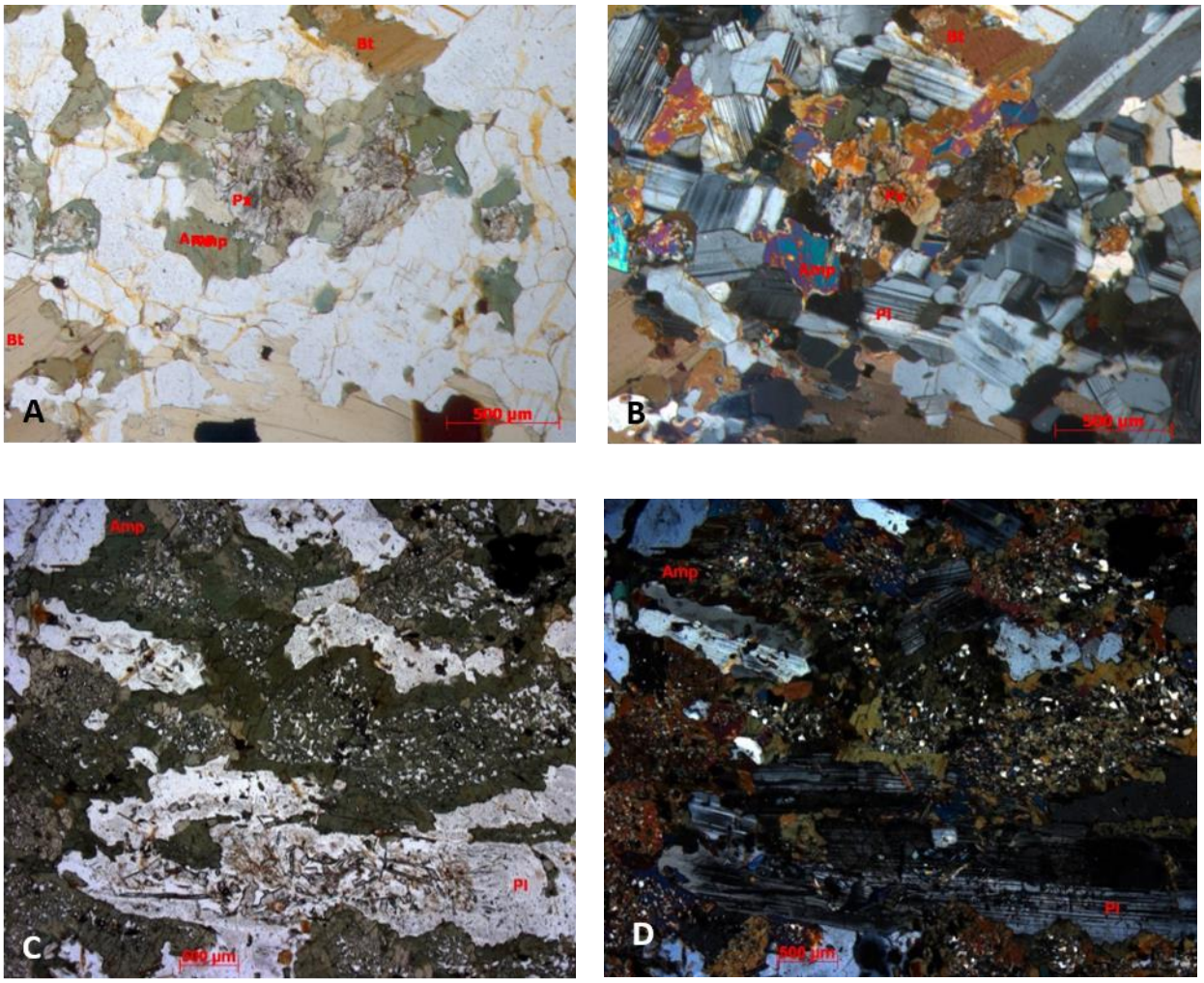

Figure 33: Thin section image of the hornblende gabbro. Photo A) show the pyroxene precursor with a green altered margin of hornblende in ppl, photo B) is the same photo in xpl. The thin section image in C) show complete alteration to amphibole, the rim probably represent hornblende and the core is probably of actinolite (ppl), and D) is the same photo in xpl.

Outcrops showing different textures and grain sizes occur near each other. Just a few meters from the medium-grained, irregularly foliated gabbro is an outcrop of coarse-grained gabbro containing 0.7-1.0 cm sized garnet. A fine-grained mafic dyke and a leucocratic pegmatite cut through the gabbro. The dyke is mesocratic but it contains a few small, scattered plagioclase crystals. The coarse-grained pegmatite composes mainly of plagioclase and a few quartz grains (Figure 34 A). There is no sign of mineral orientation in the gabbro, just close to the contact with the pegmatite the gabbro becomes more fine-grained, and segregates into a gneissose texture of light and dark minerals, and this structure has a width of 40-50 cm and is almost a bit schistose (Figure 34B)

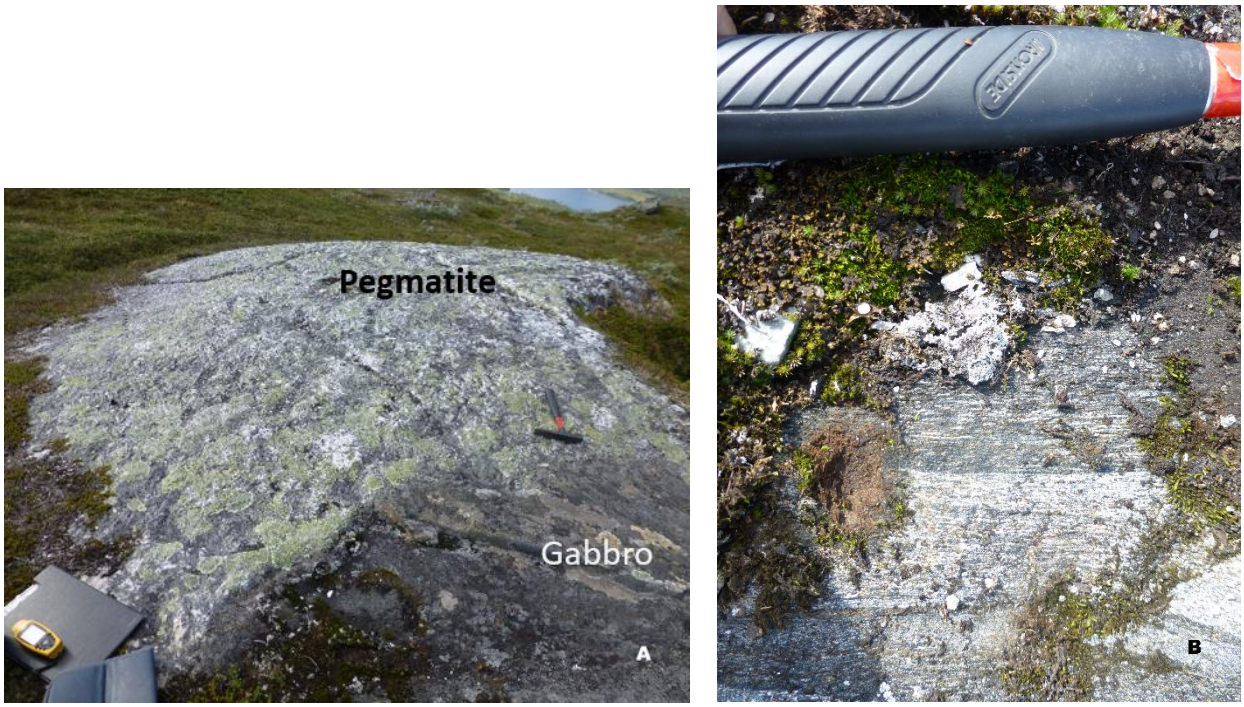

Figure 34: Photo A) show the pegmatite in contact with the gabbro. Photo B) show a close-up photo of the gneissose texture of the gabbro in contact with the pegmatite.(GPS: 483019Ø, 7338121N)

Outcrops of fine-grained hornblende gabbro are seen in contact with coarse-grained hornblende gabbro. The coarse-grained hornblende gabbro is mesocratic with an almost even distribution of white plagioclase and dark minerals of hornblende and maybe some pyroxene. The plagioclase grains occur as ca. 1.0 cm phenocrysts scattered between the dark finer-grained minerals, and twinning is visible in the phenocrysts. In contact with this coarse-grained hornblende gabbro is a fine-grained homogenous hornblende gabbro, which is massive with equal distribution of white and dark minerals. The rock is quite covered by peat, but some of the less covered parts of the outcrop show indications of that the coarse-grained gabbro may appear as lenses in the finer grained hornblende gabbro. In a few parts of the rock, there can be seen red garnet crystals in sizes from 0.5 to 1.0 cm.

Olivine gabbro*:* the olivine gabbro is mesocratic with light green and dark minerals. It is homogenous and medium-grained, and the olivine gabbro composes olivine (30-40%), pyroxene (30-40%), plagioclase (20-25%), amphibole (5-10%) and opaques (5%). The rock has a characteristic reddish, rusty surface that stands out in the field (Figure 36B), while the hornblende gabbro shows a greyish surface.

The olivine gabbro has olivine crystals surrounded by corona texture (Figure 35) The corona texture most likely consists of orthopyroxene, and probably results from fluid interaction and

reaction between olivine, plagioclase and a fluid phase. Clinopyroxene has a poikilitic texture with inclusion of olivine and opaques. The plagioclase is anhedral, occurs interstitially, and is probably one of the last crystallizing minerals, except from a later formation of the corona texture. The anhedral shape of the plagioclase can also result from reaction between the olivine, plagioclase and a hydrous phase in the formation of the corona texture.

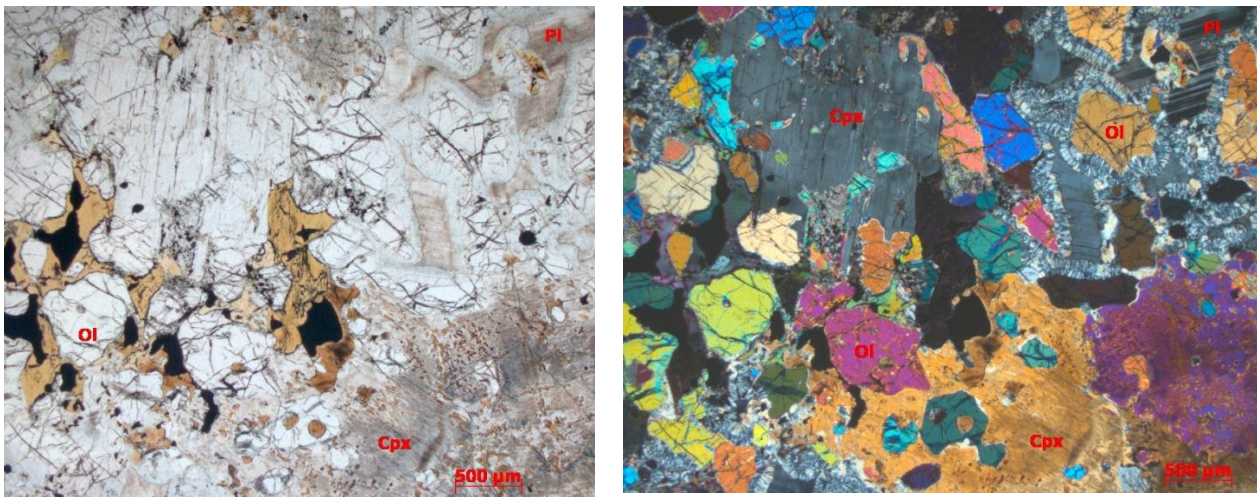

Figure 35: Thin section image of the olivine gabbro. Left photo in ppl, and right photo in xpl.

Olivine gabbro and hornblende gabbro are seen in contact with each other (Figure 36A). The outcrop in Figure 36A shows the reddish, rusty olivine gabbro in contact with a greyish hornblende gabbro. The greyish hornblende gabbro has a fine-grained matrix with both light and dark minerals, which makes up most of the rock. It also contains some randomly distributed medium- to coarse-grained white and black phenocrysts, in 2.0 – 8.0 mm sizes. The phenocrysts have mostly rounded shapes, but there are also some elongated crystals. This finer-grained hornblende gabbro with phenocrysts of plagioclase has also been seen in other outcrops in this area. The gabbro does not show any significant sign of deformation, but several mafic dykes cut through the rock.

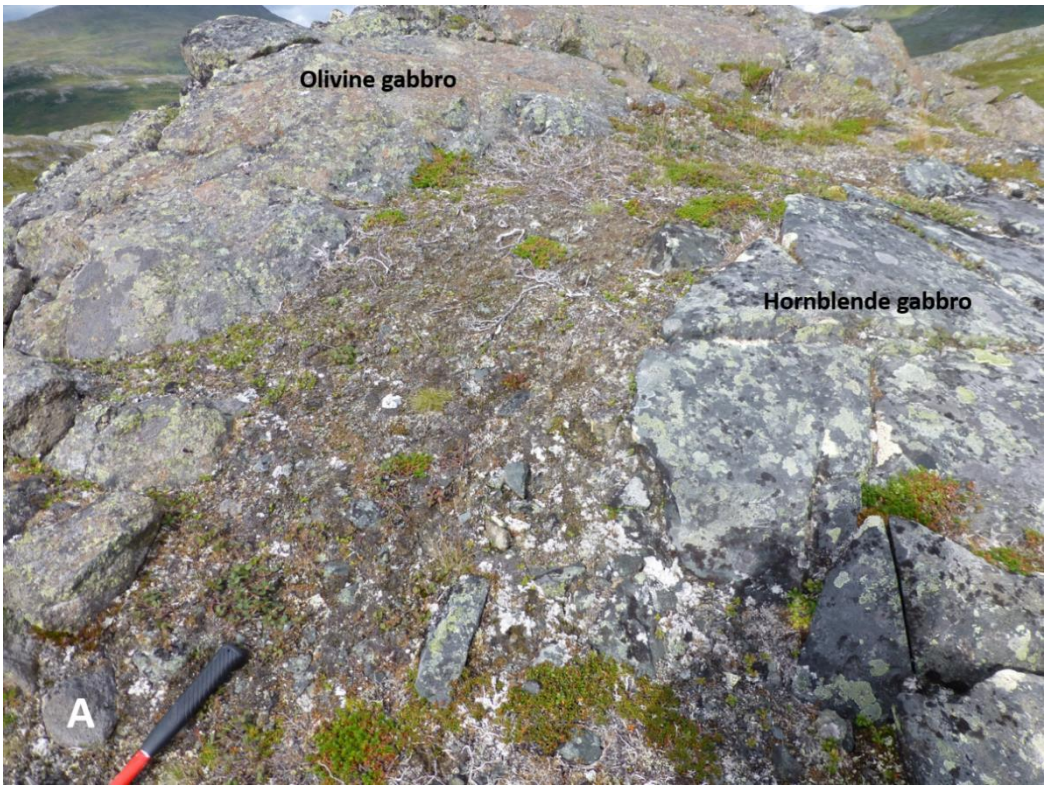

Figure 36: Field photo A) shows the olivine gabbro in contact with the hornblende gabbro. Photo B) show the characteristic rusty colour of the weathered surface of the olivine gabbro. (GPS: 483134Ø, 7338331N)

Mafic dykes

Mafic dykes are present in the hornblende gabbro, garnet-biotite gneiss at Umbukta and Østre Sauvatnet and in the quartzite at Østre Sauvatnet.

The mafic dykes mainly composes of amphibole (50-60%), plagioclase (20-30%), opaques (5-10%), pyroxene (2-5%), and accessory minerals of muscovite (<1%) and biotite (1-2%). The orientation of the dykes varies, and the widths range from about 30 cm to 3 m. The rock is very fine-grained, massive and homogenous. The rock is aphanitic and the minerals cannot be identified by hand lens. The dykes are mesocratic, have almost a black colour with just a few very fine-grained light minerals scattered between the dark minerals, making the colour dark grey. The dykes do not show any fabric. Some of the mafic dykes occur as irregular, meter-sized bodies rather than tabular dykes, and these irregular bodies are named mafic enclaves.

Most of the rock composes of amphibole and plagioclase. The amphibole is anhedral, pale green, probably secondary formed actinolite. Some samples show darker green rims, interpreted to be hornblende, and a paler core, interpreted to be actinolite, or the remains of the pyroxene precursor (Figure 37). Initially, it probably was presence of pyroxene or olivine grains that where altered and rimmed by the amphibole. The plagioclase grains are subhedral and mostly lath shaped. Some grains have lobate contacts to the amphibole, which may result from partial resorption through alteration from olivine or pyroxene to amphibole. In the samples containing pyroxene, the pyroxenes occur as scattered subhedral pheno- and glomerocrysts. In samples containing biotite, the biotite occur as very fine-grained, brown anhedral flakes always seen in contact with the green amphibole. The biotite is probably a secondary replacement. The opaques are sub-rounded to anhedral and occur as scattered grains surrounded by pale green amphibole. The magmatic texture is preserved and the minerals show no sign of orientation, so they have probably not grown during deformation, and the alteration may result from fluids.

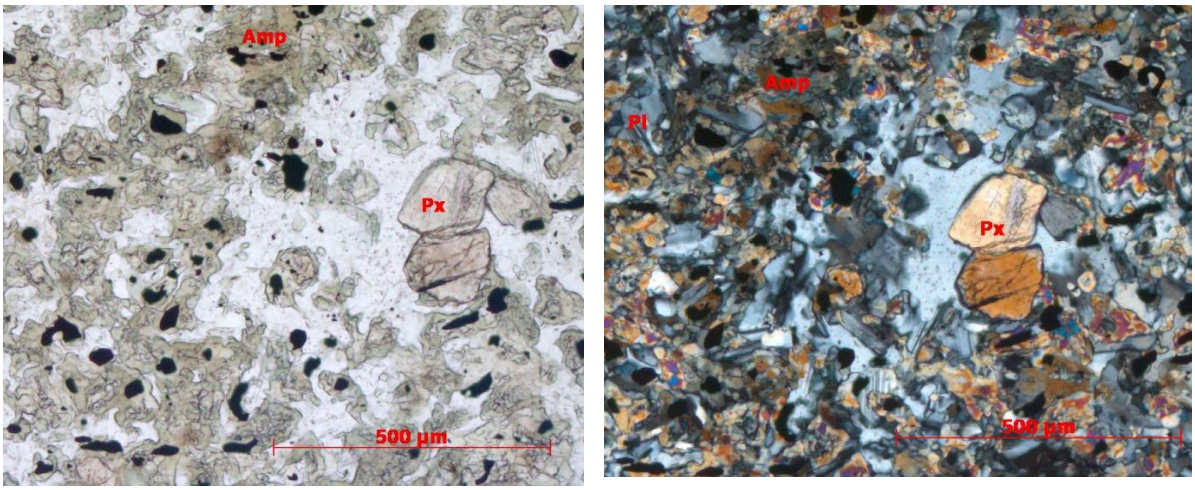

Figure 37: Thin section image of the very-fine grained mafic dyke. Left photo in ppl, and right photo in xpl.

Several mafic dykes cut through the gabbro (Figure 38). The dykes are very fine-grained, mesocratic and homogenous. The individual dykes are mostly 20 cm to 1 m wide, the extremes ranging between millimetre to 3 m. Gabbroic xenoliths are seen inside a mafic dyke. The dykes are oriented in various directions and some dykes crosscut each other. The contacts between the mafic dykes and the gabbro are always sharp, and chilled margins have not been observed. Absence of chilled margins is probably a result of intrusion shortly after emplacement of the gabbro, when both the gabbro and the mafic dykes were hot.

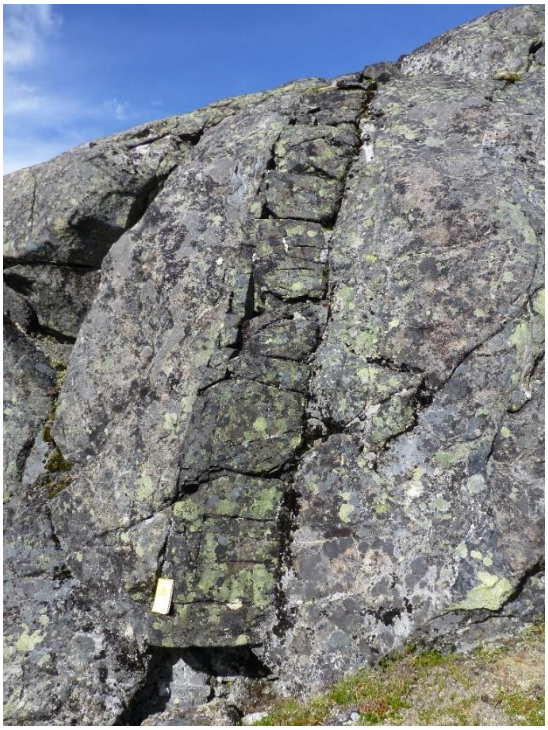

Figure 38: Field photo of a mafic dyke cutting through the gabbro. (GPS: 485990Ø, 7338443N)

In the garnet-biotite gneiss the mafic dykes are oriented in various directions (Figure 39). The dykes cut the gneissose texture in the rock (Figure 40), and must have intruded after high-grade metamorphism of the host rock. The dykes are orientatd in both E-W and N-S direction at Umbukta and Østre Sauvatnet. At Østre Sauvatnet there are also dykes orienting in SW-NE and NW-SE. These dykes are probably the same as those cutting the gabbro, an interpretation supported by the geochemical similarities discussed below. The dykes are mostly 20 cm to 1 m wide, the contacts are sharp, and there is no sign of chilled margins. Abundant mafic dykes are present in the quartzite at Østre Sauvatnet. They are typically seen in 1 to 3 meter thicknesses and oriented either in NW-SE or N-S (Figure 41)

Figure 39: Field photo of mafic dykes cutting the host rock of garnet-biotite gneiss, orienting in different directions. (GPS: 486646Ø, 7339441N)

Figure 40: Close-up photo of the mafic dyke to the left, cutting the leucocratic host rock to the right. The mafic dyke cut the gneissose texture in the host rock. (GPS: 488305Ø, 73404417N)

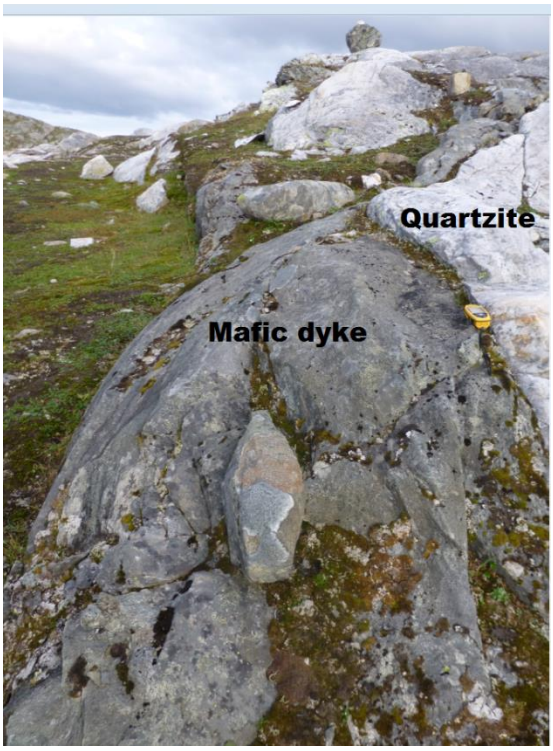

Figure 41: Mafic dyke cutting quartzite at Østre Sauvatnet. (GPS: 488548Ø, 7341012N)

The contact-zone at Østre Sauvatnet

A harp contact between the host rock and the gabbro is not occurring, but a zone between the host rock and the gabbro has been named the contact-zone. The contact-zone is a complex area with contact-zone granitoid, ductile structures, mafic dykes and enclaves, and granitic veins and bodies. At Østre Sauvatnet, there is also an area with quartzite.

Contact-zone granitoid*:* The contact-zone granitoid varies from leucocratic to mesocratic in colour. Some localities show diffuse alternating layering that is bent and wavy (Figure 42), while other localities have random distribution of light and dark minerals with no sign of alternating layers (Figure 43). The rock often occurs with mafic enclaves and cut by mafic dykes. Some outcrops shows leucocratic fragments with rectangular shape in centimetre sizes. The leucocratic fragments often contain a gneissose texture, very similar to the garnet biotite gneiss. The amount of garnet is sporadic and where it occurs, it is clustered and coarse grained between 0.5 to 2.0 mm. The contact-zone granitoid mainly consists of quartz (10-40%), feldspar (15-20%), biotite (5-30%), muscovite (25%), garnet (10%) and accessory minerals of zircon (1%) and epidote (1%).

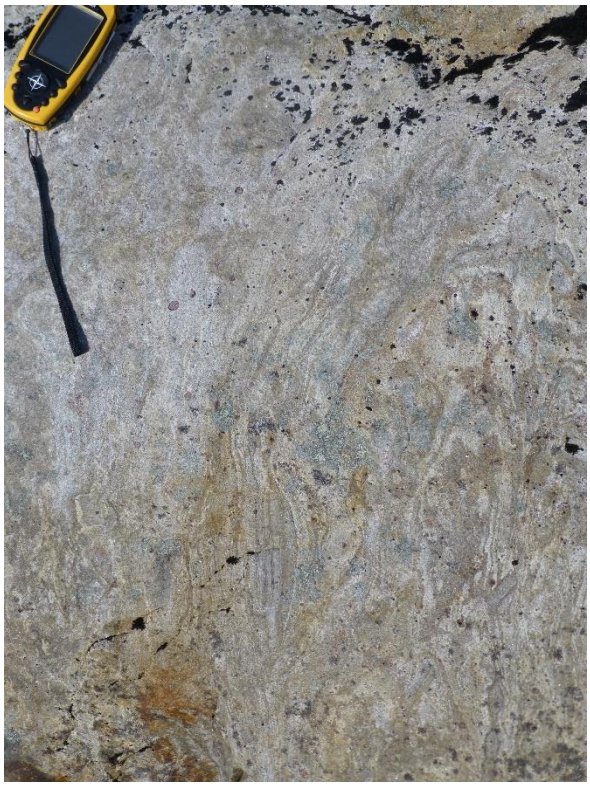

Figure 42: Field photo of the contact-zone granitoid, in the contact-zone at Østre Sauvatnet. (GPS: 488494Ø 7338872N)

Figure 43: Field photo of the contact-zone granitoid in the contact-zone at Østre Sauvatnet. (GPS: 488983Ø, 7339158N)

In thin-section, the contact-zone granitoid does not show any fabric. The biotite is fine grained, has a brown to greenish colour and subhedral- to anhedral flakes, which are randomly distributed. Muscovite also occurs as randomly distributed subhedral- to anhedral flakes. Quartz and plagioclase are anhedral and fine grained with irregular grain boundaries. Garnet varies in sizes from fine- to medium-grained, mostly with a poikilitic texture with inclusion of quartz, biotite, epidote and muscovite, but some samples have garnet with a more skeletal texture (Figure 44).

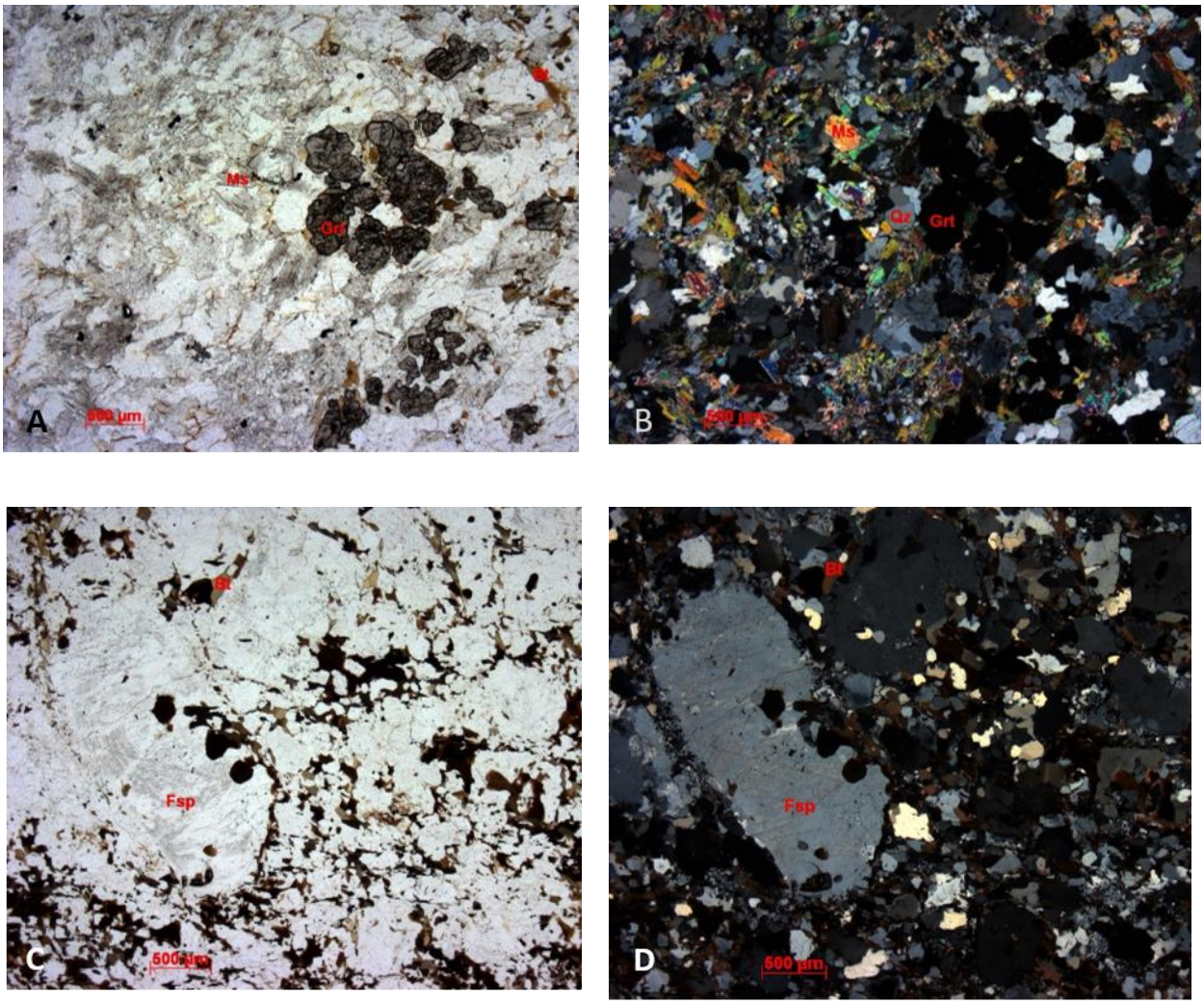

Figure 44: Thin section images of the contact-zone granitoid. Photo A) and C) in ppl, and photo B) and D) in xpl

Occurrence of structures that probably formed during highly ductile condition is present in the contact-zone. Trains of mafic material are frequently seen in the contact-zone (Figure 45A) and may result from mafic dykes disrupted into enclaves, were some of the enclaves show pillow structures (Figure 45B), and many of the mafic enclaves are cut by millimetre to centimetre thick granitic veins. Some of the mafic enclaves contain millimetre sized white crystals, as shown in the photo of the mafic pillow in Figure 46, and the crystals are probably plagioclase phenocrysts. The contact between the mafic dykes and mafic enclaves with the granitic veins are sharp. The rocks in the outcrop shown in Figure 46, looks as they have been through ductile conditions, the contact-zone granitoid which encloses the mafic enclaves looks as it is smeared out surrounding the mafic rocks.

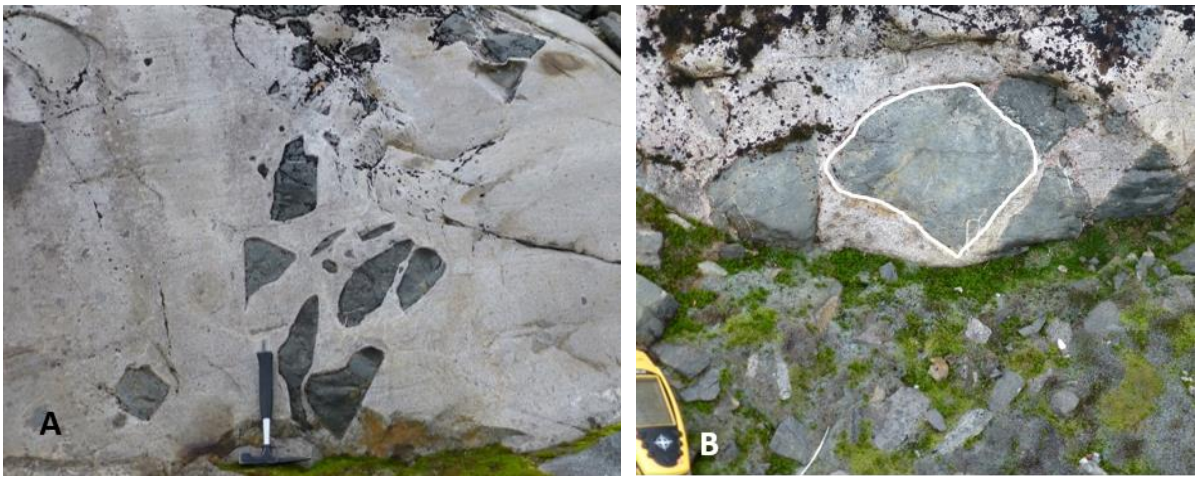

Figure 45: A) Field photo of a mafic "train", which probably is a disintegrated mafic dyke in the contact-zone granitoid at Østre Sauvatnet (GPS: 488481Ø 7338994N). B) Mafic pillow surrounded by granite in the contact-cone zone at Østre Sauvatnet (GPS: 4887240Ø, 7338718N).

Figure 46: An outcrop at Østre Sauvatnet showing an irregular mafic dyke with pillow structure, and cut by granitic veins, and the surrounding contact-zone granitoid looks smeared out in the area surrounding the dyke. (GPS: 488340Ø 7339258N)

In the contact-zone outcrops of 40 to 50 cm-wide mafic dykes, which orient NE-SW, cut through the contact-zone granitoid. Mafic dykes and mafic enclaves is shown in close relation to each other in the contact-zone. Some of the mafic enclaves have about 1.0 cm thick rim

surrounding the enclave, probably a reaction rim. The presumed reaction rim consist of leucocratic granitic composition. Sometimes the reaction rims fills in lager areas between the enclaves (Figure 47). A few of the reaction rims contain quite a lot of fine-grained garnet (Figure 47, the close-up photo).

At the southern side of Østre Sauvatnet, some outcrops show contact-zone granitoid with mafic enclaves and fragments of garnet-biotite gneiss (Figure 48). The fragments of garnet-biotite gneiss occur mostly in rectangular shapes, 40 to 60 cm long and 10 to 20 cm wide (Figure 48B). The shapes of the mafic enclaves are mostly angular or subrounded, and cut the texture in the contact-zone granitoid. The mafic enclaves vary in size, but mostly occur in sizes of about 50 to 70 cm. Inside some of the mafic enclaves, there occur white scattered phenocrysts, and the white phenocryst may be quartz or feldspar (Figure 48).

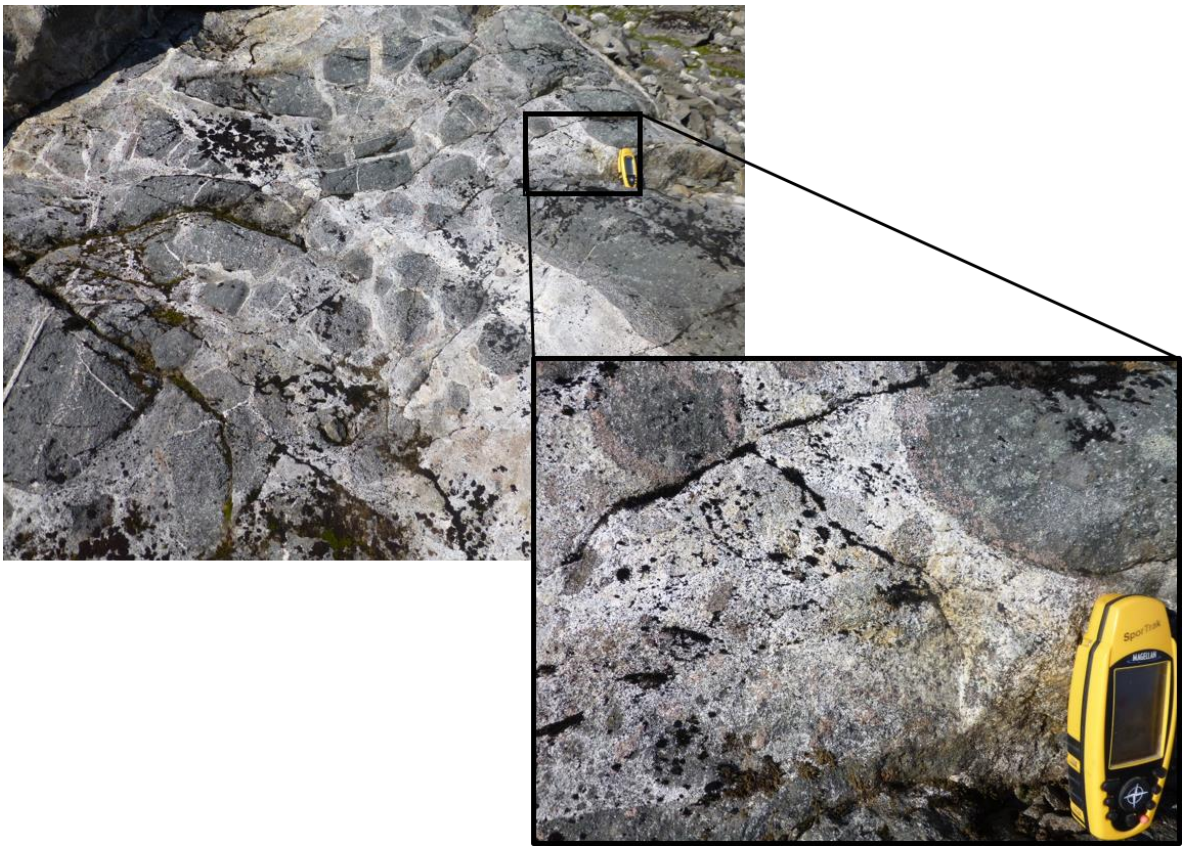

Figure 47: Mafic enclaves showing pillow structures surrounded by granite. The close-up photo to the right show fine grained red garnets in the mafic pillow at the contact to the white granite. (GPS:488494Ø 7338872N)

Figure 48: A) Locality from Østre Sauvatnet with mesocratic mafic enclaves in a leucocratic contact-zone granitoid showing fragments of the host rock. B) Close-up photo of the fragment of the host rock of garnet biotite gneiss (GPS:488494Ø 7338872N).

Several examples of enclaves are present in this contact-zone area. Close to the outcrop in Figure 48 is another locality with mafic dykes- and enclaves. The dykes are 70 to 120 cm wide, oriented N-S and NW-SE (Figure 49). A dyke cutting an enclave has been observed (Figue 50A), and the enclaves at this locality are mostly angular and shows chilled margins, but they still show relatively sharp contacts. The chilled margins at this locality occur as millimetre thick, light-coloured rims, which surrounds the enclaves (Figure 50B). The dykes do not show chilled margins, just sharp contacts.

Figure 49: Mafic dykes orienting N-S and NW-SE, cutting through the contact-zone granitoid, and mafic enclaves, some with pillow structures. . (GPS:488470Ø 7339001N)

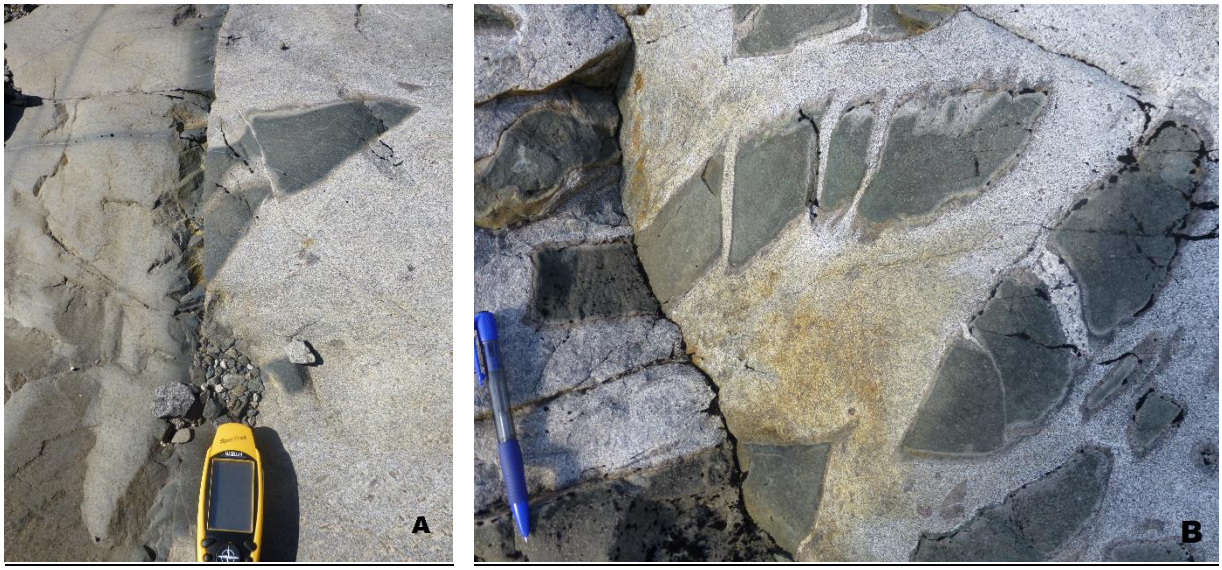

Figure 50: A) An enclave cut by a mafic dyke. B) The enclaves show thin light-coloured chilled margins (GPS:488470Ø 7339001N).

Mafic enclaves and granitic bodies also occur in the host rock, which lies in close relation to the contact-zone at Østre Sauvatnet, this area may be interpreted to be a part or a peripheral part of the contact-zone. Figure 51 is from a locality close to Sauvasshytta (Figure 12) where the mafic enclaves occur in metre-sizes, and cut through the host rock of garnet-biotite gneiss. The mafic enclaves are very fine-grained and have dark greyish colour, and contain millimetre thick

leucocratic granitic veins. The contact between the mafic enclaves and the garnet-biotite gneiss is sharp, the mafic enclaves cut the texture of the garnet-biotite gneiss, and there are no chilled margins (Figure 52). Leucocratic granitic bodies are smaller than the mafic enclaves, and the granitic bodies also cut the structures of the garnet-biotite gneiss, and the contact is sharp (Figure 52A). The granitic bodies have a granular texture and do not show any internal structures. The outcrop shown in Figure 51 looks like it may have been thorough ductile conditions, and both the granitic- and mafic enclaves clearly show evidence of cutting the texture of the garnet-biotite gneiss.

Figure 51: Metre sized mafic enclaves in the host rock. This locality is close to the Sauvasshytta at Østre Sauvatnet. (GPS:488776Ø 7340953N)

Figure 52: A) Granitic body cutting the texture of the garnet-biotite gneiss. B) The sharp contact between the mafic enclave and the garnet-biotite gneiss. (GPS:488776Ø 7340953N)

Granite*:* The granite is homogenous, leucocratic with a white colour. The texture is granular and mainly composes of light minerals of quartz (40-50 %), plagioclase (15-20%), muscovite (20-30%) and accessory minerals as K-feldspar (1-2%), biotite (1%), epidote (clinozoisite) (1%).

In thin section, the rock is fine- to medium grained. The quartz is mainly medium-grained, have mostly irregular grain-boundaries, a few grains show triple-junction and undulating extinction. The plagioclase is mainly seritizated and replaced by secondary formed muscovite (Figure 53). The muscovite is sub- to anhedral flakes, some grains are lath shaped and other show skeletal texture. The muscovite grains show no orientation. A few randomly distributed anhedral K-feldspar grains are present. Also a few biotite and epidote (clinozoisite) grains are randomly distributed, and the biotite grains are fine-grained and present as flakes, and the few epidote (clinozoisite) minerals are present as fine-grained anhedral- to subhedral crystals.

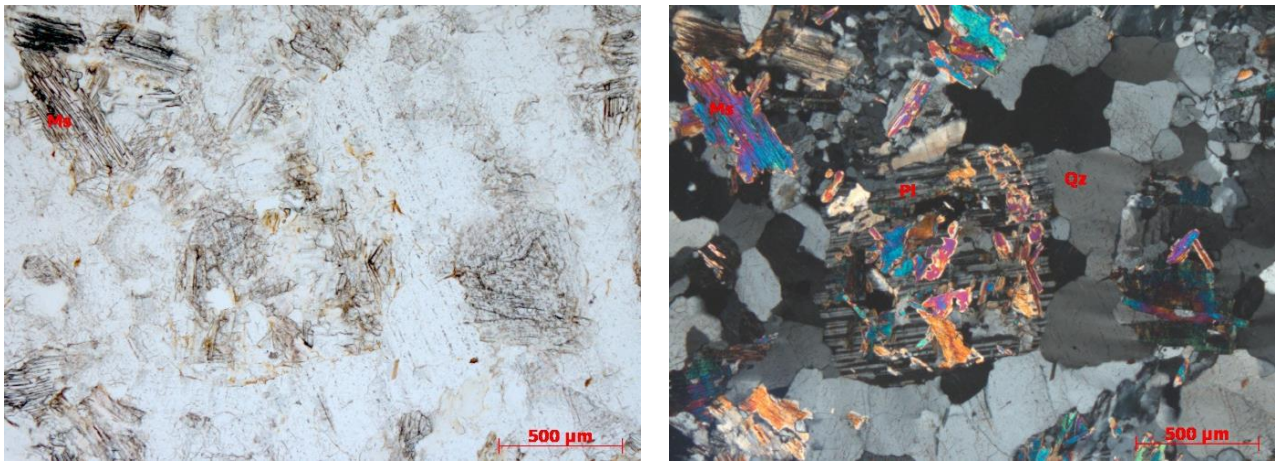

Figure 53: Thin section image of the granite. Left photo in ppl, right photo in xpl.

The leucocratic granitic veins and -bodies at Østre Sauvatnet occur in millimetre to metre sizes. The granitic veins and -bodies occur in both mafic enclaves and garnet-biotite gneiss. The granitic bodies have irregular jagged contacts and are 0.2 to 10.0 cm wide. The granitic veins form a crisscrossing pattern in the mafic enclaves and the garnet-biotite gneiss, and mostly the veins occur in millimetre to centimetre thicknesses. A large meter sized massive, very-fine grained mafic enclave, in an outcrop close to Sauvasshytta (Figure 52), contains abundant millimetre to centimetre thick granitic veins, and centimetre sized granitic bodies (Figure 54A). The mafic enclave has irregular, but sharp contacts to the fine-grained garnet-biotite gneiss, which also contains millimetre sized granitic veins. The granitic veins have a granular texture, and separates from the greyish garnet-biotite gneisses by their white colour, and no presence of garnet or gneissose texture. In the garnet-biotite gneiss, the granite also occurs as bigger bodies, which at some localities encloses the garnet-biotite gneiss, so the garnet-biotite gneiss occur as centimetre sized fragments in the granite (Figure 54B,C). The mafic enclaves are usually seen in close proximity to the granite (Figure 54D,E,F).

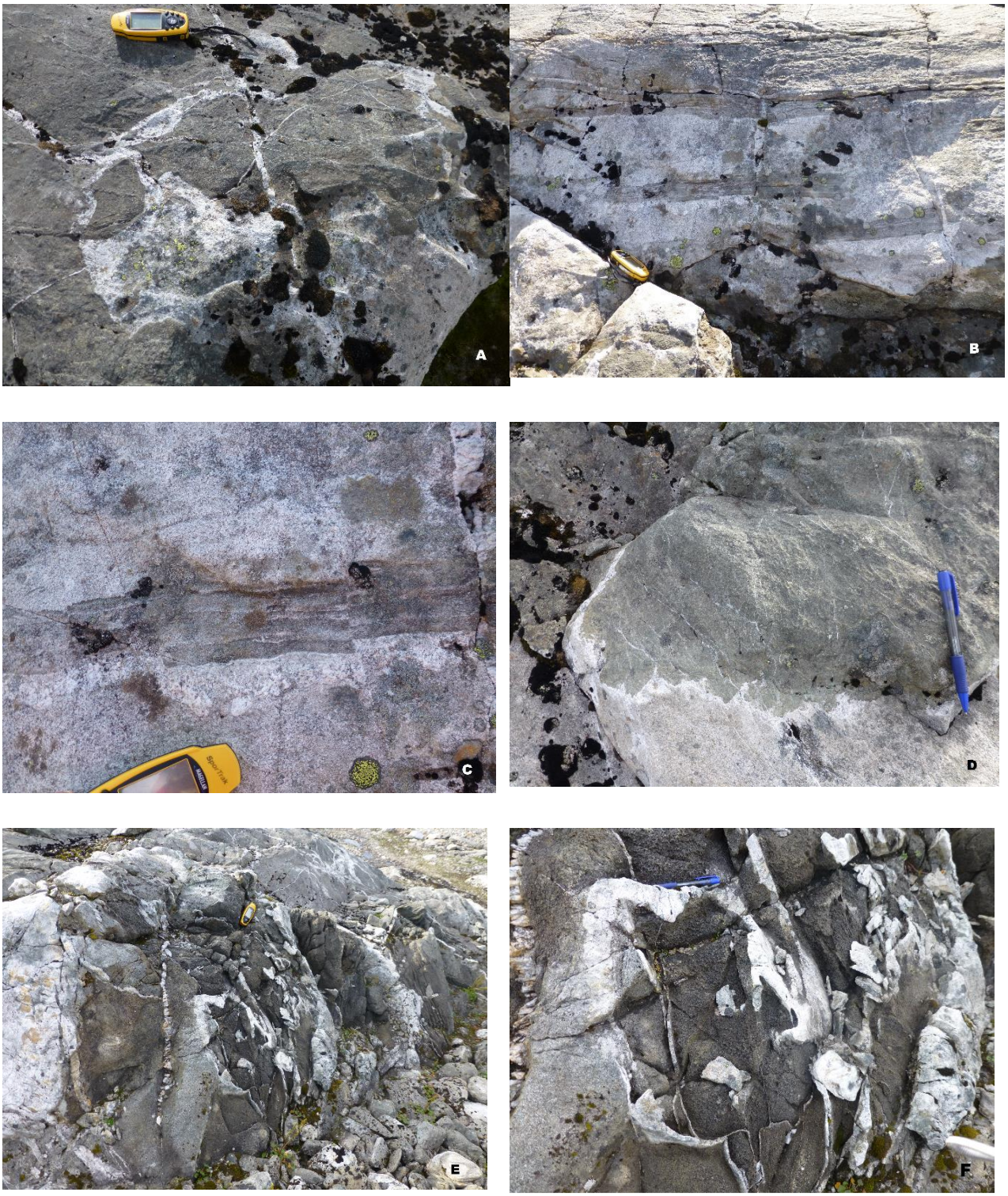

Figure 54: A) Millimetre to centimetre thick granitic veins in a mafic enclave. B) and C) Granite enclosing the garnet-biotite gneiss. D), E) and F) Granitic veins in the mafic enclaves. (A+B+C:GPS:4887276Ø 7341065N) (D+E+F: GPS:488712Ø 7341041N)

On the western side of Østre Sauvatnet garnet-biotite gneiss lies in contact with outcrops of quartzite. The amount of quartzite in the area is quite high and shown on the map. When the

garnet-biotite gneiss and quartzite are in contact, it looks like the quartzite cuts the structures of the gneiss (Figure 55). Mafic dykes are also present in the quartzite and are quite abundant. The mafic dykes occur in 1 to 3 m sizes, and orient either NW-SE or N-S (Figure 56).

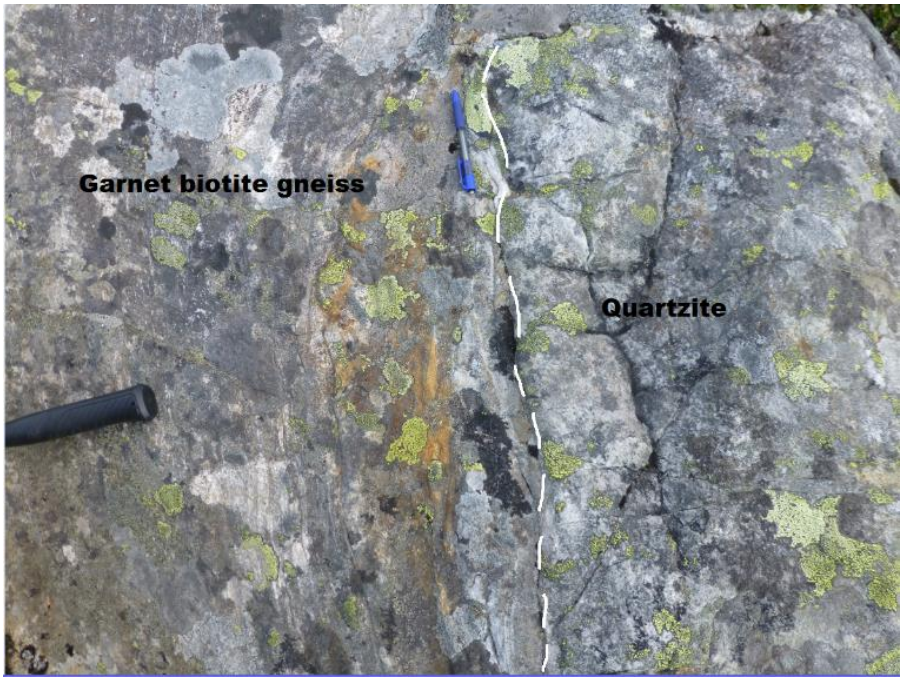

Figure 55: Contact between the garnet-biotite gneiss and the quartzite at Østre Sauvatnet. (GPS:488941Ø 7340561N)

Figure 56: Mafic dyke in the quartzite at Østre Sauvatnet. (GPS:488548Ø 7341012N)

Quartzite:The quartzite is a leucocratic fine- to medium-grained homogenous rock. The quartzite is compact, milky-white in colour and mostly impure. The rock mainly consists of quartz (90 - 95 %), muscovite (2 - 5%) and accessory minerals of biotite (1%) and apatite (1 %). In thin section, the quartz grains are anhedral and mainly medium-grained with irregular grain boundaries (Figure 57). A few grains show triple junctions, but not with straight boundaries. The extinction of the quartz grains are undulating. The muscovite is subhedral, has a lath to acicular shape and is aligned. The few biotite grains are anhedral flakes and have a light brown colour. Some biotite-grains show traces of chloritization.

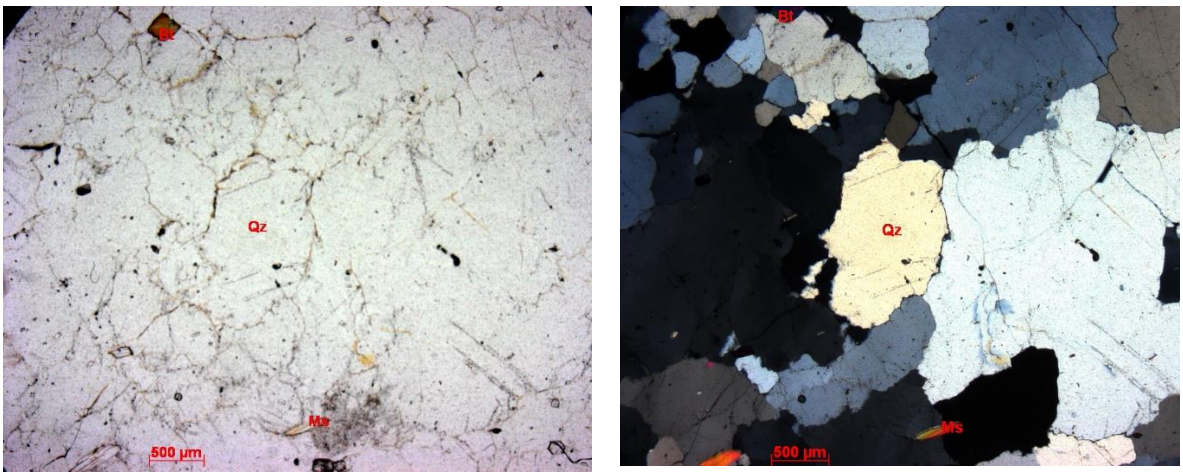

Figure 57: Thin section image of the quartzite. Left photo in ppl, and right photo in xpl.

Whole-rock geochemistry of Umbukta gabbro and mafic dykes

Major- and trace element analysis

In the following section, the major and trace elements of the mafic rocks at Umbukta will be presented, and a few trace element analysis from the contact-zone granitoid, granites and host rock will also be presented. A set of 23 samples from the Umbukta gabbro, mafic dykes were analysed for major and trace element geochemistry, and a set of 7 samples from the contact-zone granitoid, granite and host rock from Østre Sauvatnet, were analysed for trace element geochemistry. A total number of 30 samples were analysed for major and trace element geochemistry at ALS Global at Piteå in Sweden. With help from suitable diagrams made from "Igpet 2007", a geochemical analyses program, analytical results are presented below from Figure 58 to 77.

Major element data for the Umbukta gabbro and mafic dykes

The main elemental components of the gabbros show a SiO_2 content ranging from 42.3 to 58.4 wt.%, MgO from 3.9 to 18.9 wt%, Fe_2O_3 from 7.9 to 16.7 wt.%, Al_2O_3 from 10.1 to 17.8 wt.%, CaO from 5.2 to 10.4. The mafic dykes have quite similar composition and SiO_2 ranges from 48.2 to 57.0 wt.%, MgO from 7.3 to 12.8 wt.%, Fe_2O_3 from 10.6 to 14.2 wt.%, Al_2O_3 from 11.9 to 14.0 wt.%, CaO from 7.3 to 9.3 wt.% (appendix C)

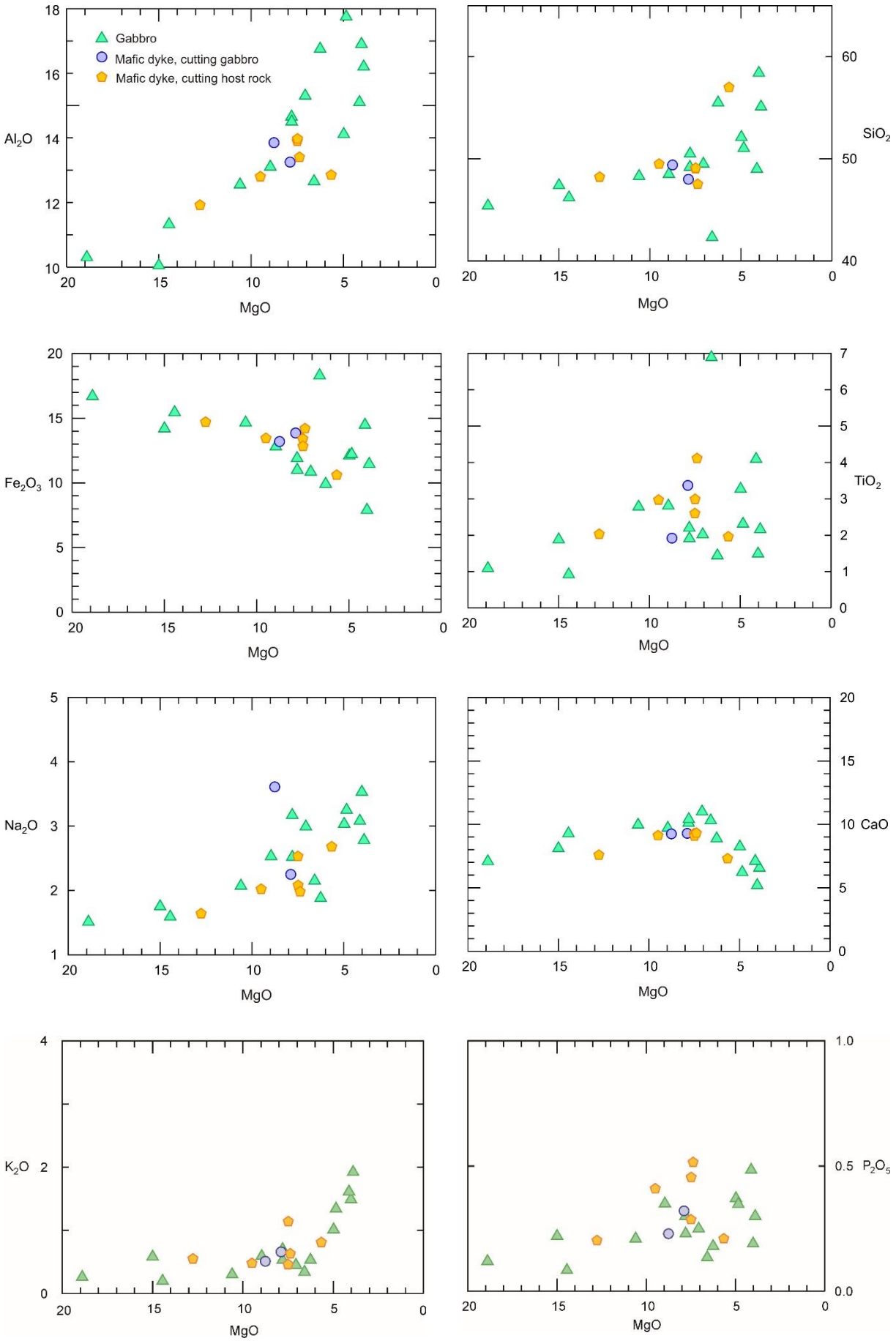
Gabbro
Mafic dyke, cutting gabbro
Mafic dyke, cutting host rock
Al2O
SiO2
Fe2O3
TiO2
Na2O
CaO
K2O
P2O5
MgO

Figure 58: Fenner diagram with data form the Umbukta gabbro and the mafic dykes. See previous page.

The Fenner diagrams (Figure 58) are used to present the major oxides. The diagrams mainly show increasing concentration of Na_2O, Al_2O_3, K_2O and SiO_2 with decreasing MgO content, while Fe_2O_3 and CaO decrease with decreasing MgO. The P_2O and TiO_2 show a slight increasing trend but mostly they are scattered. All of the diagrams show a bit of scattering, and this may be because the gabbro probably represents a cumulate mineral composition, which is a collection of minerals accumulated at different times and position in the crystallising liquid, mixed with evolved melt. The mafic dykes probably present a melt composition and not a cumulate composition, and may be the reason for showing less scatter of the presented data.

Most of the elements in the Fenner diagrams show an increasing trend with decreasing MgO concentration (more evolved magma). As the magma evolves, olivine would probably be the first mineral to fractionate, and result in decreasing MgO concentration in the melt. The decreasing concentration of Fe_2O_3, with decreasing MgO content, probably results from crystal fractionation of orthopyroxene and early removal of Fe_2O_3 with removal of MgO. The CaO first show a slight increasing trend and then decreases with decreasing MgO, this may result from removal of clinopyroxene. The clinopyroxene probably began to crystalize later than the olivine and the orthopyroxene, and may be why the CaO first slightly increased before the concentration decreased, when CaO was removed with the crystallizing clinopyroxene.

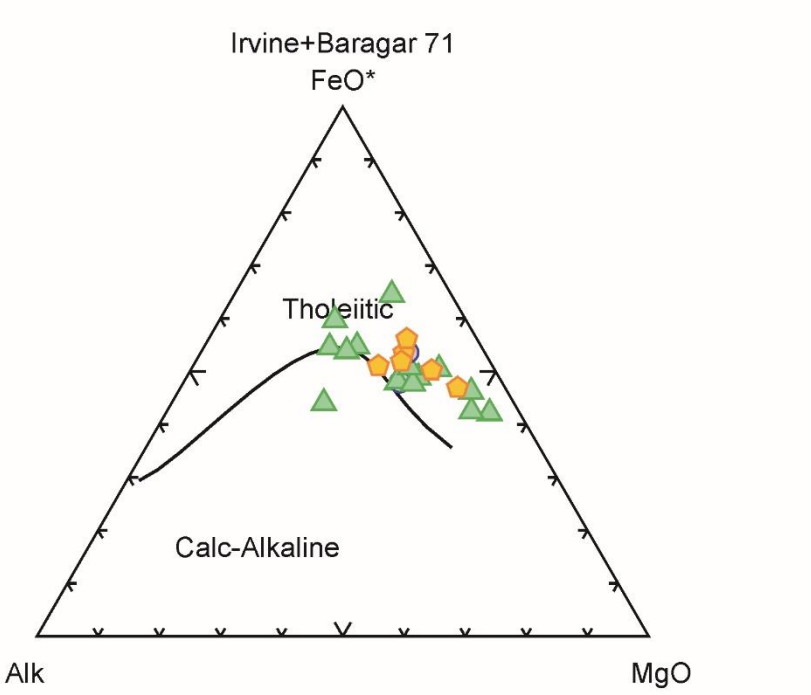

Figure 59: The AFM diagram after (Irvine and Baragar, 1971). The Umbukta gabbro and the mafic dyke plot on the tholeiitic side of the boundary line, indicating tholeiitic affinities.

All of the samples of the Umbukta gabbro and the mafic dykes (except one sample) plot on the tholeiitic side of the boundary line in the AFM diagram after Irvine and Baragar (1971) (Figure 59).

Trace element data for the Umbukta gabbro and mafic dykes

The trace elements are presented in the Chondrite -, Primitive- and MORB normalized spider diagrams (from Figure 60 to 65). The elements behave incompatibly during most partial melting and fractional crystallization processes, and the diagrams show increased incompability from right to left. Figure 60 and 61 show chondrite normalized REE values generally between 10 and 100. The rocks show an enriched pattern especially for the LREEs, and a negative trend from La to Yb, $(La/Yb)_N$ = 2.1-8.7. The Eu anomalies range from $(Eu/Eu^*)_N$ = 0.9-1.5, and most samples show a slight positive Eu anomaly.

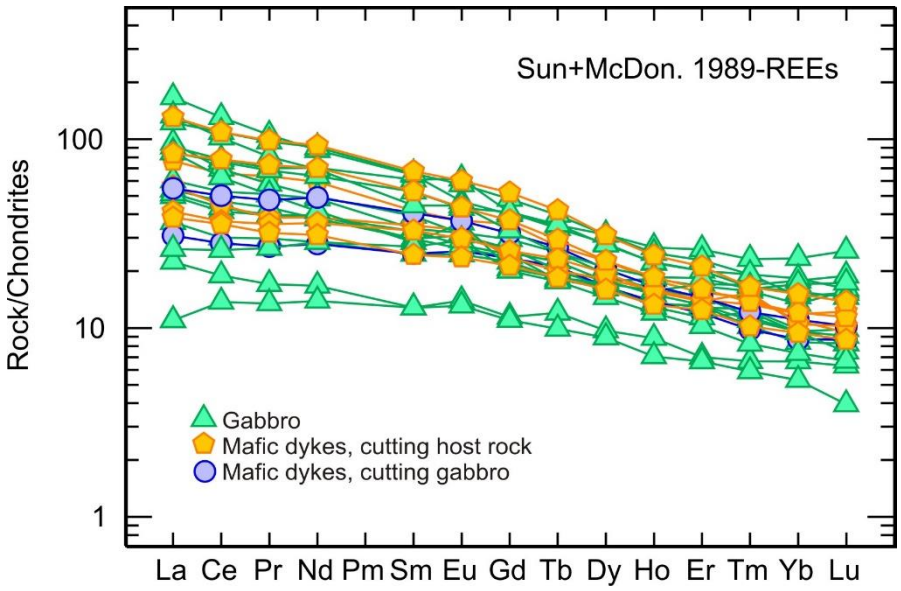

Figure 60: Chondrite normalized REE diagram after Sun and McDonough (1989). The Umbukta gabbro and the mafic dykes show enrichment in the REE, with a negative tsloping from La to Yb.

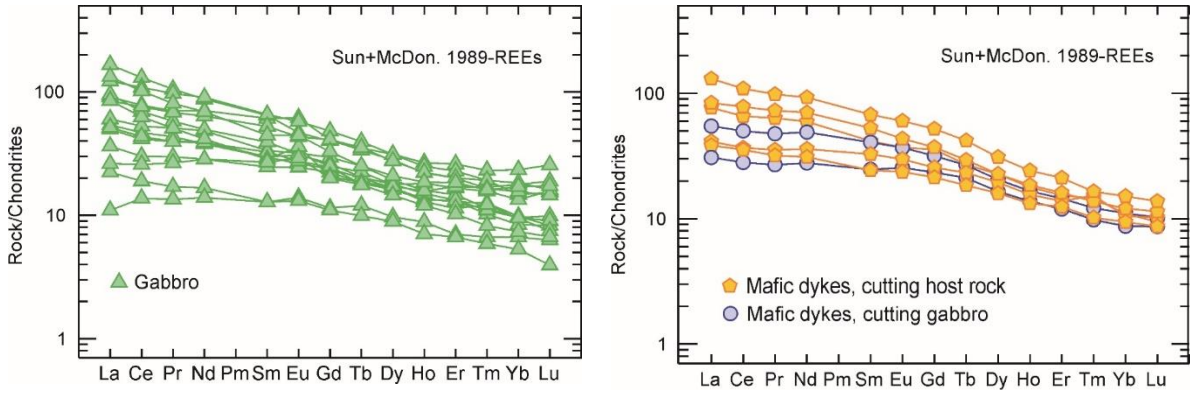

Figure 61: Chondrite normalized spider diagram after Sun and McDonough (1989), same data as presented in Figure 60. Left diagram showing the REE data from the Umbukta gabbro, and the right diagram shows the REE data from the mafic dykes.

The MORB normalized spider diagrams in Figure 62 and 63, show a pattern of variable enrichment of the trace elements, except for the two HFS elements Y and Yb, which are not enriched relative to the MORB (Pearce, 1983). The enriched pattern without depletion of Nb, Ta or Ti is an indication of a within-plate setting (Li et al., 2000) and it is suggested that this also indicates little crustal contamination (Li et al., 2000).

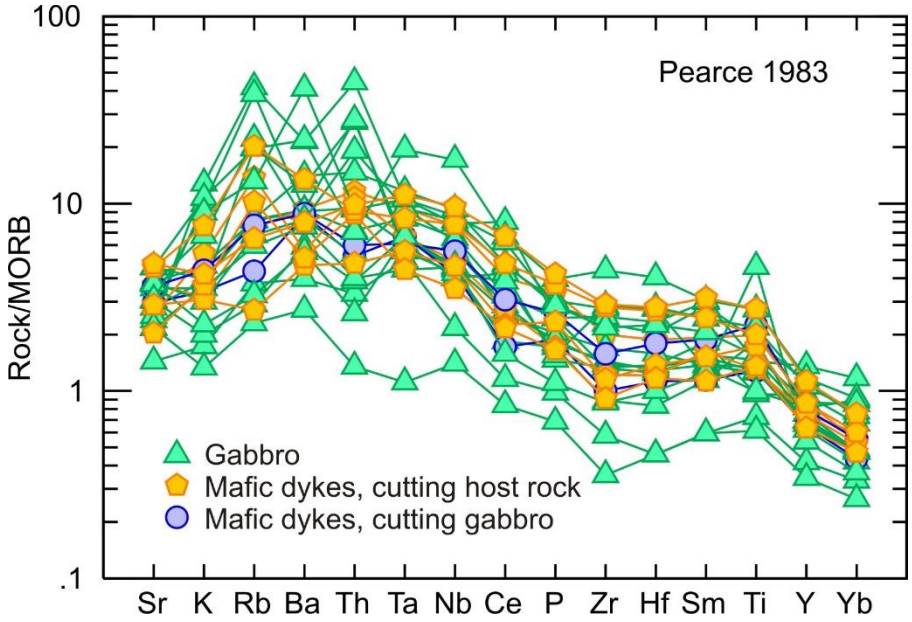

Figure 62: MORB normalized spider diagram after Pearce (1983). The Umbukta gabbro and the mafic dykes show enrichment of the trace elements relative to the MORB, except for Y and Yb.

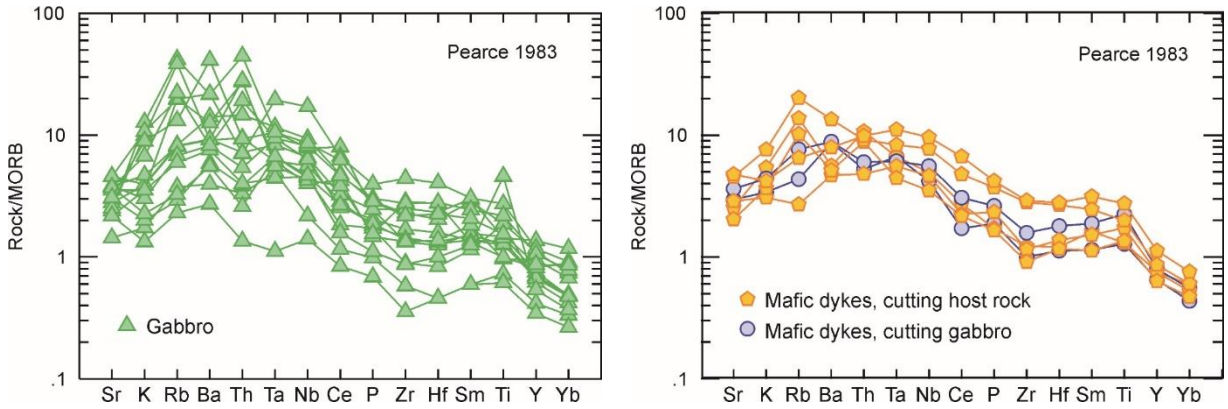

Figure 63: MORB normalized spider diagram after Pearce (1983), same data as presented in Figure 62. Left diagram showing the MORB normalised data from the Umbukta gabbro, and left figure shows the MORB normalized data from the mafic dykes.

The primitive mantle normalized spider diagram after Sun and McDonough (1989) in Figure 64 and 65 shows a "humped" pattern and a variable enriched geochemical pattern of the incompatible trace elements with respect to the primitive mantle. The enrichment in trace elements is higher than for subduction related basalts (Xia et al., 2013) and there are no negative anomalies for Nb, Ta or Ti, which indicates formation in a within-plate setting rather than in an arc related environment (Xia, 2014). Most samples show a positive Pb anomaly, which is typical for continental settings (Hofmann, 1997).

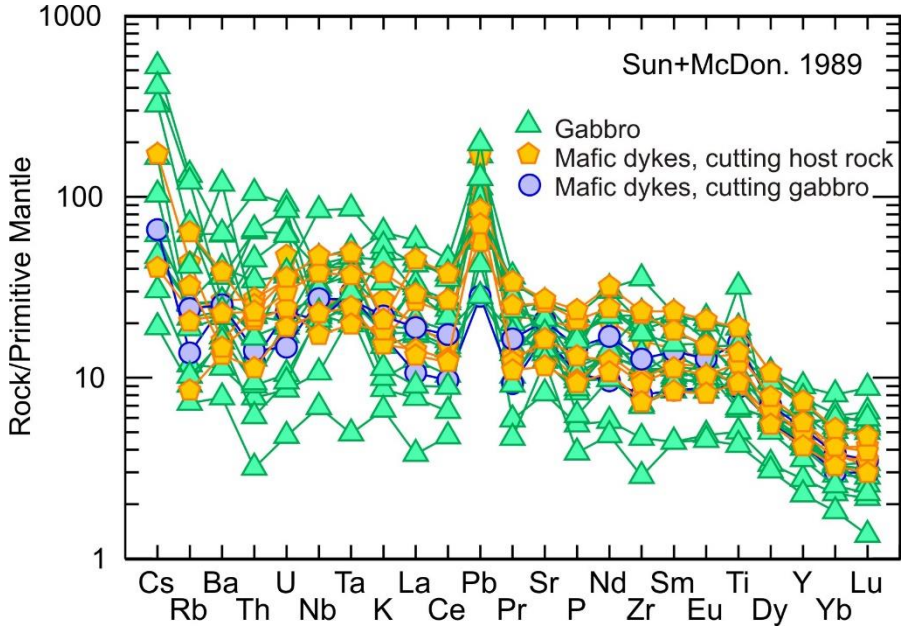

Figure 64: Primitive mantle normalized spider diagram after Sun and McDonough (1989). The Umbukta gabbro and the mafic dykes show variable enrichment in the trace elements relative to the primitive mantle.

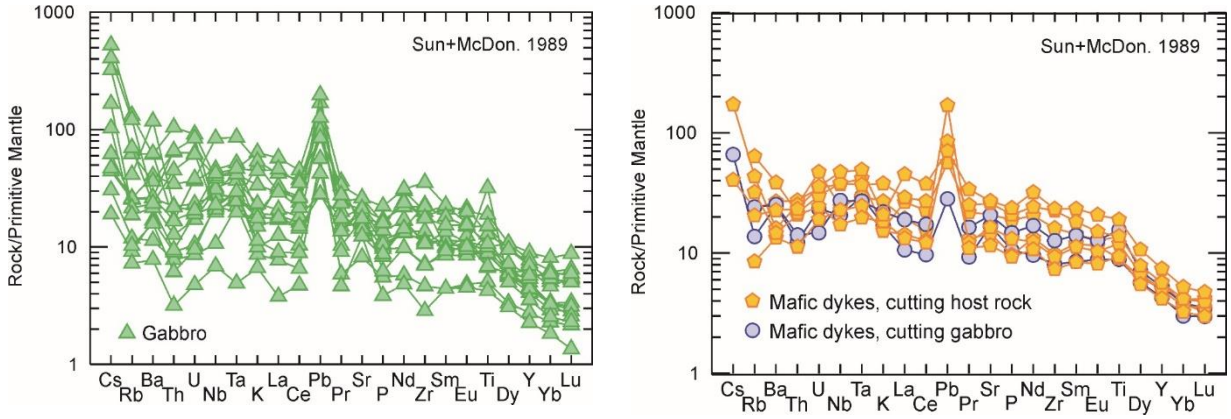

Figure 65: Primitive mantle normalized spider diagram after Sun and McDonough (1989), the same data are presented in this diagrams as in Figure 64. The left diagram shows the primitive mantle normalized data from the Umbukta gabbro, and the right diagram show the primitive mantle normalized data for the mafic dykes.

The Umbukta gabbro and the mafic dykes mainly plot as within-plate tholeiite in the Ti-Zr-Y (Figure 66), Zr/Y-Zr (Figure 67), Nb-Zr-Y (Figure 68), La-Y-Nb (Figure 69), P_2O_5-Zr (Figure 70) diagrams. The data plot relatively consistently in the fields of within-plate setting and tholeiitic composition, even with some scatter in the data presented in the different discrimination diagrams.

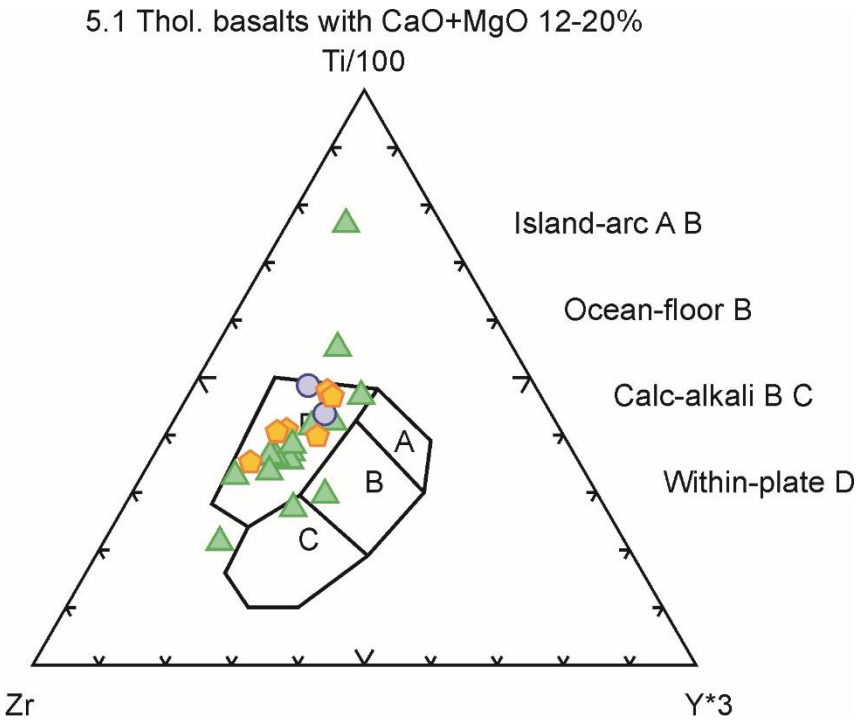

Figure 66: Ti-Zr-Y tectonic discrimination diagram after Pearce and Cann (1973). The data mainly plot in field D, which represent a within-plate setting.

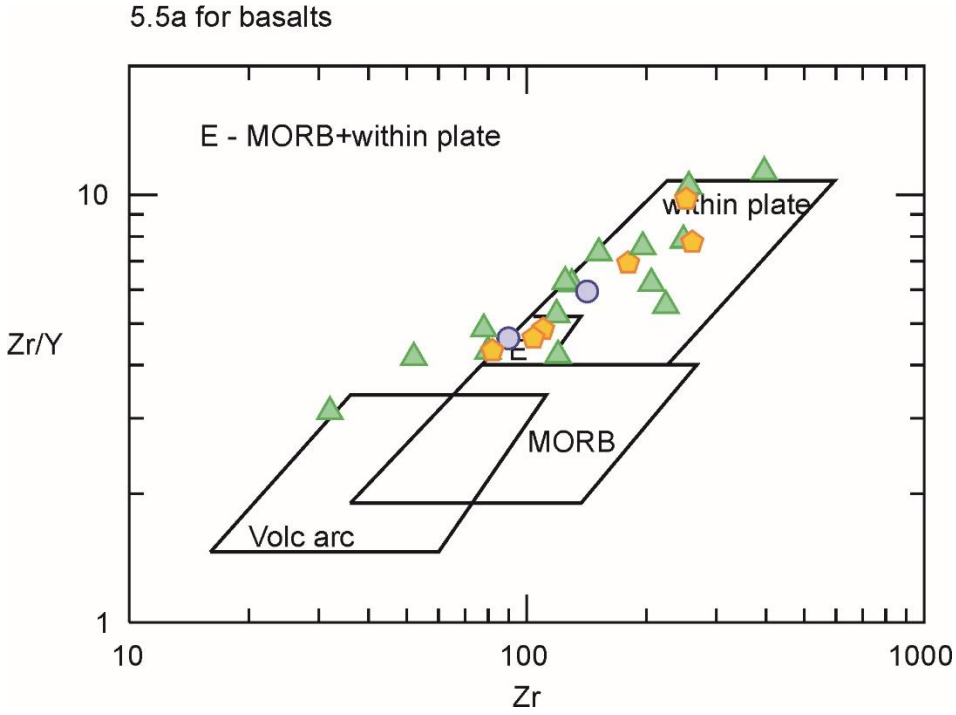

Figure 67: Zr/Y-Zr tectonic discrimination diagram after Pearce and Norry (1979). The plotted data show some scattering, but mainly concentrate in field E, which represent MORB + within plate basalts, and the field representing within plate basalts.

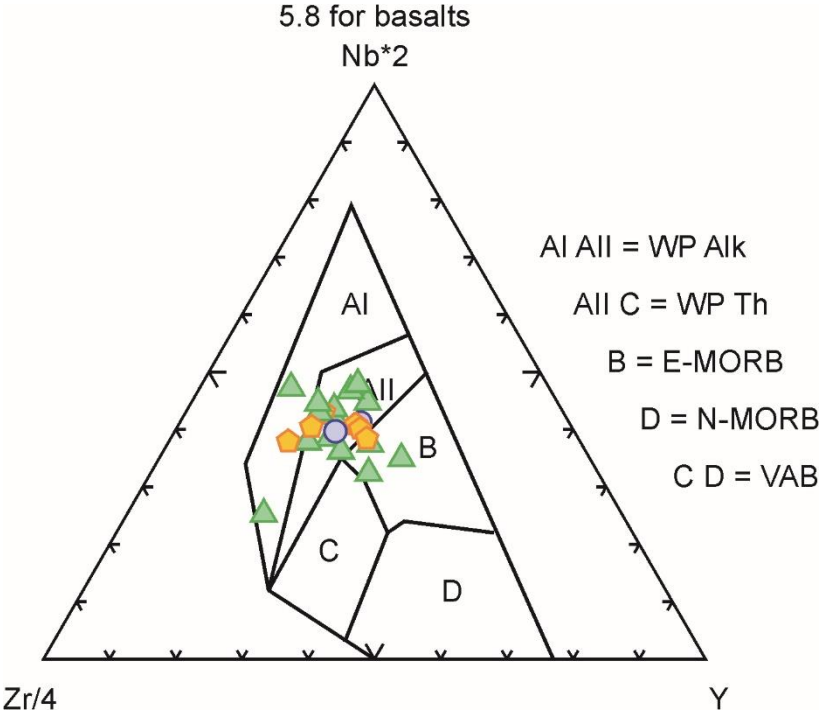

Figure 68: Zr-Nb-Y tectonic discrimination diagram after Meschede (1986). The plotted data show some scatter, but most of the samples plot in AII, which can present either within plate tholeiite or within plate alkaline magmas.

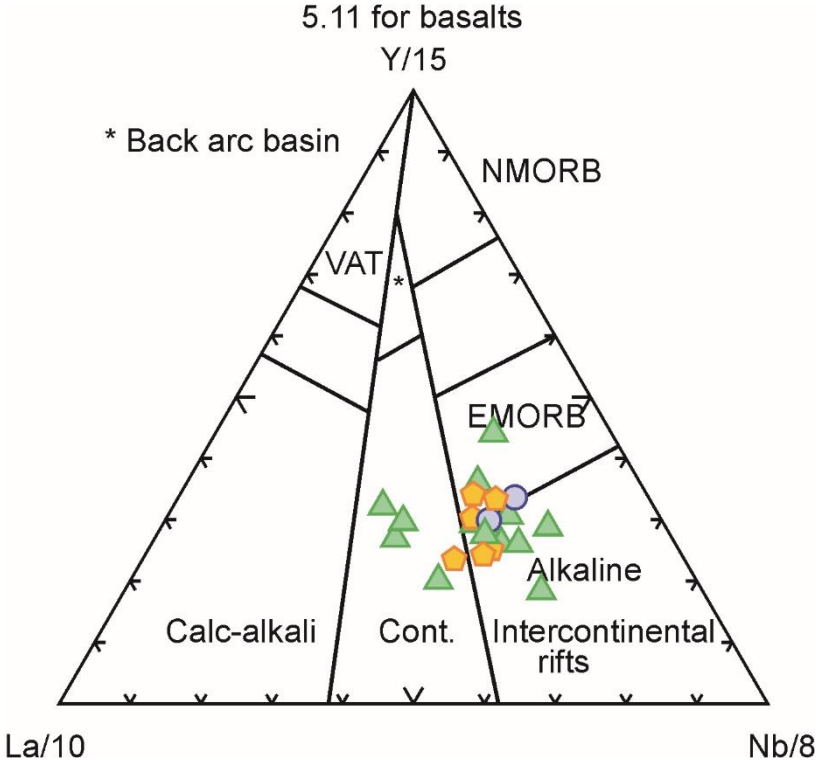

Figure 69: La-Nb-Y tectonic discrimination diagram after Cabanis (1989). The plotted data for the Umbukta gabbro and the mafic dykes show some scattering of the presented data. Mostly the data plots between E-MORB and alkaline intercontinental rifts, and a few samples plot in the field of continental affinities.

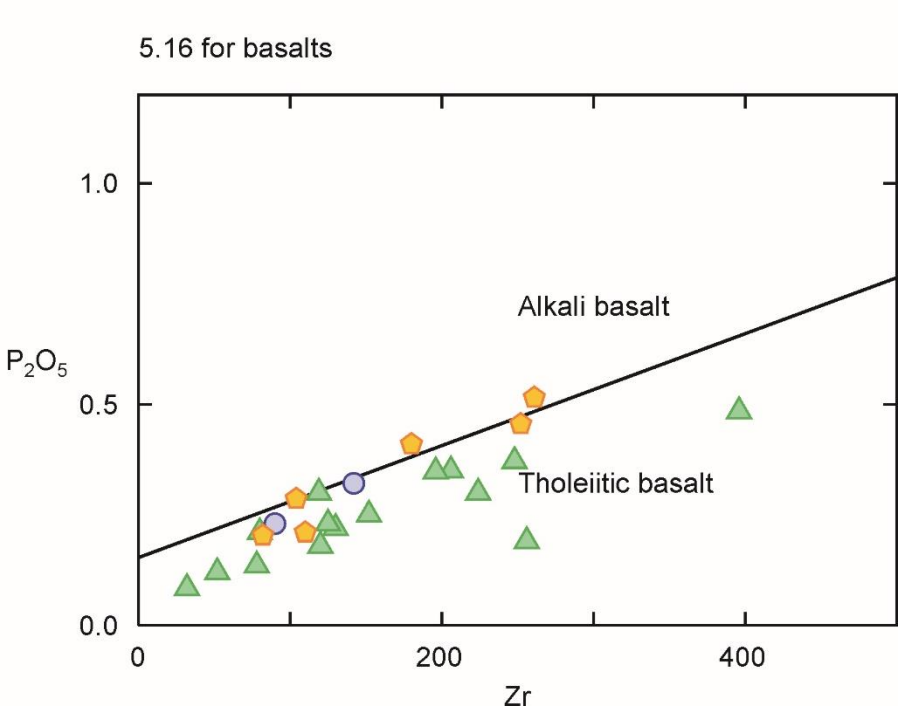

Figure 70: Zr-P_2O_5 diagram after Winchester and Floyd (1976). The Umbukta gabbro and the mafic dykes plot in the file of tholeiitic basalts.

In Figure 71 to 73 the trace element data from the Umbukta gabbro and the mafic dykes are plotted together with the trace element composition from the gabbros in the Seiland Igneous province (SIP). The data are presented in the chondrite normalized REE diagram after Sun and McDonough (1989) (Figure 71), the MORB normalized spider diagram after Pearce (1983) (Figure 72) and the primitive mantle normalized spider diagram after Sun and McDonough (1989) (Figure 73). The geochemical data from SIP is collected from unpublished data from Slagstad at the Norwegian geological survey (NGU), and from Roberts (2007). The shaded grey area is contoured after the plotted SIP data, and I have performed the countering of the SIP data. The trace element data from the gabbros in the SIP and the Umbukta gabbro and mafic dykes are very similar, and the overlap between these data is quite clear.

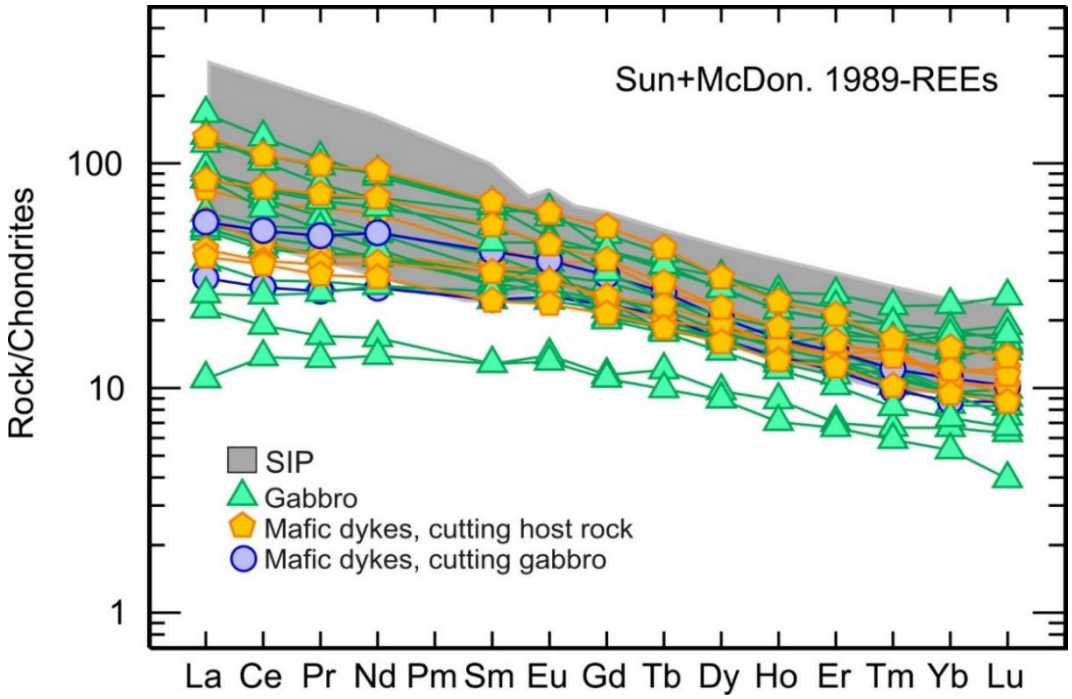

Figure 71: Chondrite normalised spider diagram after Sun and McDonough (1989). The REE data from the Umbukta gabbro and the mafic dykes plotted against the REE data of the gabbros in the SIP.

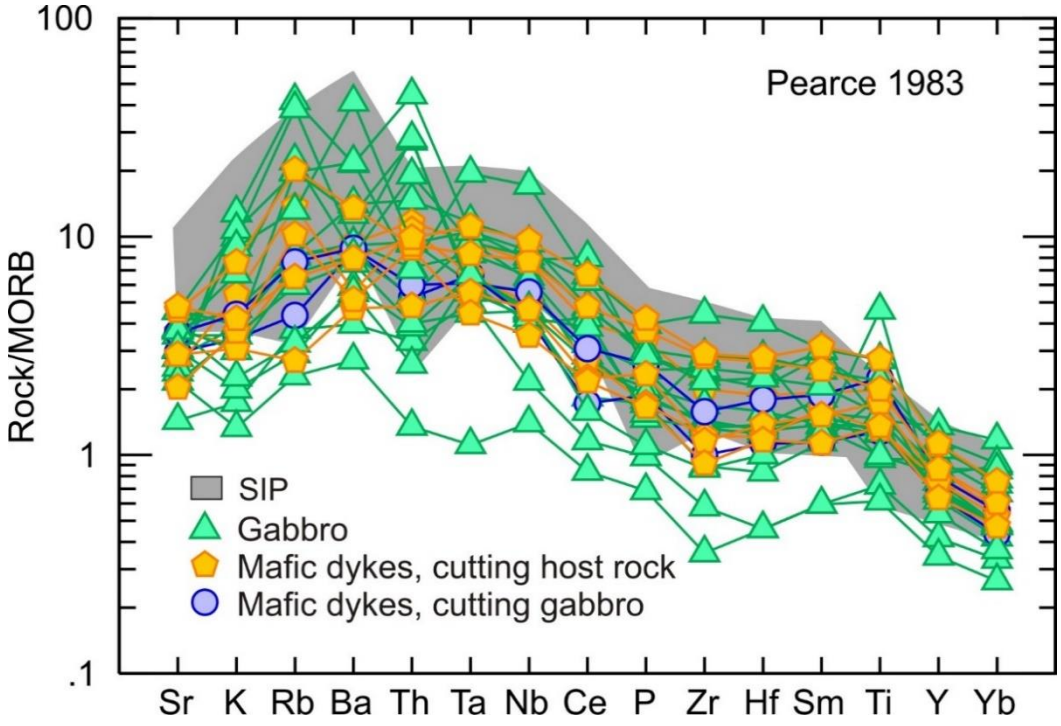

Figure 72: MORB normalized spider diagram after Pearce (1983). The MORB normalized trace elements of the Umbukta gabbro and the mafic dykes are plotted against the MORB normalized trace elements from the gabbros in SIP.

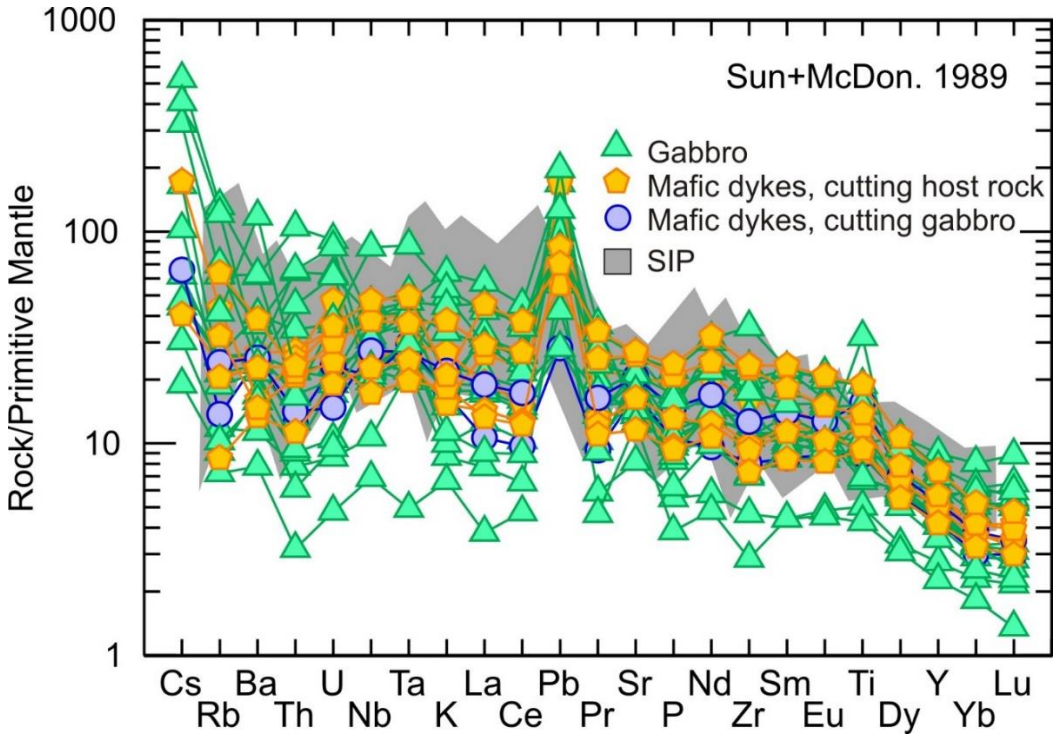

Figure 73: Primitive mantle normalised spider diagram after Sun and McDonough (1989). The primitive mantle normalized trace elements from the Umbukta gabbro and the mafic dykes are plotted against the primitive mantle normalized data from the gabbros in SIP.

Contact-zone granitoid, granites and host rock

The two granite samples have a SiO_2 content of 75.8 and 77.8 wt.%, and an A/CNK (molar $Al_2O_3/CaO+Na_2O+K_2O$) = 1.21 and 1.55, which indicates a peraluminous composition (Maas et al., 1997, Maniar and Piccoli, 1989). The contact-zone granitoid has a SiO_2 content of 60.4 wt.% and an A/CNK = 1.48, which also indicates a peraluminous composition (appendix C).

All samples (Figure 74) show significant LREE enrichment and negatively sloping REE pattern. The $(La/Yb)_N$ ratios show range of 4.7 and 5.9 for the granites, and the $(La/Yb)_N$ = 16.7 for the contact-zone granitoid. The less incompatible elements, to the right, from Gd-Lu show just a slight negative trend for the contact-zone granitoid and a relatively flat pattern for the granites. The contact-zone granitoid is a bit more enriched than the granitic samples. Both rocks are from the contact-zone area between the gabbro and the garnet-biotite gneiss. The Eu anomalies for the granite are (Eu_N/Eu^*) = 0.37 and 1.39, one has a negative Eu anomaly and the other sample show a positive Eu anomaly. The contact-zone granitoid has an (Eu_N/Eu^*) = 0.45, which is a negative Eu anomaly.

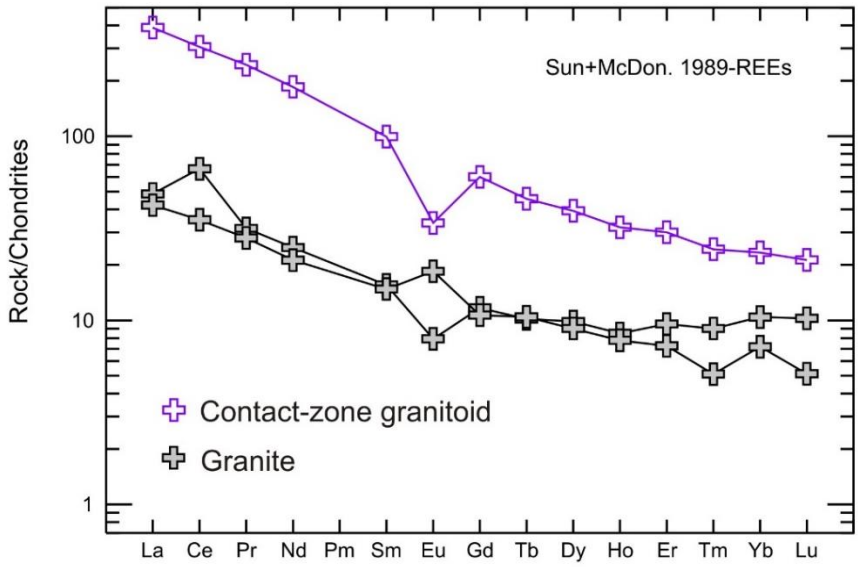

Figure 74: Chondrite normalised spider diagram after Sun and McDonough (1989). REE enriched pattern of the contact-zone granite and the granites. All samples show negative sloping for the LREE (from La-Eu), and the less incompatible elements (HFS), to the right, from Gd-Lu show just a slight negative trend for the contact-zone granitoid and a relatively flat pattern for the granites. The contact-zone granitoid and one sample of the granite show negative Eu-anomaly, and one granite sample show positive Eu-anomaly.

In Figure 75, the contact-zone granitoid and the granitic samples are plotted in a primitive mantle normalized spider diagram after Sun and McDonough (1989), which show a "humped" pattern, and the elements have variable enrichment of the incompatible elements with respect to the primitive mantle. The diagram mainly shows peaks for Cs, Th, K and Pb, and moderate peaks for Nd, U and Dy. The diagram shows troughs for Ba, Nb, Ta, P, Ti and two out of three samples show troughs for Ce.

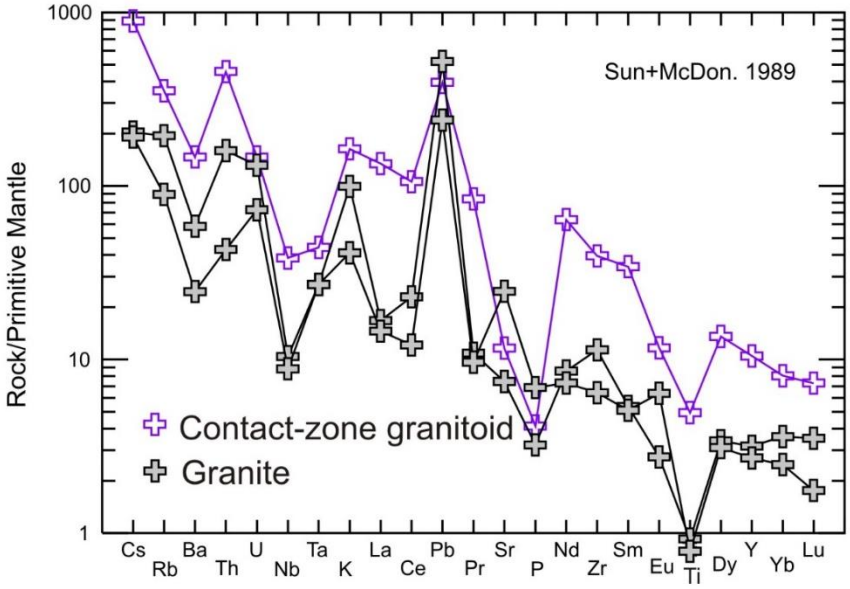

Figure 75: Primitive mantle normalised spider diagram after Sun and McDonough (1989). The trace elements of the contact-zone granitoid and the granite shows a "humped" pattern, and the elements have variable enrichment of the incompatible elements with respect to the primitive mantle.

In Figure 76 and 77 the geochemical composition of the host rock is plotted together with samples of the contact-zone granitoid and granites for comparison of the geochemical trends.

In the chondrite normalized REE diagram (Figure 76) the host rock and the contact-zone granitoid show almost similar geochemical trends, and are enriched in all the REEs, and shows negative sloping from La to Gd with a negative Eu anomaly. From Gd to Lu the slopes show just a slight negative trend, almost a flat pattern. The host rock and the contact-zone granitoid is a bit more enriched than the two granitic samples, but they do also show negative sloping from La to Gd, and just a slight negative trend, almost a flat pattern from Gd to Lu. One sample of the granites shows a positive Eu anomaly, which separates from the other samples.

In the primitive mantle normalised spider diagram (Figure 77), the rock samples show similar geochemical trends with almost the same enrichment for the elements, with respect to the primitive mantle. As in the chondrite normalized REE diagram, the host rock and the contact-zone granitoid samples show very similar trends, and the granites show almost the same trends, with just a bit slighter enrichment for most of the elements, especially from Nd to Lu.

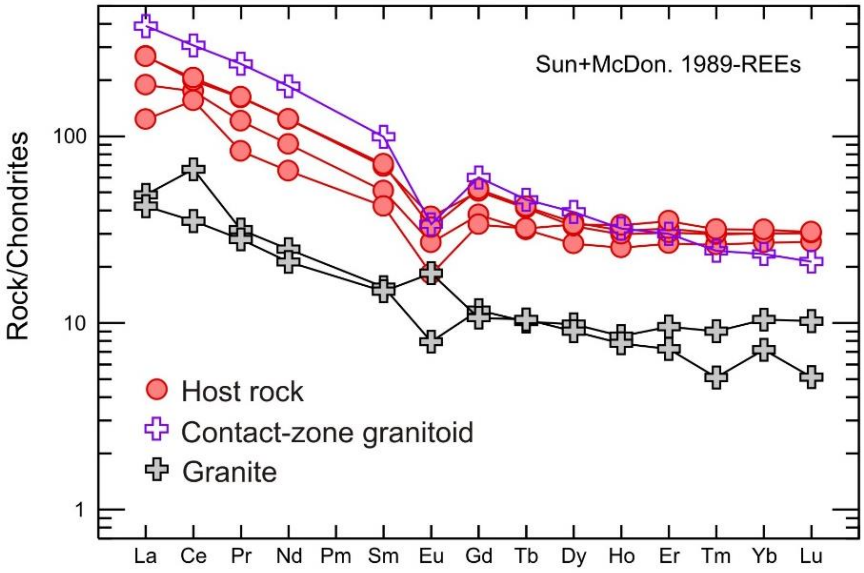

Figure 76: Chondrite normalised spider diagram after Sun and McDonough (1989). The REE data of the host rock are plotted together with the REE data from the contact-zone granitoid and the granite for geochemical comparison. The host rock and the contact-zone granitoid show almost similar geochemical trends and enrichment with respect to the condrite. The host rock and the contact-zone granitoid are a bit more enriched than the two granitic samples. All samples except for one granite sample show negative Eu-anomaly.

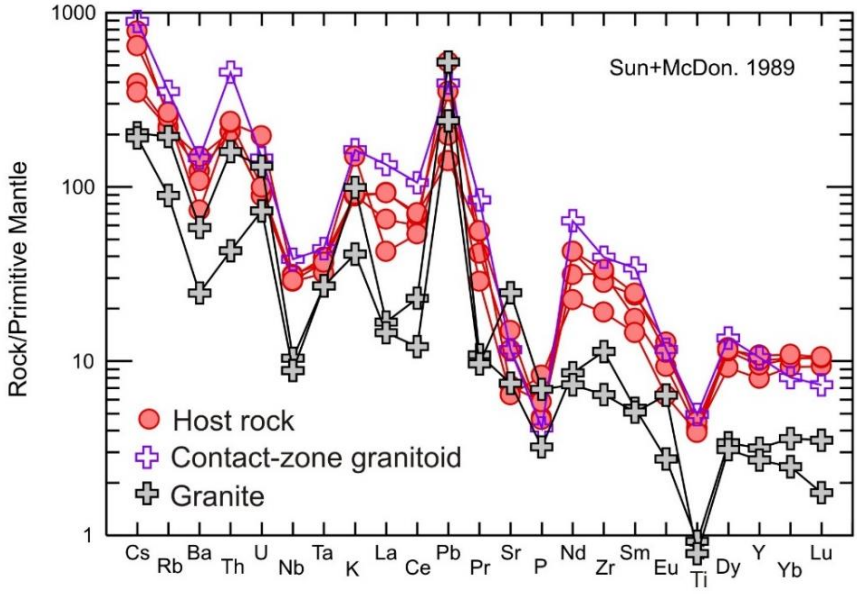

Figure 77: Primitive mantle normalised spider diagram after Sun and McDonough (1989). The rock samples show almost similar geochemical trends and enrichment with respect to the primitive mantle. The granites show similar trends as the host rock and the contact-zone granitoid whit just a slightly lower enrichment for most of the elements, especially from Nd to Lu.

Geochronology

To interpret and understand a geological region with a complex tectonic and magmatic history, reliable geochronological data are required. In this thesis U-Pb zircon dating were used for rock age determination. Zircon is common in plutonic, sedimentary and metamorphic rocks and a chemical resistant mineral that can survive weathering, transportation and metamorphism (Belousova et al., 2002).

The Umbukta gabbro has previously been dated at 576 ±7 Ma (U-Pb zircon age: Senior and Andriessen, 1990), but only in an abstract with no available data. The dated samples for this study were collected east of Mo i Rana, at Umbukta, close to the border to Sweden. The analyses were performed at the Geological Survey of Norway (NGU) with LA-ICP-MS. One gabbro and three quartzites were dated from Umbukta and Østre Sauvatnet.

Gabbro

The gabbro (sample 6.3) is medium-grained (1-2 mm), undeformed and melanocratic with almost even distribution of light and dark minerals. The light minerals mainly consist of plagioclase and the dark minerals mainly consist of pyroxene, biotite and amphibole. A very fine-grained mafic dyke cuts this gabbro sample. Ten zircons were analysed from this sample, and the zircons are prismatic, subhedral to euhedral and colourless (Figure 78). Cathodoluminescence (CL) images show internal oscillatory zoning, but no overgrowth features. The dated zircons resemble primary magmatic zircons (Hoskin, 2000).

Figure 82 shows concordia plot, with 2σ uncertainty of extracted ages from zircons in the gabbro. They are generally concordant and form a linear array with upper intercept at 565 ± 20 Ma. Since the zircons generally are concordant, and do not show significant signs of alteration, the age is interpreted to represent the crystallization age of the gabbro.

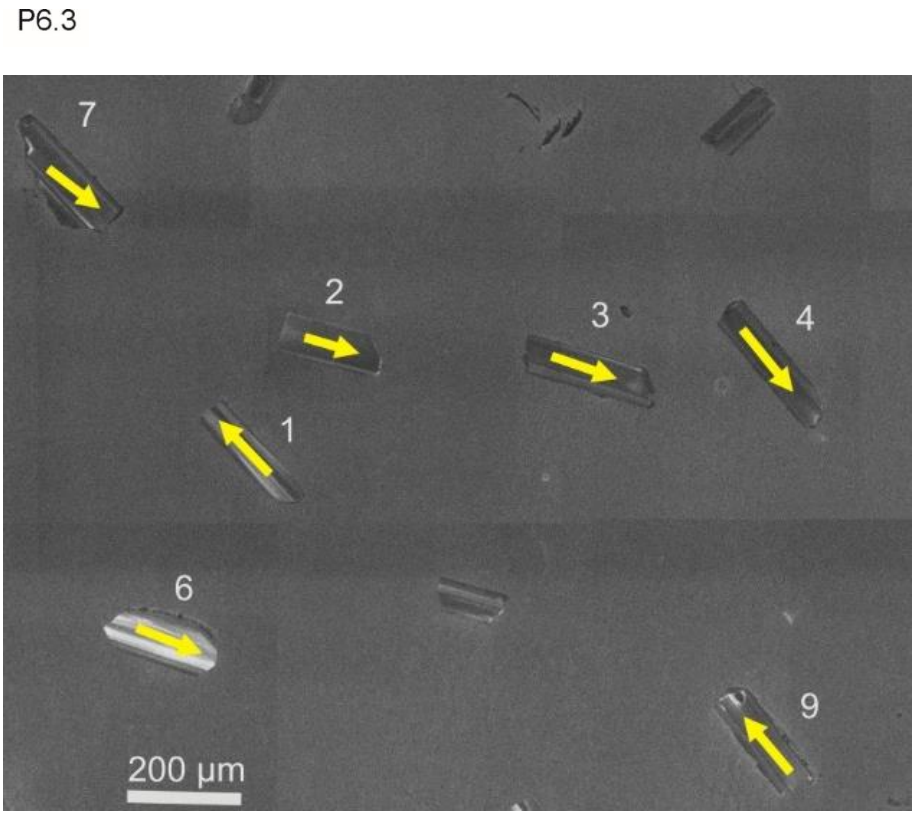

Figure 78: Cathodoluminescence (CL) image of sample P6.3. The photo shows some of the analysed zircons from the Umbukta gabbro.

Quartzite

The quartzites are homogenous, medium-grained (1-2 mm) and contain a few mica grains. Sixteen zircons were analysed from sample P8.1 (Figure 79), 26 from sample P8.6 (Figure 80) and 22 from sample P15.4 ØS (Figure 81). The zircons are rounded, subhedral to anhedral with a yellow-brown colour. Sample P8.6 contains a few prismatic grains. Zircons from sample P15.4 ØS are smaller than zircons from the two other quartzite samples. CL-images show internal growth zoning and some grains have overgrowth features. These zircons are interpreted to be detrital.

Probability density diagrams in Figure 83, 84 and 85 shows the obtained zircon ages in the quartzites. Only analyses that are <10% discordant have been plotted. Sample P8.1 has ages between 1000 and 3600 Ma, sample P8.6 from 1000 to 2800 Ma, with most grains between 1000 and 1500 Ma, and sample P15.4 ØS ages from about 1000 to 1800 Ma. The majority of zircons from all three samples show U-Pb ages between 1000 and 1500 Ma. Sampling of the quartzites is from the same geological area, in such close relations that they most likely

represent the same sedimentary sequence. The three dated rocks show a similar interval of zircon ages. The youngest age of about 1000 Ma, indicates a maximum age of deposition.

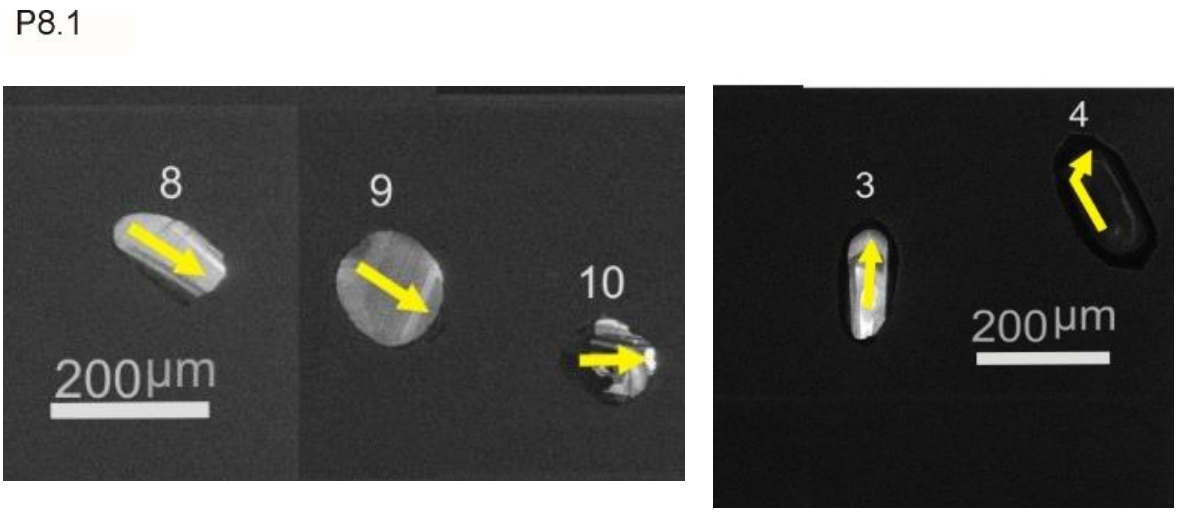

Figure 79: Cathodoluminescence (CL) image of sample P8.1. The images show some of the analysed detrital zircons from the quartzite at Østre Sauvatnet.

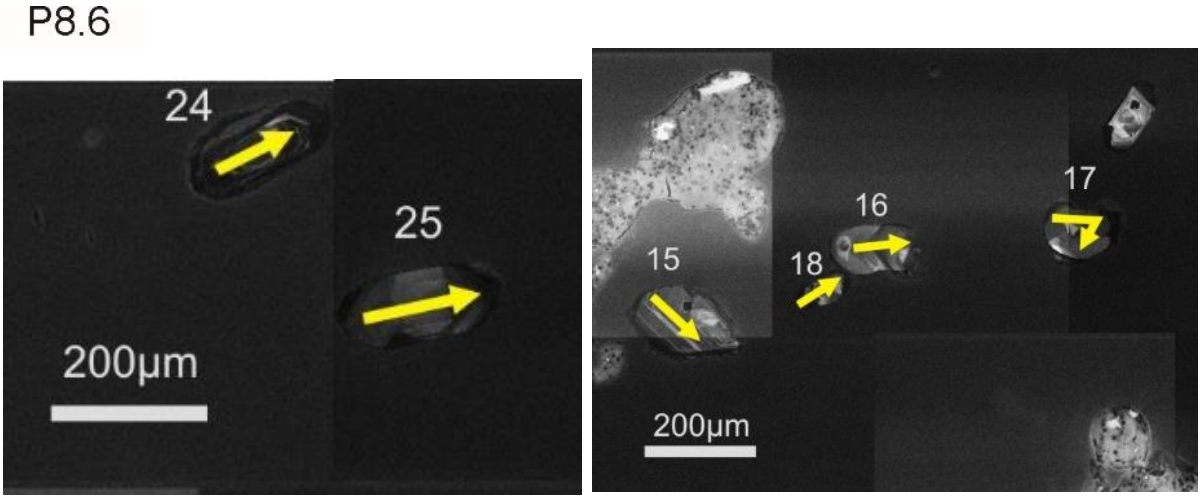

Figure 80: Cathodoluminescence (CL) image of sample P8.6. The images show some of the analysed detrital zircons from the quartzite at Østre Sauvatnet.

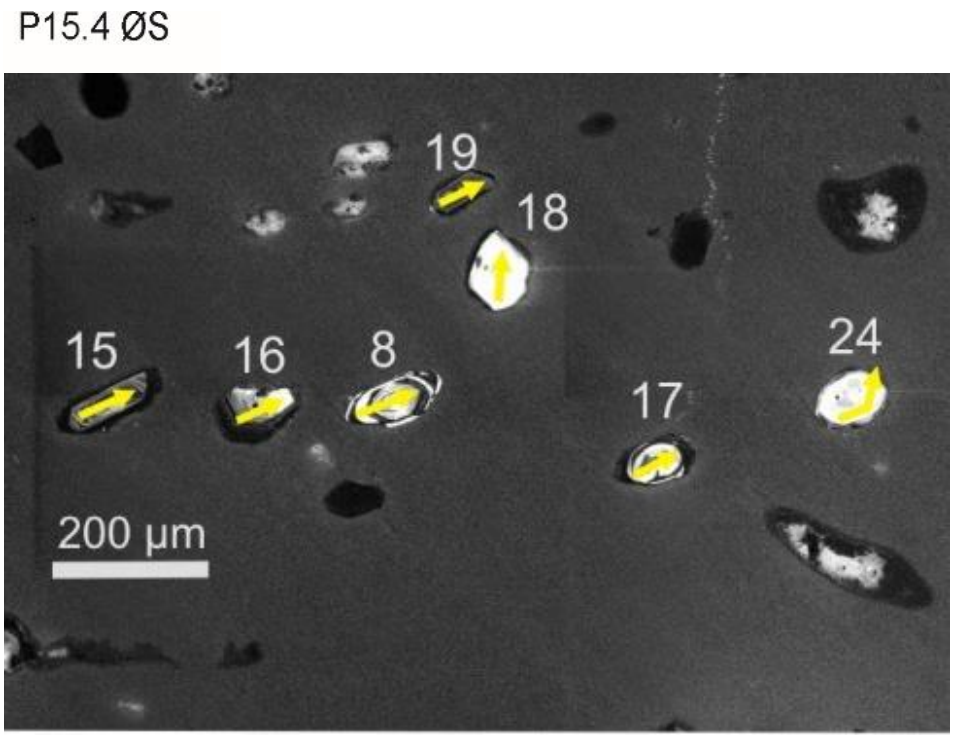

Figure 81: Cathodoluminescence (CL) image of sample P15.4 ØS. The image shows some of the analysed detrital zircons from the quartzite at Østre Sauvatnet.

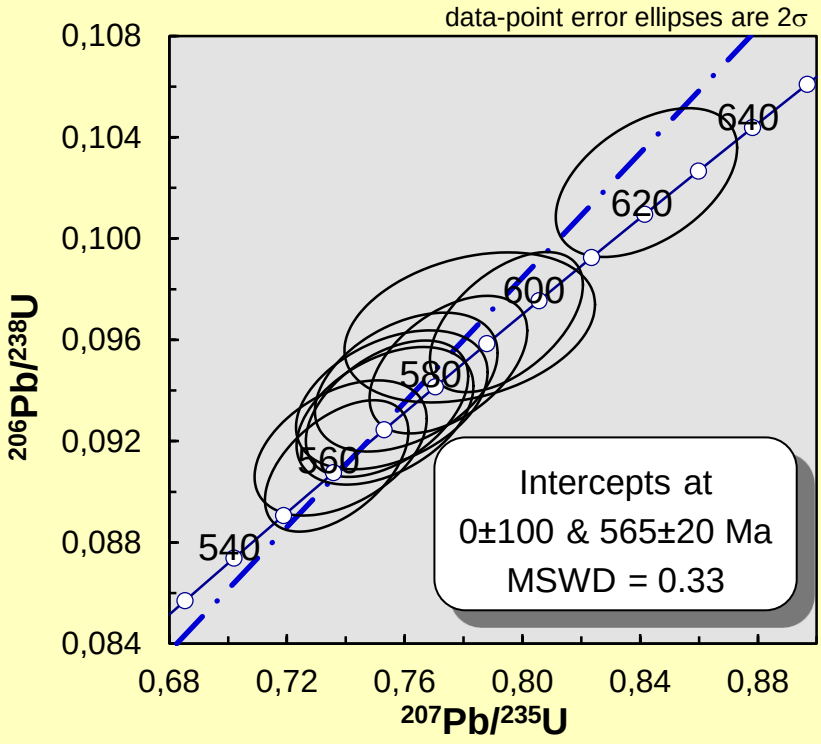

Figure 82: Concordia plot displaying zircon geochronological data from the sample P6.3 of the Umbukta gabbro. Diagram is made by the use of Isoplot.

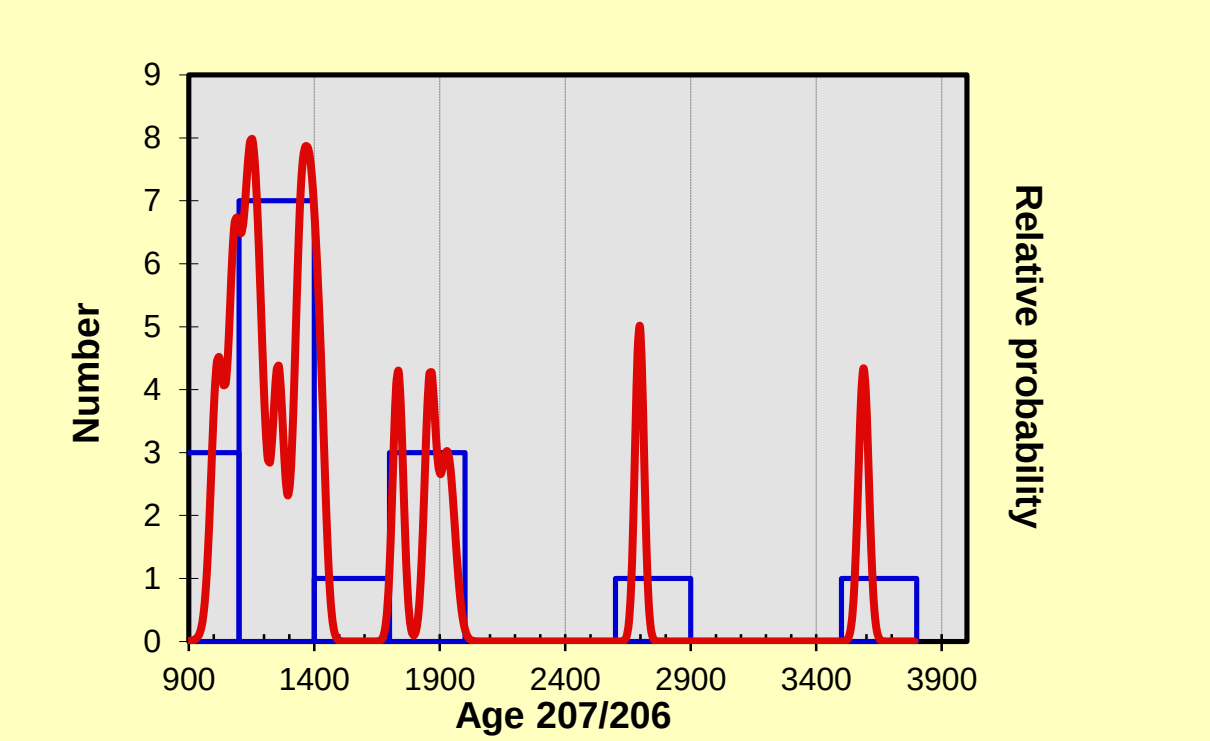

Figure 83: Sample P8.1 showing number/Relative probability versus age plot for <10% U-Pb analyses (appendix E) of detrital zircons from metasediments at Østre Sauvatnet.

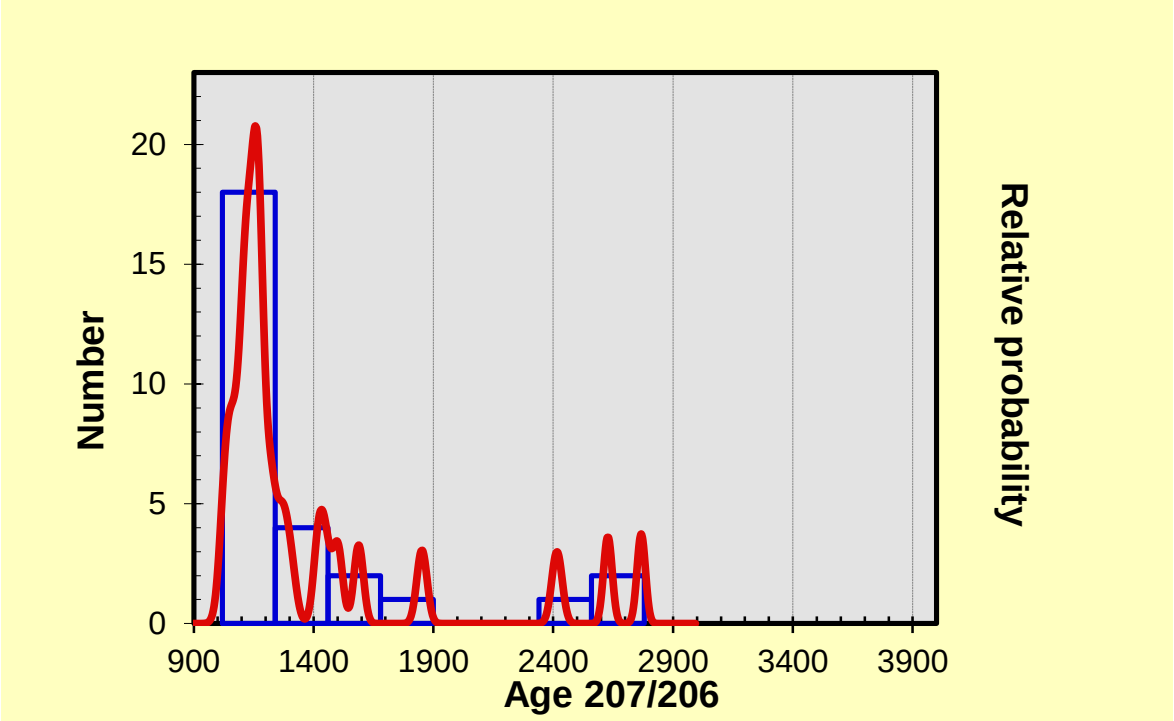

Figure 84: Sample P8.6 showing number/Relative probability versus age plot for <10% U-Pb analyses (appendix E) of detrital zircons from metasediments at Østre Sauvatnet.

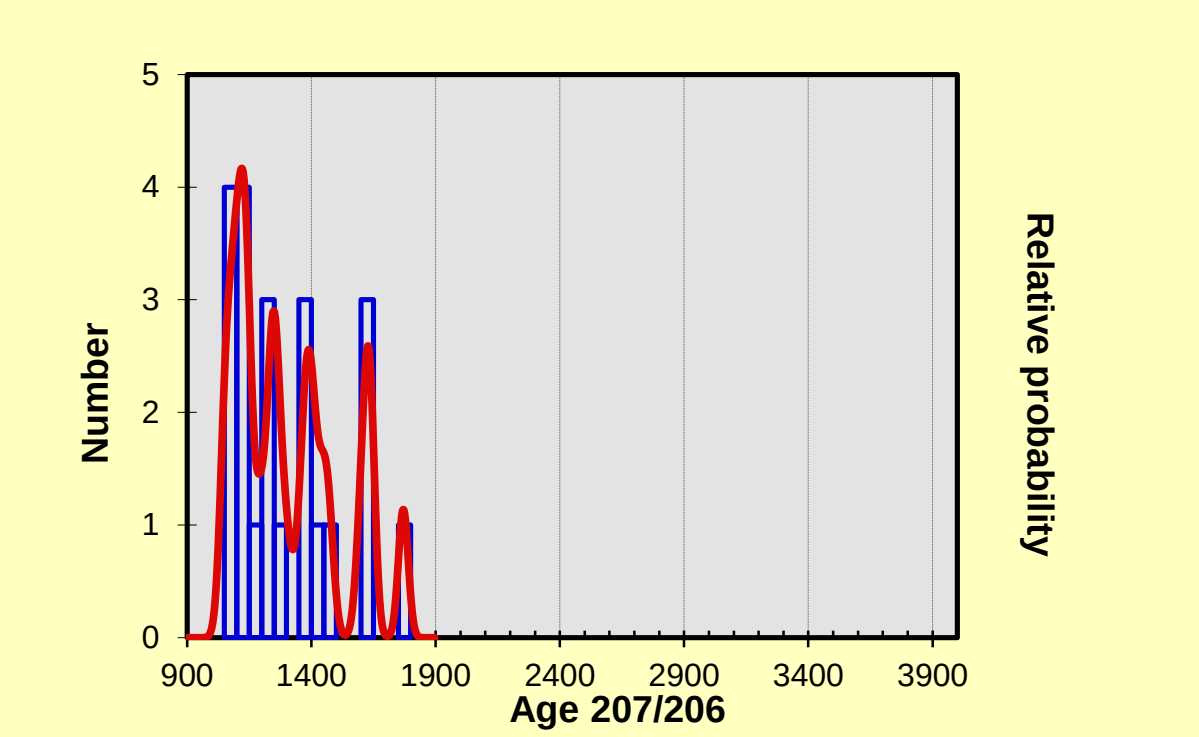

Figure 85: Sample P15.4 ØS showing number/Relative probability versus age plot for <10% U-Pb analyses (appendix E) of detrital zircons from metasediments at Østre Sauvatnet.

Sample	Lithology	UTM_E	UTM_N	Number of zircons	Age (Ma.)
P6.3	Gabbro	485990	7338443	10	565±20
P8.1	Quartzite	488718	7340688	16	Peaks at: 1000 – 1100 1400 1900 1 zircon: 2700 1 zircon: 3600
P8.6	Quartzite	488358	7340841	26	Peaks at: 1000 – 1200 1450 – 1600 1 zircon: 1850 3 zircon : 2400 - 2800
P15.4 ØS	Quartzite	488191	7340870	22	Peaks at: 1100 1250 1400 1650

Figure 86: Table showing the U-Pb age of the gabbro and the analysed U-Pb detrital zircon ages.

Discussion

Geochemical and geochronological analysis from the Umbukta gabbro and mafic dykes, together with field observation have provided interesting results, which is vital for the interpretation of the magmatic and tectonic evolution of the Umbukta gabbro and the mafic dykes. Insight into the crystallization age of the gabbro and its chemical characteristics have opened for discussion of affinities with the gabbros in the Seiland Igneous Province, which has led to further discussion of possible implication of the tectonostratigraphy of the Scandinavian Caledonides.

Field observations

Host rock

The garnet-biotite gneiss is mapped at Kallvatnet, Plurdalen, Saufjellet, Østre Sauvatnet and Umbukta. The garnet-biotite gneiss is segregated into millimetre thick bands of dark minerals of biotite, and light minerals of quartz and plagioclase. Segregation of the minerals is most likely the result of metamorphic processes (Robin, 1979, Winter, 2010).

A hypothesis is that the garnet-biotite gneiss at Kallvatnet/Plurdalen and Saufjellet may be separated from the garnet-biotite gneiss at Østre Sauvatnet and Umbukta. This hypothesis is derived from differences in field appearances. The garnet-biotite gneiss at Kallvatnet/Plurdalen and Saufjellet is medium grained, and has centimetre to metre thick alternating layers of medium-grained garnet-mica schist. In some localities at Kallvatnet/Plurdalen and Saufjellet the garnet-mica schist is the dominating lithology and is mapped as garnet-mica schist instead of garnet-biotite gneiss. At Østre Sauvatnet and Umbukta, the garnet-biotite gneiss is fine-grained and shows diffuse layering.

These differences may stem from changes in depositional environment as transgression or regression, which will change the coarsening of the deposited sediments (Boggs, 2011). Regression or transgression can also lead to unconformities, which come from periods with breaks in deposition. Regression can also result in periods with erosion before new occurrences of deposition (Boggs, 2011). An undiscovered tectonic contact between the medium- and fine-grained garnet-biotite gneisses, which has brought the sediments together, is also a possibility. Another option is just some small regional differences, where a progressive gradual contact

leads one lithology grade into another (Boggs, 2011), and that the medium- and fine-grained garnet-biotite gneisses do represent the same source.

More factors than grain-size and layering have led to a hypothesis of possible separation between the garnet-biotite gneiss at Kallvatnet/Plurdalen and Saufjellet, from Østre Sauvatnet and Umbukta. The rock unit at Kallvatnet/Plurdalen and Saufjellet contain layers of garnet amphibolite. The garnet amphibolite does not cut the layering of the rocks, and is not present at Østre Sauvatnet and Umbukta. Mafic dykes cutting the garnet-biotite gneiss and quartzite at Østre Sauvatnet, do not exist at Kallvatnet/Plurdalen and Saufjellet. At Kallvatnet/Plurdalen and Saufjellet the metasediments also contain boudinaged structures, which imply ductile and deformational conditions (Ramberg, 1955, Fossen and Gabrielsen, 2005). The boudinaged structures are not present at Østre Sauvatnet and Umbukta. Many pegmatite lenses cut the gneissose structures of the metasediments at Kallvatnet/Plurdalen and Saufjellet. Pegmatites are not present at Østre Sauvatnet, but pegmatites are found inside the gabbro at Umbukta. Based on the differences in field appearances between Kallvatnet/Plurdalen/Saufjellet and Østre Sauvatnet/Umbukta, the two rock units are interpreted as not belonging to the same rock unit. Based on field observation and the different lithologies mentioned above, it is assumed that the two rock units most likely are brought together by a tectonic contact.

Gabbro

The Umbukta gabbro has presence of both olivine gabbro and hornblende gabbro and this has led to an interpretation that the Umbukta gabbro probably is a cumulate plutonic rock. In the field, the Umbukta gabbro shows deformational structures in close proximity to undeformed rocks (Figure 87), and the deformation of the gabbro is heterogeneous.

Rocks analysed in thin sections have not developed planar fabrics, which point to non-deformational processes (Winter, 2010), and most of the magmatic texture is preserved, but many of the pyroxene grains are replaced by amphibole. As mentioned it is little sign of deformation and the alteration may result from pyroxene reacting with fluids, late magmatic reaction or changed P-T conditions (Castro and Stephens, 1992). The amphibole has preserved the shape of the pyroxene precursors. If the rock at some point is exposed to hydrothermal fluids, it can lead to hydrothermal alteration of the rock, where the original minerals are chemically replaced by new minerals, as a result of aqueous reactions between the elements in the minerals and the hydrothermal fluids (Giggenbach, 1984). If the H_2O activity increases sufficiently, amphibole becomes stable and re-equilibration might be the effect of alteration

(Castro and Stephens, 1992). Some thin sections show zoning of the amphibole, and it is assumed a more aluminous composition at the margin than in the interior, from hornblende to actinolite. This can be a magmatic process were pyroxene grains react with melt and forms hornblende at the margin while the interior, which is not in contact with the melt, form actinolite by reaction with hydrogen, were the hydrogen atoms diffuse along the grain boundaries (Castro and Stephens, 1992).

Except for the alteration of the pyroxene grains, there are few other signs of alteration. If the rock was exposed to element mobility the normalized-element plots should display strongly scattered patterns (Slagstad et al., 2004). The elements presented here display no such scatter, which implies a homogenous chemistry that has not been strongly affected by element mobility and alteration. It is assumed that the rocks reflect an approaching composition of the melt and not just cumulate phases.

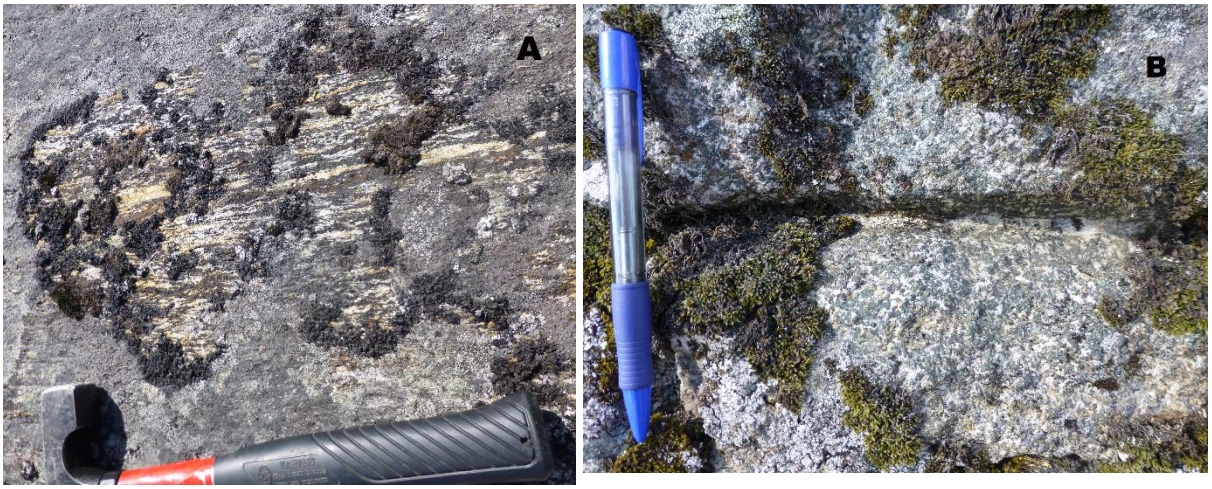

Figure 87: A) A deformed gabbro, and B) an undeformed gabbro (GPS: 483025Ø, 7338181N)

Mafic Dykes

The very-fine grained mafic dykes are present in the Umbukta gabbro, the garnet-biotite gneiss at Østre Sauvatnet and Umbukta, in the contact-zone, and in the quartzite at Østre Sauvatnet. No chilled margins have been observed between the mafic dykes and the gabbro or between the mafic dykes and the garnet-biotite gneiss. Chilled margins are known to form when a hot magma intrudes into a cold country rock (Latypov et al., 2007), and the absence of chilled margins are probably a result of intrusion shortly after emplacement of the gabbro, when both the gabbro and the mafic dykes were hot (Vernon et al., 1988). The garnet-biotite gneiss must

also been heated since there is no chilled margins between the mafic dykes and the garnet-biotite gneiss. Since the mafic dykes cut through all of the rocks at Umbukta and Østre Sauvatnet, they must post-date these rocks. Abundant field evidence shows the mafic dykes cutting the gneissose texture of the garnet-biotite gneiss (Figure 88), which indicates the mafic dykes to post-date the deformation of the garnet-biotite gneiss.

In thin section the magmatic texture of the mafic dykes is preserved, and there is no sign of mineral orientation. The mafic dykes mostly compose of amphibole and plagioclase minerals. A few pyroxene grains do occur, and a secondary formation is assumed for the amphibole in the mafic dykes, as previous discussed for the amphibole in the gabbro. Some samples show dark green rims, interpreted to be hornblende, and a paler core, interpreted to be actinolite. Initially, it probably was presence of pyroxene or olivine grains, which was altered and rimmed by the amphibole. This alteration is probably a result of the same processes as discussed for the alteration of the pyroxene grains in the gabbro. The minerals have probably not grown during deformation since the magmatic texture is preserved and the minerals do not show orientation, and most likely, the alteration is a result of either fluid interaction or a late magmatic reaction.

Figure 88: Mafic dyke cutting the host rock at Østre Sauvatnet, showing a sharp contact.

Contact-zone relationships

A sharp contact between the gabbro and the garnet-biotite gneiss is not found while mapping the area at Østre Sauvatnet, but an area between them is referred to as the contact-zone. The contact-zone shows evidence of mingling. The rocks in the contact-zone mainly consist of contact-zone granitoid, mafic- dykes and enclaves, and granitic veins.

Approaching the gabbro from Østre Sauvatnet, the gneissose texture of the garnet-biotite gneiss mostly disappears and the rock generally becomes a bit darker than the garnet-biotite gneiss, but some leucocratic outcrops are present as well, both with randomly distributed minerals. This rock has been referred to as the contact-zone granitoid (Figure 89). The contact-zone granitoid may result from the hot gabbro intruding the pre-existing host rock of mainly garnet-biotite gneiss. The intrusion of the hot mafic melt has probably superheated the garnet-biotite gneiss, decreased the viscosity and melted it to fluid conditions (Vernon et al., 1988, Blake, 1981). The viscosity contrast between the mafic magma and the melted host rock has probably prevented widespread mixing of the two melts (Morogan and Sørensen, 1994). Geochemical analyses were only performed on one sample from the contact-zone granitoid. When this sample is plotted together with the geochemical data from the host rock, they show the same geochemical trends (Figure 76 and 77). More samples of the contact-zone granitoid should be analysed before drawing any conclusion, but this indicates that the contact-zone granitoid probably resulted from melting of the host rock, with little melt-residue separation. Some places the contact-zone granitoid has inclusions of centimetre-sized patches of the host rock, which probably was the protolith of the contact-zone granitoid.

Figure 89: Contact-zone granitoid, cut by a mafic dyke. The mafic dyke lays at the left side of the pen (GPS: 488954Ø, 7339143N).

In the contact-zone, both mafic- dykes and enclaves are present. The mafic enclaves are often cut and surrounded by granitic veins. The granitic veins show several similarities to what has been referred to as net-veined complexes (Blake, 1981, Dunham, 1964, Morogan and Sørensen, 1994) or back-veining (Hoek and Schaefer, 1998, Jayananda et al., 2009). This is known to be an outcome from mingling of felsic and mafic magmas (Blake, 1981). The mafic enclaves vary from angular, subrounded to pillow shaped structures, are mesanocratic, very fine grained and do not show any internal fabric. The mafic enclaves probably entered the contact-zone as mafic dykes, and disintegrated into mafic enclaves as they rapidly entered the host rock (Morogan and Sørensen, 1994). The disintegration of the mafic dykes, and pillow structure of some mafic enclaves indicates a melt host rock, which was intruded by mafic dykes (Blake, 1981), and the two melts appears to have been coeval.

Mafic melts have a higher crystallization temperature than felsic melts and will solidify at higher temperatures (Blake, 1981). The mafic gabbro probably heated the host rock, which the mafic dykes also intruded, and this probably led to partial melting of the host rock, which than became remobilised and formed the granitic composition, which back- veined into the cooling

mafic phase (Clemens, 2003, Timoleon et al., 2012, Blake, 1981, Jayananda et al., 2009, Morogan and Sørensen, 1994). The granitic veins have been analysed geochemically to an S-type granite, which is an indication of a sedimentary protolith of the source rock (Frost et al., 2001), which agrees with field observations. Hoek and Schaefer (1998) suggested that mafic melt loses about 10% of its volume when it crystallises, and probably form small cracks when they cool. The felsic granitic melt probably was fluid long after the mafic magma solidified (Blake, 1981), and this may partially explain why the granitic melt back-veined into the cooling mafic enclaves, and formed net-veined complexes. Granitic veins also occur in the garnet-biotite gneiss and sometimes they occur as larger bodies, which cut the gneissose texture (Figure 90). Just a small amount of the granitic rock is present, and the granitic- veins and bodies are almost without exception seen in close proximity to the mafic- dykes and enclaves.

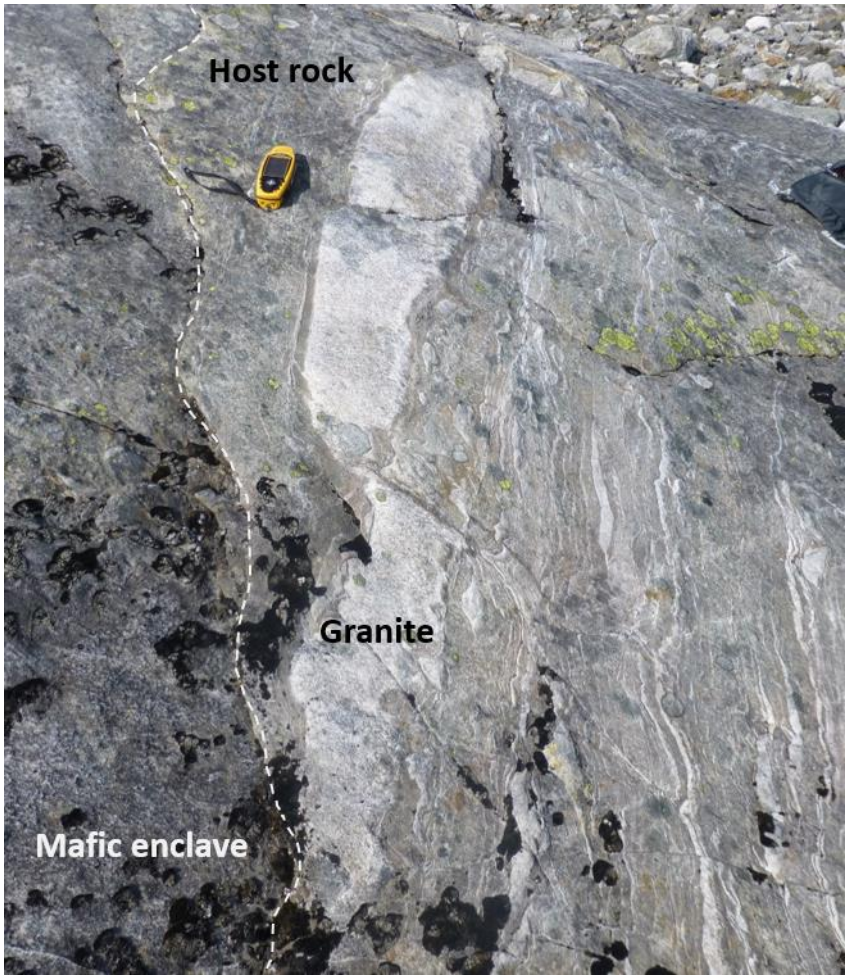

Figure 90: Millimetre to centimetre thick granitic veins and a centimetre sized granitic bodies in the garnet-biotite gneiss. The granitic bodies cut the gneissose texture. (GPS: 488673Ø, 7341089)

Mixing may have been possible between the two melts, but only in a narrow time/temperature window (Vernon et al., 1988), and if the viscosity contrast between the mafic magma and the melted host rock at some point was very low. The temperature and the viscosity contrast between the two melts probably have the largest impacts on the mixing process, but dynamic and chemical processes may also affect the degree of mixing (Sparks and Marshall, 1986). However, it is assumed that the contact-zone granitoid mainly formed from contact melting, caused by heat from the intruding mafic magma, and mingling probably was the main process between the two melts. The contact-zone granitoid at Østre Sauvatnet only occurs in an area of about 500-800 meters from the gabbro.

The mapped area shows no sign of a tectonic contact between the host rock and the gabbro, and the contact-zone relationship is interpreted to stem from heat derived from the intrusive gabbro. The intruding gabbro would not cause sufficient amount of pressure to cause the gneissose texture in the garnet-biotite gneiss. This textures must be a result of earlier deformation, as previously discussed, also indicated by mafic dykes cutting the structures in the host rock

Geochemical characteristics

The chemistry of a magma can be a tool to distinguish between different petrological processes and tectonic settings (Verma et al., 2006). Trace elements are often studied in groups, and abnormal group behaviour is helpful in distinguishing between petrological processes (Best, 2003). When a magma goes through different phases and evolves, different trace elements will be incorporated or excluded in the different processes, with much more selectivity than major elements (Winter, 2010). This provides important petrogenetic information on the origin and evolutionary process of a melt system (Best, 2003).

The AFM diagram (Figure 59) was used to determine if the gabbro and the mafic dykes belong to a tholeiitic- or calc-alkaline composition. The AFM diagram uses major elements to separate between the two types. The P_2O_5-Zr diagram combines immobile minor and trace elements, and is robust against alteration (Floyd and Winchester, 1975), and the P_2O_5-Zr diagram (Figure 70) was used to separate possible alkaline magmas from tholeiites. The analysed rock samples clearly plot in the tholeiitic field in both diagrams. Tholeiitic rocks commonly relate to zones of crustal extension (Philpotts, 2003). Typically, they develop along mid-ocean ridges (MORB) and produce thick sequences of flood basalts, but they also develop on large oceanic islands, such as Hawaii (Philpotts, 2003).

The chondrite normalized REE diagram after Sun and McDonough (1989) (Figure 60) shows enrichment of the REEs. The REE patterns of the samples mostly show similar negative slopes and indicate a similar enrichment of the light rare earth elements (LREE). The less incompatible HREEs, to the right of the diagram, show a lower enrichment than the highly incompatible elements to the left of the diagram, and overall the REE patterns show enrichment with respect to chondrite (Mandal et al., 2012). The enriched LREE pattern is characteristic for continental and ocean island basalts (Cottle and Cooper, 2006). The pattern indicates a magma that either has been through a period of fractional crystallization, melting of a mantle source with chondritic composition or enrichment from assimilation and contamination of the mafic melt (Coish and Sinton, 1992), as it intruded into the continental crust. Some samples show a very slight positive Eu anomaly, and Eu^{2+} is compatible with plagioclase and substitutes for Ca^{2+}. When Eu^{2+} substitutes for Ca^{2+} in plagioclase, the REE pattern will either show a positive or a negative anomaly on the diagram. A positive anomaly indicates a plagioclase accumulation while a negative anomaly indicates plagioclase fractionation (Winter, 2010). So this slight positive Eu anomaly probably results from plagioclase accumulation (Cottle and Cooper, 2006, Winter, 2010).

Characteristic for the within-plate tholeiitic magma relative to MORB is enrichment of the incompatible trace elements (Sr, K, Rb, Ba, Th, Ta, Nb, Ce, P, Zr, Hf, Sm, Ti), especially the most incompatible elements such as Th, Ba and Nb, whereas Y and Yb show little change (Pearce, 1982). Trace elements from the Umbukta gabbro and mafic dykes in the MORB normalized spider diagram after Pearce (1983) (Figure 62) show enrichment of the incompatible trace elements compared to the MORB, except from Y and Yb. Enrichment of Ba, Th, Nb and Ta, which means no negative anomaly for Ta and Nb, provides a good indication for a within plate setting and not a subduction related mantle source (Pearce, 1983, Coish and Sinton, 1992).

The primitive mantle normalized spider diagram after Sun and McDonough (1989) (Figure 64), also indicates a continental affinity of the trace element pattern. The diagram shows relative enrichment in the trace elements for the Umbukta gabbro and the mafic dykes, which is characteristic for intracontinental settings (Xia, 2014), and the enriched pattern also separates it from subduction related settings (Xia et al., 2013). No negative anomaly is registered for Nb, Ta, and Ti, and this supports formation in an intracontinental setting and not an arc related environment (Xia, 2014). Most of the samples show a positive Pb anomaly, which is typical for continental affinity (Hofmann, 1997).

Four different tectonic discrimination diagrams were used for further indication of possible tectonic setting of the Umbukta gabbro and the mafic dykes (Figure 66 to 69). Most of the analysed samples are of plutonic rocks, and their composition probably represents a magma (mix of melt and cumulate phases), and not a melt (Irvine, 1982). Discrimination diagrams are based on liquid composition of the rock, to perform paleo-tectonic classification (Bédard, 1994). The gabbro and the mafic dykes show quite similar geochemistry. The dykes probably represent an approximate composition of the melt, and the cumulate-bearing gabbro may not be far from having a melt composition. Despite the cumulate contents of the gabbro, and the uncertainties this brings, it is assumed that these diagrams represent valid information.

The Ti-Zr-Y- and the Zr/Y-Zr diagrams (Figure 66 and 67) mainly show samples plotting in fields of within-plate basalts, which include both ocean island basalts and continental basalts (Pearce and Cann, 1973). The Zr-Nb-Y- and La-Y-Nb diagrams (Figure 68 and 69) show a bit of scattering of the plotted data. In the Zr-Nb-Y diagram of Meschede (1986), most samples plot in the A2 field, which implies within-plate basalts. The diagram does not give a good indication if the source is alkalic or tholeiitic. Three samples plot in field A1, and this implies alkalic affinity, and two samples plot in field B, which indicates E-MORB source. No sample plot in field C, which supports within-plate tholeiitic basalt. The Zr-Nb-Y diagram has been criticized for not being able to distinguish between within-plate alkali basalts and within-plate tholeiite (Rollinson, 1993, Wang and Glover, 1992). Still it supports a within-plate setting, which is compatible with the data plotted in the other diagrams. In the La-Y-Nb diagram of Cabanis and Lecolle (1989), the samples plot in three fields of the diagram. Five samples plot in the field of continental basalts, and the rest divides between E-MORB, and alkaline continental rift. Except for the samples plotting in the field of E-MORB, this diagram also indicates some kind of continental to intracontinental rift setting.

The geochemical data presented in this thesis for the Umbukta gabbro and the mafic dykes, indicate a mantle source enriched in REEs, and the major elements in the AFM diagram show a tholeiitic rock composition. The tectonic discrimination diagram points to a within-plate setting of either ocean island basalts or continental basalts. The trace element diagrams support a within-plate setting and exclude arc- or subduction related settings. If the rocks were formed in a within-plate setting, they were most likely related to an intracontinental rifting or intracontinental back-arc extension.

The enriched trace elements and the homogenous REE pattern of the Umbukta gabbro, and the mafic dykes, are not that different from the gabbros and the mafic dykes of the Seiland Igneous

Province (SIP). Comparison between the rocks therefore seems reasonable, and will be discussed later in this thesis.

Chemical analyses were also performed on two granite samples and one contact-zone granitoid from Østre Sauvatnet. The granites have a SiO_2 content of 75.8 and 77.8 wt.%, and the geochemistry of the rock samples have given a A/CNK (molar $Al_2O_3/CaO+Na_2O+K_2O$) = 1.21 and 1.55, which indicates a peraluminous composition (Maas et al., 1997). The contact-zone granitoid has a SiO_2 content of 60.4 and an A/CNK (molar $Al_2O_3/CaO+Na_2O+K_2O$) = 1.48, which also show a peraluminous composition. A peraluminous composition is typically S-type granite and interpreted to form by melting of a sedimentary protolith (Frost et al., 2001, Chappell and White, 1974), and it is also inferred to have high SiO_2 content (64-77 wt. %) (Chappell and White, 1974). The S-type composition corresponds well with field observations, were the granitic- veins and bodies are interpreted to form from partial melting of metasediments, and that the contact-zone granitoid probably formed from contact melting of an intruding hot mafic magma.

In Figure 76 and 77 two samples of the granites is plotted together with the host rock. The granites show a lower geochemically enrichment then the host rock, especially for the REEs. Incompatible trace elements are known to preferentially partition into the melt (Winter, 2010). Accessory minerals such as zircon and monazite often concentrate most of the REEs, because these elements are essential structural components in the zircon and monazite, and the REEs will strongly partition into these minerals (Miller and Mittlefehldt, 1982, Watt and Harley, 1993, Watson and Harrison, 1984). If zircon and/or monazite is not consumed during partial melting, but stays left in the restite, the REEs will stay in the zircon and monazite rather than partition into the melt (Watt and Harley, 1993). This may be an explanation for the lower enrichment of the trace elements in the granite. Another possible explanation for the lower concentration of the trace elements may be if the incompatible trace elements did partition into the melt formed by partial melting, and if some of the melt started to crystallize, the incompatible trace elements would partition and concentrate in the remaining melt (Winter, 2010), which could have left the crystallising phase. The crystallising phase would then be depleted in the incompatible trace elements. This is only a speculation, because more samples, analyses and reach must be performed before more curtain assumptions can be made.

Geochronology

To get the most reliable interpretation and understanding of the region, a geochronological framework is important. The gabbro and the metasediments were dated by U-Pb elements in zircons, and the crystallising age of the Umbukta gabbro is 565 ± 20 Ma. This is not a common rock age dated in the Scandinavian Caledonides (Bingen and Solli, 2009). The age of the Umbukta gabbro is similar to the age of the gabbros in the SIP (Roberts et al., 2006, Roberts, 2007), and the similarity will be further discussed below. Detrital zircon ages can give indication of the metasedimentary provenance, and an approximate maximum age of sedimentary deposition (Kirkland et al., 2007). The analysed detrital zircon ages from Østre Sauvatnet present depositional ages from 3600 to 1000 Ma, and manly peaks at 1900-1850, ca. 1650-1600, ca. 1400 and ca. 1200-1000 Ma. The youngest detrital zircon age, which was analysed, had a detrital zircon depositional age of 1000 Ma, which means that the metasediments at Østre Sauvatnet was deposited after 1000 Ma ago. The metasedimentary depositional ages correlates relatively well with the metasedimentary depositional ages in the KNC, and this will also be further discussed below.

Tectonostratigraphy of the Uppermost Allochthon in Nordland

The Umbukta gabbro, mafic dykes, and metasediments of the Kjerringfjell Group are located in the Rödingsfjället Nappe Complex in the Rana region in Nordland. The Rödingsfjället Nappe Complex is interpreted to be a part of the Uppermost Allochthon, and overlain by the Helgeland Nappe Complex (Roberts et al., 2007, Barnes et al., 2007), which is structurally the highest nappe complex of the Uppermost Allochthon (Barnes et al., 2007). These two nappes dominate the Uppermost Allochthon (Roberts et al., 2007) (Figure 91).

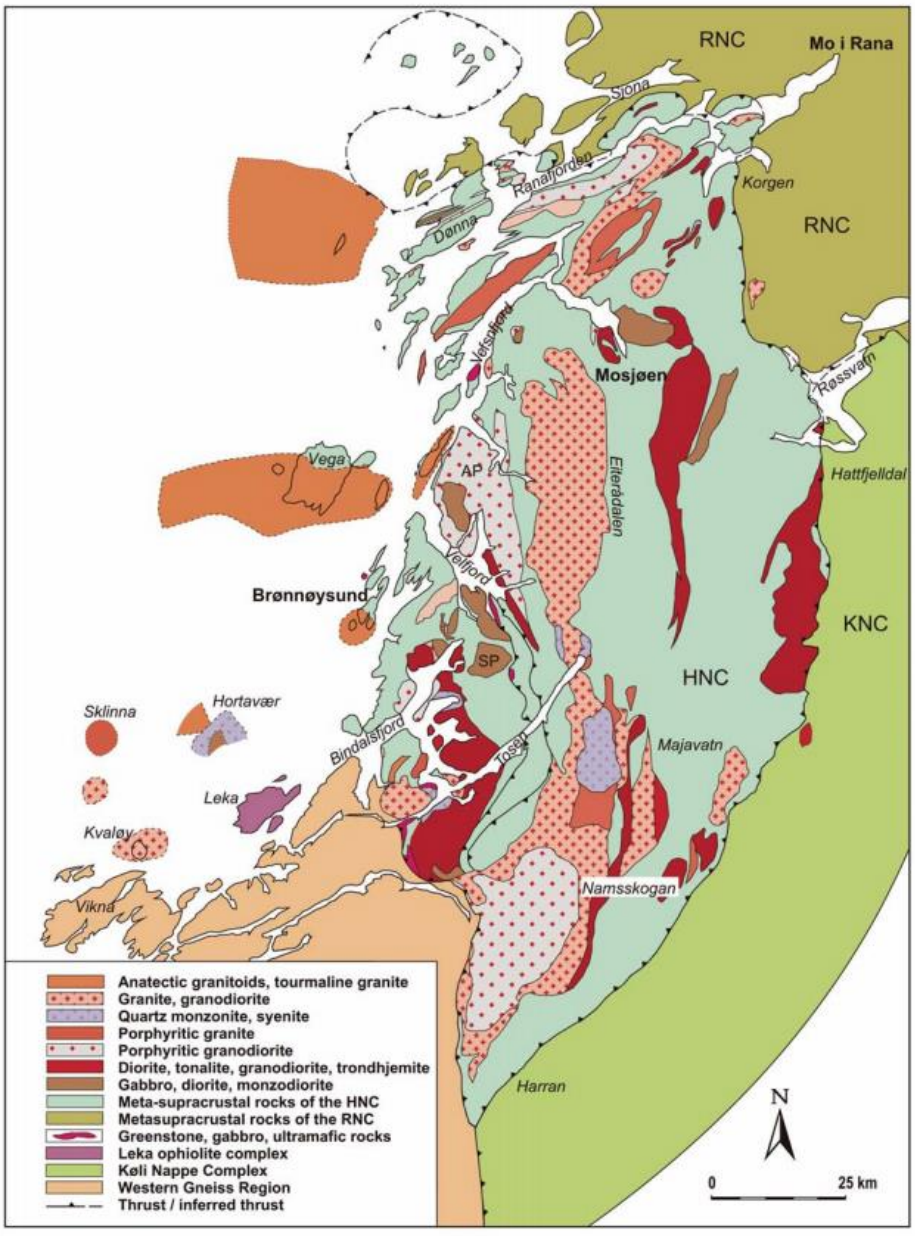

Figure 91: Geological map of Nordland in North-Central Norway. HNC = Helgeland Nappe Complex, KNC = Köli Nappe Complex (part of the Upper Allochthton), RNC = Rödingsfjället Nappe Complex. Figure from Roberts et al. (2007)

The Helgeland Nappe Complex (HNC) consists of five nappes. From structurally lowest to highest these are the Horta, Sauren-Torghatten, Lower, Middle, and Upper nappes. The Horta Nappe is the host of the Hortavær intrusion (Barnes et al., 2007, Barnes et al., 2011). The Sauren-Torghatten and Middle Nappes are characterized by a basal sliver of metaperidotite (serpentinite) and gabbro (Barnes et al., 2011). These slivers are conformably overlain by metasedimentary and metavolcanic rocks composed of metawackes, metapelites, calc-silicate rocks, and marbles, with interbedded conglomerates (Barnes et al., 2007). The rocks in these nappes were metamorphosed at amphibolite facies (Barnes et al., 2007). The Lower and Upper

Nappes consist almost entirely of metasedimentary rocks of high-grade semipelitic schist and gneiss, quartzo-feldsphatic gneiss, and marble. Most of the quartzo-feldspathic gneiss is migmatitic and indicates regional metamorphism at upper amphibolite to lower granulite facies (McArthur et al., 2014, Barnes et al., 2007). The Uppermost Allochthon hosts a number of plutonic complexes. The Bindal Batholith is the largest of these and contains more than 50 individual plutons (Roberts et al., 2007), intruding the Helgeland Nappe Complex. The rocks range from mafic gabbro to leucogranite, mainly of calc-alkaline and shoshonitic composition (Nordgulen et al., 1993). The plutonic rocks of the Bindal Batholith span over an age range from 478 to 424 Ma. (Barnes et al., 2011, Yoshinobu et al., 2002).

The Rödingsfjället Nappe Complex divides into six nappes (Figure 92) and covers most of the Rana region (Melezhik et al., 2015). Not much is known about the Rödingsfjället Nappe Complex, but the main component of the complex is medium-to high-grade metasedimentary rocks of marbles (Melezhik et al., 2015). One of the nappes in the Rödingsfjället Nappe Complex is the Ravnålia Nappe, which is separated into three lithostratigraphic units, the Kjerringfjellet Group, the Dunderland Formation, and Ørtfjellet Group, where the Kjerringfjellet Group is at the bottom of the Ravnålia Nappe (Melezhik et al., 2015). In this thesis part of the Kjerringfjellet Group has been mapped, and mainly consists of garnet-biotite gneiss, garnet-mica schist, quartzite, pegmatite, gabbro and mafic dykes. The gabbro and mafic dykes crosscut the metasedimentary rocks.

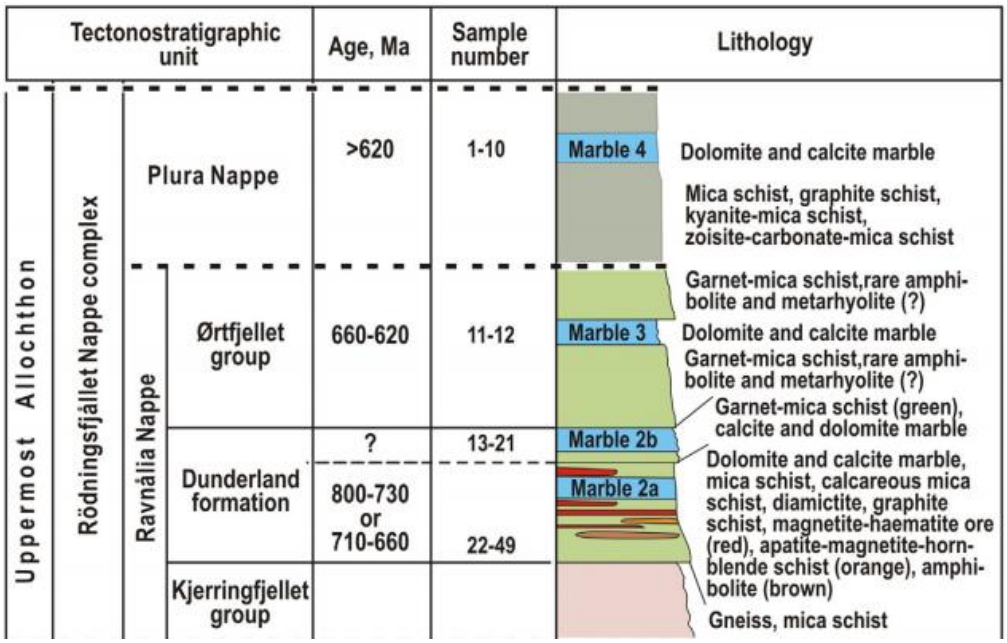

Figure 92: A simplified tectonostratigraphic column for the Rödingsfjället Nappe Complex in the Rana region. Figure is modified from Melezhik et al. (2015).

The rocks in the Helgeland Nappe Complex and the Rödingsfjället Nappe Complex contain plutonic rocks intruding metasedimentary rocks. Both nappes contain marbles, calc-silicate rocks and marbles interbedded with conglomerates or migmatitic quartzo-feldspatic gneiss.

The metasedimentary rocks in the Lower Nappe and Sauren-Torghatten Nappe of the Helgeland Nappe Complex contain quite similar ages for their metasediments. The Lower Nappe have detrital zircon ages with peaks at 900, 1150, 1450, 1800 and 2800 Ma (Barnes et al., 2007). The Sauren-Torghatten Nappe has similar detrital zircon ages as the Lower Nappe, but also contain some flysch-metasedimentary rocks of Ordovician age at about 480 Ma (Barnes et al., 2007). Except for the Ordovician age, the detrital zircon ages are quite similar to those dated in the Kjerringfjell Group of the Rödingsfjället Nappe Complex. The Middle and Upper nappes of the Helgeland Nappe Complex contain similar detrital zircons from Ordovician time about 480 Ma, and the Upper Nappe does not contain detrital zircons older than 1000 Ma (Barnes et al., 2007). This is much younger than the detrital zircon ages in the metasediments in the Kjerringfjell Group, which has ages from about 1000 Ma to Archean.

Both the Helgeland Nappe Complex and the Rödingsfjället Nappe Complex contain abundant units of marble. The marbles in Helgeland Nappe Complex have depositional ages from 650 to 590 Ma (Barnes et al., 2007, Sandøy, 2003), while the marbles dated in the Dunderland Formation, Ørtfjellet Group, and Plura Nappe, which is part of the Rödingsfjället Nappe Complex, have depositional ages from 800 to 620 Ma. (Melezhik et al., 2015). There is a little overlap between these depositional ages, but mostly the marbles in the Rödingsfjället Nappes Complex have older depositional ages than the marbles in the Helgeland Nappe Complex. The Bindal Batholith in the Helgeland Nappe Complex consists of calc-alkaline gabbro to monzodiorite and syenite (Roberts et al., 2007), the different plutons have ages from 478 to 420 Ma (Roberts et al., 2007, Yoshinobu et al., 2002). The pluton in the Kjerringfjell Group of the Rödingsfjället Nappe Complex, consist of a tholeiitic gabbro with a U-Pb age of 565 ± 20 Ma, which provides an earlier intrusion age than the plutons in the Helgeland Nappe Complex. Different geochemical chemical signatures of the plutons also imply that they most likely originated from different sources and in different tectonic settings.

The lithology of the Uppermost Allochthon are characterised with extensive carbonate formation, voluminous granitoid plutons and, in places large stratabound iron formation, which do not occur in subjacent thrust sheets (Roberts et al., 2007, Stephens and Gee, 1985). An exotic origin has generally been suggested from either Laurentia or unknown microcontinents (Roberts et al., 2007, Stephens and Gee, 1985). Interpretation of Middle Ordovician crust-

melting events, NW to W vergent thrusting, and U-Pb zircon ages in the Uppermost Allochthon have related it to the Taconian orogenesis, which is a pre-Scandian event (Yoshinobu et al., 2002, Roberts et al., 2007). The Taconic orogeny is related to an arc-continent collisional event (McKerrow et al., 2000, Ratcliffe et al., 1998, Robinson et al., 1998), and affected most of the western New England (northeastern North America). Before the arc-continent collision, it probably was a long period of subduction and continental shortening (Ratcliffe et al., 1998). The time span of the mountain-building event of the Taconic orogeny probably lasted from 495 to 450 Ma, and the most intense collisional phase between Laurentia and the magmatic arc probably was in the period of Early to Middle Ordovician (475-459 Ma) (Van Staal et al., 2007).

The Helgeland Nappe Complex and the Rödingsfjället Nappe Complex composes of both different and similar lithostratigraphy, and they are interpreted to belong to the Uppermost Allochthon, which is exotic to Baltica (Melezhik et al., 2002, Roberts et al., 2002, Yoshinobu et al., 2002). No currently available research conflicts with this interpretation. A thrust front named the Langfjell zone (Figure 12), southeast of Mo i Rana, may be a correlation point for the two Nappe Complexes. Unpublished dating of syntectonic pegmatites in the Langfjell zone has given a Taconic age of about 470 Ma, of this thrust front. The unpublished U-Pb dating was made by Slagstad from NGU.

Correlations with the Seiland Igneous Province (SIP)

The Kalak Nappe Complex (KNC) of Northern Norway is a series of stacked thrust sheets, which are separated into lower- (Kolvik and Olderfjord) and upper (Sørøy-Seiland, Havvatnet and Veines) nappes. The Sørøy-Seiland Nappe contains the Sørøy Group. The Sørøy Group is intruded by igneous rocks, which are generally referred to as the Seiland Igneous Province (SIP) (Figure 93), and the KNC is interpreted to belong to the Middle Allochthon (Roberts and Gee, 1985). The metasedimentary protolith of the KNC has classically been interpreted as a continuous depositional sequence, termed the "Sørøy Succession" (Zwaan and Roberts, 1978), originating in sedimentary basins on the continental margin of Baltica, during Ediacaran time through the development of the Iapetus Ocean (Sturt et al., 1978). Detrital zircon U-Pb dating and isotope chemostratigraphy, performed by newer research, has given the metasedimentary depositional ages of rocks in the Sørøy Succession. The ages have led to a suggestion that the metasediments of the KNC probably do not belong to a continuous depositional sequence (Slagstad et al., 2006). The lower nappes have similar detrital zircon populations, and separates from the detrital zircon ages in the upper nappes (Kirkland et al., 2007). The metasediments in

the lower nappes is now referred to as the Svaerholt Succession, and the metasediments in the upper nappes is termed the Sørøy Succession (Kirkland et al., 2007).

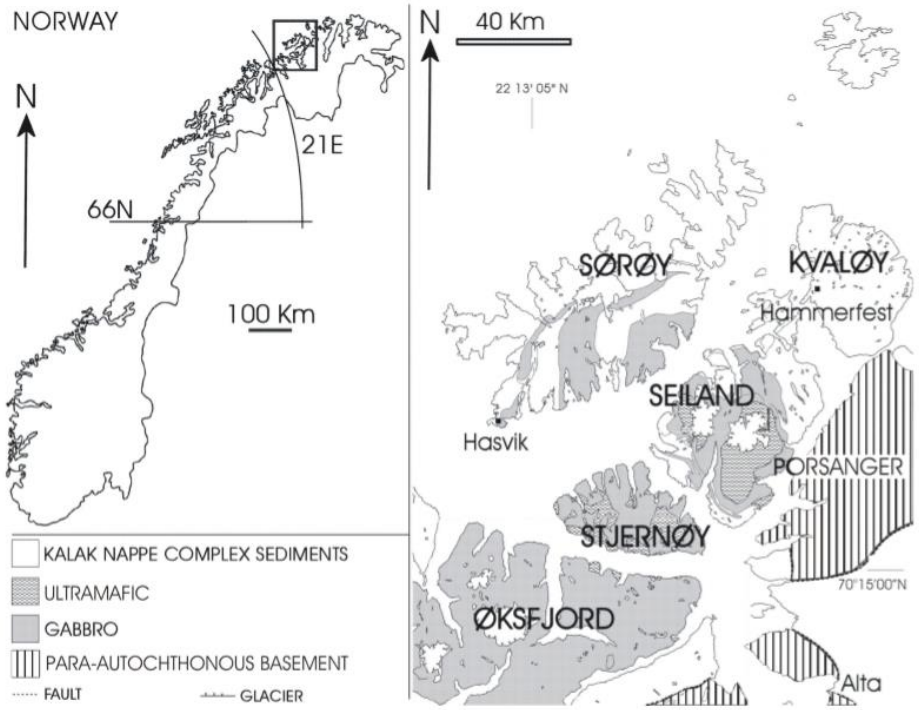

Figure 93: The square on the map of Norway on the left side, shows the location of Finnmark, and the Kalak Nappe Complex, which contains the Seiland Igneous Province. To the right a detailed map shows the distribution of the major igneous bodies within the Seiland Igneous Province. Figure from Roberts (2007).

The Sørøy Succession has late Mesoproterozoic ages with significant components of latest Paleoproterozoic grains, with peaks at 1700, ca. 1650, ca. 1600, and ca. 1500 Ma, together with a spread between 1300 and 1400 and a significant peak at 1050 Ma (Kirkland et al., 2007). The youngest zircon dated is ca. 910-920 Ma (Kirkland et al., 2007). The metasedimentary rocks of the upper nappes are believed to have been deposited between ca. 849 (from a 840 Ma granites in the Havvatnet Imbricated stack) and 910 Ma (Kirkland et al., 2007). Some consider these sediments to have an exotic origin (Kirkland et al., 2007, Slagstad et al., 2006).

The metasedimentary rocks of the Sørøy succession are intruded by numerous mantle-derived plutonic rocks (Reginiussen et al., 1995), which crosscut pre-existing fabrics. The igneous rocks range in composition from calc-alkalic to tholeiitic and alkaline gabbros (Roberts et al., 2006, Reginiussen et al., 1995) along with ultramafic plutons. Gabbroic plutons are the dominant rock in the SIP. Igneous rocks with intermediate monzonitic and dioritic (Roberts, 2007)

composition make up about 10% of the total exposed igneous rocks. Nepheline syenite, carbonatites, and granite are present as small intrusions and dykes (Roberts, 2007, Reginiussen et al., 1995). Deformation of the rocks is extremely variable. Undeformed rocks and heavily foliated and metamorphosed rocks all have the same age (Roberts et al., 2006). Mafic and felsic dykes accompany the plutons in the SIP, and intrudes the metasediment and the plutonic rocks (Reginiussen et al., 1995). The mafic dykes are dark grey, fine-grained and massive and have thicknesses from 2.5-200 cm, with an average of 35 cm (Reginiussen et al., 1995).

Many attempts on dating the plutonic rocks of the SIP have been made. Studies from the early 1990s used Sm-Nd and Rb-Sr isotopic dating. These methods have given spread ages of the gabbros in the SIP. The Hasvik gabbro was dated to 700 ± 33 Ma and the Kvalfjord and Storvik gabbros were dated to 612 ± 33 Ma and 604 ± 44 Ma, with Sm-Nd isochrons by Daly et al. (1991). Krogh and Elvevold (1990), dated the metagabbro and monzonite from the Øksfjord peninsula, which gave an Rb-Sr age of 829 ± 18 Ma. The metagabbros from Storvik on the Øksfjord peninsula were also dated by Mørk and Stabel (1990) with Sm-Nd isochrons to 502 ± 28 Ma. Cadow (1993), dated metagabbros east of the Lillebukt Alkaline Complex with Sm-Nd whole rock isochron, to an age of 517 ± 61 Ma, and the same rock with Rb-Sr age of 534 ± 6 Ma. The nepheline syenite pegmatites have given an U-Pb age of about 530 Ma (Pedersen et al., 1989). The Sm-Nd and Rb-Sr systems of isotopic dating have been criticised for possibly obtaining ages that are younger or older than the true rock age (Roberts, 2007).

The most recent zircon U-Pb analyses have obtained ages between 570-560 Ma (Roberts et al., 2006, Roberts, 2007). The alkaline magmatism has been dated to 530-520 Ma (Roberts et al., 2006), but the latest work of Roberts et al. (2010) have dated the alkaline intrusion to occur around the same time as the mafic and ultramafic plutons intruded at about 580-560 Ma.

Geochronological analysis of the Umbukta gabbro has given a zircon U-Pb age of 565 ± 20 Ma, which is the same age as the gabbros in the SIP. No alkaline rocks have been found, but the studied area is limited and the possibility of alkaline rocks cannot be dismissed. The Umbukta gabbro cuts the metasediments with detrital zircon ages mainly peaking at ca. 1900-1850, ca. 1650-1600, ca. 1400 and ca. 1200-1000 Ma. The depositional ages of the metasedimentary rocks, in Umbukta and Østre Sauvatnet, show many similar depositional ages as both the Svaerholt Succession (lower nappes) and the Sørøy Succession (upper nappes) in the KNC. The detrital zircon analysis performed on the metasediments from Umbukta and Østre Sauvatnet correlates better with the Svaerholt Succession (lower nappes), than the Sørøy Succession (upper nappes). The main reason for a better correlation with the Svaerholt Succession then the

Sørøy Succession is that no detrital zircon younger than 1000 Ma was analysed from the metasediments at Østre Sauvatnet. It is important to point out that only 64 detrital zircon where analysed from Østre Sauvatnet, so it is possible that some detrital zircon ages are not present in this analyse. Other similarities with the SIP are the mafic dykes, which are present in the gabbro and the metasediments at Umbukta and Østre Sauvatnet, and crosscut the gabbro and the gneissose texture in the metasediments.

The rare earth elements (REE) are a set of important trace elements, and the mafic plutons in the SIP show analysed REE data with an enriched pattern relative to profiles from other continental mafic intrusions. The slopes are negative from La to Lu, with only minor Eu anomalies (Roberts, 2007). The variation in the REE content is limited.

The similarities between the Umbukta gabbro and the gabbros in SIP have been pointed out above. It therefore seems proper to compare the trace element geochemistry of Umbukta gabbro and mafic dykes, with the intrusive rocks at SIP. The rock analyses from both places were performed on cumulate rocks, which also make them appropriate for comparison. The REE data from the SIP shows a relative enrichment in the trace elements, this enrichment is also seen in the REE data from the Umbukta gabbro and mafic dykes. In Figure 94 the grey shaded area shows the geochemistry of the SIP and the plotted data is from the Umbukta gabbro and mafic dykes. The overlap between the two regions is striking.

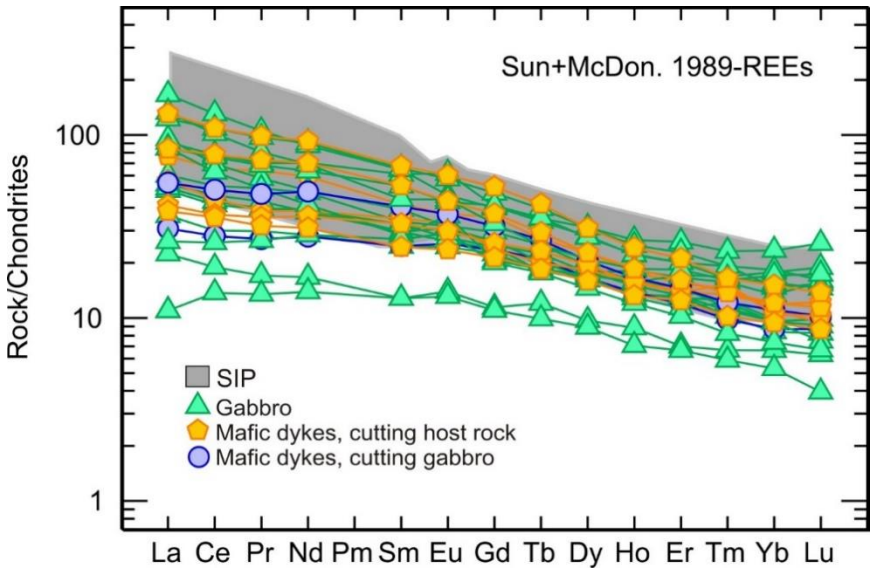

Figure 94: Chondrite normalized REE diagram after Sun and McDonough (1989). The grey shaded area is the geochemistry of the SIP, and the plotted data shows the geochemistry of the Umbukta gabbro and mafic dykes.

The primitive mantle normalised data from SIP have also been plotted in comparison with the Umbukta gabbro and mafic dykes shown in Figure 94 (left diagram), and the same for MORB normalised trace element data shown in Figure 94 (right diagram). The trace element diagrams also show very similar patterns for the gabbros and mafic dykes from the two regions.

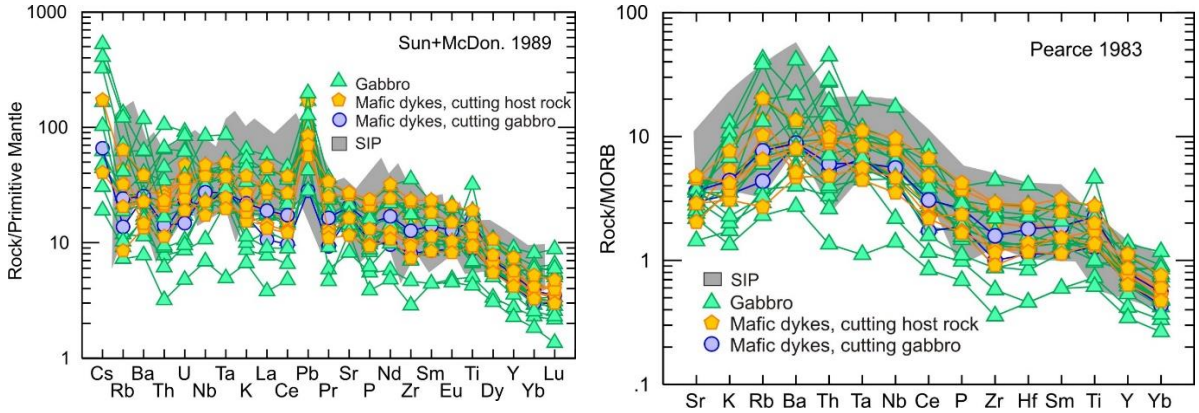

Figure 95: To the left: primitive mantle normalized spider diagram after Sun and McDonough (1989). To the right: MORB normalized spider diagram after (Pearce, 1983). The grey shaded area is the geochemistry of the SIP, and the plotted data shows the geochemistry of the Umbukta gabbro and mafic dykes.

The SIP has sometimes been referred to as a large igneous layered intrusion (LIP) (Tegner et al., 2005, Andréasson et al., 1998). Roberts (2007) compared the trace element REE data from SIP, with rocks from well-known layered intrusions such as the Bushveld Complex in South Africa, and the Skaergaard Complex in East Greenland. The SIP gabbros show homogenous enrichment in REEs relative to the other layered intrusions, and Roberts (2007) suggested to make other comparison for interpretation of magmatic sources.

The Umbukta gabbro and mafic dykes have a quite similar enriched geochemical REE pattern as the SIP. The enrichment could result from wall rock assimilation driven by the latent heat from crystallization during fractional crystallization. Crustal rocks are generally enriched in incompatible trace elements and REEs (Tegner et al., 1999). The homogeneity of the REEs argues against high degrees of fractional crystallization (Roberts, 2007), and without high degrees of fractional crystallization, it is not likely that assimilation of the wall rock would be a source of enrichment. The trace element enrichment is assumed to be a primary feature of the parental magma.

The latest interpretation of the intrusive rocks at SIP has given a short period, only about 10 m.y, of intrusion. Together with the enriched trace element composition, and the presence of mafic dykes, this has led to an interpretation of a probably extensional, tectonic regime, possibly in an intracontinental rift- or continental back-arc setting (Roberts, 2007, Roberts et al., 2006,

Reginiussen et al., 1995, Andréasson, 1994). The Umbukta gabbro is also enriched in trace elements, and shows a homogeneous pattern of the REEs. The crystallizaton age of the Umbukta gabbro is 565 ± 20 Ma, and interpreted to have intruded a metasedimentary host rock. Mafic dykes cut the Umbukta gabbro and the metasedimentary host rock. The tectonic discrimination diagrams point to either back-arc or intracontinental setting. The metasedimentary host rock was deformed prior to the intrusion of the gabbro and mafic dykes, and anticipated to be of continental affinity. These data have led to an interpretation of either an intracontinental back-arc extension or an intracontinental extensional setting for the Umbukta gabbro. This is a similar interpretation of tectonic environment as for the intrusive rocks in the SIP.

Several correlative conditions have been found between the Sørøy Group (in the SIP) and the rocks in the Kjerringfjell Group. Today the two rock units are placed in different Allochthons, SIP in the Middle Allochthon and the Kjerringfjell Group in the Uppermost Allochthon. If the Umbukta gabbro and the gabbros in SIP originated from the same source, some of the interpreted tectonostratigraphy should be reconsidered.

Implication on tectonostratigraphy

Classically, the Scandinavian Caledonides have been interpreted to composes of a variety of nappes thrust onto each other, from west to east, on to the Baltoscandian Platform (Roberts and Gee, 1985). This began with rifting of Baltica from Laurentia when the supercontinent Rodinia started to break-up at the end of the Neoproterozoic, and led to the formation of the Iapetus Ocean. It ended with collision between Laurentia and Baltica during closing of the Iapetus Ocean, and the formation of Scandinavian Caledonides, in late Silurian early Devonian times (Roberts and Gee, 1985).

Traditionally, the Kalak Nappe Complex (KNC) in northern Norway is assigned to the Middle Allochthon, which is interpreted to be a stack of basement slices derived from the margin of the Baltoscandian platform (Roberts and Gee, 1985), and this has commonly been an accepted interpretation. Based on further research, and gradual new information and understanding of the tectonic units, researchers have started to question some of the earlier interpretations. New data provide new information, and the tectonic evolution of the Scandinavian Caledonides may be more complex than originally thought.

Over several years, the KNC and the SIP have been studied, and timing of the intrusive stages has been re-evaluated several times. Earlier, the intrusive rocks of the SIP were dated between 829 ± 18 Ma (Krogh and Elvevold, 1990) and 550 ± 34 Ma (Mørk and Stabel, 1990). This gave a period of about 300 m.y. of intermittent magmatism, which is a very long period of ongoing magmatism. Some scientists questioned this time span, and the latest research has narrowed the intrusive ages to 570-560 Ma (Roberts et al., 2006). This has changed the interpretation from considering plutonic intrusion during different deformational events, to most likely a magma relating to an intracontinental rifting (Roberts et al., 2006). Reginiussen et al. (1995), also interpreted the rocks to result from continental rift processes, and explained the long time span of intrusions as possibly resulting from discrete events separated by long quiet intervals.

The sediments of the Sørøy Group (consisting of the Sørøy Succession) originally were thought to be Cambrian to late Precambrian in age, and deposited as one succession during the opening of the Iapetus Ocean (ca. 600Ma) (Roberts et al., 2006). Partly based on this interpretation the Kalak Nappe Complex has been understood to be part of the continental shelf of Baltica. Aitcheson (1990), already proposed in the 90's that the metasediments of the KNC probably had an exotic origin. New dating of the KNC metasediments has further confirmed this, and the new results show deposition substantially before opening of the Iapetus Ocean (Kirkland et al., 2006). The lower nappes (Svaerholt succession) were deposited between ca. 980 and 1030, and the upper nappes (Sørøy Succession) were deposited between 840 and 910 Ma (Kirkland et al., 2007). These results also suggest that the KNC metasediments are different fragments bound together during the Neoproterozoic (Kirkland et al., 2006). The metasedimentary ages have led to speculations if the KNC may not originate from Baltica at all, but descend from a more exotic margin (Kirkland et al., 2006, Slagstad et al., 2006). A correlation with the Seve Nappe of the Upper Allochthon (Andréasson et al., 1998, Corfu et al., 2007) has been suggested.

Corfu et al. (2007) proposed some reasons why the KNC should be related to a more exotic origin than the margin of Baltica. First, they pointed out the granitic rocks with ages of 980 to 960 Ma, 850 Ma, and 700 Ma. Together with the SIP intrusions of 570-560 Ma, and the Archean and Paleoproterozoic components found in the crystalline slices of the KNC nappes, these factors do not correlate with the orogenic Neoproterozoic rocks in the autochthonous western Baltic basement. The age patterns of the KNC and the Baltic basement do not either show geochronological resemblance. The foreland sedimentary deposits do not consist of any Cambrian to Early Ordovician deposit, which would be anticipated to represent the response to thrusting of nappes on the edge of Baltica. They also pointed out many analogies between the

KNC and the terranes developed on the eastern Laurentian margin. They suggested that the KNC most likely stemmed from western Siberia and/or the peri-Gondwana realm. They also proposed a correlation between the KNC and the Seve nappe. "There is just no simple way to rationalize a Baltic origin of the Kalak Nappe Complex" (Corfu et al., 2007, p. 452).

Slagstad et al. (2006), proposed a possible correlation between the KNC and the SIP with the Uppermost Allochthon. This assumption is based on correlated chemostratigraphy of marbles from the Falkenes formation of the KNC, with marbles of the Uppermost Allochthon, particularly from the Helgeland Nappe Complex.

Lately, the KNC has been assumed to probably belong to a more exotic terrane than stemming from the margin of Baltica. Most often it has been suggested to belong to the Upper Allochthon. This interpretation is partly based on correlative similarities to the Seve Nappe, which is interpreted to be a part of the Upper Allochthon. New data from this study has opened for further speculations if there could be a correlation between the KNC and the SIP, with the Uppermost Allochthon. The Umbukta gabbro and the gabbros in the SIP show very similar geochemical data and they have the same age of intrusion. The Umbukta gabbro and the gabbros in SIP have both intruded a metasediment, which is assumed to be of continental affinities, and the gabbros placed in Umbukta and in the SIP are both interpreted to have formed in an intracontinental rifting or an intracontinental back-arc extensional setting. The similarities between the Umbukta gabbro and the gabbros in SIP are quite striking, and do point to a correlation between the Sørøy Group placed in the Middle Allochthon, and the Kjerringfjell Group of the Uppermost Allochthon.

The Rödingsfjället Nappe Complex has not been widely studied. More research of the region is needed to reinforce this interpretation. More knowledge of the area would help, due to some reinterpretation, and a newer understanding of the Allochthons of the Scandinavian Caledonides. The simple "layer cake structure" of the tectonostratigraphy of the Scandinavian Caledonides has been a useful basis for further exploration and description of the orogen. Currently, some of the older interpretations are being questioned, and some are reinterpreted.

Conclusion

Detailed fieldwork, microscopy analysis, and whole rock geochemical and geochronological analysis has brought new interesting information about the Kjerringfjell Group, and especially the Umbukta gabbro. The main conclusions obtained from this study are the following

- The Umbukta gabbro has an age of intrusion of 565 ± 20 Ma. The intrusion age of the Umbukta gabbro is not a common age in the Scandinavian Caledonides.
- Based on the geochemical data the Umbukta gabbro is interpreted to have formed in an intracontinental rift or a back-arc setting.
- The garnet-biotite gneiss, which is the host rock of the gabbro, was dated to a depositional age younger than 1000 Ma, and the host rock was deformed and metamorphosed prior to the intrusion of the gabbro.
- Based on field observation it is assumed that there may be a tectonic contact separating the garnet biotite gneiss at Plurdalen, Kallvatnet and Saufjellet from the garnet-biotite gneiss at Østre Sauvatnet and Umbukta.
- The geochemistry of the Umbukta gabbro and mafic dykes indicate a mantle source enriched in the REEs, this geochemical enrichment is very similar to the gabbros in the Seiland Igneous Province (SIP), and they have the same age of about 560-570 Ma. The host rock and field relation of the Umbukta gabbro and mafic dykes also show similarities with the SIP, which has led to a speculation of a possible correlation with the SIP.
- The correlation of the Umbukta gabbro in the Kjerringfjell Group with the Sørøy Group and the SIP do not fit into the traditionally tectonostratigraphic interpretation of Scandinavian Caledonides. Today the Kjerringfjell Group and the Umbukta gabbro are situated in the Uppermost Allochthon, while the Sørøy Group and the SIP is interpreted to belong to the Middle Allochthon. If the two areas are correlated as suggested in this thesis, the Sørøy Group and the SIP should belong to the same allochthon as the Kjerringfjell Group and the Umbukta gabbro. At this point I am in no position to launch an alternative to the traditional interpretation of the tectonostratigraphy of the Scandinavian Caledonides, but some of the older interpretations are being questioned.

Future work

- To increase the geological knowledge of the Rödingsfjället Nappe Complex continued geological mapping of the rocks should be performed in the area.
- More detailed mapping of the Umbukta gabbro considering both geochemical and structural variations. More detailed mapping of the Umbukta gabbro should reveal if there is presence of alkaline bodies within the pluton. Further geochemical analysis could be interesting in terms of mineral resource, for example in terms of PGE minerals.
- Structural analysis should be performed to increase the understanding of the rocks-, and the regional geological history of the Rödingsfjället Nappe Complex.
- Perform more detailed detrital zircon analysis on the host rock, to see if there could be a correlation with the Sørøy Succession.

References

AITCHESON, S. J. 1990. Nd isotopic evidence for exotic detritus in the Kalak Nappe Complex, north Norwegian Caledonides. *Journal of the Geological Society,* 147**,** 923-926.

ANDERSEN, T. 2005. Detrital zircons as tracers of sedimentary provenance: limiting conditions from statistics and numerical simulation. *Chemical Geology,* 216**,** 249-270.

ANDERSEN, T. B. & JAMTVEIT, B. 1990. Uplift of deep crust during orogenic extensional collapse: A model based on field studies in the Sogn-Sunnfjord Region of western Norway. *Tectonics,* 9**,** 1097-1111.

ANDRÉASSON, P.-G., SVENNINGSEN, O. M. & ALBRECHT, L. 1998. Dawn of Phanerozoic orogeny in the North Atlantic tract; evidence from the Seve-Kalak superterrane, scandinavian caledonides. *GFF,* 120**,** 159-172.

ANDRÉASSON, P. 1994. The Baltoscandian margin in Neoproterozoic-early Palaeozoic times. Some constraints on terrane derivation and accretion in the Arctic Scandinavian Caledonides. *Tectonophysics,* 231**,** 1-32.

BARNES, C. G., FROST, C. D., YOSHINOBU, A. S., MCARTHUR, K., BARNES, M. A., ALLEN, C. M., NORDGULEN, Ø. & PRESTVIK, T. 2007. Timing of sedimentation, metamorphism, and plutonism in the Helgeland Nappe Complex, north-central Norwegian Caledonides. *Geosphere,* 3**,** 683-703.

BARNES, C. G., REID, K., FROST, C. D., BARNES, M. A., ALLEN, C. M. & YOSHINOBU, A. S. 2011. Ordovician and Silurian magmatism in the Upper Nappe, Uppermost Allochthon, Helgeland Nappe Complex, north-central Norway. *Norwegian Journal of Geology,* 91**,** 121-136.

BAU, M. 1991. Rare-earth element mobility during hydrothermal and metamorphic fluid-rock interaction and the significance of the oxidation state of europium. *Chemical Geology,* 93**,** 219-230.

BÉDARD, J. H. 1994. A procedure for calculating the equilibrium distribution of trace elements among the minerals of cumulate rocks, and the concentration of trace elements in the coexisting liquids. *Chemical Geology,* 118**,** 143-153.

BELOUSOVA, E., GRIFFIN, W. & O'REILLY, S. Y. 2006. Zircon crystal morphology, trace element signatures and Hf isotope composition as a tool for petrogenetic modelling: examples from Eastern Australian granitoids. *Journal of Petrology,* 47**,** 329-353.

BELOUSOVA, E., GRIFFIN, W. L., O'REILLY, S. Y. & FISHER, N. 2002. Igneous zircon: trace element composition as an indicator of source rock type. *Contributions to Mineralogy and Petrology,* 143**,** 602-622.

BEST, M. G. 2003. *Igneous and metamorphic petrology,* Blackwell publishing.

BINGEN, B. & SOLLI, A. 2009. Geochronology of magmatism in the Caledonian and Sveconorwegian belts of Baltica: synopsis for detrital zircon provenance studies. *Norwegian Journal of Geology/Norsk Geologisk Forening,* 89.

BLAKE, D. 1981. Intrusive felsic-mafic net-veined complexes in north Queensland. *BMR Journal of Australian Geology and Geophysics,* 6**,** 95-99.

BOGGS, S. J. 2011. *Principles of sedimentology and stratigraphy,* Pearson Prentice Hall.

BRYHNI, I. & STURT, B. 1985a. Caledonides of southwestern Norway. *The Caledonide Orogen—Scandinavia and Related Areas. Wiley, Chichester***,** 89-107.

BRYHNI, I. & STURT, B. 1985b. Caledonides of southwestern Norway. *The Caledonide Orogen—Scandinavia and Related Areas***,** 89-107.

CABANIS, B. 1989. Le diagramme La/10-Y/15-Nb/8: unoutil pour la discrimination des series volcaniques et la mise en evidence des processus de melande et/ou de contamination crustale. *CR Acad. Sci. Ser. II,* 309**,** 2023-2029.

CADOW, R. 1993. Sm-Nd and Rb-Sr ages of hornblende clinopyroxenite and metagabbro from the Lillebukt alkaline complex, Seiland Igneous Province. *Norsk geologisk tidsskrift,* 73**,** 243-249.

CASTOR, S. B. & HEDRICK, J. B. 2006. Rare earth elements. *Industrial minerals volume, 7th edition: Society for mining, metallurgy, and exploration, Littleton, Colorado***,** 769-792.

CASTRO, A. & STEPHENS, W. E. 1992. Amphibole-Rich Polycrystalline Clots In Calc-Alkaline Granitic Rocks And Their Enclaves. *Canadian Mineralogist* 30**,** 1093-1112.

CHAPPELL, B. & WHITE, A. 1974. Two contrasting granite types. *Pacific geology,* 8**,** 173-174.

CHERNIAK, D., HANCHAR, J. & WATSON, E. 1997. Rare-earth diffusion in zircon. *Chemical Geology,* 134**,** 289-301.

CHERNIAK, D. & WATSON, E. 2001. Pb diffusion in zircon. *Chemical Geology,* 172**,** 5-24.

CHERNIAK, D. J. & WATSON, E. B. 2003. Diffusion in zircon. *Reviews in mineralogy and geochemistry,* 53**,** 113-143.

CLEMENS, J. 2003. S-type granitic magmas—petrogenetic issues, models and evidence. *Earth-Science Reviews,* 61**,** 1-18.

COCKS, L. & TORSVIK, T. 2006. European geography in a global context from the Vendian to the end of the Palaeozoic. *MEMOIRS-GEOLOGICAL SOCIETY OF LONDON,* 32**,** 83.

COISH, R. & SINTON, C. 1992. Geochemistry of mafic dikes in the Adirondack mountains: implications for late Proterozoic continental rifting. *Contributions to Mineralogy and Petrology,* 110**,** 500-514.

CORFU, F., ANDERSEN, T. B. & GASSER, D. 2014a. *The Scandinavian Caledonides: main features, conseptual advances and critical questions* London, Geological society

CORFU, F., GASSER, D. & CHEW, D. M. 2014b. *New perspectives on the Caledonides of Scandinavia and related areas: introduction,* London, Geological Society, London.

CORFU, F., HANCHAR, J. M., HOSKIN, P. W. & KINNY, P. 2003a. Atlas of zircon textures. *Reviews in mineralogy and geochemistry,* 53**,** 469-500.

CORFU, F., RAVNA, E. & KULLERUD, K. 2003b. A Late Ordovician U–Pb age for the Tromsø Nappe eclogites, uppermost allochthon of the Scandinavian Caledonides. *Contributions to Mineralogy and Petrology,* 145**,** 502-513.

CORFU, F., ROBERTS, R. J., TORSVIK, T. H., ASHWAL, L. D. & RAMSAY, D. M. 2007. Peri-Gondwanan elements in the Caledonian nappes of Finnmark, northern Norway: implications for the paleogeographic framework of the Scandinavian Caledonides. *American Journal of Science,* 307**,** 434-458.

CORTÉS, J. A. 2009. On the harker variation diagrams; a comment on "the statistical analysis of compositional data. Where are we and where should we be heading?" by Aitchison and Egozcue (2005). *Mathematical Geosciences,* 41**,** 817-828.

COTTLE, J. M. & COOPER, A. F. 2006. The Fontaine Pluton: An early Ross Orogeny calc-alkaline gabbro from southern Victoria Land, Antarctica. *New Zealand Journal of Geology and Geophysics,* 49**,** 177-189.

DALY, J., AITCHESON, S., CLIFF, R., GAYER, R. & RICE, A. 1991. Geochronological evidence from discordant plutons for a late Proterozoic orogen in the Caledonides of Finnmark, northern Norway. *Journal of the Geological Society,* 148**,** 29-40.

DOBRZHINETSKAYA, L. F., EIDE, E. A., LARSEN, R. B., STURT, B. A., TRØNNES, R. G., SMITH, D. C., TAYLOR, W. R. & POSUKHOVA, T. V. 1995. Microdiamond in high-grade metamorphic rocks of the Western Gneiss region, Norway. *Geology,* 23**,** 597-600.

DODSON, M., COMPSTON, W., WILLIAMS, I. & WILSON, J. 1988. A search for ancient detrital zircons in Zimbabwean sediments. *Journal of the Geological Society,* 145**,** 977-983.

DUNHAM, A. 1964. A petrographic and geochemical study of back-veining and hybridization at a gabbro-felsite contact in Coire Dubh, Rhum, Inverness-shire. *Mineralogical Magazine,* 33**,** 887-902.

EGOZCUE, J. J. 2009. Reply to "on the Harker variation diagrams;…" by JA Cortés. *Mathematical Geosciences,* 41**,** 829-834.

EVENSEN, N., HAMILTON, P. & O'NIONS, R. 1978. Rare-earth abundances in chondritic meteorites. *Geochimica et Cosmochimica Acta,* 42**,** 1199-1212.

FEDO, C. M., SIRCOMBE, K. N. & RAINBIRD, R. H. 2003. Detrital zircon analysis of the sedimentary record. *Reviews in Mineralogy and Geochemistry,* 53**,** 277-303.

FLOYD, P. & WINCHESTER, J. 1975. Magma type and tectonic setting discrimination using immobile elements. *Earth and Planetary science letters,* 27**,** 211-218.

FOSSEN, H. & GABRIELSEN, R. H. 2005. *Strukturgeologi,* Norge, Fagbokforlaget.

FOWLER, A., PROKOPH, A., STERN, R. & DUPUIS, C. 2002. Organization of oscillatory zoning in zircon: analysis, scaling, geochemistry, and model of a zircon from Kipawa, Quebec, Canada. *Geochimica et Cosmochimica Acta,* 66**,** 311-328.

FROST, B. R., BARNES, C. G., COLLINS, W. J., ARCULUS, R. J., ELLIS, D. J. & FROST, C. D. 2001. A geochemical classification for granitic rocks. *Journal of petrology,* 42**,** 2033-2048.

GEE, D. 1975. A tectonic model for the central part of the Scandinavian Caledonides. *American Journal of Science,* 275**,** 468-515.

GEE, D. G., FOSSEN, H., HENRIKSEN, N. & HIGGINS, A. K. 2008. From the early Paleozoic platforms of Baltica and Laurentia to the Caledonide Orogen of Scandinavia and Greenland. *Episodes,* 31**,** 44.

GEE, D. G. & ZACHRISSON, E. 1979. *The Caledonides in Sweden*, na.

GEHRELS, G., KAPP, P., DECELLES, P., PULLEN, A., BLAKEY, R., WEISLOGEL, A., DING, L., GUYNN, J., MARTIN, A. & MCQUARRIE, N. 2011. Detrital zircon geochronology of pre-Tertiary strata in the Tibetan-Himalayan orogen. *Tectonics,* 30.

GIGGENBACH, W. F. 1984. Mass transfer in hydrothermal alteration systems—a conceptual approach. *Geochimica et Cosmochimica Acta,* 48**,** 2693-2711.

GRENNE, T., IHLEN, P. & VOKES, F. 1999. Scandinavian Caledonide metallogeny in a plate tectonic perspective. *Mineralium Deposita,* 34**,** 422-471.

GRIFFIN, W., STURT, B., O'NEILL, C., KIRKLAND, C. & O'REILLY, S. Y. 2013. Intrusion and contamination of high-temperature dunitic magma: the Nordre Bumandsfjord pluton, Seiland, Arctic Norway. *Contributions to Mineralogy and Petrology,* 165**,** 903-930.

HANCHAR, J. & RUDNICK, R. 1995. Revealing hidden structures: the application of cathodoluminescence and back-scattered electron imaging to dating zircons from lower crustal xenoliths. *Lithos,* 36**,** 289-303.

HANSON, G. N. 1980. Rare earth elements in petrogenetic studies of igneous systems. *Annual Review of Earth and Planetary Sciences,* 8**,** 371.

HARLOV, D. E. & AUSTRHEIM, H. 2013. Metasomatism and the chemical transformation of rock: rock-mineral-fluid interaction in terrestrial and extraterrestrial environments. *Metasomatism and the Chemical Transformation of Rock.* Springer.

HASTIE, A. R., KERR, A. C., PEARCE, J. A. & MITCHELL, S. 2007. Classification of altered volcanic island arc rocks using immobile trace elements: development of the Th–Co discrimination diagram. *Journal of Petrology,* 48**,** 2341-2357.

HENDERSON, P. 1984. *Rare earth element geochemistry,* Elsevier.

HOEK, J. & SCHAEFER, B. 1998. Palaeoproterozoic Kimban mobile belt, Eyre Peninsula: timing and significance of felsic and mafic magmatism and deformation. *Australian Journal of Earth Sciences,* 45**,** 305-313.

HOFMANN, A. 1997. Mantle geochemistry: the message from oceanic volcanism. *Nature,* 385**,** 219-229.

HOSKIN, P. W. 2000. Patterns of chaos: fractal statistics and the oscillatory chemistry of zircon. *Geochimica et Cosmochimica Acta,* 64**,** 1905-1923.

IRVINE, T. 1982. Terminology for layered intrusions. *Journal of Petrology,* 23**,** 127-162.

IRVINE, T. & BARAGAR, W. 1971. A guide to the chemical classification of the common volcanic rocks. *Canadian journal of earth sciences,* 8**,** 523-548.

JACKSON, S. E., PEARSON, N. J., GRIFFIN, W. L. & BELOUSOVA, E. A. 2004. The application of laser ablation-inductively coupled plasma-mass spectrometry to in situ U–Pb zircon geochronology. *Chemical Geology,* 211**,** 47-69.

JAYANANDA, M., MIYAZAKI, T., GIREESH, R., MAHESHA, N. & KANO, T. 2009. Synplutonic mafic dykes from late Archaean granitoids in the Eastern Dharwar Craton, Southern India. *Journal of the Geological Society of India,* 73**,** 117-130.

KIRKLAND, C., DALY, J. & WHITEHOUSE, M. 2006. Granitic magmatism of Grenvillian and late Neoproterozoic age in Finnmark, Arctic Norway—constraining pre-Scandian deformation in the Kalak Nappe Complex. *Precambrian Research,* 145**,** 24-52.

KIRKLAND, C. L., DALY, J. S. & WHITEHOUSE, M. J. 2007. Provenance and terrane evolution of the Kalak Nappe Complex, Norwegian Caledonides: implications for Neoproterozoic paleogeography and tectonics. *The Journal of Geology,* 115**,** 21-41.

KROGH, E. J. & ELVEVOLD, S. 1990. A Precambrian age for an early gabbro–monzonitic intrusive on the Øksfjord peninsula, Seiland Igneous Province, northern Norway. *Norsk Geologisk Tidsskrift,* 70**,** 267-273.

LABROUSSE, L., HETÉNYI, G., RAIMBOURG, H., JOLIVET, L. & ANDERSEN, T. B. 2010. Initiation of crustal-scale thrusts triggered by metamorphic reactions at depth:

Insights from a comparison between the Himalayas and Scandinavian Caledonides. *Tectonics,* 29.

LATYPOV, R., CHISTYAKOVA, S. & ALAPIETI, T. 2007. Revisiting problem of chilled margins associated with marginal reversals in mafic–ultramafic intrusive bodies. *Lithos,* 99**,** 178-206.

LEE, J. K., WILLIAMS, I. S. & ELLIS, D. J. 1997. Pb, U and Th diffusion in natural zircon. *Nature,* 390**,** 159-162.

LI, X.-H., SUN, M., WEI, G.-J., LIU, Y., LEE, C.-Y. & MALPAS, J. 2000. Geochemical and Sm–Nd isotopic study of amphibolites in the Cathaysia Block, southeastern China: evidence for an extremely depleted mantle in the Paleoproterozoic. *Precambrian Research,* 102**,** 251-262.

LUGWIG, K. 2010. Isoplot/Ex version 4, a geochronological toolkit for Microsoft Excel. *Berkeley Geochronology Center Special Publication: Berkeley, CA, USA*.

LUNDMARK, A. & CORFU, F. 2008. Late-orogenic Sveconorwegian massif anorthosite in the Jotun Nappe Complex, SW Norway, and causes of repeated AMCG magmatism along the Baltoscandian margin. *Contributions to Mineralogy and Petrology,* 155**,** 147-163.

LUNDMARK, A., CORFU, F., SPÜRGIN, S. & SELBEKK, R. 2007. Proterozoic evolution and provenance of the high-grade Jotun Nappe Complex, SW Norway: U–Pb geochronology. *Precambrian Research,* 159**,** 133-154.

LYUBETSKAYA, T. & KORENAGA, J. 2007. Chemical composition of Earth's primitive mantle and its variance: 1. Method and results. *Journal of Geophysical Research: Solid Earth (1978–2012),* 112.

MAAS, R., NICHOLLS, I. A. & LEGG, C. 1997. Igneous and metamorphic enclaves in the S-type Deddick Granodiorite, Lachlan Fold Belt, SE Australia: petrographic, geochemical and Nd-Sr isotopic evidence for crustal melting and magma mixing. *Journal of Petrology,* 38**,** 815-841.

MANDAL, A., RAY, A., DEBNATH, M. & PAUL, S. P. 2012. Petrology, geochemistry of hornblende gabbro and associated dolerite dyke of Paharpur, Puruliya, West Bengal: Implication for petrogenetic process and tectonic setting. *Journal of earth system science,* 121**,** 793-812.

MANIAR, P. D. & PICCOLI, P. M. 1989. Tectonic discrimination of granitoids. *Geological society of America bulletin,* 101**,** 635-643.

MASUDA, A., NAKAMURA, N. & TANAKA, T. 1973. Fine structures of mutually normalized rare-earth patterns of chondrites. *Geochimica et Cosmochimica Acta,* 37**,** 239-248.

MCARTHUR, K. L., FROST, C. D., BARNES, C. G., PRESTVIK, T. & NORDGULEN, Ø. 2014. Tectonic reconstruction and sediment provenance of a far-travelled oceanic nappe, Helgeland Nappe Complex, west-central Norway. *Geological Society, London, Special Publications,* 390**,** 583-602.

MCKEEGAN, K. & DAVIS, A. 2003. Early solar system chronology. *Treatise on Geochemistry,* 1**,** 431-460.

MCKERROW, W., MAC NIOCAILL, C. & DEWEY, J. 2000. The Caledonian orogeny redefined. *Journal of the Geological Society,* 157**,** 1149-1154.

MELEZHIK, V., GOROKHOV, M., FALLICK, A., ROBERTS, D., KUZNETSOV, A., ZWAAN, K. & POKROVSKY, B. 2002. Isotopic stratigraphy suggests Neoproterozoic ages and Laurentian ancestry for high-grade marbles from the North-Central Norwegian Caledonides. *Geological Magazine,* 139**,** 375-393.

MELEZHIK, V., IHLEN, P., KUZNETSOV, A., GJELLE, S., SOLLI, A., GOROKHOV, I., FALLICK, A., SANDSTAD, J. & BJERKGÅRD, T. 2015. Pre-Sturtian (800–730Ma) depositional age of carbonates in sedimentary sequences hosting stratiform iron ores in the Uppermost Allochthon of the Norwegian Caledonides: A chemostratigraphic approach. *Precambrian Research,* 261**,** 272-299.

MESCHEDE, M. 1986. A method of discriminating between different types of mid-ocean ridge basalts and continental tholeiites with the Nb▪ 1bZr▪ 1bY diagram. *Chemical geology,* 56**,** 207-218.

MILLER, C. F. & MITTLEFEHLDT, D. W. 1982. Depletion of light rare-earth elements in felsic magmas. *Geology,* 10**,** 129-133.

MILNES, A., WENNBERG, O., SKÅR, Ø. & KOESTLER, A. 1997. Contraction, extension and timing in the South Norwegian Caledonides: the Sognefjord transect. *Geological Society, London, Special Publications,* 121**,** 123-148.

MOROGAN, V. & SØRENSEN, H. 1994. Net-veined complexes in the Oslo Rift, southeast Norway. *Lithos,* 32**,** 21-45.

MØRK, M. & STABEL, A. 1990. Cambrian Sm-Nd dates for an ultramafic intrusion and for high-grade metamorphism on the Øksfjord peninsula, Finnmark, North Norway. *Norsk Geologisk Tidsskrift,* 70**,** 275-291.

NALLUSAMY, B. 2014. Morphology, Trace, and Rare Earth Elements of Detrital Zircon of Kayamkulam, Thottappally Placers, South West India—Implication on Provenance. *Marine Georesources & Geotechnology*.

NORDGULEN, Ø., BICKFORD, M., NISSEN, A. & WORTMAN, G. 1993. U-Pb zircon ages from the Bindal Batholith, and the tectonic history of the Helgeland Nappe Complex, Scandinavian Caledonides. *Journal of the Geological Society,* 150**,** 771-783.

PEARCE, J. 1996. A user's guide to basalt discrimination diagrams.

PEARCE, J. A. 1982. Trace element characteristics of lavas from destructive plate boundaries. *Andesites***,** 525-548.

PEARCE, J. A. 1983. Role of the subcontinental lithosphere in magma genesis at active continental margins.

PEARCE, J. A. & CANN, J. 1973. Tectonic setting of basic volcanic rocks determined using trace element analyses. *Earth and planetary science letters,* 19**,** 290-300.

PEARCE, J. A. & NORRY, M. J. 1979. Petrogenetic implications of Ti, Zr, Y, and Nb variations in volcanic rocks. *Contributions to mineralogy and petrology,* 69**,** 33-47.

PEARCE, T. 1968. A contribution to the theory of variation diagrams. *Contributions to Mineralogy and Petrology,* 19**,** 142-157.

PEDERSEN, R., DUNNING, G. & ROBINS, B. 1989. U-Pb ages of nepheline syenite pegmatites from the Seiland Magmatic Province, N. Norway. *The Caledonide Geology of Scandinavia***,** 3-8.

PHILPOTTS, A. R. 2003. *Petrography of Igneous and Metamorphic Rocks,* United State of America, Waveland Press, Inc.

PIRAJNO, F. 2009. *Hydrothermal Processes and Mineral Systems*.

PRESTVIK, T. 1982. Basic volcanic rocks and tectonic setting. A discussion of the Zr-Ti-Y discrimination diagram and its suitability for classification purposes. *Lithos,* 15**,** 241-247.

PUPIN, J. 1980. Zircon and granite petrology. *Contributions to Mineralogy and Petrology,* 73**,** 207-220.

PUTNIS, A. & AUSTRHEIM, H. 2010. Fluid-induced processes: metasomatism and metamorphism. *Geofluids,* 10**,** 254-269.

RAMBERG, H. 1955. Natural and experimental boudinage and pinch-and-swell structures. *The Journal of Geology***,** 512-526.

RAMBERG, I. B. 1967. *Kongsfjell-områdets geologi, en petrografisk og struktruell undersøkelse i Helgeland, Nord-Norge,* Universitetsforlaget.

RAMSAY, D., STURT, B., ZWAAN, K. & ROBERTS, D. 1985. Caledonides of northern Norway. *The Caledonian Orogen: Scandinavia and related areas. Edited by DG Gee and BA Sturt. Wiley, Chichester, UK***,** 163-184.

RATCLIFFE, N. M., HAMES, W. E. & STANLEY, R. S. 1998. Interpretation of ages of arc magmatism, metamorphism, and collisional tectonics in the Taconian orogen of western New England. *American Journal of Science,* 298**,** 791.

REGINIUSSEN, H., RAVNA, E. & BERGLUND, K. 1995. Mafic dykes from Øksfjord, Seiland Igneous Province, northern Norway: geochemistry and palaeotectonic significance. *Geological Magazine,* 132**,** 667-681.

RIDDLE, C. 1993. *Analysis of geological materials,* Marcel Dekker, Inc.

ROBERTS, D. 2003. The Scandinavian Caledonides: event chronology, palaeogeographic settings and likely modern analogues. *Tectonophysics,* 365**,** 283-299.

ROBERTS, D. & GEE, D. 1985. An introduction to the structure of the Scandinavian Caledonides. *The Caledonide orogen–Scandinavia and related areas,* 1**,** 55-68.

ROBERTS, D., MELEZHIK, V. & HELDAL, T. 2002. Carbonate formations and early NW-directed thrusting in the highest allochthons of the Norwegian Caledonides: evidence of a Laurentian ancestry. *Journal of the Geological Society,* 159**,** 117-120.

ROBERTS, D., NORDGULEN, Ø. & MELEZHIK, V. 2007. The Uppermost Allochthon in the Scandinavian Caledonides: From a Laurentian ancestry through Taconian orogeny to Scandian crustal growth on Baltica. *Geological Society of America Memoirs,* 200**,** 357-377.

ROBERTS, R., CORFU, F., TORSVIK, T., ASHWAL, L. & RAMSAY, D. 2006. Short-lived mafic magmatism at 560–570 Ma in the northern Norwegian Caledonides: U–Pb zircon ages from the Seiland Igneous Province. *Geological Magazine,* 143**,** 887-903.

ROBERTS, R., CORFU, F., TORSVIK, T., HETHERINGTON, C. & ASHWAL, L. 2010. Age of alkaline rocks in the Seiland Igneous Province, Northern Norway. *Journal of the Geological Society,* 167**,** 71-81.

ROBERTS, R. J. 2007. *The Seiland Igneous Province, Northern Norway: Age, Provenance, and Tectonic Significance* University of the Witwatersrand.

ROBIN, P.-Y. F. 1979. Theory of metamorphic segregation and related processes. *Geochimica et Cosmochimica Acta,* 43**,** 1587-1600.

ROBINSON, P., TUCKER, R. D., BRADLEY, D., BERRY IV, H. N. & OSBERG, P. H. 1998. Paleozoic orogens in New England, USA. *GFF,* 120**,** 119-148.

ROCK, N. 1987. The need for standardization of normalized multi-element diagrams in geochemistry: a comment. *Geochemical Journal,* 21**,** 75-84.

ROFFEIS, C., CORFU, F. & AUSTRHEIM, H. 2012. Evidence for a Caledonian amphibolite to eclogite facies pressure gradient in the Middle Allochthon Lindås Nappe, SW-Norway. *Contributions to Mineralogy and Petrology,* 164**,** 81-99.

ROLLINSON, H. R. 1993. *Using Geochemical Data: Evolution, Presentation, Interpretation*

SANDØY, R. 2003. Geological variations in marble deposits: The geometry, internal structure and geochemical variations of the industrial mineral marble deposits in the Velfjord area.

SENIOR, A. & ANDRIESSEN, P. A. M. 1990. U/Pb And K/Ar Determinations In The Upper And Uppermost Allochtons, Central Scandinavian Caledonides. *Geonytt,* 1.

SHETH, H. C., TORRES-ALVARADO, I. S. & VERMA, S. P. 2002. What is the" calc-alkaline rock series"? *International Geology Review,* 44**,** 686-701.

SKÅR, Ø. 2002. U–Pb geochronology and geochemistry of early Proterozoic rocks of the tectonic basement windows in central Nordland, Caledonides of north-central Norway. *Precambrian Research,* 116**,** 265-283.

SLAGSTAD, T., CULSHAW, N. G., JAMIESON, R. A. & KETCHUM, J. W. 2004. Early Mesoproterozoic tectonic history of the southwestern Grenville Province, Ontario: constraints from geochemistry and geochronology of high-grade gneisses. *Geological Society of America Memoirs,* 197**,** 209-241.

SLAGSTAD, T., MELEZHIK, V., KIRKLAND, C., ZWAAN, K., ROBERTS, D., GOROKHOV, I. & FALLICK, A. 2006. Carbonate isotope chemostratigraphy suggests revisions to the geological history of the West Finnmark Caledonides, northern Norway. *Journal of the Geological Society,* 163**,** 277-289.

SLAGSTAD, T., PIN, C., ROBERTS, D., KIRKLAND, C. L., GRENNE, T., DUNNING, G., SAUER, S. & ANDERSEN, T. 2014. Tectonomagmatic evolution of the Early Ordovician suprasubduction-zone ophiolites of the Trondheim Region, Mid-Norwegian Caledonides. *Geological Society, London, Special Publications,* 390**,** 541-561.

SPARKS, R. & MARSHALL, L. 1986. Thermal and mechanical constraints on mixing between mafic and silicic magmas. *Journal of Volcanology and Geothermal Research,* 29**,** 99-124.

STEPHENS, M., FURNES, H., ROBINS, B. & STURT, B. 1985a. Igneous activity within the Scandinavian Caledonides. *The Caledonide Orogen—Scandinavia and Related Areas,* 2**,** 623-656.

STEPHENS, M. & GEE, D. 1985. A tectonic model for the evolution of the eugeoclinal terranes in the central Scandinavian Caledonides. *The Caledonide Orogen—Scandinavia and Related Areas***,** 953-978.

STEPHENS, M., GUSTAVSON, M., RAMBERG, I. & ZACHRISSON, E. 1985b. The Caledonides of central-north Scandinavia—a tectonostratigraphic overview. *The Caledonide orogen–Scandinavia and related areas***,** 135-162.

STURT, B., PRINGLE, I. & RAMSAY, D. 1978. The Finnmarkian phase of the Caledonian orogeny. *Journal of the Geological Society,* 135**,** 597-610.

SUN, S.-S. 1982. Chemical composition and origin of the Earth's primitive mantle. *Geochimica et Cosmochimica Acta,* 46**,** 179-192.

SUN, S.-S. & MCDONOUGH, W. F. 1989. Chemical and isotopic systematics of oceanic basalts: implications for mantle composition and processes. *Geological Society, London, Special Publications,* 42**,** 313-345.

TEGNER, C., ROBINS, B., REGINIUSSEN, H. & GRUNDVIG, S. 1999. Assimilation of crustal xenoliths in a basaltic magma chamber: Sr and Nd isotopic constraints from the Hasvik Layered Intrusion, Norway. *Journal of Petrology,* 40**,** 363-380.

TEGNER, C., WILSON, J. R. & ROBINS, B. 2005. Crustal assimilation in basalt and jotunite: Constraints from layered intrusions. *Lithos,* 83**,** 299-316.

TIMOLEON, N., SYLVESTRE, G., PAUL, N. J., BERNHARD, S., DEPESQUIDOUX, T. T. & EMMANUEL, S. C. 2012. Geochemistry and geochronology of Peraluminous high-K granitic leucosomes of Yaoundé series (Cameroon): evidence for a unique Pan-African magmatism and melting event in north equatorial fold belt. *International Journal of Geosciences,* 3**,** 525.

TUCKER, R. D., ROBINSON, P., SOLLI, A., GEE, D. G., THORSNES, T., KROGH, T. E., NORDGULEN, Ø. & BICKFORD, M. 2004. Thrusting and extension in the Scandian hinterland, Norway: new U-Pb ages and tectonostratigraphic evidence. *American Journal of Science,* 304**,** 477-532.

VAN ACHTERBERGH, E., RYAN, C., JACKSON, S. & GRIFFIN, W. 2001. Data reduction software for LA-ICP-MS. *Laser-Ablation-ICPMS in the earth sciences—principles and applications. Miner Assoc Can (short course series),* 29**,** 239-243.

VAN STAAL, C., DEWEY, J., MAC NIOCAILL, C. & MCKERROW, W. 1998. The Cambrian-Silurian tectonic evolution of the northern Appalachians and British Caledonides: history of a complex, west and southwest Pacific-type segment of Iapetus. *Geological Society, London, Special Publications,* 143**,** 197-242.

VAN STAAL, C., WHALEN, J., MCNICOLL, V., PEHRSSON, S., LISSENBERG, C. J., ZAGOREVSKI, A., VAN BREEMEN, O. & JENNER, G. 2007. The Notre Dame arc and the Taconic orogeny in Newfoundland. *Geological Society of America Memoirs,* 200**,** 511-552.

VAVRA, G. 1993. A guide to quantitative morphology of accessory zircon. *Chemical Geology,* 110**,** 15-28.

VERMA, S. P., GUEVARA, M. & AGRAWAL, S. 2006. Discriminating four tectonic settings: Five new geochemical diagrams for basic and ultrabasic volcanic rocks based on log—ratio transformation of major-element data. *Journal of Earth System Science,* 115**,** 485-528.

VERMEESCH, P. 2006. Tectonic discrimination diagrams revisited. *Geochemistry Geophysics Geosystems,* 7.

VERNON, R., ETHERIDGE, M. & WALL, V. 1988. Shape and microstructure of microgranitoid enclaves: indicators of magma mingling and flow. *Lithos,* 22**,** 1-11.

WANG, P. & GLOVER, L. 1992. A tectonics test of the most commonly used geochemical discriminant diagrams and patterns. *Earth-Science Reviews,* 33**,** 111-131.

WATSON, E. & HARRISON, T. 1984. Accessory minerals and the geochemical evolution of crustal magmatic systems: a summary and prospectus of experimental approaches. *Physics of the Earth and Planetary Interiors,* 35**,** 19-30.

WATT, G. & HARLEY, S. 1993. Accessory phase controls on the geochemistry of crustal melts and restites produced during water-undersaturated partial melting. *Contributions to Mineralogy and Petrology,* 114**,** 550-566.

WIEDENBECK, M., ALLE, P., CORFU, F., GRIFFIN, W., MEIER, M., OBERLI, F., QUADT, A. V., RODDICK, J. & SPIEGEL, W. 1995. Three natural zircon standards for U-Th-Pb, Lu-Hf, trace element and REE analyses. *Geostandards newsletter,* 19**,** 1-23.

WILSON, M. 1993. Magmatic differentiation. *Journal of the Geological Society,* 150**,** 611-624.

WINCHESTER, J. & FLOYD, P. 1976. Geochemical magma type discrimination: application to altered and metamorphosed basic igneous rocks. *Earth and Planetary Science Letters,* 28**,** 459-469.

WINTER, J. D. 2010. *Principles of igneous and metamorphic petrology,* Prentice Hall New York.

WOOD, D. A., JORON, J.-L. & TREUIL, M. 1979. A re-appraisal of the use of trace elements to classify and discriminate between magma series erupted in different tectonic settings. *Earth and Planetary Science Letters,* 45**,** 326-336.

XIA, L.-Q. 2014. The geochemical criteria to distinguish continental basalts from arc related ones. *Earth-Science Reviews,* 139**,** 195-212.

XIA, L., XIA, Z., XU, X., LI, X. & MA, Z. 2013. Late Paleoproterozoic rift-related magmatic rocks in the North China Craton: Geological records of rifting in the Columbia supercontinent. *Earth-Science Reviews,* 125**,** 69-86.

YOSHINOBU, A. S., BARNES, C. G., NORDGULEN, Ø., PRESTVIK, T., FANNING, M. & PEDERSEN, R. 2002. Ordovician magmatism, deformation, and exhumation in the Caledonides of central Norway: An orphan of the Taconic orogeny? *Geology,* 30**,** 883-886.

ZWAAN, K. & ROBERTS, D. 1978. *Tectonostratigraphic succession and development of the Finnmarkian nappe sequence, North Norway,* Universitetsforlaget.

Appendix

Appendix A - Sample Coordinates

Appendix B – Thin Section Descriptions

Appendix C – Whole-rock analysis

Appendix D – Cathodoluminescence (CL) images of the analysed zircons

Appendix E – Zircon geological data

Appendix A – Sample coordinates

Sample	Rock	East	North
P1.1	Pegmatite	-	-
P2.1	Mafic dyke	-	-
P2.2	Mafic dyke	-	-
P 4.1	Garnet-bitote gneiss	-	-
P 4.2	Garnet-mica schist	-	-
P 4.3	Garnet-bitote gneiss	490574	7345730
P 4.4	Garneb-mica schist	490872	7345301
P 4.5	Biotite gneiss	491588	7344842
P 5.1	Mafic dyke	485155	7338781
P 5.2	Gabbro	485193	7338574
P 5.3	Pegmatite	485565	7338285
P 6.1	Gabbro	485972	7338503
P 6.2	Garnet-bitote gneiss	486011	7339012
P 6.3	Gabbro	485990	7338443
P 6.4	Gabbro	487351	7338543
P 7.1	Gabbro	485986	7338454
P 7.2	Mafic dyke	486113	7338491
P 7.3	Gabbro	486671	7338591
P 7.4	Gabbro	487351	7338543
P 7.5	Gabbro	487088	7338899
P 8.1	Kvartsitt	488718	7340688
P 8.2	Garnet-bitote gneiss	488592	7340703
P 8.3	Garnet-mica schist	488499	7340637
P 8.4	Garnet-bitote gneiss	487641	7339284
P 8.5	Gabbro	488378	7340410
P 8.6	Quartzite	488358	7340841
P 9.1	Garnet-bitote gneiss	489269	7339572
P 9.2	Gabbro	489306	7339225
P 9.3	Gabbro	488481	7338994
P 9.4	Gabbro	487909	7339147
P10.1 UM	Gabbro	481429	7336148
P10.2 UM	Gabbro	-	-
P11.1 KV	Garnet-mica schist	490061	7346298
P11.2 ØS	Granite	-	-
P12.1A KV	Garnet-biotite gneiss	-	-
P12.1B KV	Garnet-mica schist	-	-
P13.1 KV	Granat biotitt gneis	490207	7346150
P13.2 KV	Garnet-mica schist	490190	7346136
P13.3 KV	Garnet amphibolite	490236	7346018
P13.4 KV	Garnet amphibolite	490052	7346299

Sample	Rock	East	North
P14.3 (a) KV	Garnet-mica schist	490722	734506
P14.3 (b) KV	Garnet-bitite gneiss	490722	734506
P14.4 KV	Garnet amphibolite	491391	7344961
P14.5 KV	Two-mica geniss	491581	7344841
P15.1ØS	Garnet-bitote gneiss	488673	7341089
P15.2A ØS	Mafic rock	488725	7340941
P15.2B ØS	Granite	488725	7340941
P15.3 ØS	Mafic dyke	488548	7341012
P15.4 ØS	Quartzite	488191	7340870
P16.1 ØS	Mafic dyke	488992	7340464
P16.2A ØS	Mafic dyke	488494	7338872
P16.2B ØS	Gabbro	488494	7338872
P16.3A ØS	Impure quartzite	488440	7340560
P16.3B ØS	Garnet-bitote gneiss	488440	7340560
P17.1 ØS	Contat-zone granitoid	488494	7338872
P17.2 ØS	Mafic dyke	483132	7338336
P17.3 ØS	Mafic dyke	488305	7340291
P18.1 PL	Two-mica geniss	488526	7347580
P18.2 PL	Chloritified garnet-biotit	487614	7345587
P19.1 UM	Mafic dyke	483074	7338224
P19.2 UM	Olivin-gabbro	483134	7338331
P19.3 UM	Gabbro	483132	7338336
P19.4A UM	Gabbro	483181	7338346
P19.4B UM	Coarse-grained garnet hornblende gabbro	483181	7338346
P19.5 UM	Mafic dyke	483254	7338374
P19.6A UM	Mafic rock	483019	7338121
P19.6B UM	Gabbro		
P20.1 UM	Garnet gabbro	482019	7338121
P20.2A UM	Gabbro	483409	7338069
P20.2B UM	Gabbro		
P22.1 PL	Marble	486959	7344769
P22.2 PL	Gneiss	487051	7344680
P23.1 SF	Gneiss	489906	7342926
P23.2 SF	Garnet amphibolite	489876	7342673

Appendix B – Thin Section Descriptions

Thin section: P1.1

Rock name: Pegmatite

Hand specimen

The pegmatite is coarse grained and leucocratic with a white colour, and some scattered occurrence of micas. The rock mainly consists of coarse-grained plagioclase where twinning is visible, and medium-grained milky-white quartz is present in a lesser amount. The mica grains are scattered and consist of muscovite and biotite. Some of the biotite grains show a greenish colour.

Minerals

Main minerals: Plagioclase (60%), quartz (25 - 30%), muscovite (5%)

Accessorise: chlorite (2-5%), biotite (1%), titanite (<1%), epidote (clinozoisite) (<1 %)

Description

The pegmatite is coarse-grained and manly consist of plagioclase and quartz grains. The coarse plagioclase grains have a dusty surface and have poikilitic texture with inclusion of quartz, muscovite, chlorite and biotite. The grains are anhedral and the grain boundaries are irregular. Quartz grains are anhedral and occurs both inter- and intragranular. The quartz show undulating extinction, mostly irregular grain-boundaries, and a few coarser grains show triple junction. Muscovite and biotite are medium- to coarse grained, have lath shape and occur interstitial between grain contacts and as inclusions in plagioclase. Most biotite grains are altered to chlorite.

Grain size

Plagioclase: 2.5 mm -1.4 cm, quartz: 0.25-1.2 cm, muscovite: 0.25-4.5 mm, biotite: 0.25-3.7 mm, chlorite: 2.7 mm -1.0 cm, epidote (clinozoisite): 0.3-3.5 mm, titanite: 1.0-2.7 mm

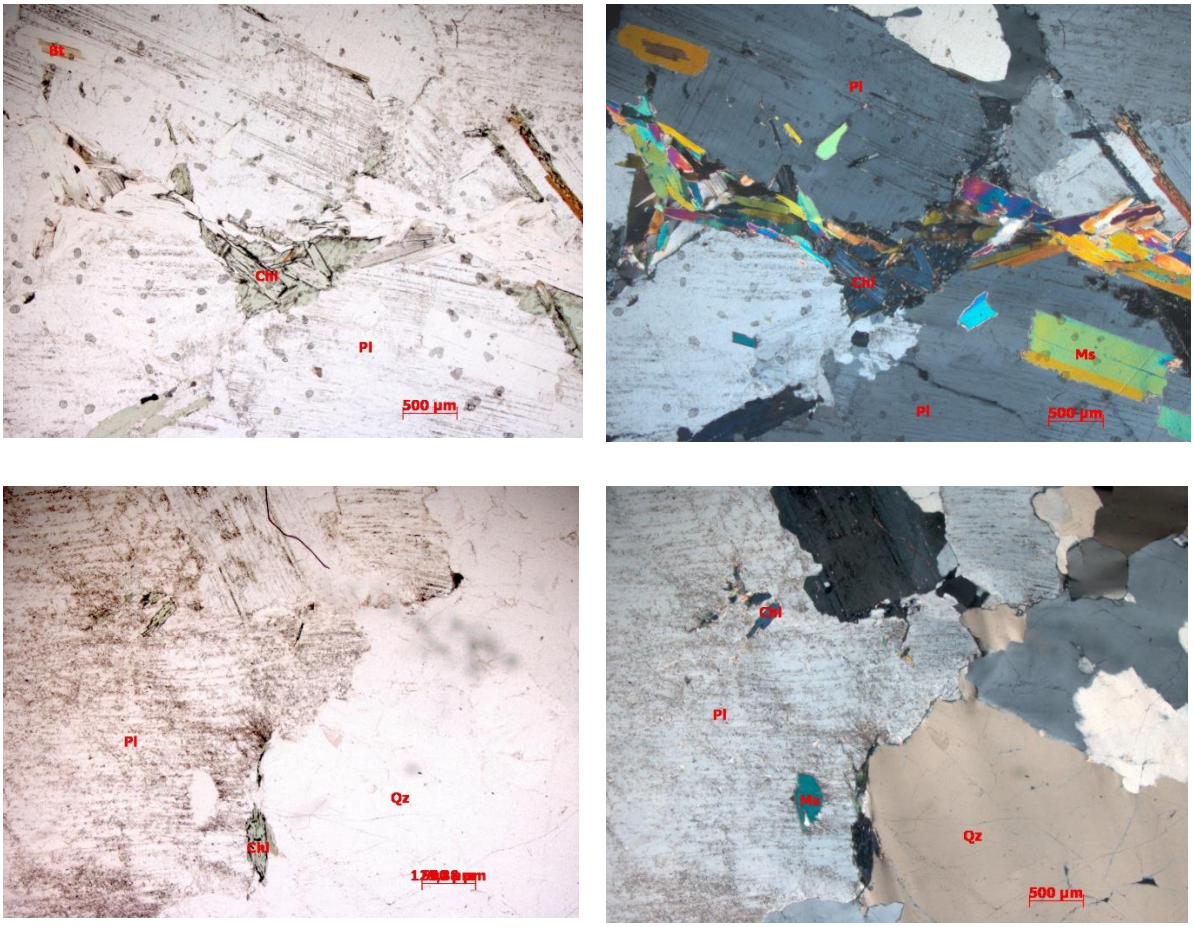

Thin section images of the pegmatite. Left photos in plan-polarized light (ppl), and right photos in cross-polarised light (xpl)

Thin section: P2.1

Rock name: **Mafic dyke**

Hand specimen

The mafic dyke is a massive, homogenous and mesocratic. The rock is very-fine grained and the minerals cannot be identified by hand lens. Occurrence of a few light minerals gives the rock a dark grey colour.

Minerals

Amphibole (50-60%), plagioclase (30%), pyroxene (2-5%), opaque (10%)

Description

The dyke is very fine-grained and undeformed. The amphibole is anhedral, pale green, probably secondary formed actinolite, which probably replaced the primary mafic mineral. The plagioclase grains are subhedral, and some grains are lath shaped and other occur with lobate contacts to the amphibole. The lobate contacts may result from partly reabsorption or results from simultaneous growth. Pyroxene appears randomly as a few subhedral pheno- and glomerocrystals. The opaques are sub-rounded to anhedral, and occur as scattered grains surrounded by pale green amphibole. The minerals do not show any orientation, so they have not grown during deformation. A few tiny cracks occur in the thin section cutting through the mafic dyke in about 0.2 mm width.

Grain size

Amphibole: 0.1 – 0.3 mm, plagioclase: 0.03 – 1.2 mm, pyroxene: 0.5 – 2.0 mm, opaquer: 0.04 – 1.5 mm.

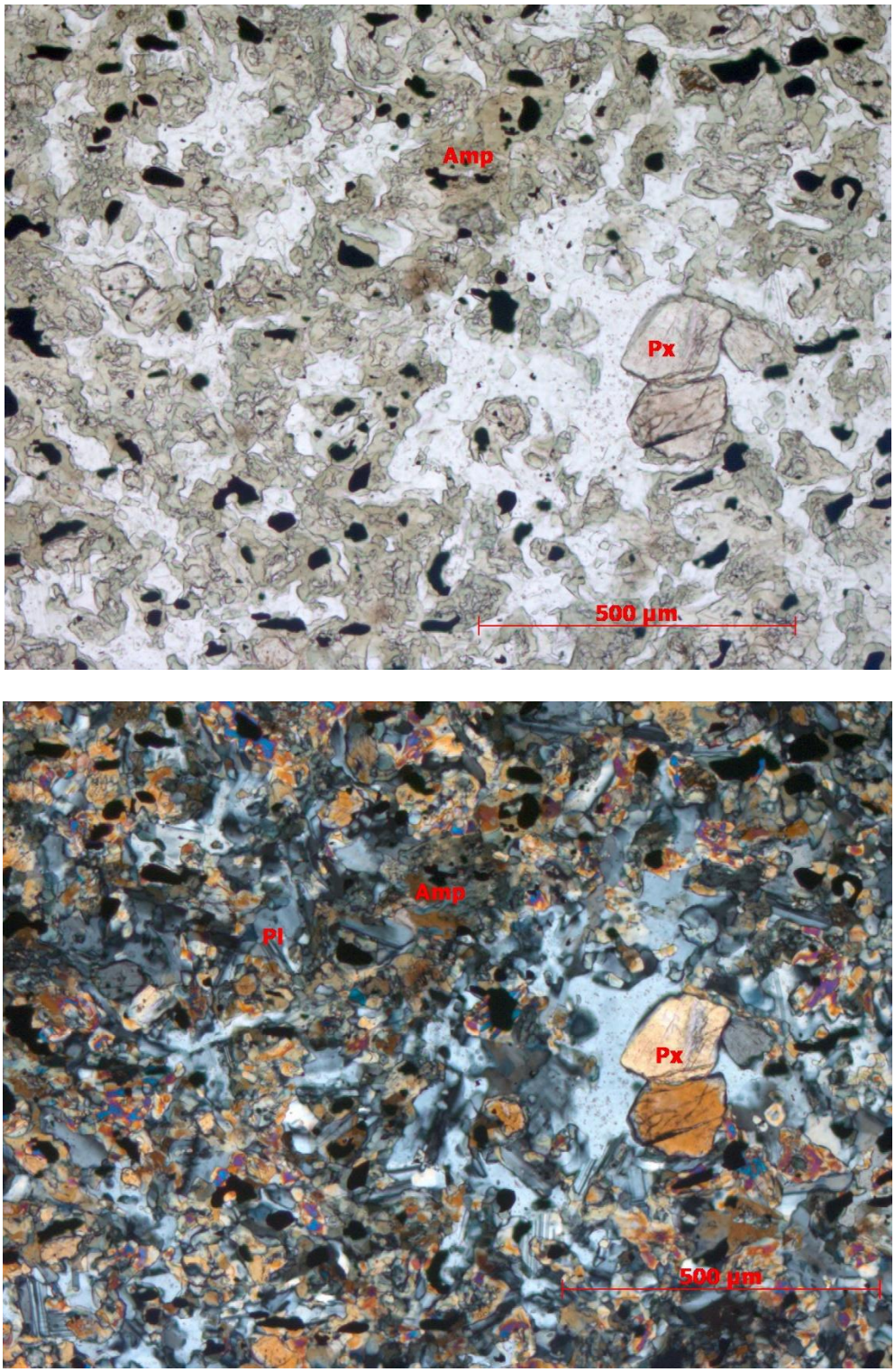

Thin section image of the mafic dyke. Upper photo in ppl, and lower photo in xpl.

Thin section: P4.1

Rock name: Garnet-biotite gneiss

Hand specimen

The garnet-biotite gneiss is leucocratic, medium-grained and heterogenic. The rock is separated in white and dark millimetre to centimetre thick layers. The dark mineral of biotite has a flaky dark brown colour, and the light minerals consist of white plagioclase grains and milky white quartz. The rock also contain small red garnets.

Minerals

Main minerals: Quartz (40%), biotite (25%), plagioclase (15%), garnet (10%), titanite (5%)

Accessories: Muscovite (1%), chlorite (1%), zircon (1%), apatite (1%), allanite (epidote) (1-2%)

Description

The garnet biotite gneiss is fine- to medium-grained and characterised by thin layers of aligned biotite. The biotite grains have brown colour, are lath shaped and show a slight trend of foliation in the rock. The medium-grained biotite has inclusions of garnet, titanite and allanite, and a few grains are chloritified. The quartz is fine- to medium grained, have irregular grain-boundaries and undulating extinction. The plagioclase is randomly distributed throughout the rock, fine- to medium grained and have irregular grain-boundaries. A few plagioclase grains show a dusty surface and slight seritization. The garnet is mostly medium-grained and almost euhedral and randomly distributed with a poikilitic texture and inclusions of quartz and titanite.

Grain size

Quartz: 0.1-2.2 mm, biotite: 0.2 -4.2 mm, plagioclase: 0.3-1.8 mm, garnet: 0.32-1.05 mm, titanite: 0.02-0.5 mm, muscovite: 0.07-0.4 mm, chlorite: 0.2-0.4 mm, zircon: 0.06-0.5 mm, apatite: 0.1-0.2 mm, allanite: 0.07-0.2 mm.

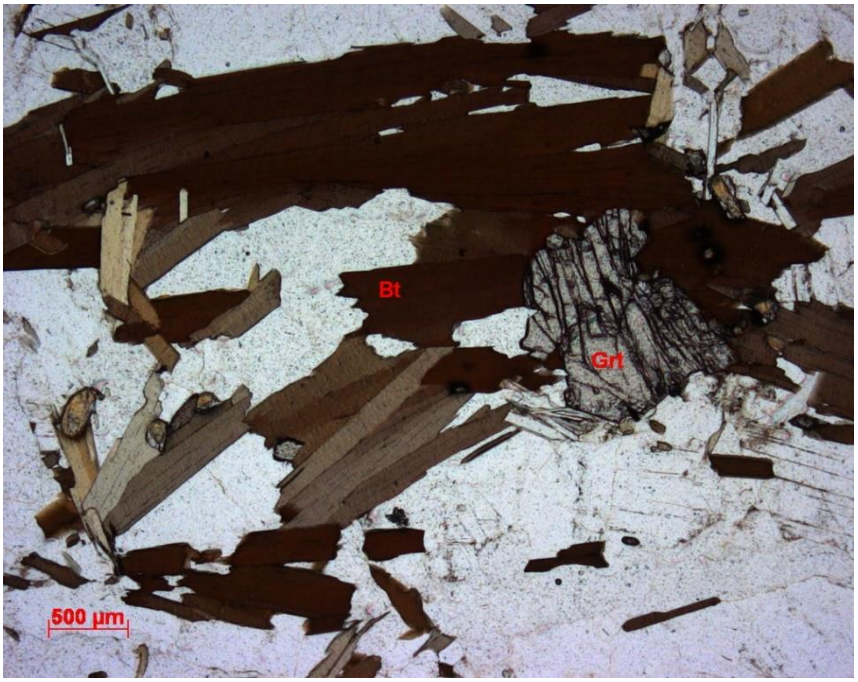

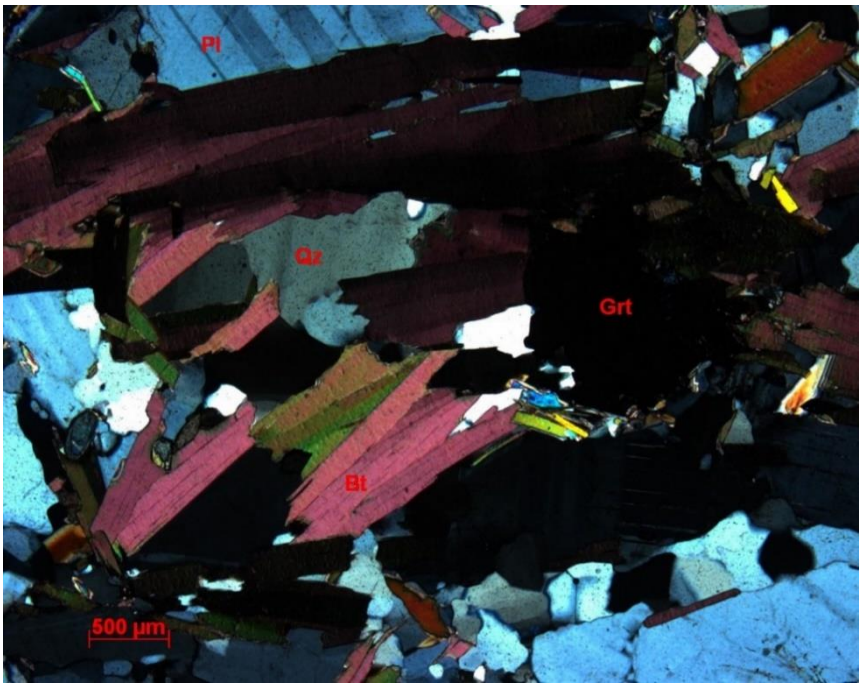

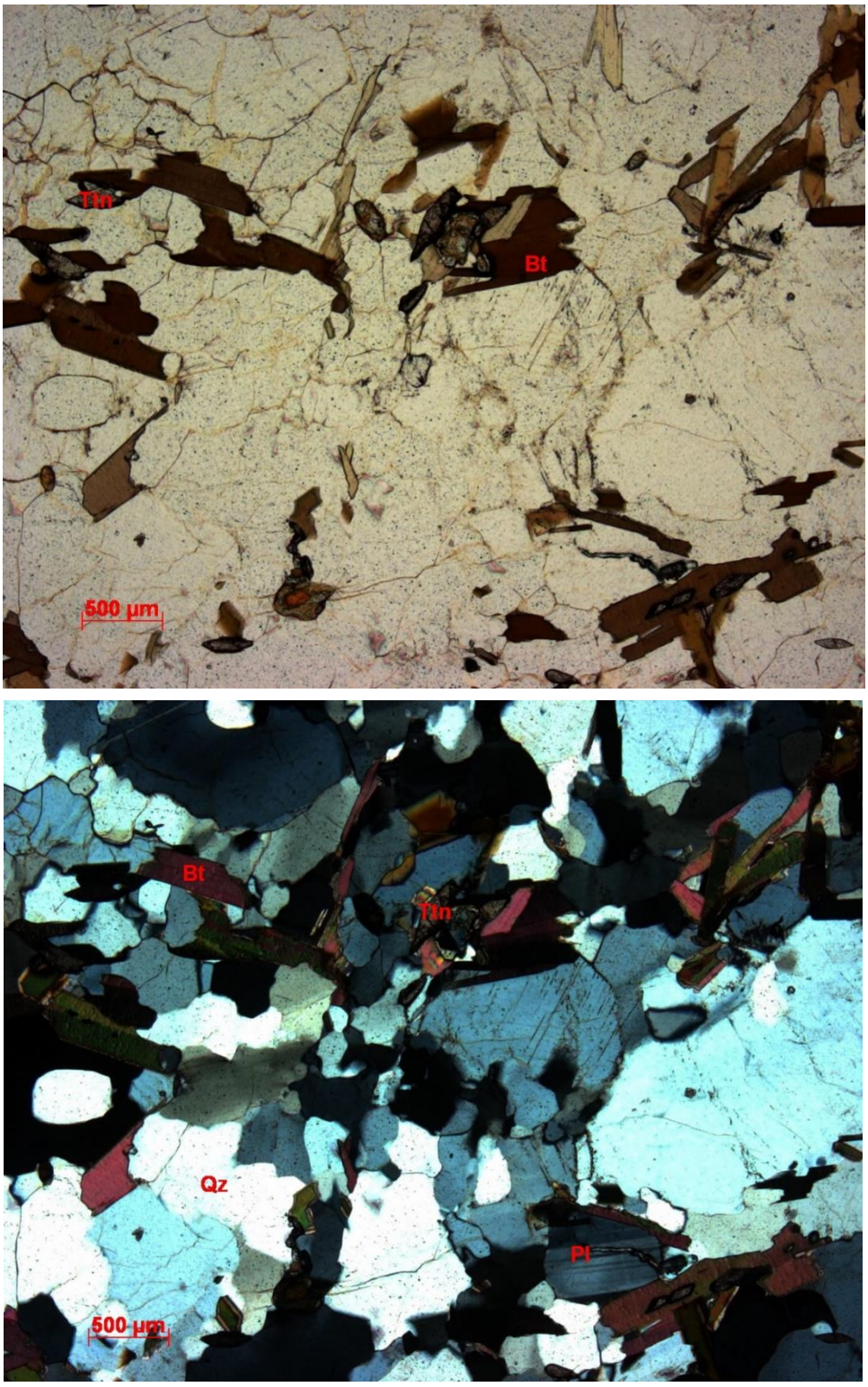

Thin section images of the Garnet-biotite gneiss.

Thin section: P4.3

Rock name: Garnet-biotite gneiss

Hand specimen

The garnet-biotite gneiss is leucocratic medium-grained and heterogenic. The rock is separated in white and dark millimetre to centimetre thick layers. The white layers mainly consist of quartz and plagioclase, and the dark layers has a high occurrence of biotite in addition to quartz and plagioclase. Small garnet is mainly concentrated in the darker layers.

Minerals

Main minerals: Quartz (40%), plagioclase (25%), garnet (15%), biotite (10%).

Accessories: Apatite (10%), zircon (<1%)

Petrographic Description

The garnet biotite gneiss is fine- to medium grained and characterised by centimetre thick layers, richer and poorer in garnet and biotite. The rock is relatively quartz rich, and the quartz is fine- to medium grained, have mostly irregular grain-boundaries, but some of the coarser quartz-grains show triple junction. The plagioclase is anhedral, fine- to medium grained and randomly distributed throughout the rock. Some of the plagioclase grains show a dusty surface in plan polarized light. The biotite is aligned and defines a foliation in the rock. The layering most likely represents primary layering. The brown biotite is lath shaped and a few grains are altered to chlorite. The dark layering separates from the light layering mainly because of higher concentration of biotite, but it is also a slightly higher concentration of garnet in the biotite rich layers. The garnet is almost euhedral and varies from fine- to medium grained. The garnet has a poikilitic texture with inclusions of quartz, biotite and chlorite. Accessory phases are apatite, including some relatively large apatite grains, and zircon.

Grain size

Quartz: 0.1 – 1.25mm, plagioclase: 0.4 – 1.5mm, garnet: 0.55 – 1.3mm, biotite: 0.36 – 4.0mm, chlorite: 0.1 – 0.6mm, apatite: 0.2 – 1.1mm, zircon: <0.1 mm

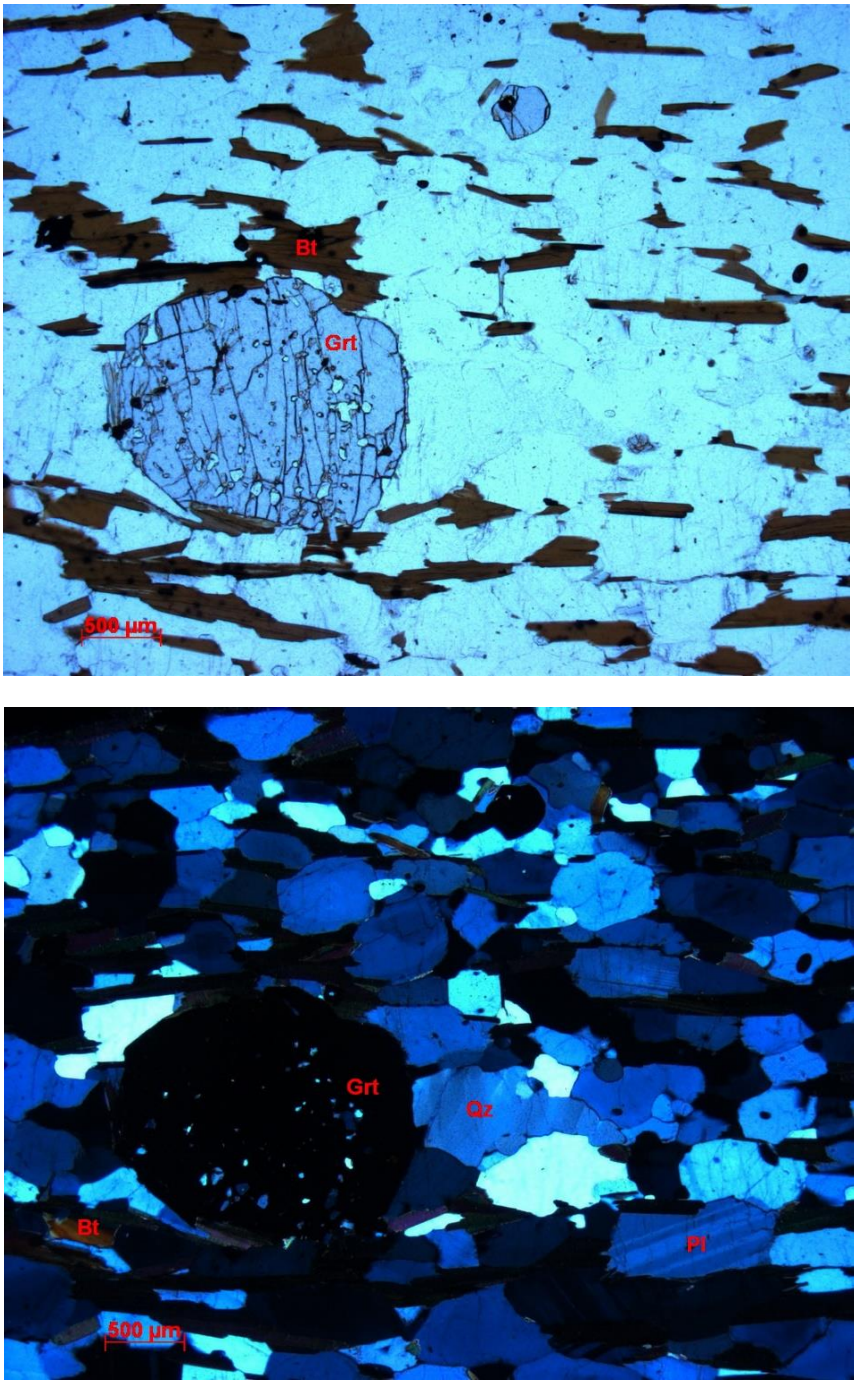

Thin section image of the garnet rich layer.

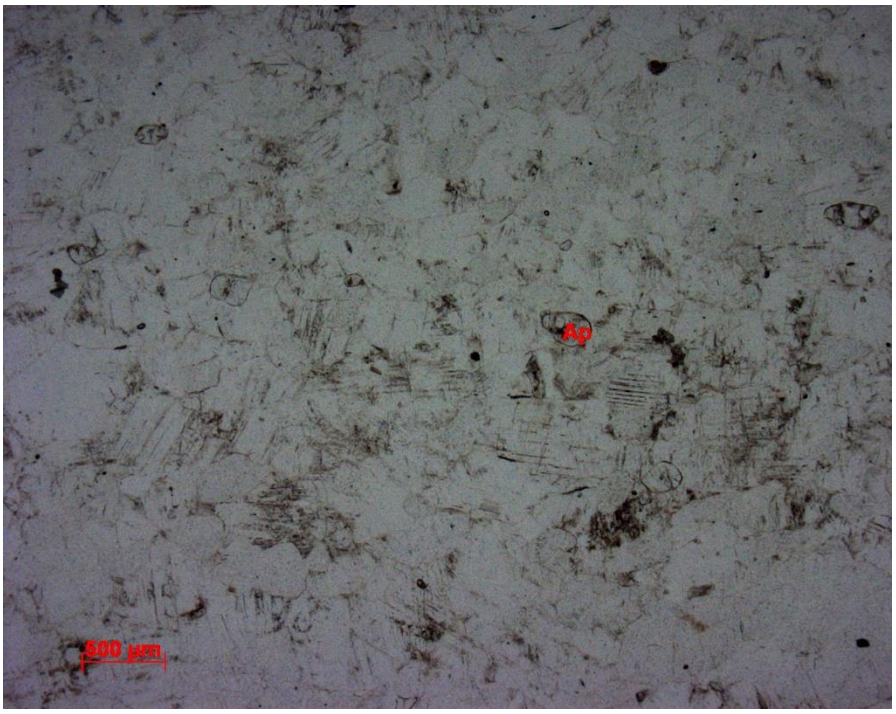

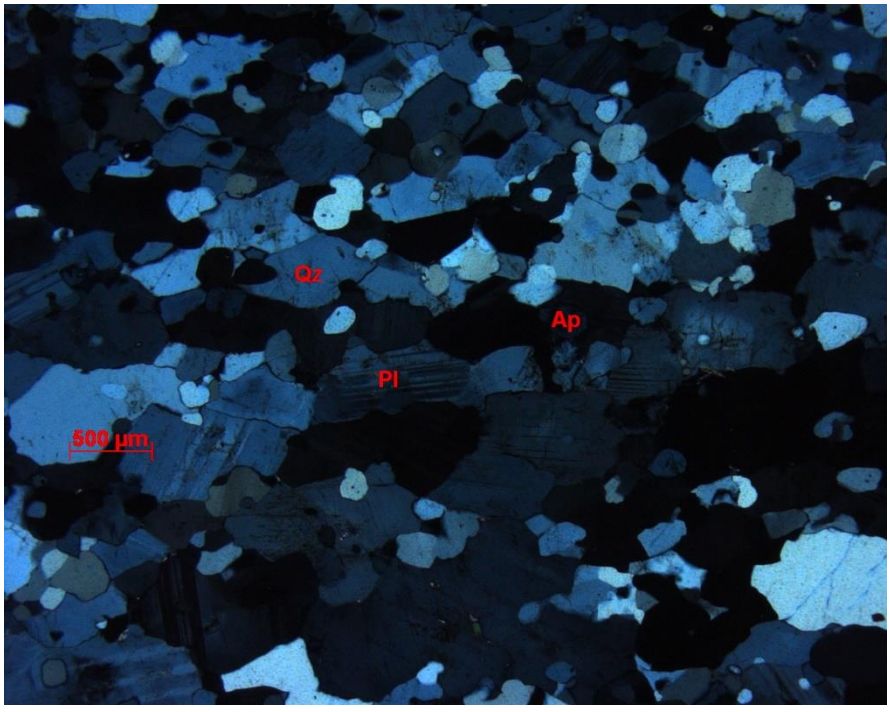

Thin section images of the garnet poor layer

Thin section: P4.4

Rock name: Garnet-mica schist

Hand specimen

The garnet-mica schist is medium grained, schistoses and mica rich. It mainly consist of quartz, muscovite, biotite and garnet. The mica-grains are aligned and show crenulation folding and the quartz-grains are distributed in-between the micas. The garnets are red and medium-grained in 1-2 mm sizes.

Minerals

Main minerals: Quartz (40%), muscovite (40%), biotite (10%) garnet (5-10%)

Accessorise: Plagioclase (1%)

Description

The garnet-mica schist is medium grained and deformed. The muscovite is characteristic with kink-banding and folds around garnet grains. The garnet are almost euhedral and have a poikilitic texture with inclusion of quartz. The biotite occur in-between the muscovite grains, some biotite grains show pleochroic halos and one grain is chloritized. The quartz grains are fine to medium-grained, have anhedral shape, irregular grain-boundaries and undulating extinction.

Grain size

Quartz: 0.1 - 2.0mm, muscovite: 0.3 – 5.5mm, biotite: 0.2 – 1.3mm, garnet: 0.9 – 2.4mm, plagioclase: 0.3 – 0.7mm

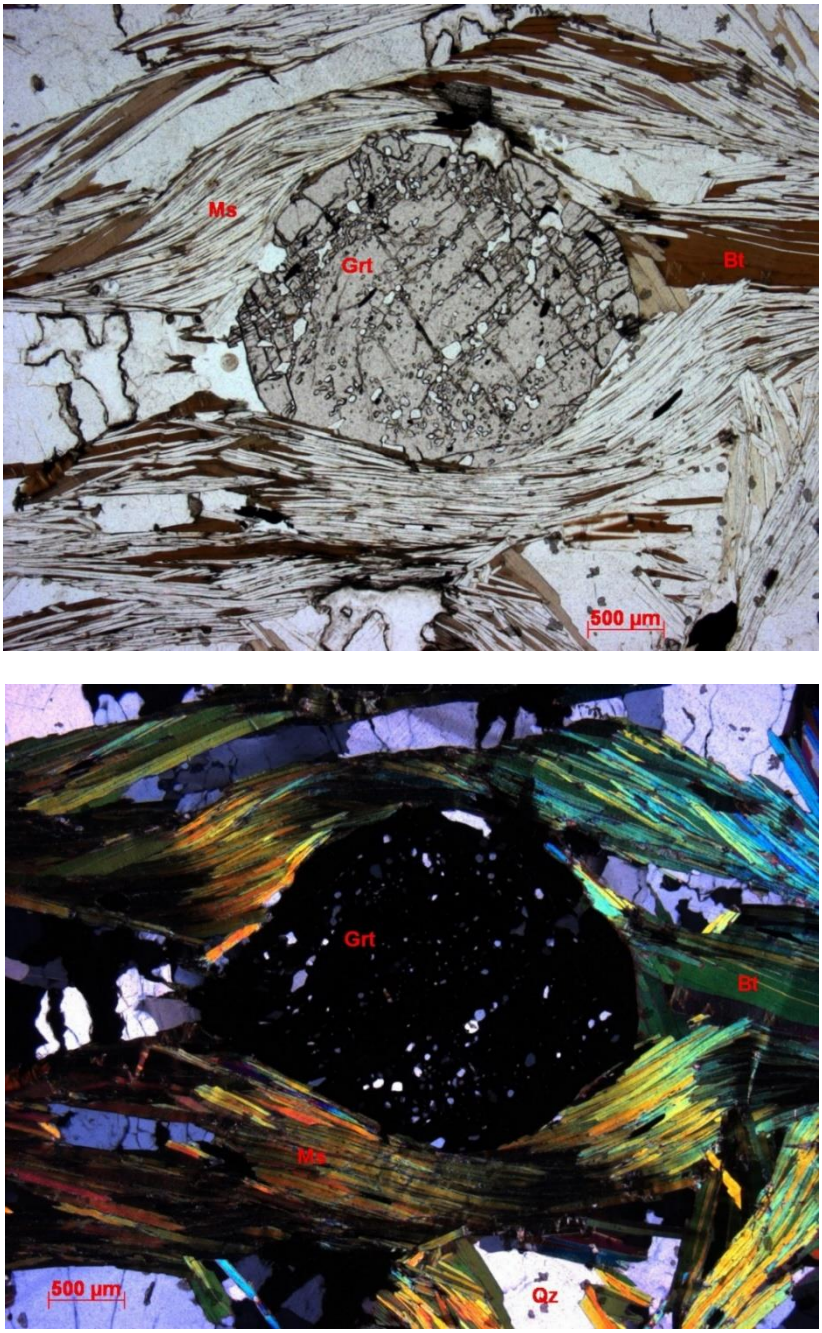

Thin section images of the garnet-mica schist. Upper photo in ppl and lower photo in xpl

Thin section: P5.2

Rock name: Gabbro

Hand specimen

Medium-grained melanocratic gabbro with almost even distribution of white and dark minerals, with presence of a few scattered coarse-grained dark minerals. The light minerals are mainly of plagioclase and the dark consist of pyroxene, biotite and amphibole. The grain sizes are about 1-2 mm.

Minerals

Main minerals: Plagioclase (40%), (clino-)pyroxene (30%), biotite (15%), amphibole (10%),

Accessories: apatite (1%), quartz (1%), opaque (1-5%)

Description

The gabbro is fine- to medium-grained and undeformed. The Pyroxene is subhedral, and the plagioclase grains are lathy with irregular grain boundaries. Plagioclase and pyroxene occur in a sub-ophitic texture and many of the pyroxene grains have an altered rim of green amphibole (most likely hornblende). Biotite grains occur as both dark brown anhedral flakes and subhedral-elongated grains. The concentration of the biotite increases closer to the mafic dyke, which cut the gabbro. The opaques occur as inclusions in pyroxene and biotite.

The mafic dyke, which cut the gabbro mainly contain plagioclase and biotite. The thin section only covers a small part of the mafic dyke and most likely represents the contact between them. In the contact, the plagioclase grains are mostly coarser than in the rest of the thin section and the biotite occur in a larger concentration, and there may be presence of few small quartz grains as well.

Grain size

Plagioclase: 0.14-1.6 mm, pyroxene: 0.1-1.25 mm, biotite: 0.08-1.4 mm, amphibole: 0.04-0.2 mm, Opaque: 0.01-0.15 mm, quartz: 0.15-0.75 mm

.

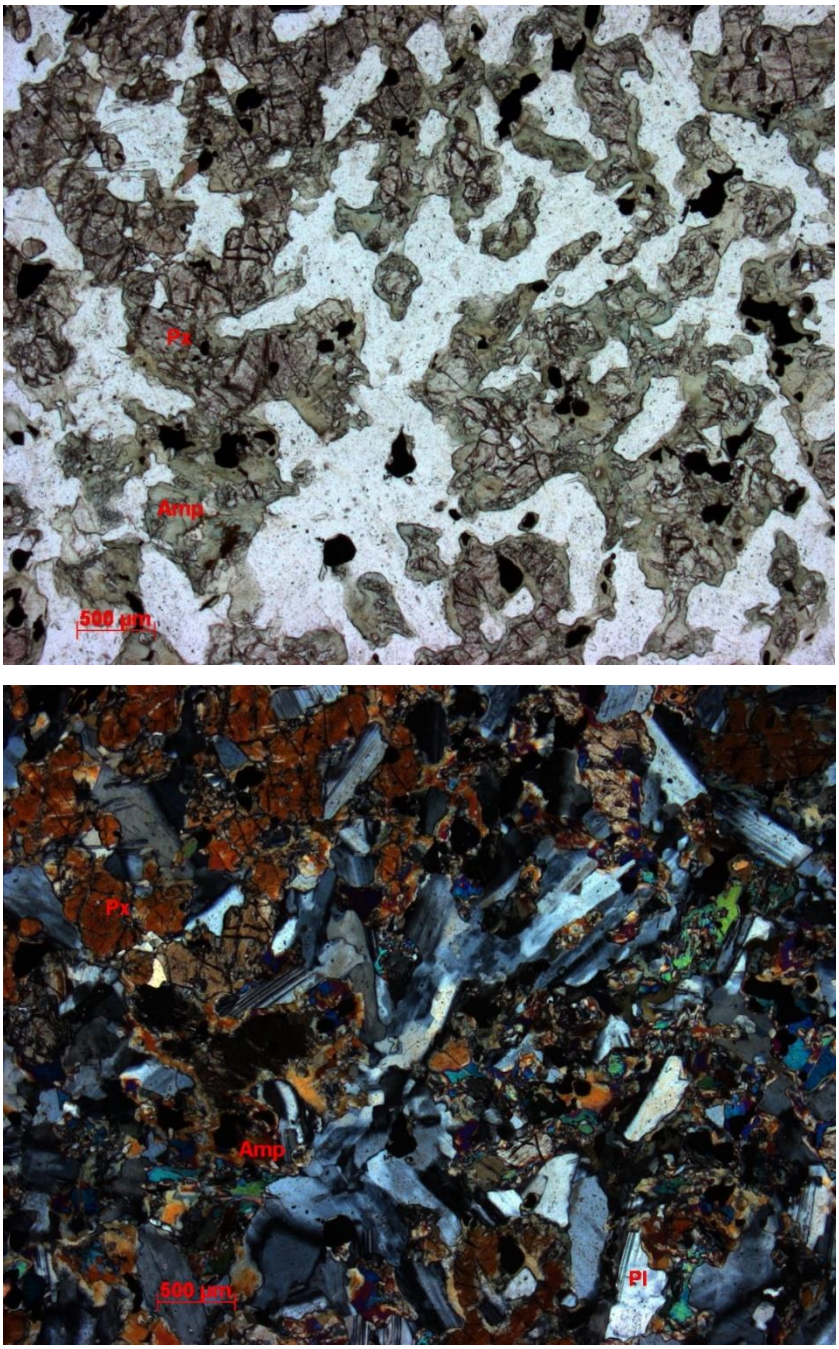

Thin section images of the gabbro. Upper photo in ppl, and lower photo in xpl

Thin section: P5.3

Rock name: Pegmatite

Hand specimen

The rock is leucocratic and medium-grained. It mainly consists of white plagioclase and milky-white quartz, but some silver coloured scattered muscovite grains are also occurring. The rock has no orienting minerals, and plagioclase and quartz lies interchangeably.

Minerals

Plagioclase (50%), quartz (35 – 40%), muscovite (10 – 15%)

Description

The pegmatite is medium- to coarse grained and manly consist of plagioclase and quartz. The plagioclase are subhedral, has a dusty surface, seritizated and a poikilitic texture with inclusion of quartz grains. The grain boundaries of the plagioclase are irregular. Quartz grains are anhedral and occur both intergranular and as inclusions. The quartz show undulating extinction and irregular grain-boundaries. The muscovite is mostly anhedral, and the very fine-grained muscovite occurs inside plagioclase grains as secondary formed minerals. Some medium-grained muscovites have undeveloped crystal shape, kind of skeletal texture, and they always occur inside plagioclase grains with the same crystal orientation. These muscovite grains probably grew secondary from the plagioclase. A few muscovite grains are present with a lath shape.

Grain size

Quartz: 1.1-2.9 mm, plagioclase: 0.6-4.5 mm, muscovite: 0.35-1.2 mm

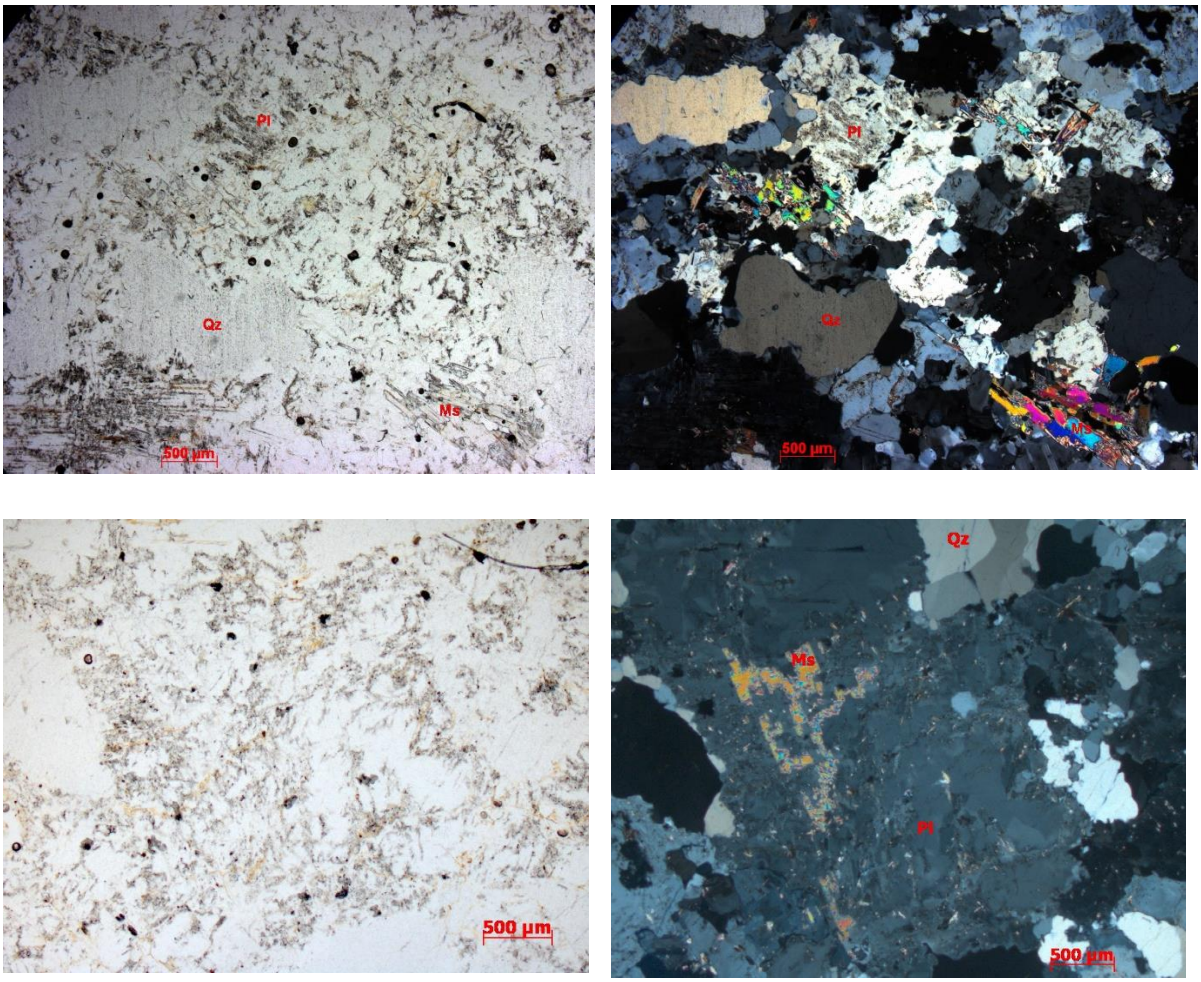

Thin section images of the pegmatite with plan-polarized light (ppl) to the left and with cross-polarised light (xpl) to the right.

Thin section: P6.2

Rock name: Garnet-two-mica gneiss

Hand specimen

The garnet-two-mica gneiss is leucocratic and fine-grained, it is heterogenic and separated in millimeter thick layers of light and dark minerals. Muscovite is present in both light and dark layers, but the light layers contains a larger amount of the muscovite. Light minerals consist of quartz, plagioclase and muscovite and dark minerals mainly of biotite. It is a relatively large amount of garnet in 0.5-1.0 mm sizes, and the garnet occur in both light and dark layers. The minerals in the dark layers show orientation.

Minerals:

Main minerals: Quartz (30%), plagioclase (25%), garnet (20%), biotite (10-15%), muscovite (5-10%)

Accessories: Rutil (1-5%)

Description:

The rock is fine grained and separates into layers, which is richer and poorer in garnet. The layers which is rich in garnet mainly consist of garnet and quartz with a lesser amount of plagioclase and micas. The garnet is present as subhedral to almost euhedral crystals, the quartz grains are very-fine to fine grained, have irregular grain boundaries and undulating extinction. The plagioclase is fine-grained and show irregular grain boundaries. Just a few mica grains are present in the garnet-rich layers, and the biotite occur as light brown minerals with a flaky shape and show poorly alignment. The few muscovite grains that are present in the garnet-rich layer is more elongated then the biotite. The garnet-poor layer mainly consist of micas and quartz, with a lesser amount of garnet and plagioclase. The micas show a poor alignment, and the biotite has a light brown color and are flaky to lath shaped. The muscovite are a bit coarser and more elongated than the biotite, and has a lath shape. The quartz and the plagioclase are very-fine grained to fine grained, have irregular grain boundaries and the quartz show undulating extinction. The few garnet grains that are present in the garnet-poor layer is fine grained and subhedral. The rutile is randomly distributed in the thin section.

Grain size:

Quartz: 0.04 – 0.9 mm, plagioclase: 0.18 – 0.5 mm, garnet: 0.1 – 1.0 mm, biotite: 0.18 – 1.0 mm, muscovite: 0.2 – 1.46 mm, rutil: 0.1 – 0.2 mm

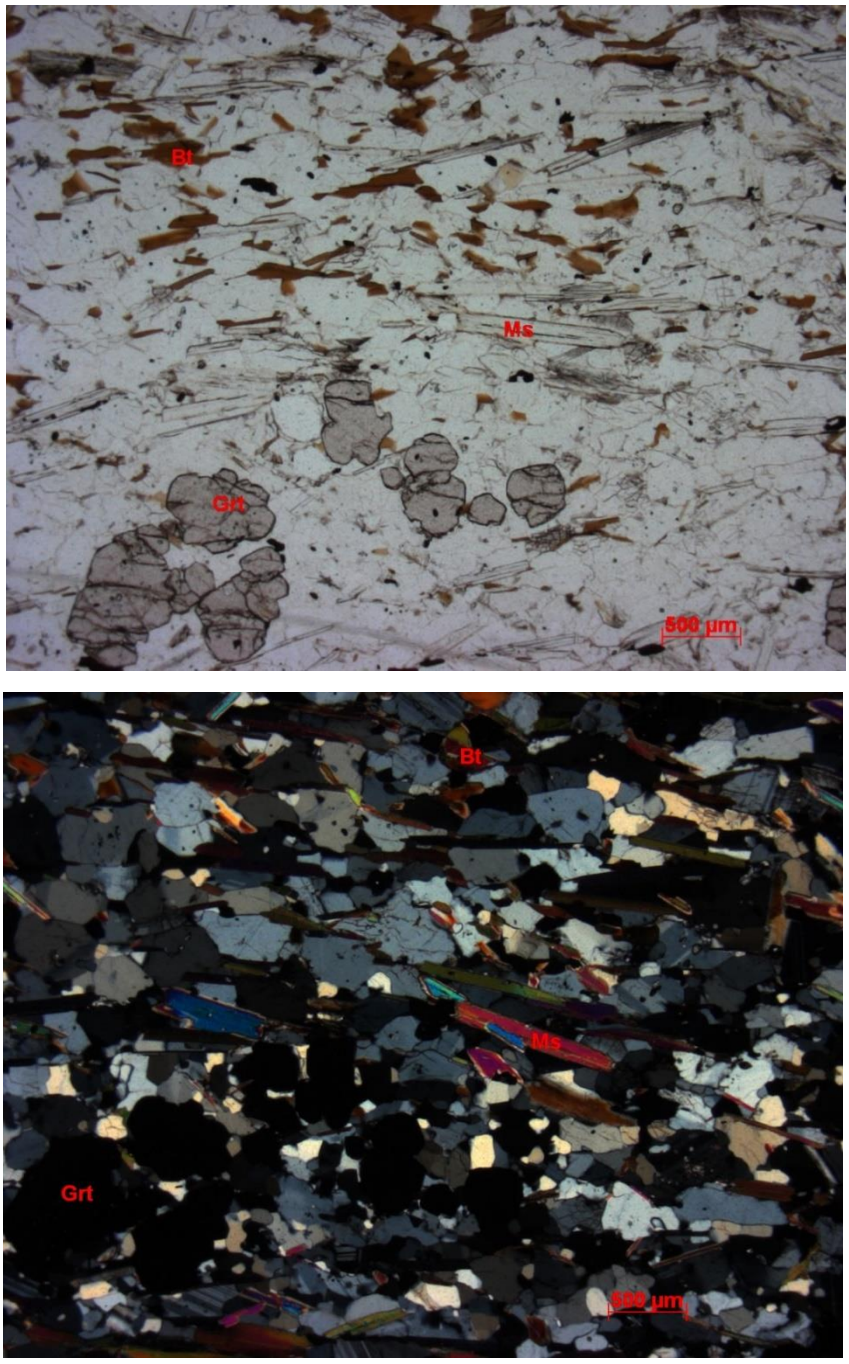

Thin section images of the garnet-two mica gneiss. Upper photo in ppl, and lower photo in xpl.

Thin section: P6.3

Rock name: Meta-gabbro

Hand specimen

Medium-grained melanocratic gabbro with almost even distribution of white and dark minerals. The light minerals consist of plagioclase and the dark minerals of pyroxene and amphibole. The grain size is about 1-2 mm. This rock lays in contact with a mafic dyke.

Minerals

Main minerals: Plagioclase (40%), Biotite (20%), Amphibole (20%), Pyroxene (15%)

Accessorise: quartz (1-3%), apatite (1%), zircon (1%),

Description

The gabbro is medium grained and undeformed, and cut by a fine-grained mafic dyke. Pyroxene is sub- to anhedral and is altered and rimmed by secondary replacement of green amphibole. Dark brown and green biotite occurs both as anhedral flakes and as lathy grains, and has inclusions of oxides. Biotite show occurrence of pleicoric halos, which indicate presence of zircons. Plagioclase is subhedral and lath shaped with irregular grain boundaries, which indicates a magmatic origin.

The mafic dyke which cut the gabbro is very fine-grained mainly consist of amphibole, biotite and plagioclase. The mafic and felsic minerals are segregated into millimetre thick layers oriented parallel to the margin of the mafic dyke.

Grain size

Gabbro: Plagioclase: 0.3-2.0 mm, biotite: 0.12-2.3 mm, amphibole: 0.3-1.0 mm, pyroxene: 0.3-1.2 mm, quartz: 0.1-1.1 mm, apatite: 0.16-0.3 mm, quartz: 0.01-0.04 mm, zircon: <0.01 mm
Dyke: Plagioclase: 0.13-0.44 mm, amphibole: 0.2-0.3 mm, biotite: 0.05-0.18 mm, pyroxene: 0.27-0.35 mm.

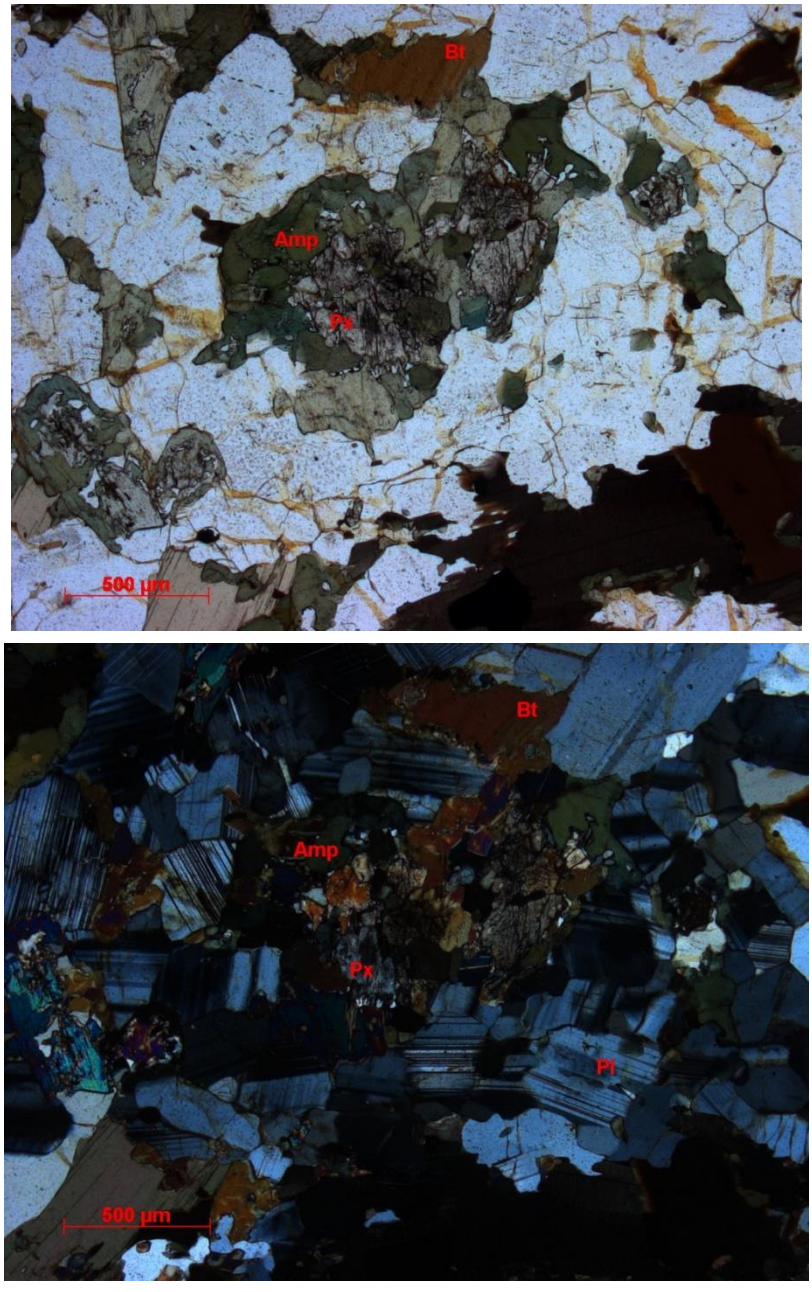

Thin section images of the gabbro. Upper photo in ppl, lower photo in xpl

Thin section: P7.2

Rock name: Mafic dyke

Hand specimen

A mesocratic very fine-grained mafic dyke. The rock is massive, homogenous and mainly consisting of black minerals. A few very fine-grained light minerals are scattered between the dark minerals.

Minerals

Main minerals: Amphibole (50-60%), plagioclase (25-30%), opaque (5-10%)

Accessories: biotite (1-2%), pyroxene (1%), muscovite (<1%),

Description

The mafic dyke is very fine-grained, and the minerals are so small that they sometimes are challenging to classify. Mainly the mafic dykes consist of amphibole and plagioclase. The amphibole may be a secondary formed mineral, and initially it may have been presence of pyroxene or olivine grains. The pyroxene or the olivine grains have probably been altered and rimmed by secondary replaced, green amphibole and the core of the mineral show a dusty pale colour in plan polarised light. Some amphibole grains show corona texture surrounding the core. The plagioclase is subhedral and lath shape and some grains show lobate contacts to the amphibole. The biotite is very fine grained, occurs as brown anhedral flakes, and appears in contact with the green amphibole. The biotite may have formed secondary. The opaques are scattered and they always occur surrounded by amphibole grains. The magmatic texture is preserved and there is no sign of deformation, so the alteration may result from fluids.

Grain size

Main minerals: Amphibole: 0.4 -1.0 mm, plagioclase: 0.1-0.9 mm, opaques: 0.04-0.4 mm

Accessories: Muscovite: 0.05-0.2 mm, biotite: 0.04-0.3 mm

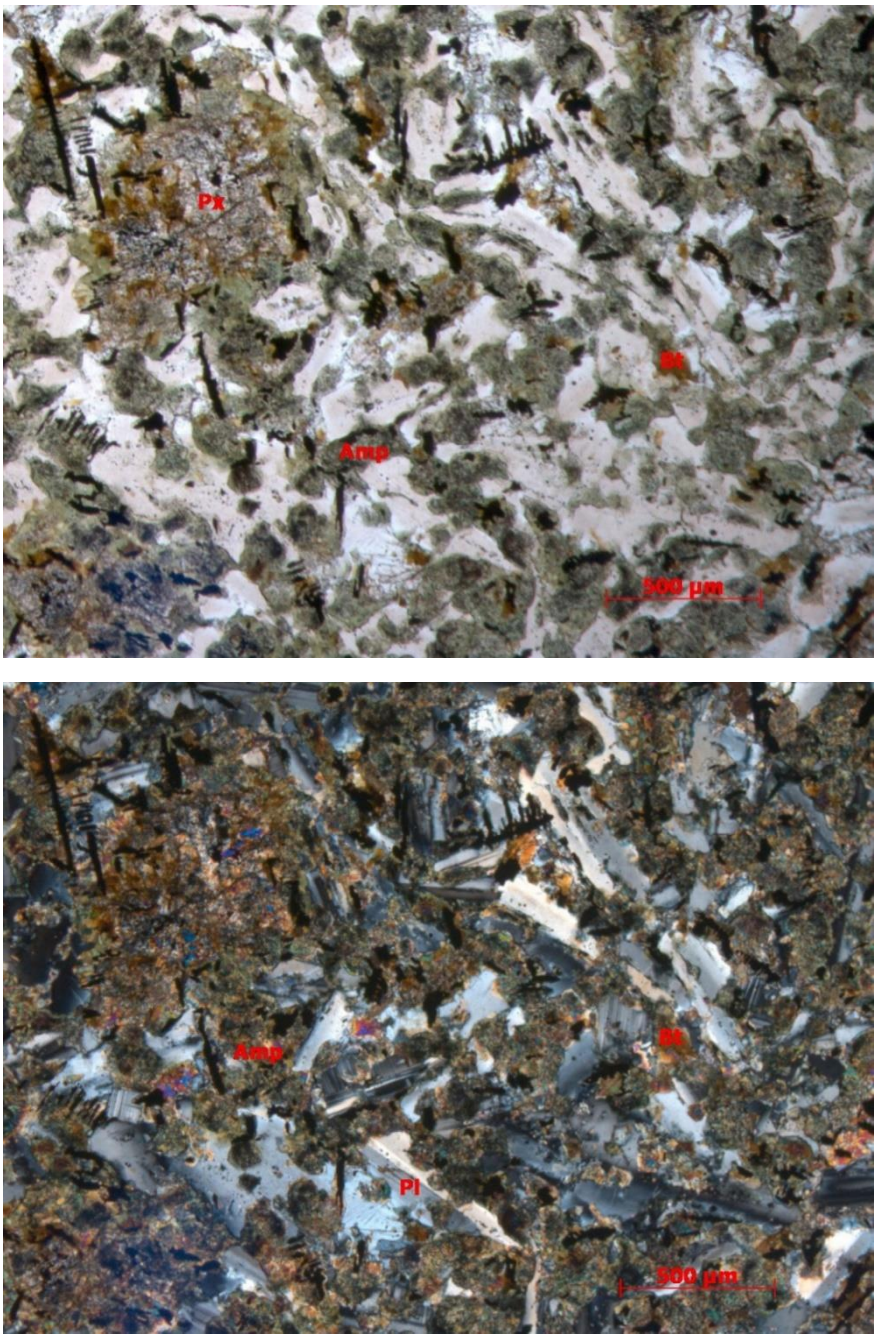

Thin section images of the mafic dyke. Upper picture show plane-polarized light, and lower picture show cross-polarized light.

Thin section: P7.4

Rock name: Gabbro

Hand specimen

The gabbro is homogeneous, melanocratic and fine- to medium-grained. The light and dark minerals are randomly distributed relative to each other. The light minerals has a bit smaller grain sizes than the darker minerals, and it is an overweight of dark minerals. A few of the dark minerals have a bit bigger grain-size then the rest of the rock, and they are about 1-2 mm in size.

Minerals

Pyroxene (40%), plagioclase (40%), amphibole (10%), biotite (5%), Opaque (5%)

Petrographic Description

The gabbro is fine grained and undeformed. Pyroxene is sub- to anhedral and the plagioclase grains are lathy with irregular grain boundaries. Plagioclase and pyroxene occur in an ophitic to sub-ophitic texture and a few pyroxene grains are altered to amphibole. Biotite is dark brown and occurs as anhedral flakes. A few coarse-grained amphiboles are present, they occur with a skeletal texture and with inclusions of pyroxene and plagioclase. The amphibole grains have probably grown at a later stage or secondary replaced the pyroxene.

Grain size

Pyroxene: 0.1-0.3 mm, plagioclase: 0.1-0.6 mm, amphibole: 0.23-1.0 mm, biotite: 0.16 -1.2 mm, opaque: 0.06 -0.7 mm

Coarse-grained amphibole: 1.2 -2.0 mm

.

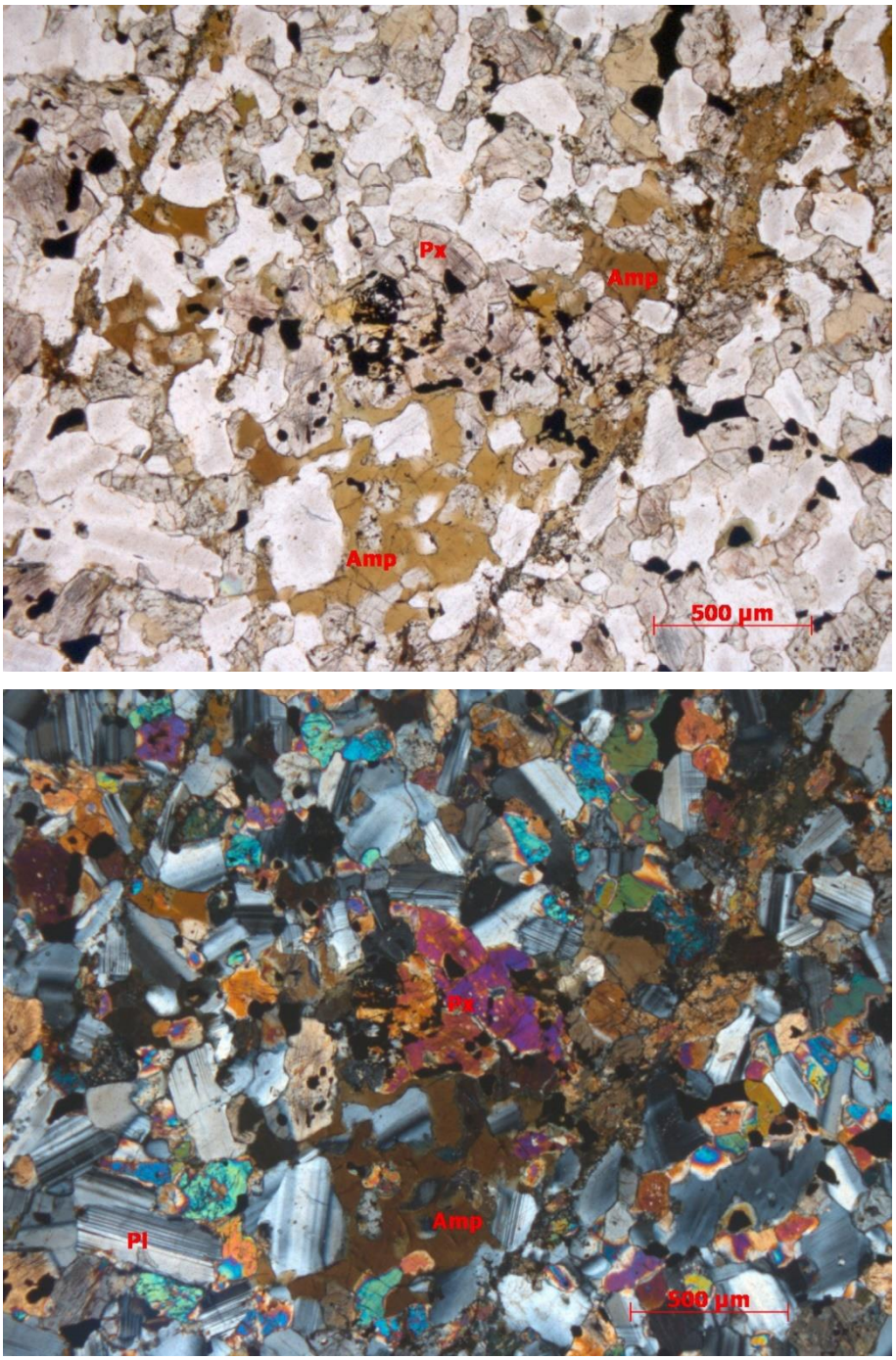

Thin section images of the gabbro. The upper picture is of in ppl and the lower picture is xpl.

Thin section: P7.5

Rock name: Contact-zone granitoid

Hand specimen

The rock is fine-grained, mesocratic with almost equal distribution of light and dark minerals. The light and dark minerals are randomly distributed relative to each other. The dark minerals mainly consist biotite, and the light mineral mainly consists of K-feldspar, plagioclase and quartz. A few phenocrystals of plagioclase are present, and the phenocrystals show twinning. Garnet occurs scattered in the rock with grain sizes of 0.5-1.0 mm.

Minerals

Main minerals: Biotite (30%), K-feldspar (20%), plagioclase (15%), quartz (10%), garnet (10%), opaques (5%)

Accessories: Muscovite (1%), zircon (<1%), epidote (<1 %)

Description

This specimen of contact-zone granitoid is fine grained and do not show any orientation of the minerals. The biotite is fine grained, has a brown to greenish colour and are sub- to anhedral flakes that are randomly distributed. The K-feldspar act as subhedral phenocrysts, and at the contacts there is not unusual to find myrmekite. Some of the orthoclase grains contain inclusion of biotite, quartz and muscovite. The garnets are fine- to medium grained, subhedral and poikilitic with inclusion of quartz, biotite, epidote and muscovite. Some of the garnets have a dusty surface. Plagioclase is anhedral and fine-grained.

Grain size:

Biotite: 0.08-0.45mm, quartz: 0.02-0.48 mm, orthoclase: 0.42-1.85 mm, plagioclase: 0.28-0.9 mm, garnet: 0.2-1.5 mm, muscovite: 0.14-0.25 mm, zircon: 0.16 mm.

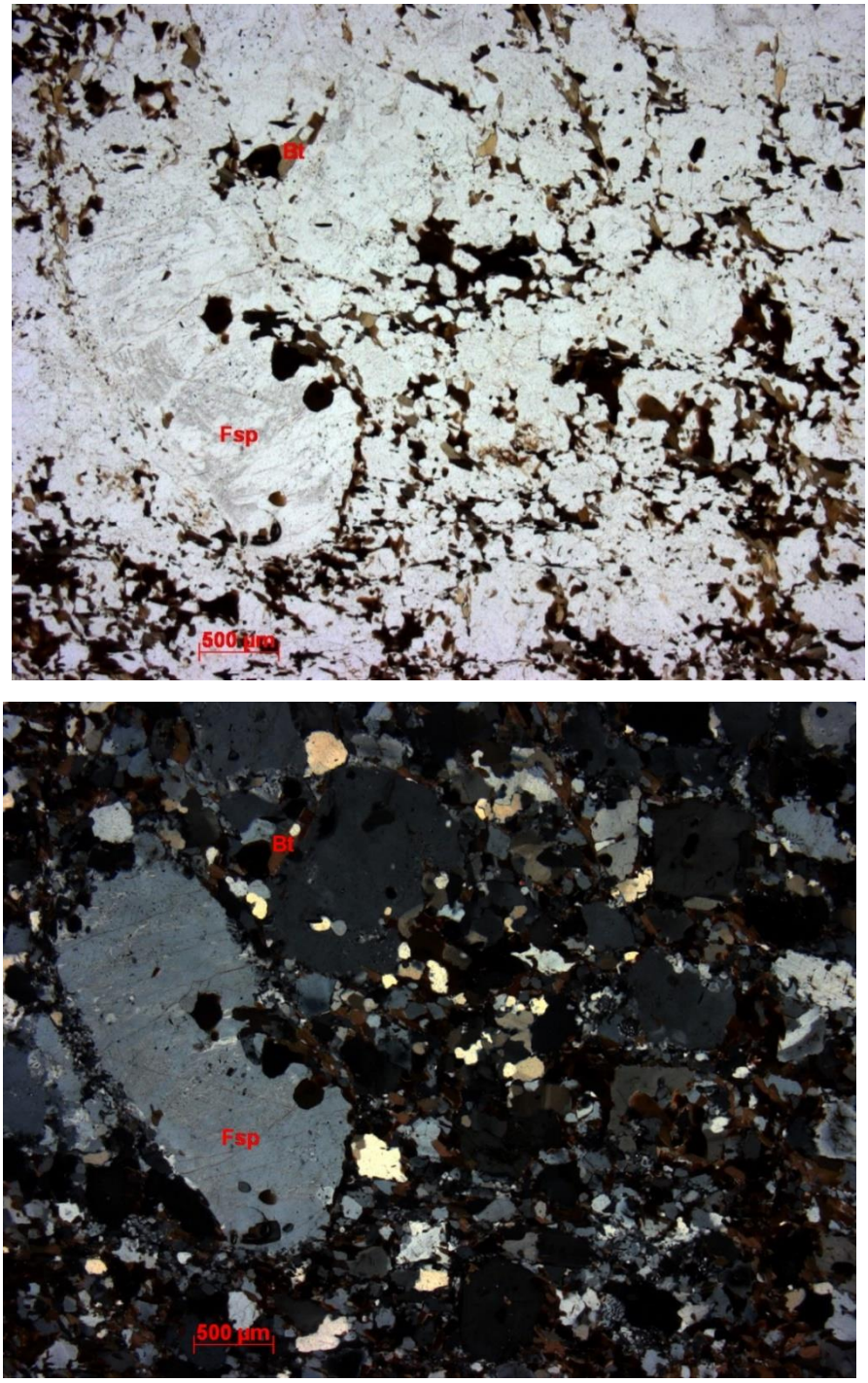

Thin section image of the contact-zone granitoid. Upper photo in ppl, lower photo in xpl

Thin section: P8.1

Rock name: (Impure) Quartzite

Hand specimen

A leucocratic fine- to medium-grained homogenous rock. The quartzite are compact and milky-white in colour. A few black minerals of biotite occur scattered in the rock.

Minerals

Main minerals: Quartz (90 - 95 %), muscovite (2 - 5%)

Accessory: Biotite (1%), apatite (1 %)

Description

The quartzite is anhedral and mainly medium-grained with mostly irregular grain boundaries. A few triple junction are present, but not with straight boundaries with undulating extinction. The muscovite is subhedral, has a lathy to acicular shape and is aligned. The few biotite grains are anhedral flakes and have a light brown colour, and some of the biotite grains show traces of chloritification.

Grain size

Quartz: 0.16-2.5 mm, muscovite: 0.17-0.8 mm, biotite: 0.14 -0.52 mm, apatite: 0.04-0.2 mm.

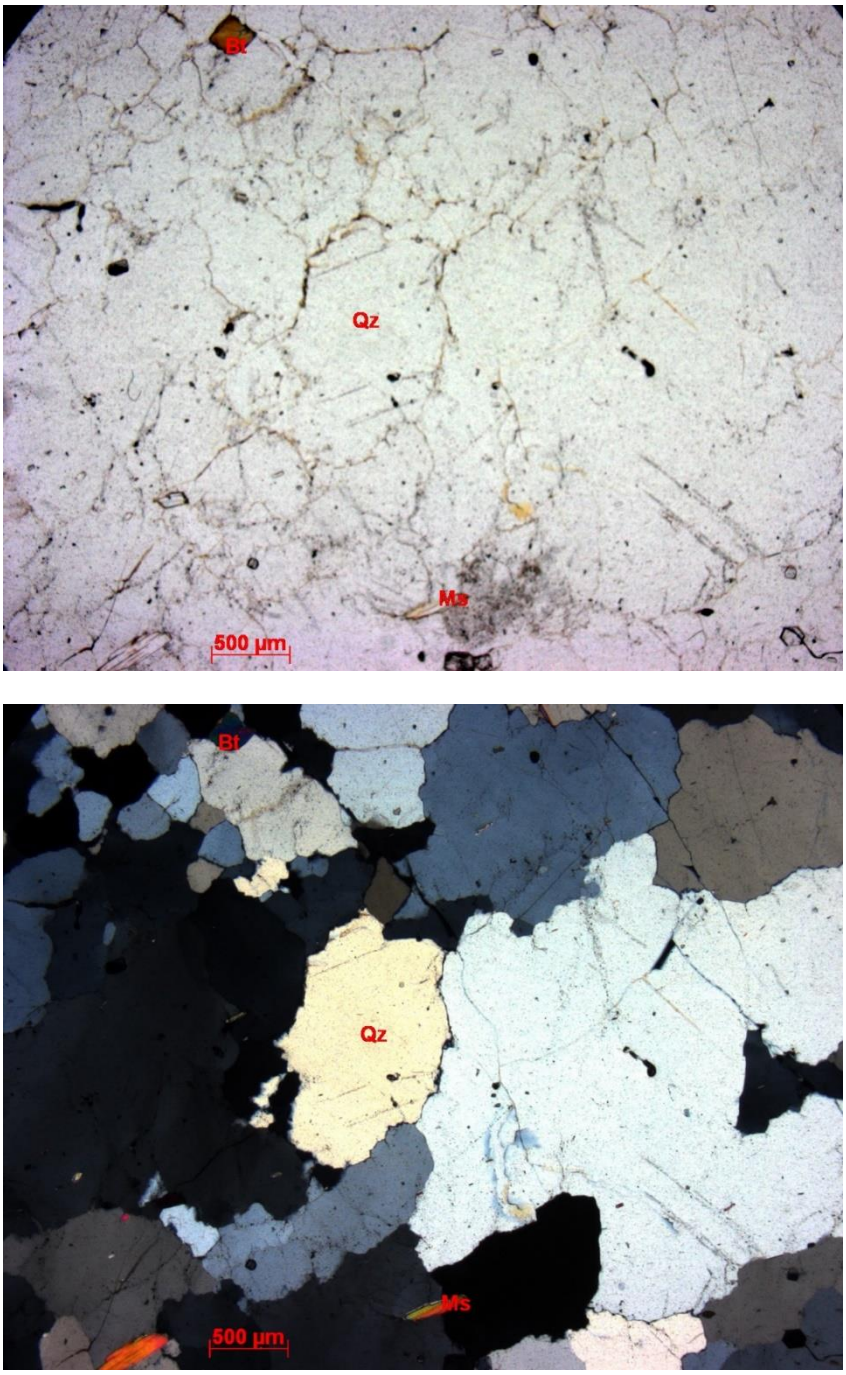

Thin section image of the (impure) quartzite. Upper photo in ppl, and lower photo in xpl

Thin section: P8.2

Rock name: Garnet-biotite gneiss

Hand specimen

The rock is fine-grained, heterogenic and separated in light and dark layers. The layer thickness between the leucocratic and the mesocratic layers varies from millimetre to centimetre in sizes. The rock contain small garnet mainly concentrated in the darker layers.

Minerals

Main minerals: Quartz (45%), Biotite (40%), garnet (5-10%),

Accessories: Plagioclase (1%), muscovite (<1%), clinozoesitt (1-2%), chlorite (1%), opaque (1-3%)

Description

The garnet biotite gneiss is fine grained and rich in biotite, and characterised with millimetre to centimetre thick layers richer and poorer in biotite. The biotite is aligned and occurs as relatively small subhedral flakes and defines a foliation in the rock. Biotite also show pleochroic haloes. Most garnet occurs in the biotite rich layers and appears in cluster of small anhedral grains. In the biotite poorer layers, anhedral quartz grains are the dominating mineral, and the alignment of the biotite grains is not as clear in this layer as in the biotite-rich layers. A few of the biotite grains show chloritization.

Grain size

Quartz: 0.07-0.65 mm, biotite: 0.16-1.1 mm, garnet: 0.12-2.1 mm, opaque: 0.02-0.75 mm, muscovite: 0.14-0.5 mm, plagioclase: 0.14-0.6 mm, clinozoisite: 0.14-0.28 mm, chlorite: 0.3-0.6 mm.

Thin section images of the garnet-biotite gneiss. Upper photo in ppl, and lower photo in xpl.

Thin section: P8.4

Rock name: Garnet-two-mica gneiss

Hand specimen

The rock is fine-grained and separates into 1-2 mm thick layers of light and dark minerals. The dark minerals mainly consist of biotite, and the light minerals mainly consist of quartz and plagioclase. Muscovite is present in both layers. Red garnet grains occur in 2-7 mm sizes.

Minerals

Quartz (35%), biotite (30%), muscovite (20%), garnet (5-10%), plagioclase (5%), opaque: (1%)
Accessories: Chlorite (<1%)

Description

The garnet-two-mica gneiss is mainly fine grained and the micas define a foliation in the rock. The biotite are mostly fine grained, has a light brown colour and a few grains are chloritized. The chloritized grains occur as inclusions or in the contact with garnet. The biotite varies from flaky to lath shaped, and are aligned and defines a foliation in the rock. The muscovite are very fine- to fine grained, occur as both flaky and lath shaped and defines a foliation in the rock together with the biotite. The mica grains bends around the larger garnet grains and some of the coarser quartz and plagioclase grains. The quartz is very fine- to fine grained, have irregular grain boundaries and undulating extinction. A few of the larger quartz grains show triple junction contacts. The plagioclase are very fine- to fine grained, subhedral and has irregular grain boundaries. Some coarser plagioclase grains show seritization. The garnet is fine to medium grained and subhedral, and show skeletal to poikilitic texture, with inclusion of biotite, quartz and a few chlorite grains.

Grain size

Quartz: 0.2 – 0.75 mm, biotite: 0.06 – 0.8 mm, muscovite: 0.08 – 0.6 mm, garnet: 0.1 – 1.3 mm, plagioclase: 0.47 – 0.7 mm

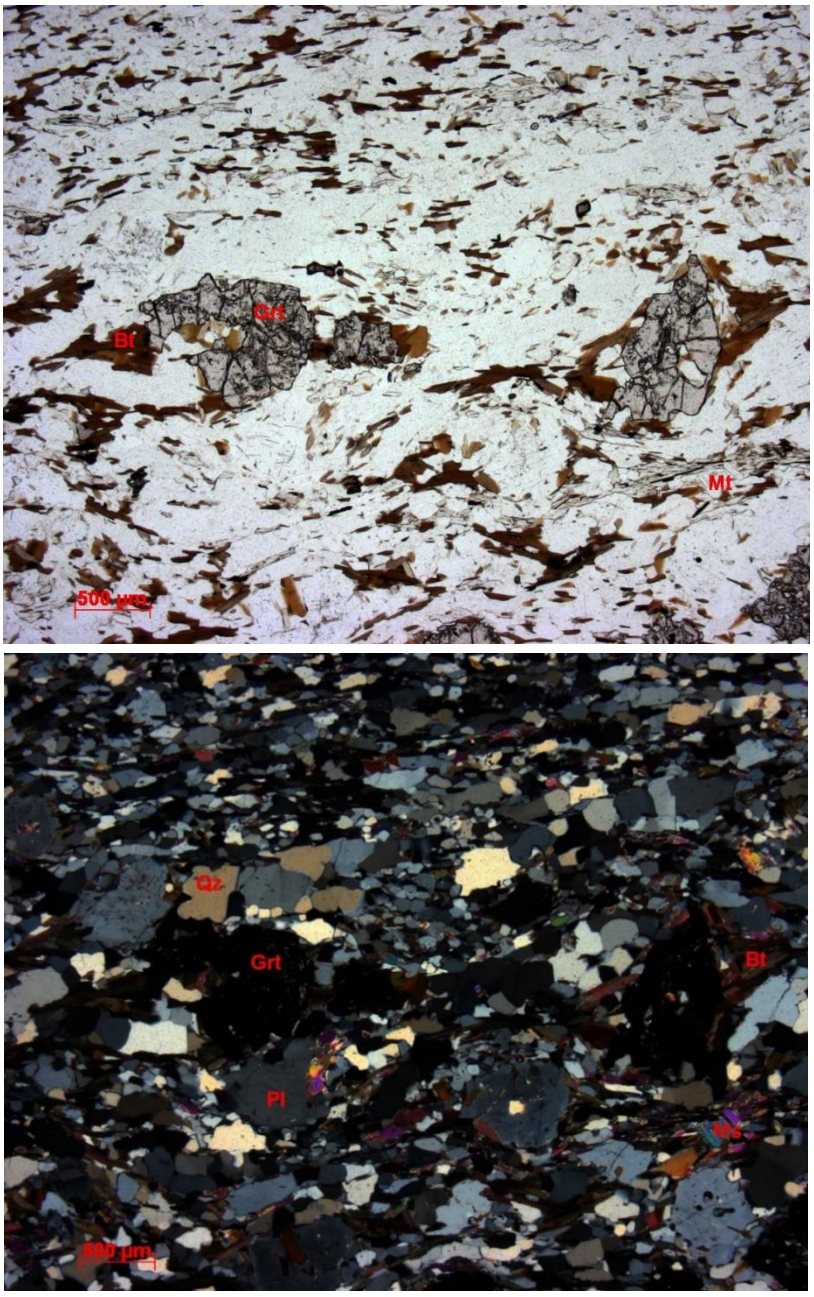

Thin section imags of the garnet-two mica gneiss. Upper photo in ppl, and lower photo in xpl

Thin section: P11.2 ØS

Rock name: Granite

Handspeciman

The granite is homogenous, leucocratic with a white colour. The texture is granular and mainly consists of light minerals of quartz, plagioclase and muscovite.

Minerals

Main minerals: Quartz (40-50 %), plagioclase (15-20%), muscovite (20-30%),
Accessories: K-feldspar (1-2%), biotite (1%), epidote (clinozoisite) (1%)

Petrographic description

The rock is fine- to medium grained. The quartz is mainly medium-grained, have mostly irregular grain-boundaries, whit a few grains showing triple-junction. The quartz grains show undulating extinction. The plagioclase is mainly seritizated and replaced by secondary formed muscovite. The muscovite is sub- to anhedral flakes, some grains are lath shaped and other show skeletal texture. A few anhedral K-feldspar grains are present and randomly distributed. A few biotite and epidote (clinozoisite) grains are randomly distributed in the thin section. Both the biotite and the and the epidote (clinozoisite) are fine grained, and the biotite occurs as anhedral flakes and the epidote (clinozoisite) as anhedral- to subhedral grains.

Grain size

K-feldspar: 0.06-1.9 mm, plagioclase: 0.4-0.8 mm, muscovite: 0.1-0.9 mm, K-feldspar: 0.5-0.6 mm, biotite: 0.04-0.2 mm

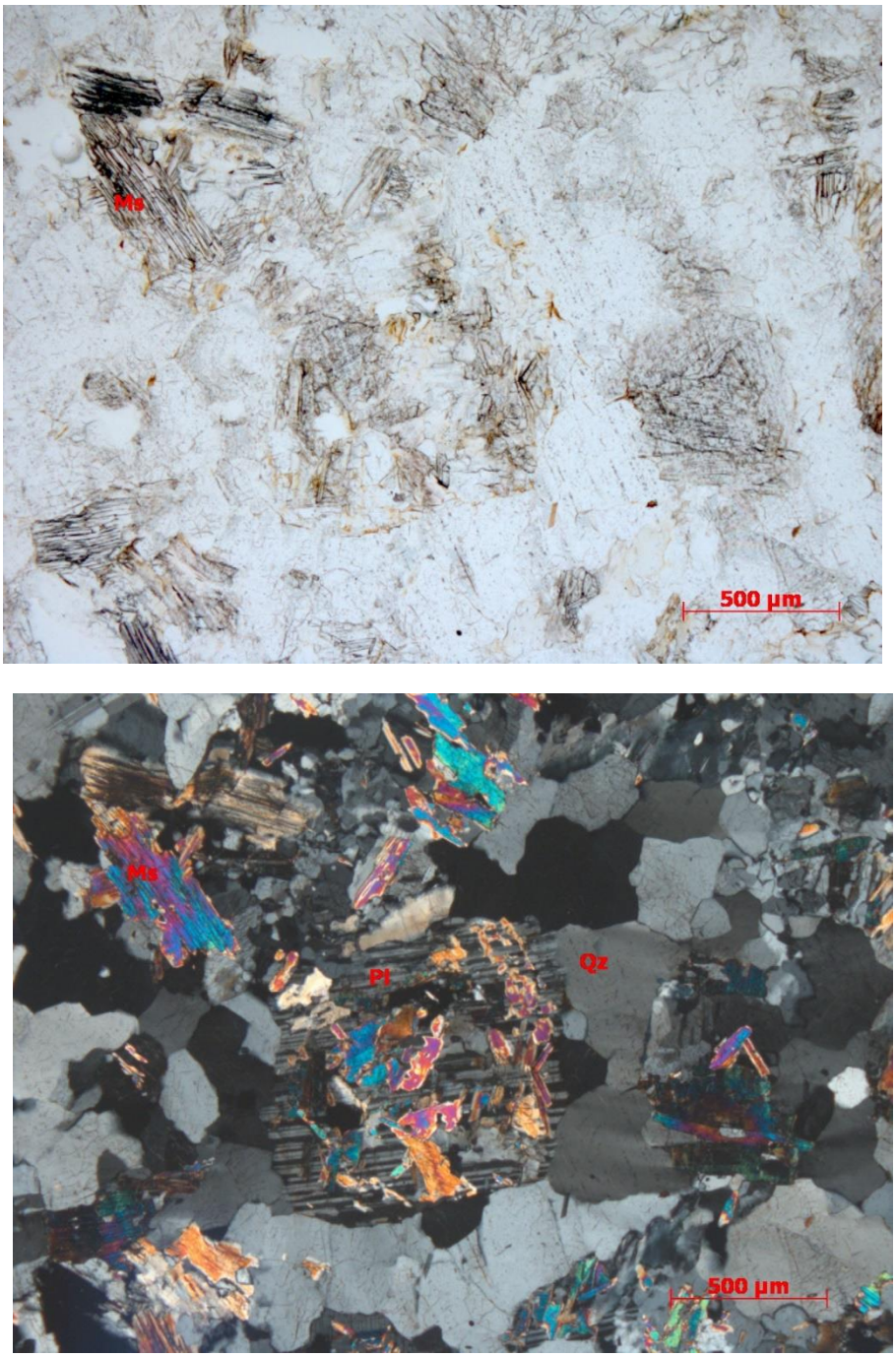

Thin section image of the granite. Upper photo in ppl, and lower photo in xpl

Thin section: P16.3B ØS

Rock name: Garnet-two mica gneiss

Hand specimen

The leucocratic garnet-two mica gneiss is fine-grained, heterogeneous and separates into 0.5-1.0 cm thick layers of light and dark minerals. The light layers mainly consist of quartz and muscovite and the dark layers mainly consist of biotite. Garnet is present in both layers, but has a larger concentration in the dark biotite rich layers. The garnet occurs in 2.0 to 1.5 cm sizes.

Minerals

Main minerals: Quartz (40%), muscovite (30%), biotite (10%), garnet (10%),

Accessories: Apatite (1%), plagioclase (1%)

Description

The rock is very fine grained, and defined by centimetre thick layers richer and poorer in garnet and biotite. The garnet and biotite poor layers mainly consist of muscovite and quartz. The muscovite is mostly very fine grained and lath shaped, and they show poorly alignment. The quartz is generally very fine grained, have irregular grain boundaries and undulating extinction. The layers rich in garnet and biotite are darker than the garnet and biotite poor layers. In the garnet and biotite rich layers, the biotite show poorly alignment and are very fine grained. The biotite is brown in colour and mostly shows flaky shape, but a few lath shaped grains are present. The garnet are mostly fine grained and subhedral. Some of the garnet crystals occur as small-subrounded crystals, and some larger crystals show poikilitic texture with inclusion of quartz and biotite. Muscovite and quartz are also present in the garnet and biotite rich layers. The poor alignment of the micas, suggest that the layering represents primary compositional layering rather than segregation during metamorphic deformation.

Grain size

Quartz: 0.03-0.29 mm, muscovite: 0.02 -0.32 mm, garnet: 0.06-0.6 mm, biotite: 0.05-0.27 mm, plagioclase: 0.1-0.15 mm, opaquer: 0.05-0.13 mm, apatite: 0.02-0.07 mm

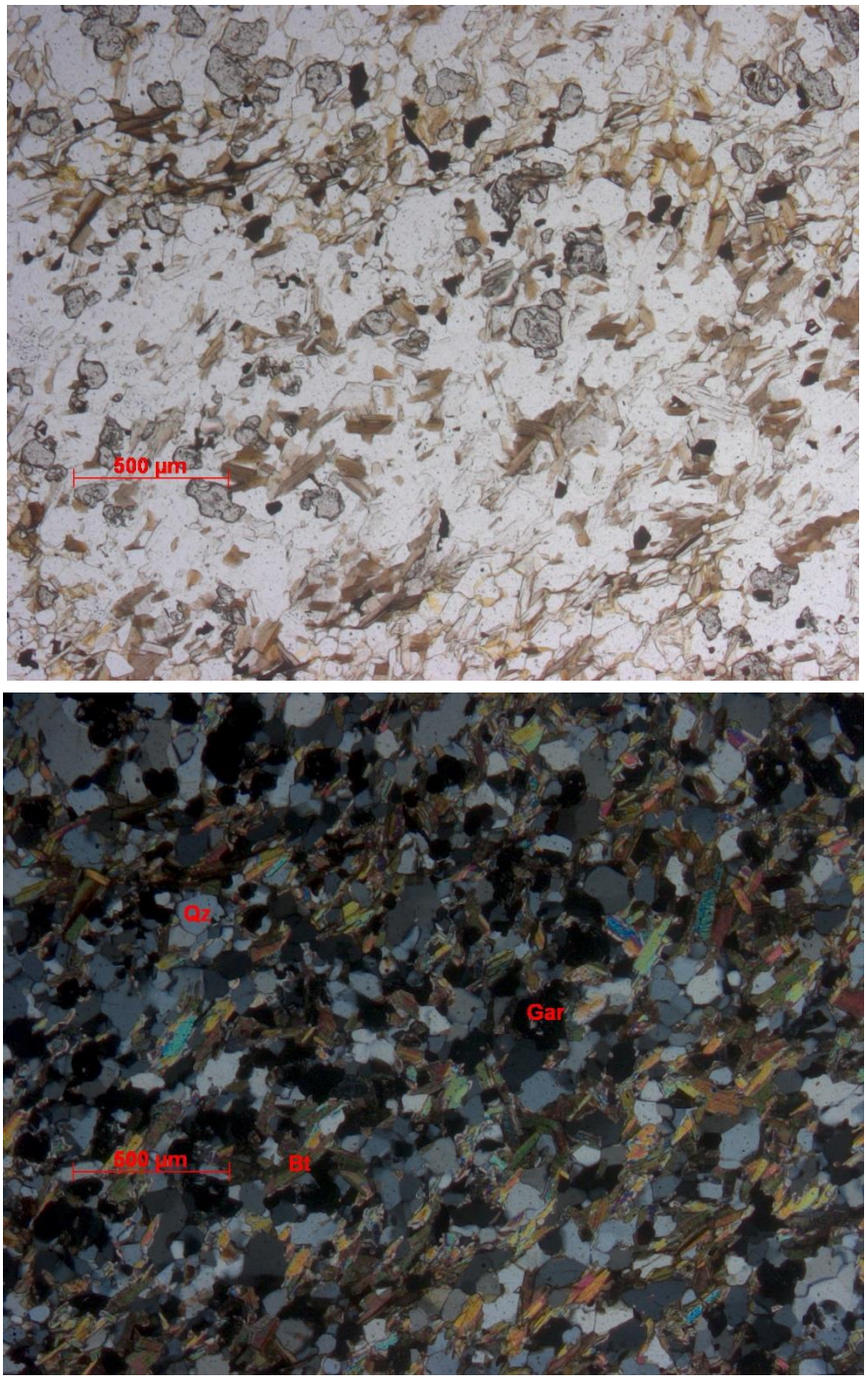

Thin section image of the garnet and biotite rich layers. Upper photo in ppl, and lower photo in xpl

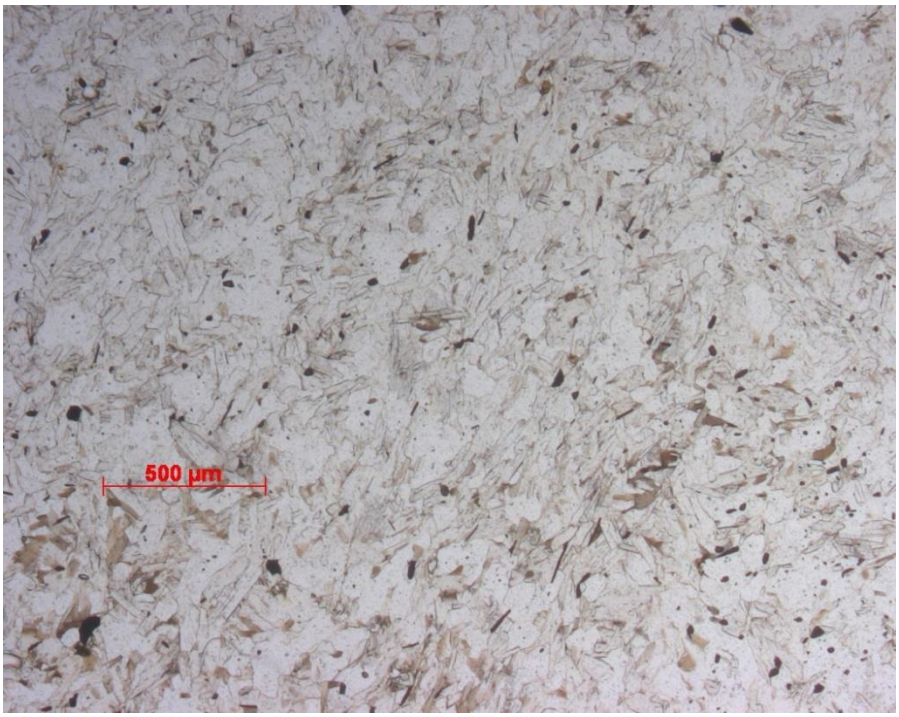

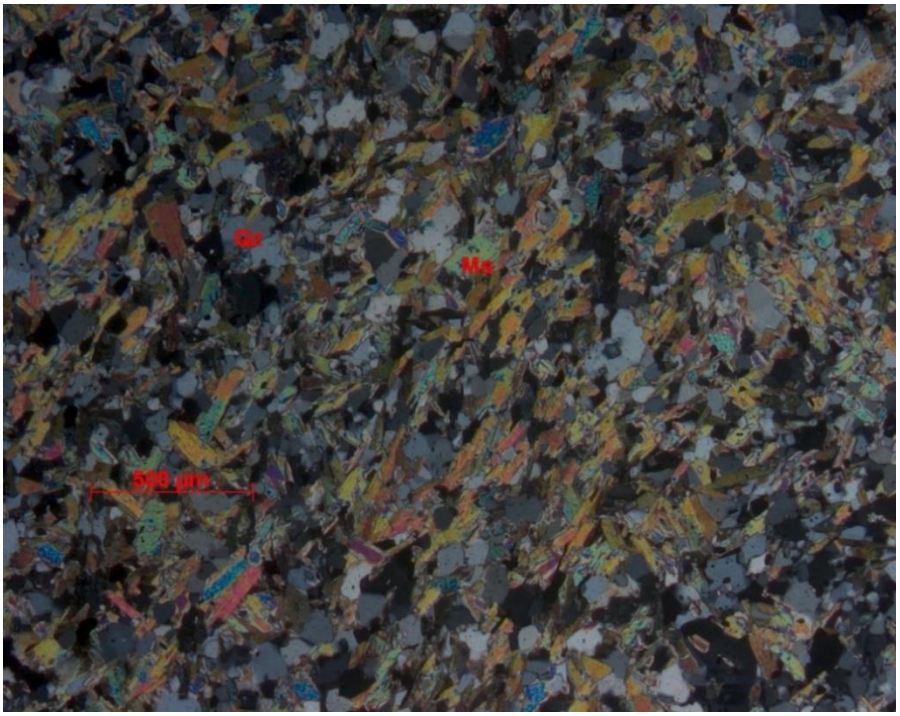

Thin section image of the garnet and biotite poor layers. Upper photo in ppl, and lower photo in xpl

Thin section: P17.1 ØS

Rock name: contact-zone granitoid

Hand specimen

The contact-zone granitoid is leucocratic and heterogeneous. The rock is fine grained consist of light and dark minerals. The light minerals mainly consist of quartz, muscovite and plagioclase, and the dark minerals mainly consist of biotite. Garnet occurs randomly in the rock and has a red colour.

Minerals

Quartz (40%), muscovite (25-30%), plagioclase (20%), garnet (10%), biotite (5%)

Description

This contact-zone granitoid is very fine- to fine grained, and this sample is very garnet rich. The rock is rich in micas, and the muscovite is very fine- to fine grained, occur mostly as flakes, but some minerals show lath shaped grains. The muscovite is randomly distributed and occur both inter- and intragranular. The biotite is mostly very fine grained, and occurs as light-brown flakes and is randomly distributed. The biotite occur both inter- and intragranular. The garnet varies in size from fine- to medium grained, and are randomly distributed in the thin section. The medium-grained garnet mostly show a skeletal texture, and the fine grained garnet mostly show poikilitic texture with mainly inclusion of quartz, but also with a few mica grains. Quartz and plagioclase are anhedral and fine-grained with irregular grain boundaries and undulating extinction. Some of the plagioclase grains show seritization.

Grain size

Quartz: 0,1 – 0,5 mm, muscovite: 0,1 – 0,4 mm, plagioclase: 0,2 - 0,7 mm, garnet: 0,11 – 1,4 mm, biotite: 0,03 – 0,4 mm

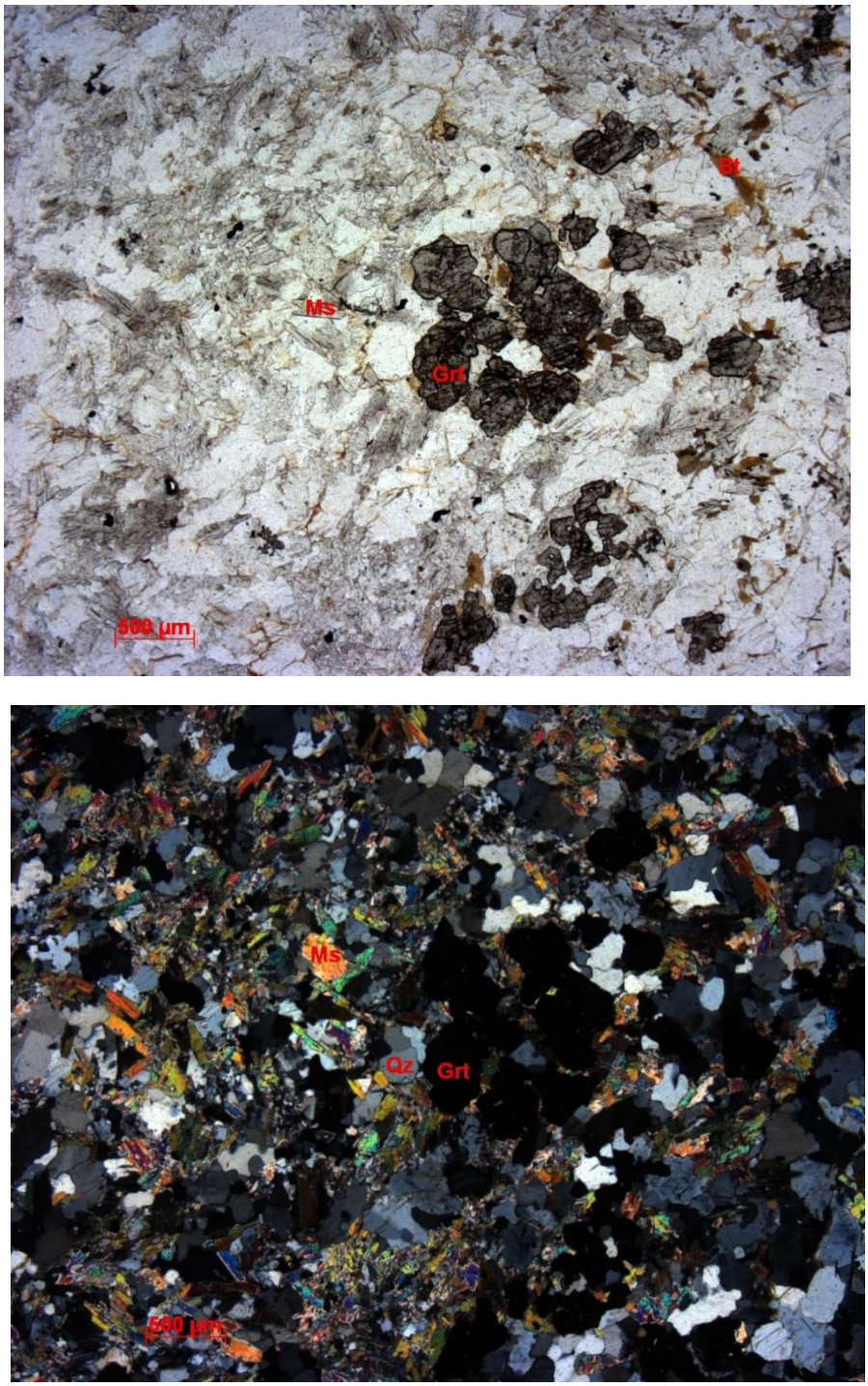

Thin section image of the contact-zone granitoid. Upper photo in ppl, and lower photo in xpl

Thin section: P18.1 PL

Rock name: Two-mica gneiss

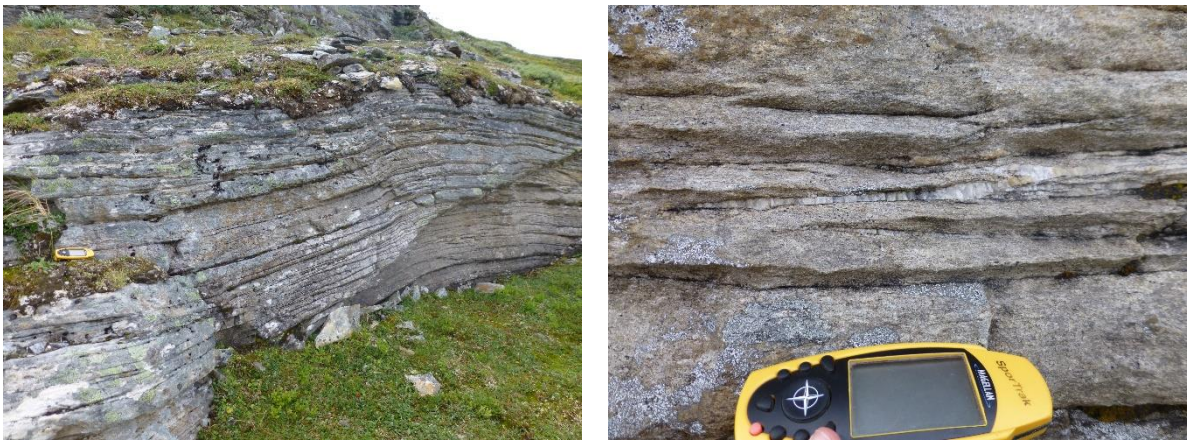

The two-mica gneiss, how it looks in the field.

Hand specimen

The two-mica gneiss is leucocratic, has a gneissose texture and mostly fine- to medium grained. The rock is heterogenic and separates into millimetre to centimetre thick layers, which is more or less rich in micas. The mica-rich layers are a bit darker in colour than the mica-poor layers, probably because of a slightly higher concentration of biotite. The micas occur as aligned minerals in the rock. The mica-poor layers have a light colour and mainly consist of K-feldspar, quartz and plagioclase, and a few mica grains are present in these layers as well.

Minerals

Main minerals: K-feldspar (30%), muscovite (30%), quartz (20%), biotite (10%), plagioclase (5-10%)

Accessorise: Apatite (1-3%), opaque (1%)

Description

The two-mica gneiss is fine grained and characterised with clear orientation of the mica minerals. Muscovites are aligned and defines a foliation in the rock, some places accompanied by greenish-brown anhedral biotite. The rock is relatively muscovite rich. K-feldspar, feldspar

and especially the quartz show undulating extinction and some quartz grains also show ribbon-like extinction, which often indicates rock deformational processes. The feldspars and the quartz have subhedral grain shape and irregular grain boundaries. The rock has gneissose texture.

Grain size

K-feldspar: 0.2 – 0.9 mm, muscovite: 0.1 – 1.9 mm, quartz: 0.03 – 1.0 mm, biotite: 0.09 – 0.5 mm, feldspar: 0.2 – 0.4 mm, apatite: 0.05 – 0.2 mm

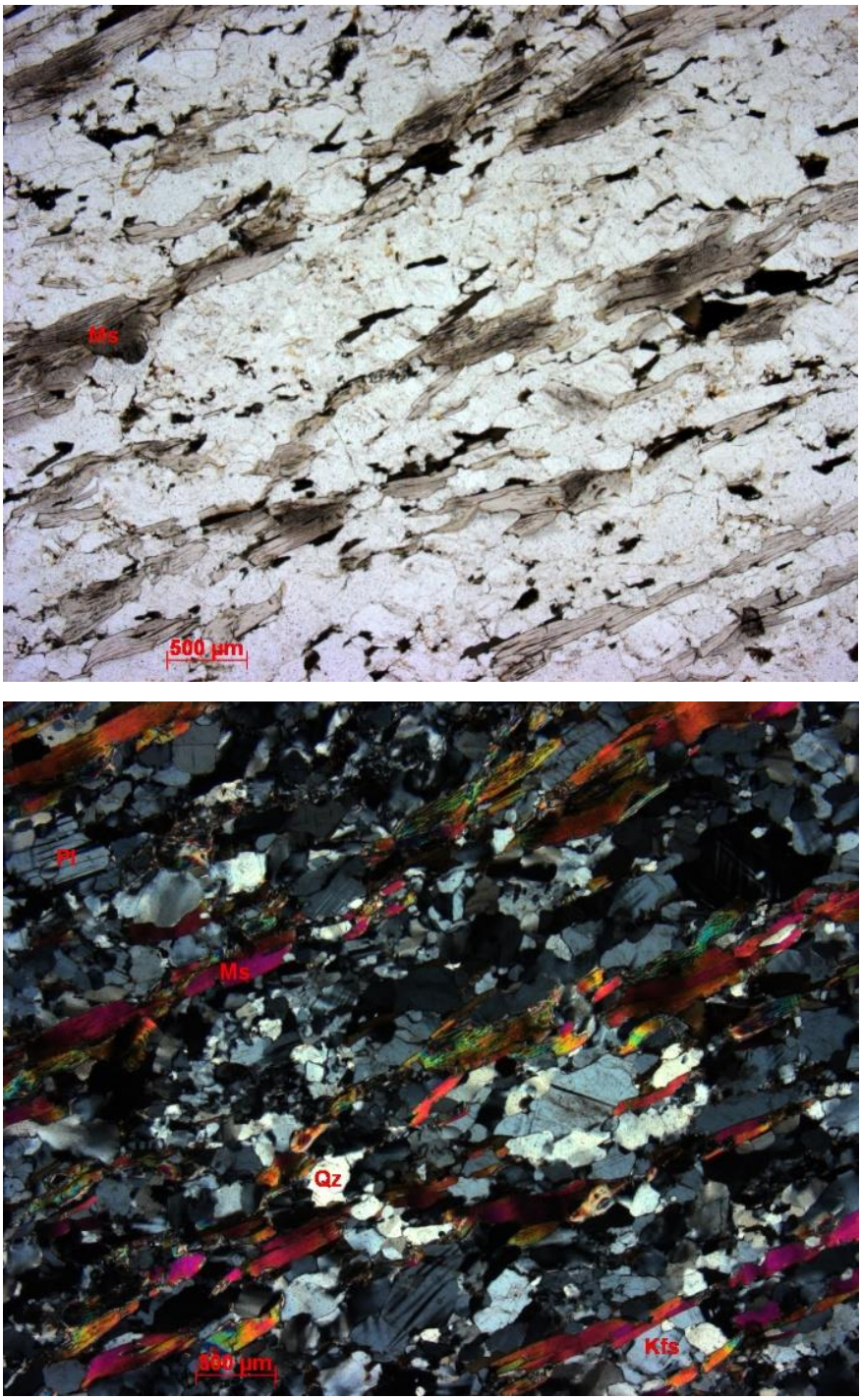

Thin section images of the two-mica gneiss. Upper photo in ppl, and lower photo in xpl

Thin section: P18.2 PL

Rock name: Chloritised garnet-biotite gneiss

Hand specimen:

The chloritised garnet-biotite gneiss has a gneissose texture, are mesocratic, and separates into very fine-grained dark layers, and fine-grained lighter layers. The darker and lighter layers vary from millimetre to centimetre thicknesses. The dark layers mainly consist of chlorite and biotite, and the lighter layers mainly consist of quartz, plagioclase and biotite. Garnet occurs in both layers in 0.5 to 1.0 cm sizes, but have largest concentration is in the lighter layers, and has a brown-red colour.

Minerals:

Main minerals: Quartz (20-25 %), plagioclase (20-25 %), biotite (5-10 %), chlorite (20-25 %), garnet (5 %), epidote + clinozoisite (5 %), calcite (5 %), opaque (5 %)

Accessories: titanite (1 %), apatite (1 %)

Description

The chloritised garnet-biotite gneiss is mainly fine-grained and characterised by relatively aligned layers of biotite and chlorite. The biotite is fine-grained, mainly lath shaped and has a brown colour, and most of the biotite grains are altered to chlorite. The chlorite has a light green colour. The quartz is mostly fine-grained, have irregular grain-boundaries and show undulating extinction. A millimetre thick quartz vein is cutting through the rock. The vein has medium-grained quartz with relatively straight grain-boundaries, and some grain contacts show triple

junction. The plagioclase is fine-grained and most of the plagioclase is partly seritizated. It is also a millimetre thick vein of calcite cutting the chloritised garnet-biotite gneiss. The calcite is fine-grained and mainly found in the vein, but a few calcite grains are also randomly distributed in the thin-section. The garnet and the epidote + clinozoisite occur mostly in the layering where the biotite is least altered to chlorite. The garnet is medium-grained, subhedral and has a poikilitic texture. The epidote + clinozoisite are fine- to medium grained, subhedral and some grains show poikilitic texture. Accessory phases are titanite and apatite.

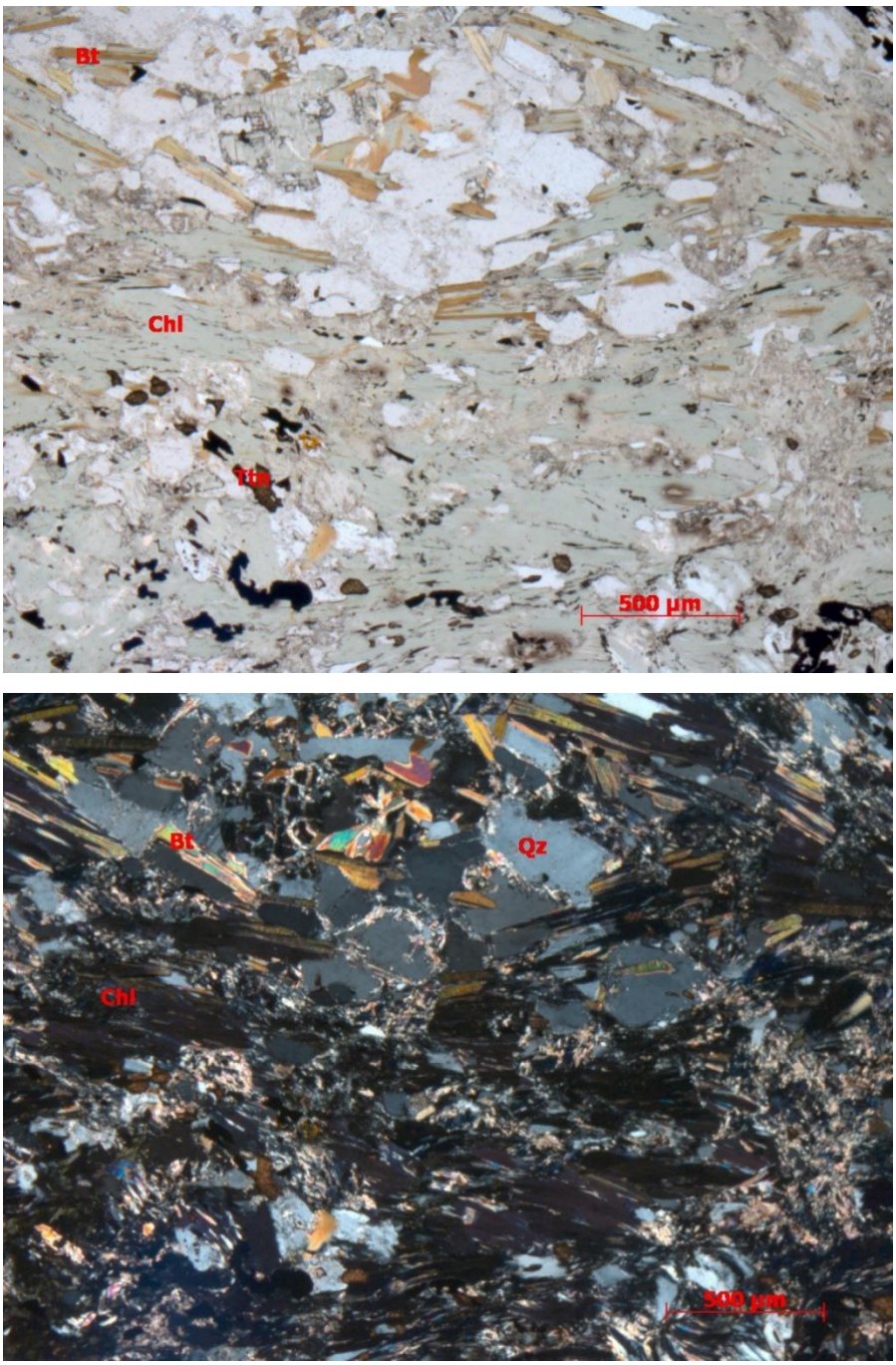

Thin section image of the chlorite rich layer. Upper photo in ppl, and lower photo in xpl

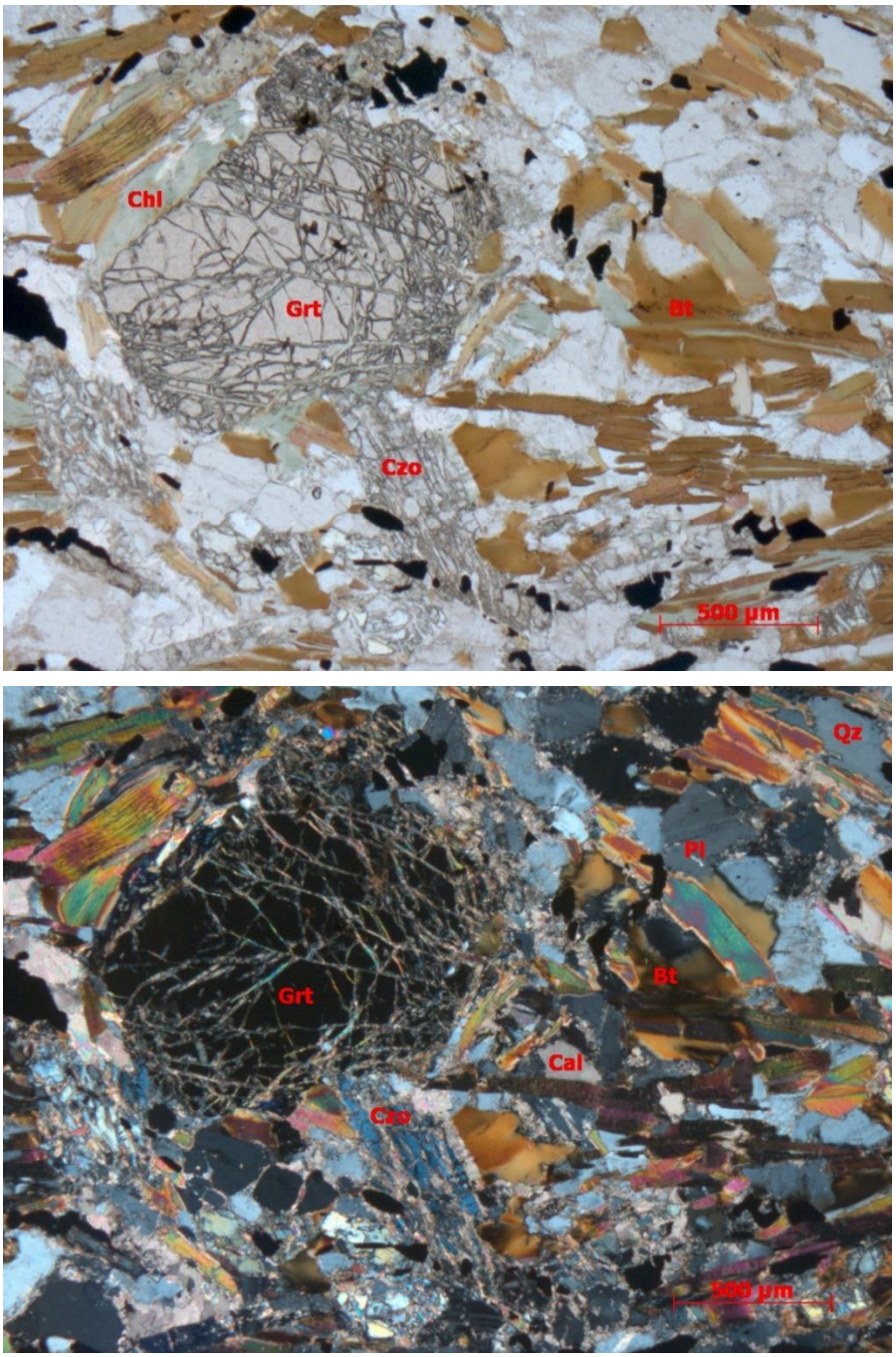

Thin section image of the garnet and epidote rich layer. Upper photo in ppl, and lower photo in xpl

Thin section: P19.2 UM

Rock name: Olivine gabbro

Hand specimen

The olivine gabbro is mesocratic and has a brown rusty weathered surface. The rock is massive, homogeneous and medium-grained, and composes of grey pyroxene, dark green olivine and a few light minerals of plagioclase.

Minerals

Olivine (35%), clinopyroxene (35%), plagioclase (20%), amphibole (5%), Opaques (5%)

Description

The olivine gabbro is medium grained and undeformed. The rock is characteristic by corona textures, probably of orthopyroxene, surrounding the olivine grains. The alteration of olivine to orthopyroxene is most likely a result of fluid interaction. The anhedral pyroxene has a poikilitic texture with inclusion of olivine and opaques. The plagioclase is anhedral and occurs interstitially between the olivine and the pyroxene, and is probably one of the last crystallizing minerals, except from a later formation of the corona texture.

Grain size

Olivine: 0.09-1.73 mm, pyroxene: 0.9-2.0 mm, plagioclase: 0.3-0.6 mm, amphibole: 0.15-1.2 mm, orthopyroxene: < 1.0 mm, opaques: 0.06-1.2 mm.

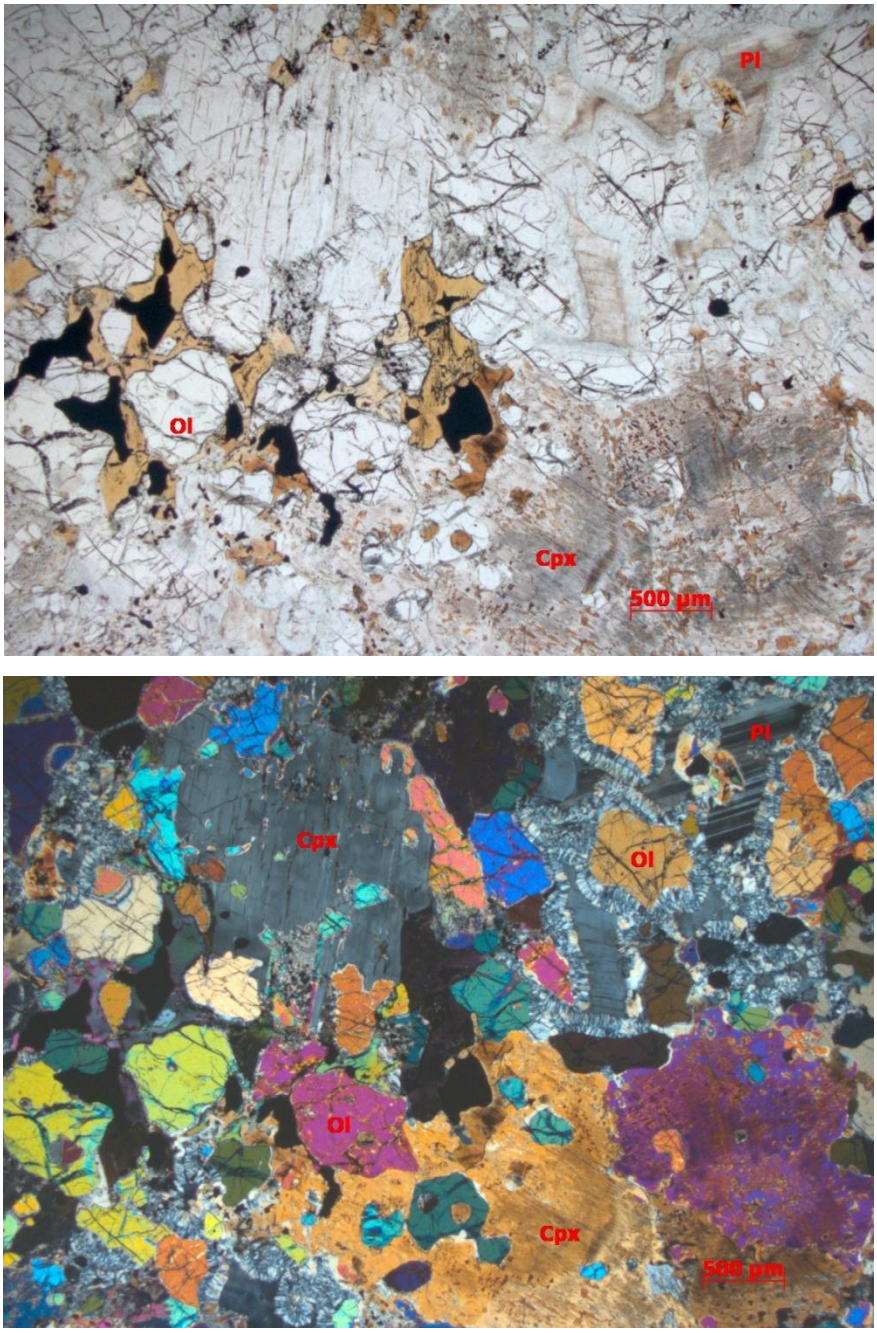

Thin section image of the olivine gabbro. Upper photo in ppl, and lower photo in xpl

Thin section: P19.4B UM

Rock name:

Coarse-grained garnet hornblende gabbro

Hand specimen

A coarse-grained melanocratic gabbro. The rock is homogenous and consists of an almost even distribution of light and dark minerals. The light minerals mainly consist of plagioclase and the dark minerals mainly consist of amphibole. Corse garnet grains are randomly distributed throughout the rock.

Minerals

Main minerals: Plagioclase (40%), amphibole (hornblende + actinolite) (45%), garnet (5%)

Accessorise: Clinozoisite (1%), quartz (1-3%), biotite (<1%), epidote (<1%), zircon (<1%), titanite (<1%), opaquer (1-2%), apatite (<1%)

Description

The coarse-grained garnet hornblende gabbro mainly shows pyroxene grains altered to hornblende and actinolite. The cores of the pyroxene are mostly transformed to actinolite, and the green rims are probably hornblende. The amphibole grains have a poikilitic texture with many small inclusions of quartz grains, which may be a result of excess silica in the alteration from pyroxene to amphibole. The plagioclase occurs with lath shape and some grains are slightly saussuritizated by fine-grained clinozoisite and epidotes. The garnet is coarse grained and have a scattered distribution, so only two grains can be seen in this thin section. The coarse-grained gabbro is cut by a fine grained dyke that mainly consist of amphibole.

Grain size

Plagioclase: 0.2-9.0 mm, amphibole (hornblende): 0.9-6.6 mm, biotite: 0.1-0.8 mm, clinozoisite: 0.08-0.22 mm, garnet: 0.4-2.3 mm, apatite: 0.1-0.5 mm, zircon: 0.5 mm, titanite: 0.2 mm

Dyke: Amphibole (hornblende): ca. 0.08 mm

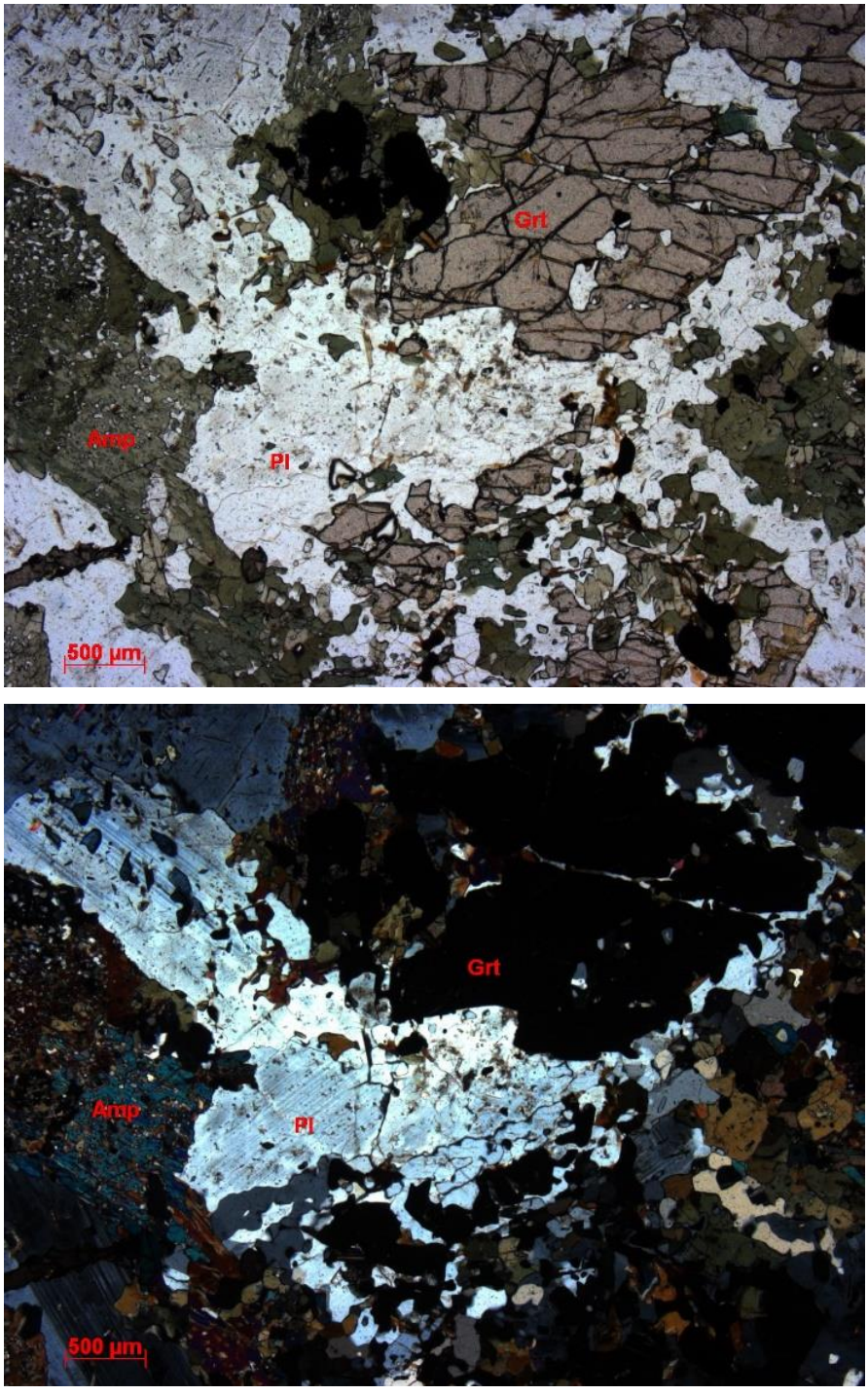

Thin section image of a garnet in the coarse-grained hornblende gabbro.

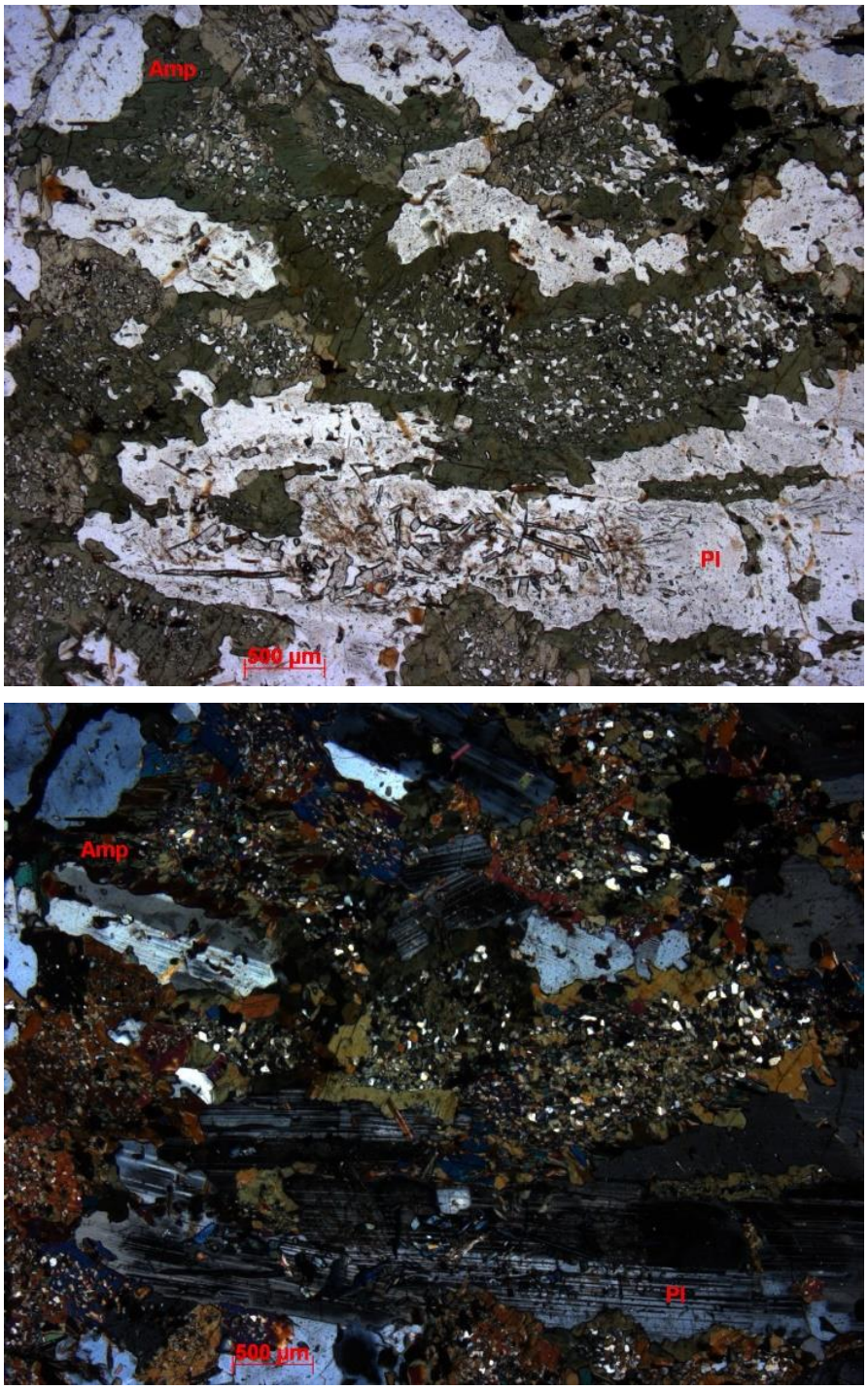

Thin section image, which show alteration of the pyroxene to amphibole and seritization of the coarse plagioclase grains

Appendix C – Whole rock analyses

SAMPLE	UM46	P7.4	P9.4	P6.1	UM61	UM1A	P7.2	UM1D
Rock type	Gabbro	Gabbro	Gabbro	Gabbro	Gabbro	Mafic dyke, cutting gabbro	Mafic dyke	Gabbro
UTM_E33	488127	487351	487909	485972	482451	481390	486113	481390
UTM_N33	7336112	7338543	7339147	7338503	7336086	7337541	7338491	7337541
SiO2	45,4	47,4	48,3	48,5	49,2	49,4	49,5	49,5
Al2O3	10,3	10,05	12,55	13,1	14,65	13,85	12,8	15,3
Fe2O3	16,7	14,2	14,65	12,8	11,9	13,2	13,45	10,85
CaO	7,08	8,1	9,96	9,71	10,1	9,25	9,12	11
MgO	18,9	15	10,6	8,96	7,81	8,76	9,5	7,07
Na2O	1,51	1,75	2,07	2,53	3,17	3,61	2,02	2,99
K2O	0,26	0,58	0,3	0,59	0,7	0,51	0,48	0,45
Cr2O3	0,03	0,07	0,06	0,05	0,06	0,05	0,04	0,03
TiO2	1,09	1,88	2,78	2,81	2,2	1,92	2,97	2,02
MnO	0,21	0,18	0,2	0,16	0,16	0,18	0,17	0,14
P2O5	0,12	0,22	0,21	0,35	0,3	0,23	0,41	0,25
SrO	<0.01	0,03	0,03	0,04	0,04	0,02	0,04	0,04
BaO	0,01	0,02	0,01	0,02	0,02	0,02	0,02	0,02
LOI	-0,59	-0,25	-0,1	0,39	0,06	0,35	0,08	0,92
Total	101,02	99,23	101,62	100,01	100,37	101,35	100,6	100,58
Ba	79,3	182	118	282	185	173,5	187	164
Ce	11,6	28,6	18,4	47,8	32,3	17,2	40,2	25,4
Cr	210	470	380	450	380	320	270	160
Cs	0,24	0,35	0,15	0,37	0,49	0,52	0,32	1,31
Dy	2,46	4,22	4,1	7,13	4,91	4,19	5,75	4,53
Er	1,16	2,13	2,17	3,32	2,43	1,98	2,54	2,19
Eu	0,81	1,52	1,42	3,58	1,85	1,48	2,14	1,79
Ga	12,6	16,4	17,3	25,2	21	20,2	19,4	18,5
Gd	2,35	4,9	4,6	8,38	6,06	4,82	7,34	5,4
Hf	1,1	3,1	2	4,9	3	2,7	4,5	3,8
Ho	0,5	0,77	0,76	1,25	0,9	0,78	1,01	0,85
La	5,3	12,8	8,6	21,6	14,3	7,3	18,2	11,8
Lu	0,16	0,21	0,21	0,39	0,25	0,22	0,24	0,23
Nb	7,6	19,6	15,6	32,7	23	14,7	26,7	22,1
Nd	7,8	17,7	13,3	32,9	22,6	13	27,7	18,4
Pr	1,62	4,12	2,83	6,67	4,85	2,56	6,04	3,76
Rb	7,5	16,2	5,8	16,6	16,4	8,7	14,9	13,6
Sm	1,96	4,53	3,77	9,34	5,12	3,78	6,38	4,54
Sn	2	1	1	2	2	1	2	1
Sr	172,5	335	364	552	457	355	440	459
Ta	0,9	1,1	1,2	2,1	1,5	1,2	1,7	1,7
Tb	0,45	0,75	0,68	1,26	0,94	0,79	1,01	0,76
Th	0,66	1,89	0,77	2,93	1,44	1,05	2,32	1,08
Tm	0,17	0,32	0,26	0,49	0,29	0,25	0,37	0,28
U	0,18	0,49	0,22	0,77	0,42	0,49	0,73	0,36
V	144	191	196	306	199	213	210	162
W	<1	<1	<1	<1	<1	<1	<1	<1
Y	12,5	21	18,6	33,2	22,7	19,5	26	20,8
Yb	1,13	1,67	1,43	2,5	1,63	1,48	1,86	1,63
Zr	52	130	80	206	119	90	180	152
Ag	<0.5	<0.5	<0.5	<0.5	<0.5	<0.5	<0.5	<0.5
As	<5	<5	<5	<5	<5	<5	<5	5
Cd	<0.5	<0.5	<0.5	<0.5	<0.5	<0.5	<0.5	<0.5
Co	99	71	60	47	44	47	54	40
Cu	52	57	43	43	39	55	44	51
Li	<10	10	<10	30	10	10	20	20
Mo	<1	<1	<1	1	<1	1	1	<1
Ni	604	492	269	200	116	160	245	111
Pb	4	8	3	9	2	2	4	2
Sc	16	21	27	24	25	20	22	22
Tl	<10	<10	<10	<10	<10	<10	<10	<10
Zn	134	122	128	130	114	136	132	92

SAMPLE	UM5	P6.3	P6.4	P5.1	P5.2	MO 030-2	AS05-05	AS08-06
Rock type	Gabbro	Gabbro	Gabbro	Mafic dyke	Gabbro	Mafic dyke, cutting gabbro	Gabbro	Gabbro
UTM_E33	481387	485990	487351	485155	485193	487131	481974	482436
UTM_N33	7336546	7338443	7338543	7338781	7338574	7336648	7336169	7335116
SiO2	50,5	55,1	55,5	57	58,4	48	42,32	49
Al2O3	14,5	16,2	16,75	12,85	16,9	13,25	12,65	15,1
Fe2O3	11	11,45	9,91	10,6	7,9	13,86	18,3	14,48
CaO	10,4	6,56	8,88	7,3	5,19	9,29	10,3	7,1
MgO	7,8	3,9	6,26	5,66	4,02	7,89	6,59	4,13
Na2O	2,52	2,78	1,88	2,68	3,53	2,25	2,15	3,08
K2O	0,53	1,92	0,53	0,81	1,49	0,66	0,34	1,61
Cr2O3	0,07	0,02	0,04	0,03	0,02	0,04	<0.01	<0.01
TiO2	1,91	2,16	1,44	1,96	1,49	3,37	6,89	4,09
MnO	0,15	0,15	0,13	0,14	0,09	0,17	0,17	0,18
P2O5	0,23	0,3	0,18	0,21	0,19	0,321	0,135	0,484
SrO	0,03	0,02	0,01	0,02	0,03	0,05	0,04	0,06
BaO	0,02	0,04	0,02	0,01	0,02	0,03	0,02	0,06
LOI	0,56	0,18	0,34	0,41	0,36	0,42	-0,16	0,59
Total	100,22	100,78	101,87	99,68	99,63	99,59	99,75	99,96
Ba	151	431	252	112	184	176,5	110,5	437
Ce	26,6	79,9	42,5	27,4	38,4	30,7	15,8	66,6
Cr	460	90	290	160	130	270	20	10
Cs	0,81	4,15	2,55	1,36	3,22	49,2	50,4	34,5
Dy	4,27	7,94	4,49	4,62	4,37	5,21	3,69	7,9
Er	1,88	4,31	2,75	2,32	2,83	2,4	1,69	3,78
Eu	1,59	2,71	1,83	1,92	2,09	2,14	1,69	3,34
Ga	18,4	25,2	21,4	18,9	20,5	19,4	21,8	27
Gd	5,04	8,21	5,14	4,86	4,24	6,52	4,12	9,9
Hf	3,2	5,6	3,3	2,9	6,6	4,3	2,4	9,7
Ho	0,73	1,51	1,03	0,9	0,89	0,94	0,68	1,41
La	12,2	39,4	22,6	13,3	20,2	13	6,2	29
Lu	0,19	0,65	0,4	0,31	0,48	0,26	0,17	0,41
Nb	16	27,4	14	17,3	14,9	19,5	16,3	60
Nd	18,1	40,8	23,2	18	19,4	22,9	13,3	42,2
Pr	3,76	9,99	5,5	3,64	4,83	4,52	2,52	9,22
Rb	11,9	83,7	39,9	27,5	76,9	15,3	6,5	39,4
Sm	4,98	9,88	6	5,33	4,35	6,22	4,12	10,05
Sn	2	4	2	3	2	2	1	3
Sr	424	287	261	306	302	435	450	548
Ta	0,8	1,9	1,1	1,2	1	1,1	1,2	3,5
Tb	0,67	1,31	0,84	0,75	0,69	1	0,66	1,48
Th	0,8	8,89	5,46	2,14	5,61	1,2	0,52	1,41
Tm	0,31	0,59	0,4	0,34	0,43	0,31	0,21	0,49
U	0,4	1,92	1,32	0,99	1,77	0,31	0,2	0,8
V	195	222	183	190	113	215	692	197
W	<1	1	<1	1	<1	1	<1	1
Y	20	40,7	28,5	22,7	24,5	23,9	16,1	35,1
Yb	1,61	3,98	2,28	2,02	3,03	1,88	1,25	3,11
Zr	125	224	120	110	256	142	78	396
Ag	<0.5	<0.5	<0.5	<0.5	<0.5	<1	<1	<1
As	5	<5	<5	<5	<5			
Cd	<0.5	<0.5	<0.5	<0.5	<0.5			
Co	40	28	35	37	25	49,2	50,4	34,5
Cu	39	23	21	15	29	39	108	25
Li	20	30	30	20	30			
Mo	1	1	<1	1	<1	2	<2	<2
Ni	136	26	84	91	84	146	53	17
Pb	<2	12	7	12	14	<5	<5	6
Sc	22	24	22	19	15	0,4	0,16	0,38
Tl	<10	<10	<10	<10	<10	<0.5	<0.5	<0.5
Zn	92	122	99	109	93	152	180	183

SAMPLE	AS08-07	AS08-09	MO 030-1	MO 028	MO 031	MO 034	MO 017	P7.5
Rock type	Gabbro	Gabbro	Gabbro, Umbukta	Mafic dyke	Mafic dyke	Mafic dyke	Mafic dyke	CZ-granitoid
UTM_E33	517269	481479	467472	486659	486824	484743	484881	487088
UTM_N33	7425612	7335324	7343218	7335775	7337335	7338416	7339613	7338899
SiO2	46,21	52,12	51,04	49,04	48,22	49,1	47,52	60,4
Al2O3	11,32	14,11	17,75	13,9	11,92	13,97	13,4	16,95
Fe2O3	15,45	12,1	12,22	13,41	14,7	12,83	14,2	6,98
CaO	9,28	8,24	6,22	9,27	7,58	9,08	9,31	2,12
MgO	14,45	4,98	4,85	7,5	12,77	7,49	7,38	1,95
Na2O	1,59	3,03	3,25	2,53	1,64	2,08	1,98	3,86
K2O	0,2	1,01	1,34	0,46	0,55	1,14	0,63	4,92
Cr2O3	0,08	0,01	0,02	0,04	0,05	0,04	0,03	0,01
TiO2	0,92	3,27	2,31	2,6	2,03	2,99	4,11	1,07
MnO	0,2	0,15	0,17	0,17	0,18	0,16	0,18	0,06
P2O5	0,084	0,371	0,348	0,286	0,203	0,455	0,515	0,09
SrO	0,03	0,05	0,04	0,04	0,03	0,06	0,06	0,02
BaO	0,01	0,02	0,11	0,02	0,01	0,04	0,02	0,1
LOI	0,08	-0,03	0,15	0,57	-0,21	0,45	0,39	0,51
Total	99,9	99,44	99,81	99,83	99,68	99,88	99,72	99,04
Ba	54,3	164,5	824	93,6	102,5	269	158,5	1025
Ce	8,4	46,4	62,3	22,5	21,7	47,8	66,7	187,5
Cr	550	100	120	270	340	290	200	60
Cs	79,2	36,9	31,4	40,1	65,2	43,6	47,3	7,04
Dy	2,26	7	5,31	4,95	4,05	5,77	7,86	9,98
Er	1,1	3,32	3,04	2,29	2,06	2,66	3,5	4,97
Eu	0,76	2,5	2,58	1,73	1,37	2,52	3,49	1,96
Ga	13,1	23,7	23,6	19,9	15,5	20,9	24,2	29,3
Gd	2,26	8,44	6,73	5,26	4,39	7,63	10,7	12,35
Hf	1,1	6,7	5,4	3,3	2,8	6,4	6,7	10,7
Ho	0,4	1,26	1,05	0,88	0,75	1,05	1,37	1,81
La	2,6	20,1	31,5	9,8	9,1	19,9	31	92,3
Lu	0,1	0,37	0,44	0,26	0,22	0,29	0,35	0,54
Nb	4,9	28,5	30,1	16,2	12,3	27,1	33,6	27,4
Nd	6,5	29,7	32,3	16,8	14,5	32,8	43,3	86,5
Pr	1,28	6,48	7,66	3,37	3,03	6,92	9,34	23,2
Rb	4,6	44,4	26,3	5,4	20,4	40,4	13	224
Sm	1,96	8,05	6,81	5,01	3,73	8,09	10,35	15,2
Sn	<1	4	1	1	1	2	4	5
Sr	261	446	369	345	244	547	572	245
Ta	0,2	1,7	1,9	1	0,8	1,5	2	1,8
Tb	0,37	1,32	0,94	0,87	0,69	1,1	1,57	1,71
Th	0,27	3,82	1,86	0,96	1,76	1,83	1,97	38,7
Tm	0,15	0,42	0,41	0,39	0,26	0,35	0,42	0,62
U	0,1	1,29	0,43	0,4	0,51	0,63	0,75	3,08
V	132	207	165	207	168	191	250	97
W	<1	5	2	2	1	4	1	<1
Y	10,3	31,7	26	22,5	19	25,8	33,7	47,6
Yb	0,9	2,64	2,9	1,78	1,6	2,05	2,57	3,97
Zr	32	248	196	104	82	252	261	442
Ag	<1	<1	<1	<1	<1	<1	<1	<0.5
As								<5
Cd								<0.5
Co	79,2	36,9	31,4	40,1	65,2	43,6	47,3	16
Cu	51	59	35	21	54	32	43	13
Li								40
Mo	<2	3	<2	2	<2	2	2	<1
Ni	395	54	63	120	418	149	124	30
Pb	<5	6	9	6	<5	<5	5	28
Sc	0,09	1,83	0,48	0,21	0,82	0,83	0,63	12
Tl	<0.5	<0.5	<0.5	<0.5	<0.5	<0.5	<0.5	<10
Zn	119	174	157	140	133	158	165	95

SAMPLE	P11.1 OS	P15.2B OS	MO 008	MO 012	MO 016	MO 028771		
Rock type	Granite	Granite	Host rock	Host rock	Host rock	Host rock		
UTM_E33		488725	483310	482875	484647	485826		
UTM_N33		7340941	7338840	7338835	7339694	7338733		
SiO2	77,8	75,8	64,25	63,5	63,85	61,9		
Al2O3	12,9	13,2	16,75	17,39	18,3	16,65		
Fe2O3	1,38	1,93	6,52	6,61	7,16	7,8		
CaO	0,61	2,38	2,5	2,54	1,24	1,03		
MgO	0,31	0,67	2,14	2,26	1,67	2,88		
Na2O	2,76	4,5	2,74	2,9	3	1,04		
K2O	2,99	1,24	2,69	2,66	2,73	4,5		
Cr2O3	<0.01	0,01	0,01	0,01	0,01	0,01		
TiO2	0,2	0,17	0,88	0,9	0,97	0,84		
MnO	0,01	0,03	0,15	0,14	0,1	0,09		
P2O5	0,07	0,15	0,103	0,1	0,127	0,18		
SrO	0,01	0,05	0,03	0,04	0,02	0,02		
BaO	0,05	0,02	0,11	0,13	0,06	0,09		
LOI	1,02	0,98	0,82	0,7	0,66	1,5		
Total	100,11	101,13	99,69	99,87	99,89	98,5		
Ba	409	172	861	1040	512	757		
Ce	40,7	21,5	106,5	121,5	125,5	95		
Cr	10	40	60	60	60	70		
Cs	1,61	1,51	3,09	2,75	6,18	5,08		
Dy	2,5	2,29	6,75	8,38	8,76	8,56		
Er	1,58	1,2	4,4	5,04	5,29	5,81		
Eu	0,46	1,07	1,56	2,15	1,88	1,06		
Ga	15,7	17,3	24,1	25,6	26,5	26,9		
Gd	2,4	2,19	7,79	10,4	10,7	6,91		
Hf	4,5	2,3	9,9	8,6	10,2	6,3		
Ho	0,48	0,44	1,43	1,69	1,77	1,89		
La	11,5	10	44,6	63,6	63,2	29,2		
Lu	0,26	0,13	0,69	0,77	0,77	0,78		
Nb	7,4	6,3	20,4	22,3	21,9	20,6		
Nd	11,6	9,9	42,3	57,5	57,6	30,4		
Pr	3	2,66	11,45	15,25	15,4	7,9		
Rb	123,5	56,7	140,5	137,5	158,5	169,5		
Sm	2,38	2,26	7,79	10,55	10,85	6,45		
Sn	6	1	1	2	4	3		
Sr	157,5	521	244	315	152	134,5		
Ta	1,1	1,1	1,3	1,5	1,6	1,5		
Tb	0,38	0,39	1,18	1,54	1,57	1,2		
Th	13,55	3,65	17,5	17,6	19,8	20,1		
Tm	0,23	0,13	0,67	0,76	0,77	0,81		
U	2,76	1,53	1,87	1,86	4,11	2,09		
V	9	20	60	66	77	83		
W	1	1	1	1	2	1		
Y	14,4	12,3	36,1	43	45,8	49		
Yb	1,77	1,22	4,57	5,12	5,12	5,37		
Zr	127	72	358	315	373	213		
Ag	<0.5	<0.5	<1	<1	<1	<1		
As	5	<5						
Cd	<0.5	<0.5						
Co	2	4	14,8	14	13,9	18,4		
Cu	4	6	5	12	7	7		
Li	10	<10						
Mo	<1	1	<2	<2	<2	<2		
Ni	4	14	29	29	26	31		
Pb	37	17	37	25	10	14		
Sc	4	3						
Tl	<10	<10	<0.5	<0.5	0,5	<0.5		
Zn	22	18	126	110	114	106		

Appendix D – Cathodoluminescence (CL) images of the analysed zircons

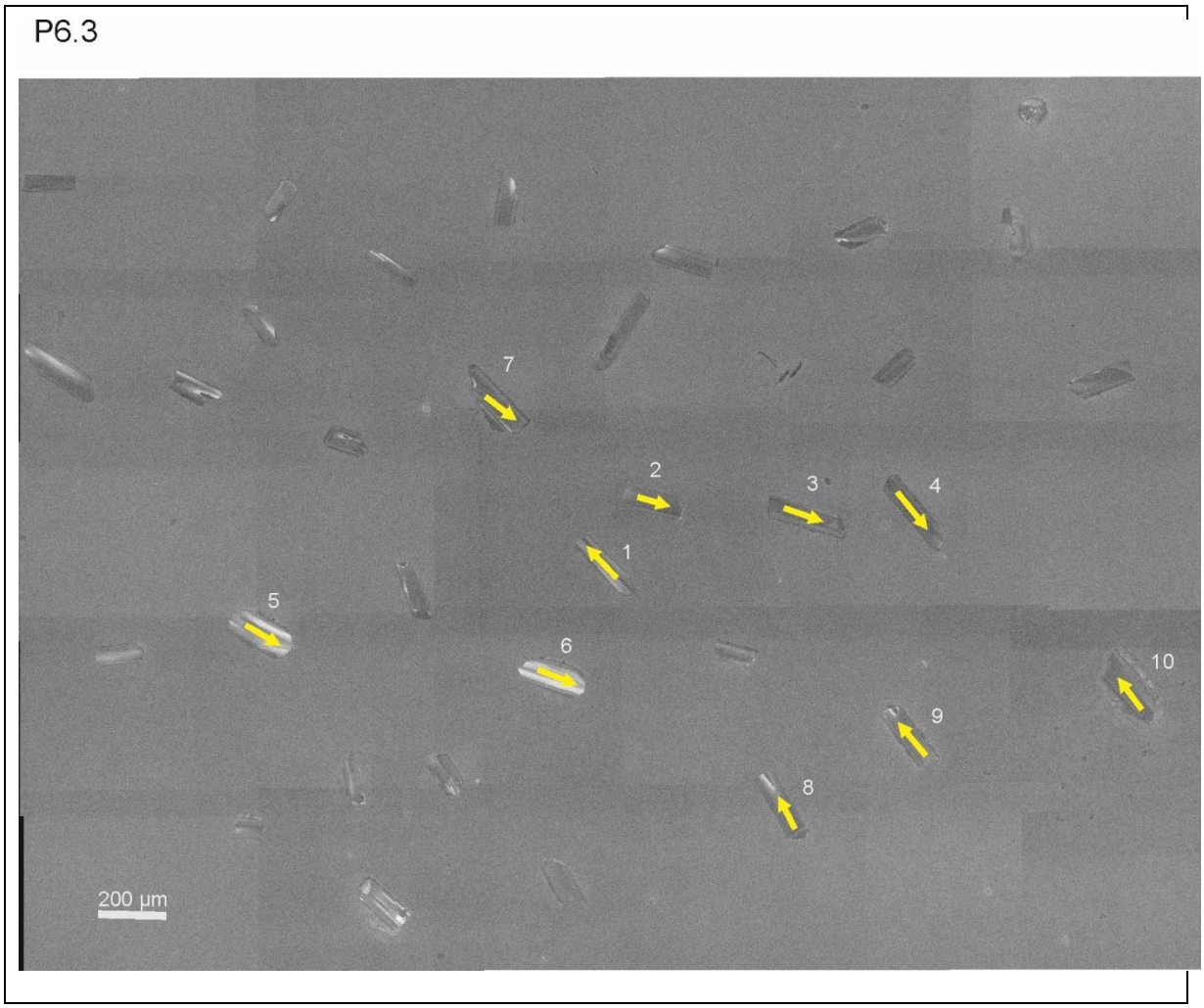

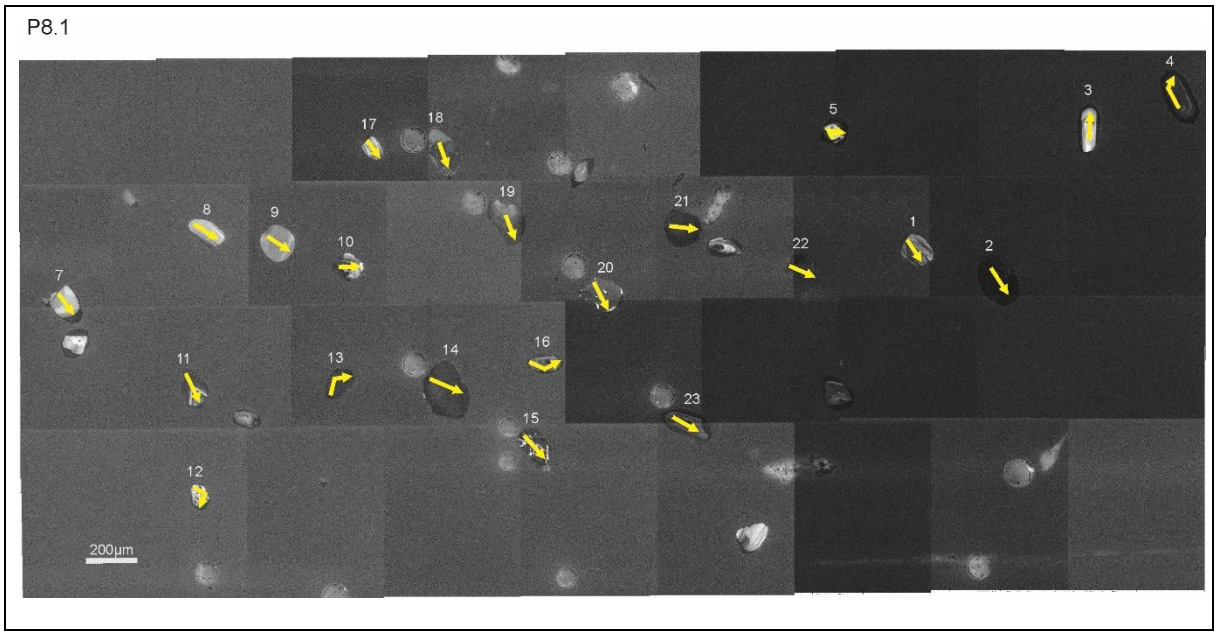
P8.1
1
2
3
4
5
7
8
9
10
11
12
13
14
15
16
17
18
19
20
21
22
23
200µm

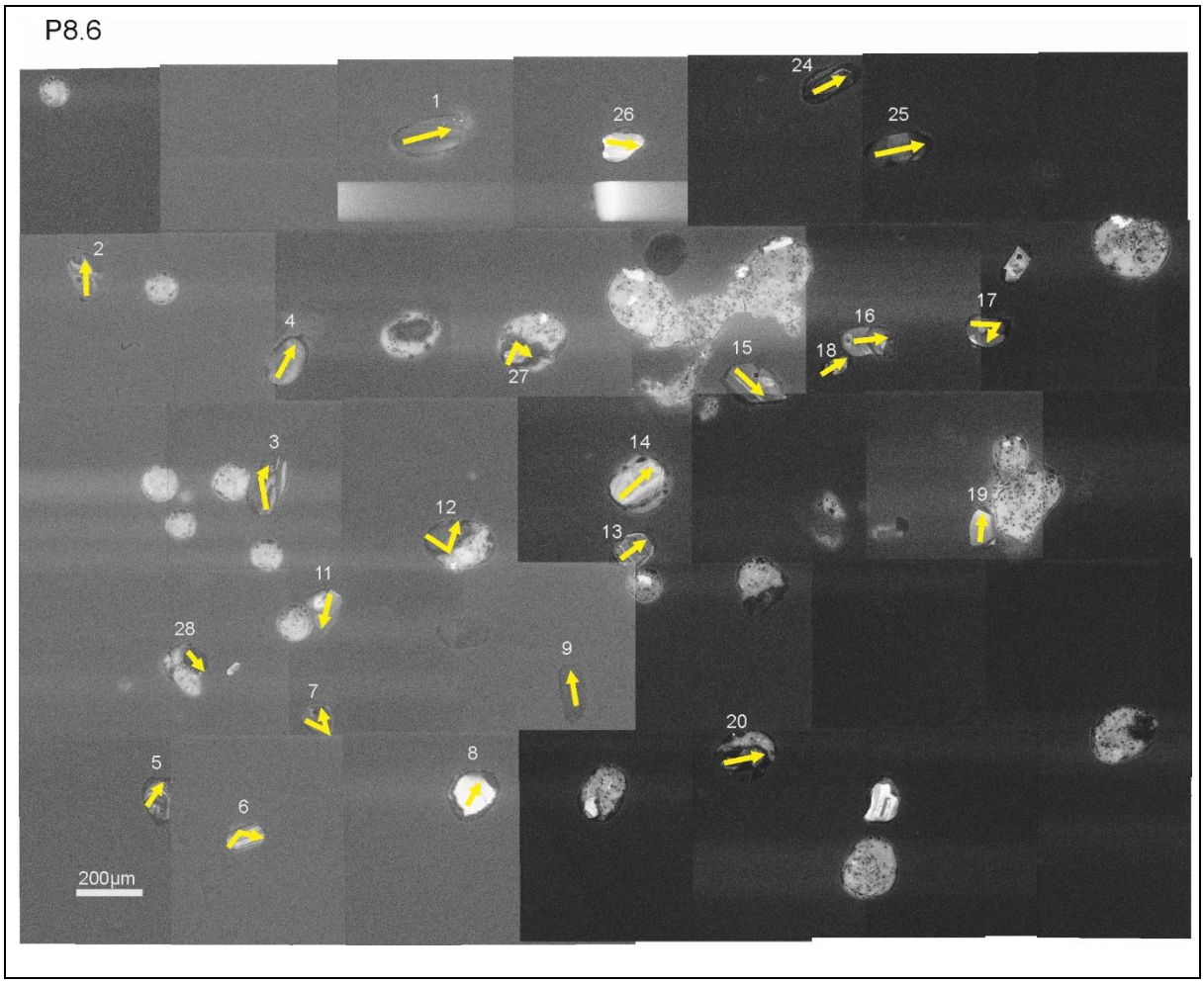
P8.6
1
2
3
4
5
6
7
8
9
11
12
13
14
15
16
17
18
19
20
24
25
26
27
28
200µm

P15.4 ØS

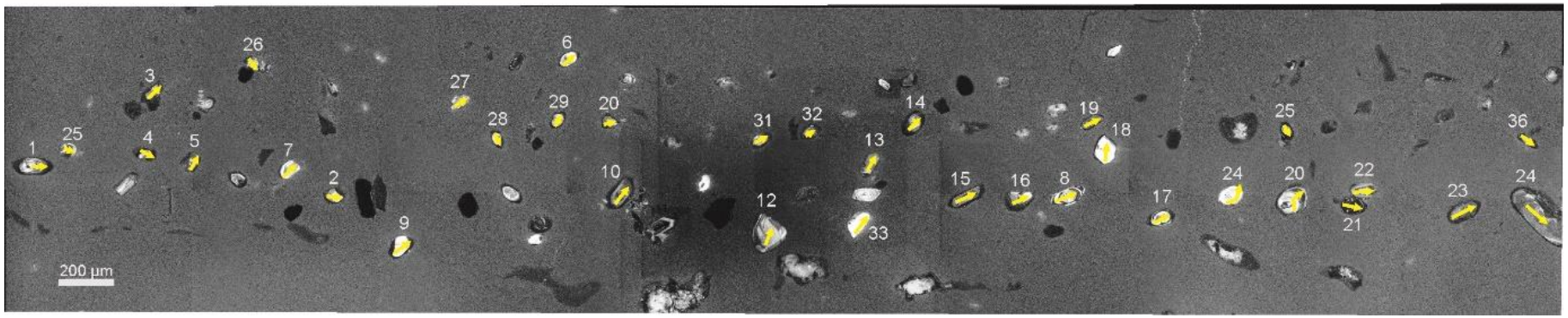
1
25
3
4
26
5
7
2
9
27
28
29
6
20
10
31
32
12
13
33
14
15
16
8
19
18
17
25
24
20
22
21
23
36
24
200 µm

Appendix E – Zircon geochronological data

	Isotope ratios										Age estimates (ma)					Concentrations			
	Concordia output				Terra-Wasserburg output														
Analysis #	Pb207/U235	1s%	Pb206/U238	1s%	roh	238/206	1s%	207/206	1s%		Pb207/Pb206	1s	Pb207/U235	1s	Pb206/U238	1s	conc	Th/U	U	Th	Pbtot
P6-3_01	0,7383	1,62	0,09173	1,19	0,43	10,9016	1,19	0,05838	1,54		543,9	33,39	561,4	6,98	565,7	6,44	104,0	1,01	246	248	31
P6-3_02	0,7540	1,49	0,09328	1,18	0,47	10,7204	1,18	0,05863	1,40		553,3	30,4	570,5	6,52	574,9	6,48	103,9	1,16	433	502	57
P6-3_03	0,7749	1,41	0,09502	1,17	0,49	10,5241	1,17	0,05915	1,32		572,6	28,33	582,6	6,26	585,1	6,55	102,2	1,19	416	495	57
P6-3_04	0,7946	1,34	0,0967	1,17	0,53	10,3413	1,17	0,05960	1,22		589	26,41	593,8	6,01	595,1	6,62	101,0	1,26	492	619	69
P6-3_05	0,7533	1,63	0,093	1,19	0,43	10,7527	1,19	0,05875	1,55		557,9	33,56	570,1	7,11	573,3	6,52	102,8	0,70	216	152	27
P6-3_06	0,7556	1,76	0,09363	1,20	0,40	10,6803	1,20	0,05854	1,69		549,8	36,62	571,5	7,69	577	6,62	104,9	0,61	134	82	16
P6-3_07	0,7369	1,35	0,09102	1,16	0,52	10,9866	1,16	0,05872	1,24		556,8	26,86	560,6	5,82	561,6	6,26	100,9	0,88	446	393	57
P6-3_08	0,7605	1,67	0,09433	1,19	0,42	10,6011	1,19	0,05848	1,59		547,7	34,46	574,3	7,32	581,1	6,62	106,1	0,91	181	165	23
P6-3_09	0,7821	2,22	0,09649	1,25	0,31	10,3638	1,25	0,05879	2,19		559,3	47,09	586,7	9,91	593,8	7,09	106,2	0,97	136	132	18
P8-1_001	2,9542	1,31	0,23861	1,14	0,51	4,1909	1,14	0,08980	1,22		1421,1	23,15	1395,9	9,93	1379,5	14,16	97,1	0,33	163	53	47
P8-1_003	2,1447	2,25	0,19831	1,28	0,29	5,0426	1,28	0,07844	2,24		1158	43,78	1163,3	15,60	1166,2	13,62	100,7	0,88	33	29	9
P8-1_004	2,1469	1,41	0,20053	1,15	0,47	4,9868	1,15	0,07765	1,34		1138	26,32	1164,1	9,77	1178,1	12,38	103,5	0,39	155	61	37
P8-1_005	2,6536	1,75	0,22399	1,21	0,38	4,4645	1,21	0,08592	1,70		1336,4	32,61	1315,6	12,89	1302,9	14,22	97,5	0,19	55	11	14
P8-1_006	5,0386	1,31	0,32108	1,15	0,51	3,1145	1,15	0,11382	1,22		1861,2	21,88	1825,8	11,09	1795	17,99	96,4	0,42	85	36	34
P8-1_007	5,2856	1,74	0,32419	1,25	0,40	3,0846	1,25	0,11825	1,69		1930	30	1866,5	14,85	1810,1	19,65	93,8	0,84	40	33	18
P8-1_008	1,8883	2,74	0,18156	1,36	0,24	5,5078	1,36	0,07543	2,76		1080,1	54,22	1077	18,21	1075,5	13,46	99,6	1,09	31	34	8
P8-1_009	33,0721	1,46	0,74054	1,29	0,52	1,3504	1,29	0,32391	1,36		3588,5	20,68	3582,8	14,42	3572,6	35,49	99,6	0,65	31	20	35
P8-1_011	2,1727	1,53	0,19922	1,16	0,43	5,0196	1,16	0,07910	1,47		1174,7	28,66	1172,3	10,62	1171,1	12,49	99,7	0,35	93	33	21
P8-1_015	2,6808	1,20	0,22049	1,13	0,56	4,5354	1,13	0,08818	1,10		1386,5	20,95	1323,2	8,91	1284,5	13,13	92,6	0,15	479	73	120
P8-1_018	11,7739	1,20	0,4623	1,13	0,56	2,1631	1,13	0,18472	1,09		2695,7	17,86	2586,6	11,18	2449,7	23,03	90,9	0,15	284	44	162
P8-1_019	1,7052	1,31	0,16945	1,14	0,51	5,9014	1,14	0,07299	1,22		1013,5	24,53	1010,5	8,39	1009,1	10,64	99,6	0,23	343	78	66
P8-1_020	2,6099	1,28	0,21867	1,14	0,52	4,5731	1,14	0,08657	1,19		1350,9	22,76	1303,4	9,42	1274,8	13,17	94,4	0,16	131	21	33
P8-1_021	1,7233	1,21	0,16557	1,13	0,56	6,0397	1,13	0,07549	1,10		1081,5	22	1017,3	7,77	987,7	10,33	91,3	0,05	1060	51	191
P8-1_022	2,2526	1,25	0,19816	1,14	0,54	5,0464	1,14	0,08245	1,15		1256,2	22,18	1197,6	8,80	1165,4	12,09	92,8	0,42	397	169	97
P8-1_023	4,4971	1,24	0,30741	1,14	0,54	3,2530	1,14	0,10610	1,14		1733,5	20,8	1730,4	10,32	1727,9	17,22	99,7	0,29	278	81	102

	Isotope ratios									Age estimates (ma)							Concentrations			
	Concordia output					Terra-Wasserburg output														
Analysis_#	Pb207 U235	1s%	Pb206 U238	1s%	roh	238/206	1s%	207/206	1s%	Pb207 Pb206	1s	Pb207 U235	1s	Pb206 U238	1s	conc	Th/U	U	Th	Pbtot
P8-6_001	2,5516	1,37	0,21933	1,17	0,51	4,5593	1,17	0,08437	1,27	1301,1	24,38	1286,9	9,97	1278,3	13,53	98,2	0,60	193	115	52
P8-6_002	2,0518	1,24	0,18879	1,15	0,57	5,2969	1,15	0,07883	1,12	1167,8	22,01	1132,9	8,47	1114,8	11,77	95,5	0,56	196	109	46
P8-6_003	1,8197	1,22	0,17749	1,14	0,57	5,6341	1,14	0,07436	1,09	1051,2	21,82	1052,6	7,96	1053,2	11,14	100,2	0,50	323	161	70
P8-6_004	1,9868	1,27	0,18833	1,15	0,55	5,3098	1,15	0,07651	1,15	1108,5	22,9	1111	8,58	1112,3	11,77	100,3	0,36	147	53	33
P8-6_005	3,8111	1,20	0,28178	1,15	0,58	3,5489	1,15	0,09809	1,08	1588,2	20	1595,1	9,68	1600,3	16,24	100,8	0,41	261	106	90
P8-6_006	2,0759	1,34	0,1954	1,16	0,52	5,1177	1,16	0,07705	1,23	1122,5	24,44	1140,9	9,19	1150,6	12,21	102,5	0,47	130	61	31
P8-6_007	2,1621	1,21	0,19917	1,14	0,58	5,0208	1,14	0,07873	1,08	1165,4	21,3	1169	8,38	1170,9	12,25	100,5	0,15	345	51	77
P8-6_008	9,1767	1,40	0,42589	1,20	0,51	2,3480	1,20	0,15627	1,30	2415,7	21,86	2355,8	12,79	2287,2	23,11	94,7	0,77	46	36	27
P8-6_009	1,6342	1,20	0,16135	1,14	0,58	6,1977	1,14	0,07346	1,08	1026,6	21,51	983,5	7,53	964,3	10,22	93,9	0,55	718	394	143
P8-6_010	1,9415	1,59	0,18967	1,19	0,44	5,2723	1,19	0,07424	1,51	1048	30,18	1095,5	10,63	1119,6	12,19	106,8	0,27	682	187	151
P8-6_011	2,3231	1,27	0,20692	1,15	0,54	4,8328	1,15	0,08143	1,17	1231,8	22,61	1219,4	9,03	1212,4	12,70	98,4	0,47	135	63	34
P8-6_012	1,9947	1,25	0,18897	1,15	0,56	5,2918	1,15	0,07656	1,14	1109,7	22,61	1113,7	8,48	1115,8	11,74	100,5	0,77	238	183	58
P8-6_013	2,1375	1,24	0,19213	1,15	0,56	5,2048	1,15	0,08069	1,12	1213,9	21,9	1161	8,56	1132,9	11,89	93,3	0,31	211	65	48
P8-6_014	5,0133	1,30	0,32108	1,16	0,53	3,1145	1,16	0,11325	1,19	1852,1	21,36	1821,6	10,98	1795	18,15	96,9	3,16	62	197	40
P8-6_015	2,0392	1,24	0,18953	1,14	0,56	5,2762	1,14	0,07804	1,13	1147,8	22,22	1128,7	8,46	1118,8	11,75	97,5	0,27	213	57	47
P8-6_016	2,0990	1,24	0,19284	1,15	0,56	5,1856	1,15	0,07894	1,13	1170,7	22,17	1148,5	8,54	1136,7	11,92	97,1	0,38	207	79	47
P8-6_017	13,5153	1,19	0,50813	1,14	0,58	1,9680	1,14	0,19292	1,07	2767,2	17,53	2716,4	11,30	2648,6	24,75	95,7	0,70	177	124	124
P8-6_018	2,8655	1,22	0,22195	1,14	0,57	4,5055	1,14	0,09364	1,10	1500,9	20,68	1372,9	9,16	1292,2	13,34	86,1	0,25	321	80	84
P8-6_019	2,0708	1,36	0,19063	1,15	0,50	5,2458	1,15	0,07879	1,27	1166,9	24,82	1139,2	9,30	1124,8	11,91	96,4	0,32	89	28	20
P8-6_020	1,7986	1,24	0,17325	1,14	0,56	5,7720	1,14	0,07530	1,13	1076,5	22,6	1045	8,12	1030	10,85	95,7	0,27	257	68	51
P8-6_021	2,1034	1,31	0,19273	1,15	0,52	5,1886	1,15	0,07916	1,21	1176,1	23,79	1149,9	9,03	1136,1	11,96	96,6	0,24	264	64	59
P8-6_022	1,9182	1,67	0,17805	1,19	0,40	5,6164	1,19	0,07814	1,61	1150,5	31,63	1087,4	11,15	1056,3	11,58	91,8	0,99	50	50	12
P8-6_023	11,3746	1,21	0,46524	1,14	0,57	2,1494	1,14	0,17733	1,09	2628	18,03	2554,3	11,27	2462,7	23,33	93,7	0,16	184	30	105
P8-6_024	2,8578	1,23	0,23098	1,14	0,56	4,3294	1,14	0,08974	1,11	1419,9	21,11	1370,9	9,22	1339,6	13,77	94,3	0,38	323	122	88
P8-6_025	2,0093	1,20	0,18868	1,13	0,57	5,3000	1,13	0,07724	1,09	1127,4	21,58	1118,7	8,16	1114,2	11,60	98,8	0,57	1114	636	264
P8-6_026	1,9314	1,70	0,1828	1,19	0,40	5,4705	1,19	0,07664	1,64	1111,7	32,45	1092	11,37	1082,2	11,83	97,3	1,05	44	47	11
P8-6_027	3,1852	1,29	0,2534	1,14	0,53	3,9463	1,14	0,09117	1,18	1450,1	22,47	1453,6	9,97	1456	14,92	100,4	0,34	124	42	37
P8-6_028	2,0022	1,21	0,17503	1,13	0,55	5,7133	1,13	0,08297	1,11	1268,5	21,28	1116,2	8,22	1039,8	10,88	82,0	0,24	1116	266	227
P15-4-OS_11	1,8238	1,19	0,17745	1,12	0,56	5,6354	1,12	0,07454	1,09	1055,8	22,12	1054	7,78	1053	10,82	99,73		1287	574	274
P15-4-OS_12	4,6775	1,19	0,31337	1,12	0,55	3,1911	1,12	0,10825	1,10	1770,1	19,91	1763,2	9,95	1757,3	17,16	99,28		309	23	110
P15-4-OS_13	1,7910	1,23	0,16928	1,12	0,53	5,9074	1,12	0,07673	1,15	1114,2	22,64	1042,2	8,01	1008,2	10,43	90,49		393	217	83
P15-4-OS_14	1,9366	1,23	0,18501	1,12	0,53	5,4051	1,12	0,07591	1,15	1092,8	22,81	1093,8	8,26	1094,3	11,25	100,14		427	162	93
P15-4-OS_16	2,0472	1,26	0,19098	1,12	0,52	5,2362	1,12	0,07774	1,17	1140,3	23,13	1131,4	8,56	1126,7	11,58	98,81		403	116	89
P15-4-OS_17	3,9018	1,24	0,28123	1,12	0,53	3,5558	1,12	0,10062	1,15	1635,6	21,29	1614,1	10,01	1597,5	15,85	97,67		293	294	114
P15-4-OS_18	2,8006	1,41	0,22904	1,14	0,46	4,3660	1,14	0,08868	1,35	1397,2	25,62	1355,7	10,59	1329,5	13,73	95,15		126	76	36
P15-4-OS_22	1,8450	1,25	0,17944	1,11	0,52	5,5729	1,11	0,07457	1,17	1056,6	23,7	1061,7	8,24	1063,9	10,95	100,69		556	94	113
P15-4-OS_23	1,8842	1,27	0,17601	1,12	0,50	5,6815	1,12	0,07763	1,20	1137,5	23,59	1075,5	8,44	1045,1	10,79	91,88		746	249	151
P15-4-OS_24	1,8152	1,23	0,17368	1,11	0,52	5,7577	1,11	0,07580	1,15	1089,8	22,75	1051	8,03	1032,3	10,62	94,72		334	403	84
P15-4-OS_25	2,2461	1,24	0,20416	1,11	0,52	4,8981	1,11	0,07979	1,15	1191,7	22,66	1195,6	8,69	1197,6	12,17	100,50		575	218	141
P15-4-OS_27	2,3053	1,54	0,20381	1,15	0,41	4,9065	1,15	0,08203	1,50	1246,2	28,81	1213,9	10,93	1195,8	12,60	95,96		181	61	44
P15-4-OS_28	2,6057	1,46	0,22457	1,14	0,44	4,4530	1,14	0,08415	1,40	1295,9	27,11	1302,2	10,72	1306	13,52	100,78		166	40	43
P15-4-OS_29	2,5361	1,31	0,21107	1,12	0,49	4,7378	1,12	0,08714	1,24	1363,6	23,66	1282,5	9,52	1234,5	12,61	90,53		364	169	90
P15-4-OS_30	2,3687	1,31	0,20925	1,12	0,49	4,7790	1,12	0,08210	1,24	1247,8	24,19	1233,2	9,39	1224,8	12,52	98,16		382	267	97
P15-4-OS_34	3,4547	1,40	0,27691	1,13	0,46	3,6113	1,13	0,09048	1,34	1435,5	25,27	1516,9	10,99	1575,8	15,87	109,77		117	59	40
P15-4-OS_35	2,4325	1,28	0,21506	1,12	0,49	4,6499	1,12	0,08203	1,22	1246,2	23,6	1252,2	9,24	1255,7	12,73	100,76		391	94	97
P15-4-OS_36	3,6023	1,27	0,2643	1,12	0,50	3,7836	1,12	0,09884	1,19	1602,4	22,14	1550	10,07	1511,8	15,04	94,35		399	177	128